DESIGN AND SYNTHESIS OF MICROCAPSULES USING MICROFLUIDICS FOR AUTONOMIC SELF-HEALING IN CEMENTITIOUS MATERIALS

Lívia Ribeiro de Souza

Department of Engineering

University of Cambridge

This dissertation is submitted for the degree of Doctor of Philosophy

Clare Hall College

July 2017

DECLARATION

I hereby declare that this dissertation is the result of my own work and includes nothing, which is the outcome of work done in collaboration except where specifically indicated in the text. The contents of this dissertation are original and have not been previously submitted, or, are being concurrently submitted, in part or whole, for consideration for a degree or diploma or other qualification at the University of Cambridge or any other University or similar institution except as declared in the Preface and specified in the text.

In accordance with the Department of Engineering guidelines, this thesis does not exceed 65,000 words, inclusive of appendices, footnotes, tables and equations and it does not contain more than 150 figures.

Lívia Ribeiro de Souza

Cambridge, July 2017

ACKNOWLEDGEMENTS

Thanks to Abir for accepting me as a PhD student and give me intellectual, emotional and financial support to perform the research. Thank you very much for not giving up, even in the moments I was lost.

Thanks to the Brazilian Labour Party (*Partido dos Trabalhadores*, PT) for all the investment in education which enabled me to be where I am right now. In particular, to the President Dilma Rousseff, for being an example strength and courage; I'm sorry for the coup. The financial support from the Science without Borders/Brazil (BEX 9185/13-5) is gratefully acknowledged.

I'm filled with gratitude for the research group and all the amazing people I had the pleasure to meet in the last 4 years. This PhD would have been completely different if it was not by the grace, intelligence and charm of the M4L team: Antonis, Chrysoula, Petros, Rami, Wenting and Tanvir. Thanks for being around for the good and bad moments, and sharing the dreams and disenchantments of the research process. A special thanks to Dr. Antonis for all the guidance, Dr. Fei Jin for being always so cheerful and willing to help, and to Dr. Chrysoula for proof-reading my no tea no shade ramblings. Indeed, reading is fundamental.

Thanks to Chris and Len for being always so helpful and cheerful and playful and the best technicians. Thanks to the support offered by the Engineering Department and its canteen, the Hot Numbers café. I'm really grateful for Sue Jackson, Alhinha, John, Ken and all the staff for making my days in the department as pleasant as possible. I also gratefully appreciate the existence of Hot Numbers, bringing me comfort in a form of an 8-oz-mocha-to-go.

Thanks to all my friends in Cambridge whom supported me during this long and winding road, filling my heart with happiness and warmth. Giorgia, Isabelle, Sinan, Marie, Juan, Rasha, Penny, Tristan, Paula, Luna and Nico: thanks for all the hugs and the amazing advices. Special thanks to: Lyn for being so calm, so graceful, so smart and so efficient; Ivo, oh-my-goodness, thanks for existing in this other place; Angel for believing in me and in my strength (Card VIII, my card); Tuzinho and Maricota, for showing me kindness and friendship and assertiveness and the magic of friendship, day after day. I'm also really grateful for the support given by Clare Hall College and the amazing people I had the pleasure to meet. Carlita and Laura: you are sunshine on a cloud day!

Gratitude, immense gratitude, for Rachael, Dave and the Samatha group. I wish I knew the words to express how grateful I am for everything you taught me. This thesis is dedicated to you.

Last, but more importantly, thanks to the giants shoulders of my parents. Today and always. And all my Brazilian friends and family. And Jacque, for the Faith and the English. We did it!

ABSTRACT

A capsule-based self-healing cementitious material, capable of autonomically repairing its own cracks, can extend the service life of concrete structures and decrease the costs associate with repair and maintenance actions. However, the size, shell thickness, shell material and mechanical properties of the capsules still need to be optimised to ensure self-healing performance. Thus, the objective of this research was to explore the controlled microfluidic encapsulation to investigate the production of microcapsules for physically triggered self-healing in cementitious materials. A flow-focusing microfluidic device was used to produce double emulsions to be selectively photopolymerised to generate a core-shell structure. Subsequently, the physical triggering was assessed by embedding the produced microcapsules in cement paste, fracturing it and observing the cracked surface in the SEM. The results showed the production of microcapsules with 80-140 μm of diameter with excellent control over size and shell thickness. Using water-in-oil-in-water (w/o/w) double emulsion, microcapsules were synthesised containing water, colloidal silica solution and sodium silicate solution as core material. In addition, an oil-in-oil-in-water (o/o/w) double emulsion was used to encapsulate mineral oil and emulsified healing agents. The formation of the core-shell structure with aqueous and organic cores was characterised using optical microscopy and SEM. It was demonstrated that the water is not retained inside of the capsule, resulting in the formation of dimples and buckled capsules, particularly for shells thickness ~7 μm. On the other hand, TGA confirmed the retention of mineral oil for shells thickness of ~2 μm and the encapsulation efficiency was demonstrated to be 66%. When the capsules were added to the cement paste, four key factors were observed to prevent physical triggering: (i) thick shells, (ii) buckling of thinner shells due to the loss of water core, (iii) mechanical properties and (iv) poor interfacial bonding. As a result, a mechanical characterisation of the shell material was performed, indicating brittle fracture at room temperature, reduced Young's modulus when compared with cementitious matrix and stress at rupture of 15-36 MPa. In addition, an innovative methodology was proposed to functionalise the surface of the microcapsules with hydrophilic groups in order to increase the interfacial bonding between the cement paste and the microcapsules. Thus, microcapsules with low tensile strength, low shell thickness, organic core and good interfacial bonding were successfully synthesised and demonstrated to rupture upon crack formation. These results experimentally demonstrate the importance of reduced shell thickness, core retention and interfacial bonding as valuable guides during the design of microcapsules for physically triggered self-healing in cementitious materials.

LIST OF CONTENTS

LIST OF FIGURES

LIST OF TABLES

a	gravitational acceleration
A_c	maximum load
BisGMA	bisphenol A glycerolate dimethacrylate
bwoc	by weight of cement
Ca	capillary number
$Ca(OH)_2$	calcium hydroxide
CaO	calcium oxide
CO_2	carbon dioxide
CS	colloidal silica
DCPD	dicyclopentadiene
DETA	diethylenetriamdiethylenetriamineine
di	internal diameter of microcapsules
do	external diameter of microcapsules
E	elastic modulus
EDX	Energy-dispersive X-ray spectroscopy
ETMPTA	trimethylolpropane ethoxylate triacrylate
h	shell thickness to radius ratio
h_c	contact depth
HDDA	1,6-hexanediol diacrylate
h_{max}	maximum penetration depth
IBOA	isobornyl acrylate
L	diameter of the flow
MMA	methyl methacrylate
MU3603	Miwon urethane diacrylate
Na_2PO_3F	sodium monofluorophosphate
NH_4OH	ammonium hydroxide
o/o/w	oil-in-oil-in-water
ODTMS	trimethoxy(octadecyl)silane
OM	optical microscope
PEA	poly(2-phenoxyethyl acrylate)
PEG	poly(ethylene glycol)
PEG-DA	poly(ethylene glycol) diacrylate
PLA	poly(lactic acid)
P_{max}	maximum applied load
PMMA	Poly(methyl methacrylate)
PMVB	poly(o-(α-methyl)vinylbenzaldehyde)
pNIPAM	poly(N-isopropylacrylamide)
PS	polystyrene
PUF	poly(urea formaldehyde)
PVA	poly(vinyl alcohol)
Q	flow rate
Q_i	inner flow rate
Q_m	middle flow rate
Q_o	outer flow rate

SEM	scanning electron microscope
SS	Sodium silicate
tan δ	loss factor
TEOS	tetraethyl orthosilicate
TETA	triethylenetetramine
T_g	Glass transition temperature
TGA	thermogravimetric analysis
UV	Ultraviolet
UVC	Ultraviolet C
V_f	volume fraction
w/o/w	water-in-oil-in-water
XCT	X-ray computed tomography
γ	interfacial tension
η	viscosity
ν	flow speed
ρ	density

1. INTRODUCTION

1.1. PROBLEM AND RATIONALE

Concrete is still the most widely used material on the world, surpassed only by water in terms of consumption. The estimated production of Ordinary Portland Cement, the precursor of concrete, was estimated in 4.2 billion tons in 2016 (U.S. Geological Survey 2017). More than half of this production is accounted to China, which used 6.6 billion tons of cement between 2011 and 2013, more than the U.S. used in the entire 20th Century (Bill Gates 2014). The continued growth of key world economies results in an increasing demand for construction materials to be used to expand urban areas and provide ways to reduce poverty. As a result, the predicted amount of annual cement production in 2050 is ~ 6 billion tons (Müller and Harnisch 2007). However, the large volume of cement produced every year has an environmental impact due to the energy consumption, raw material consumption, waste generation and CO_2 emissions (Meyer 2009). Worldwide, the cement industry was estimated to be responsible for 5% of the global anthropogenic CO_2 generated (Humphreys and Mahasenan 2002). Aiming at sustainable development, Portland cement has been partially substituted by locally available minerals, recycled materials and waste, such as fly ash and ground granulated blast furnace slag (Meyer 2009). Furthermore, the development of resilient infrastructures is also desirable, as it could not only enhance the service life but also reduce the demand for new structures.

However, concrete is inherently susceptible to the formation of cracks that impair its durability. Once formed, the cracks facilitate the ingress of water and carbon dioxide, leading to an increased damage in cement and the corrosion of the reinforcement. To control the damage, repair is necessary, where a sound, cementitious, non-shrinking repair material may be used (Broomfield 2007). The UK alone spent ~£50 billion in 2016 on repair and maintenance of concrete structures, which accounts for 35% of the total expenditure in construction (Office for National Statistics 2016). In the US, the cost for repair, rehabilitation, strengthening and protection of the concrete structures was estimated between $18 to $21 billion/year (Emmons and Sordyl 2006). In addition, a study released by the U.S. Federal Highway Administration (FHWA) in 2002 estimated the annual direct cost of corrosion in the infrastructure in $22.6 billion (NACE International; Koch et al. 2002). Furthermore, indirect costs due to traffic jams and loss of productivity calculated through life cycle analyses can be more than 10 times the direct cost of maintenance and repair (Freyermuth 2001; van Breugel 2007). Thus, preventing the crack propagation in concrete would make it more robust, extending the service-life and reducing repair and maintenance. To date, the common design philosophy has been based on *damage prevention*, namely developing stronger construction

materials to postpone the effects of deterioration. To a certain degree, compositional enhancement of cementitious binders has improved their overall performance. Nevertheless, the formation of cracks is difficult to eliminate, leading materials scientists towards another approach: accept the inevitability of crack formation. As a result, emerged the notion of *damage recovery* where the formation of damage is not problematic as long as it is counteracted by a subsequent process of *healing* (van der Zwaag 2007).

The healing process in concrete is divided into two categories: the first is autogenous healing, associated with intrinsic properties of cementitious materials; and the second is autonomic healing, based on the embedding of healing agents in the matrix (de Rooij et al. 2013). Autogenous healing has as principal healing mechanism the secondary hydration of the unhydrated cement particles and the precipitation of calcium carbonate in the cracks (Edvardsen 1999). However, this autogenous healing is limited by crack width – the crack needs to be roughly below 200 μm and preferably lower than 50 μm (Reinhardt et al. 2013; Fan and Li 2015). A wide array of materials have been added to the matrix to promote autogenous healing, such as the minerals to enhance carbonate precipitation, superabsorbent polymers to promote hydration and fibres to limit the crack width (de Rooij et al. 2013). Alternatively, the healing of larger cracks can be achieved through the use of capsules or vascular systems to store healing agents, which are released when the damage occurs (Van Tittelboom and De Belie 2013). Regarding feasibility, capsule-based self-healing allows the easy addition of capsules during the mixing of concrete followed by controlled release of the healing agent upon damage. This healing agent can be polymeric, mineral and/or biological based and are reported to heal crack up to 1 mm (Wang et al. 2014).

The performance of capsule based autonomic self-healing is controlled by the synergy between the properties of the shell, responsible for triggering, and the core material, responsible for healing. These properties need to be considered during the choice of method to produce the capsules. Although a variety of sophisticated capsule materials capable of responding to an external trigger have been developed (Wang et al. 2013; Wang et al. 2014; Xiong et al. 2015; Lv et al. 2016b; Kanellopoulos et al. 2017), there is no optimum encapsulation methodology yet. This drawback presents a technological challenge for the practical application of capsule-based self-healing on cementitious materials. Cost-effective and simple methodologies for the encapsulation of healing agent have used pelletisation and pan-coating techniques (Alghamri et al. 2016; Tziviloglou et al. 2016). However, these methodologies result in the encapsulation of solid cores, which rely in the ingress of water to promote the self-healing. This limitation can be mitigated by the encapsulation of liquid cores to act as healing agent or as carrier for the healing agent (Wang et al. 2013; Wang et al. 2014; Perez et al. 2015a; Kanellopoulos et al. 2016; Araújo et al. 2016). This methodology

typically relies on the use of emulsification polymerisation processes and results in core-shell structures containing the healing agent. However, the polymerisation process is affected by the properties of the core material (and vice versa), which limits the diversity of cargo and shell material combination that can be used. Moreover, the latter limitation narrows the understanding about the core-shell and shell-matrix interactions, thus limiting the knowledge about self-healing performance.

A promising route to provide detailed understanding of the impact of different cargo and shell material is the encapsulation using microfluidics to form a double emulsion template. By using acrylate monomers as the middle oil fluid and loading it with a photoinitiator, double emulsions can be consolidated into solid capsules through UV polymerisation (Utada et al. 2005). In this process, the laminar flow conditions help to circumvent the reactivity issues encountered using less-controlled conventional emulsification techniques and enable the encapsulation of several core materials (Chen et al. 2014b; Zieringer et al. 2015). Double emulsion templating also allows the fine control of the template dimensions and offers high diversity to the materials to be used as precursors for the capsule shell (Chen et al. 2012; Vilanova et al. 2013; Zieringer et al. 2015). This versatile microfluidic encapsulation is a robust platform where several healing agents and shell material could be produced. Although promising, this technology has not been used for the production of microcapsules for the self-healing concrete.

1.2. AIM AND OBJECTIVES

The overall aim of this thesis is to develop and optimise a microfluidic encapsulation protocol for mechanically triggered self-healing in cementitious materials. Hence, the specific objectives of this research are discussed in different sections of the thesis:

- Set-up a microfluidic station to produce double emulsion, followed by photopolymerisation for production of microcapsules (Section 4.1);
- Investigate the role of flow regimes on the production of double emulsion and the control over size and shell thickness (Section 4.2);
- Synthesise microcapsules containing aqueous (Section 4.3) and organic-based (Section 4.4) core material and acrylate shell;
- Investigate the behaviour of the microcapsules in the cementitious materials, focusing on survival during integration, dispersion, shell properties and physical triggering (Section 5.1);
- Investigate the mechanical properties of specific materials suitable to be used as shell for physical triggering (Section 5.2);

- Synthesise microcapsules with shell suitable for physical triggering, focusing on shell functionalisation, core retention and tuning shell properties (Section 5.3).

1.3. THESIS OUTLINE

This thesis is divided into six chapters; each aiming to answer a question in the scope of the PhD. Chapter 2 provides a comprehensive literature review on the topic of self-healing, presenting recent state of the art developments in the field. Focusing on capsule-based autonomic self-healing, the main healing agents used to promote self-healing are presented, as well as the typical encapsulation process and the expected properties of the shell. Last, a comprehensive literature review on encapsulation using microfluidics is presented, focusing on fabrication and design of the microcapsules, as well as upscaling production. Chapter 3 describes the characteristics of materials and experimental protocols employed in this research. In Chapter 4 the results on the use of microfluidics to produce microcapsules are presented, focusing on the control over size and shell thickness. In addition, four different shells were used to investigate the encapsulation of water- and oil-based cores containing sodium silicate and colloidal silica. The incorporation of microcapsules in cementitious paste to explore survival, dispersion and physical triggering upon crack is discussed in Chapter 5. Additionally, the design of the microcapsules was explored to obtain the mechanically triggered release of the healing agent. Finally, in Chapter 6 the main findings and conclusions are summarised and an outlook towards future research is presented.

2. Literature Review

The purpose of this chapter is to provide an overview on the fundamental concepts associated with capsule-based self-healing of cementitious materials. It starts with a brief overview about the challenges related to concrete industry and the proposed solutions to tackle these challenges, including autogenous and autonomic self-healing. Then, the methods to produce the capsules for autonomic self-healing are presented, examining the encapsulation of solid and liquid cores and the microencapsulation of liquid materials. Next, the shell properties required for self-healing are discussed, focusing at the triggering, mechanical properties and permeability of the shell. To conclude, microfluidics is proposed as a universal technique to encapsulate all liquid core healing agents and the mechanism of encapsulation is elucidated. It is also explained how microfluidics encapsulation can be exploited to fine-tuning microcapsules' permeability and mechanical properties to ensure triggering for capsule-based self-healing.

2.1. Cementitious materials – use and limitations

Concrete is the most used material in the development of infrastructure networks vital in driving economic growth and creating conditions for poverty reduction (UNCTAD Infrastructure Report 2001). The reason behind concrete's popularity is its excellent mechanical and durability properties. In addition, the material is mouldable, generally available, affordable and it can be engineered to satisfy most set of performance specifications (Meyer 2009). These properties are the consequence of the synergy between aggregates, sand, water and Portland cement, the main cementitious material currently used. Portland cement is a powder mixture of mineral oxides which reacts in the presence of water to form hydration products capable of binding particles together. Unfortunately, the cement production is a highly energy-intensive process, mainly due to the calcination of raw materials (limestone, clay and other minerals). As a consequence of the sheer volumes of produced material, the cement industry now contributes ~5% of annual anthropogenic global CO_2 production, with China's booming construction industry producing 3% alone (Worrell et al. 2001; Crow 2008). In order to produce a more sustainable concrete, several materials have been investigated as partial substitutes for Portland cement - in particular materials that are by-products of industrial processes, such as fly ash and ground granulated blast furnace slag (Meyer 2009). In addition, the environmental impact of the concrete industry can be reduced by improving the durability, resulting in an extended life of infrastructures and cost savings (Mehta 2001).

However, the durability of concrete infrastructures is impaired by the formation of cracks. Although concrete is strong in compression, it is prone to cracking due to its limited tensile strength. Cracks may be caused due to freeze-thaw cycles, thermal effects, early-age shrinkage, mechanical loading,

chemical attack or a combination of these causes and it leads to mechanical degradation of concrete. To overcome this limitation, reinforcement is used to improve the tensile load capacity. In this scenario, cracks are not considered as failure of reinforced concrete as long as a crack width criterion is not exceeded (Huang et al. 2016). However, the microcracks provide preferential pathways for ingress of aggressive agents, such as chloride, sulphates and carbonates. These aggressive agents can induce corrosion of embedded steel reinforcement and the corrosion products are expansive thereby accelerating crack formation, spalling and potential premature structural failure. Once formed, cracks lead to leakage, affecting water tightness, a crucial serviceability requirement for many structures such as basements, retaining walls, reservoirs, dams, tunnels, pipelines and waste repositories.

To repair this cracks, conventionally synthetic fillers are used, such as epoxy, grout and resins, applied manually to fill them (Kumar et al. 2011). However these methodologies have several implications: first, this type of one-time quick repair is applied repeatedly over the life of a structure. Secondly, the cracks may also be present in parts of structures inaccessible, making it difficult to be detected and repaired. Furthermore, there are huge costs associated with repeated inspection, repair and maintenance. In the UK only, repair and maintenance actions resulted in a cost of ~£50 billion/year (Office for National Statistics 2016). In the Netherlands, the maintenance of road infrastructure is ~ €68 million/year, and the backlog in maintenance can get as high as €350 million (Klatter et al. 2009). In the United States, a study reported that concrete structure owners nationwide pay ~$18 to $21 billion/year on repair, protection and strengthening (Emmons and Sordyl 2006). In addition, the associated costs for maintenance due to steel corrosion reach $23 billion/year in the U.S. only (NACE International; Koch et al. 2002).

To overcome the limitations associated with crack formation, two material design principles have been explored: *damage prevention* and *damage management* (van der Zwaag 2007). Damage prevention aims at creating a stronger material with microstructures which oppose and/or delay the formation of micro-cracks. However, the formation of damage during use cannot be excluded, and the structures still need periodic inspection to monitor damage development and repair actions. Alternatively, damage management is based on the notion that the formation of damage is not problematic as long as it is counteracted by a subsequent autonomous process of “removing” or “healing” the damage. Thus, the concept of equipping our concrete infrastructure with the ability to repair itself, or *self-heal*, without external intervention has emerged as a possibility to overcome the on-going degradation of our civil infrastructure. As shown in Figure 2.1a, the performance of conventional and high performance concrete structures decreases with the lapse of time until the moment repair is needed; thus the total cost of the structure is periodically increased (Figure 2.1b).

Alternatively, the performance of a structure made with self-healing material remains steady (Figure 2.1c), and although the initial costs are high, the absence of repair costs can result in an overall financially positive situation (Figure 2.1d) (van Breugel 2007).

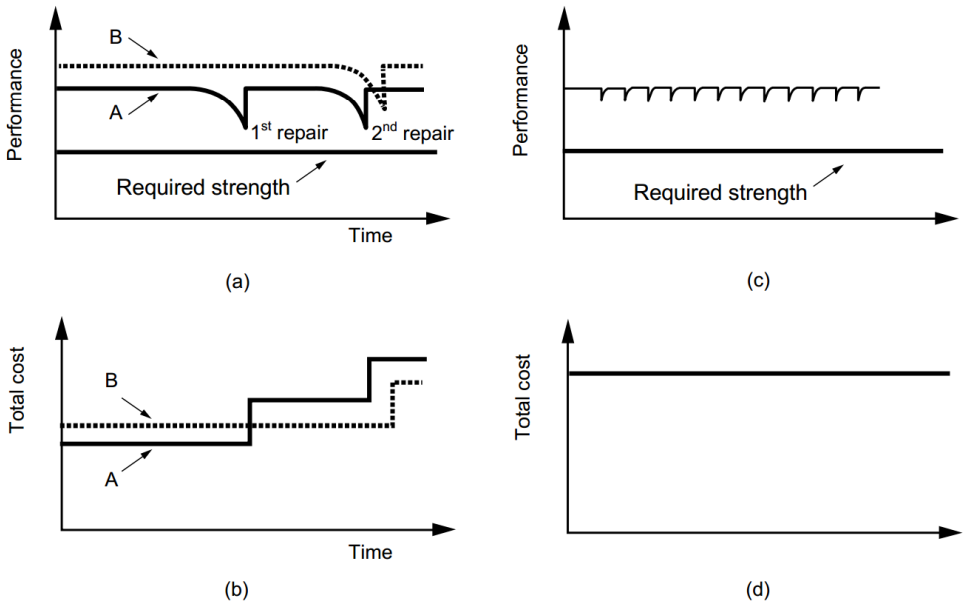

Figure 2.1 – Conceptual performance (a) and costs (b) with elapse of time for normal (A) and high quality (B) structures. Performance (c) and costs (d) of a structure made with self-healing concrete with elapse of time (van Breugel 2007)**.**

2.2. SELF-HEALING CEMENTITIOUS MATERIALS

The field of self-healing materials is based on the concept of "damage management" whereby the development of damage as a function of time is considered (van der Zwaag 2007). For self-healing the formation of damage is not problematic as long as it is counteracted by an autonomous process of healing the damage. In other words, it relies on a self-initiated response of the system to detect and recover autonomically, without external interaction. The general mechanism involves the detection of damage, followed by healing of the created crack and restoring the mechanical properties of the system. For cementitious materials, the mechanisms for achieving self-healing are grouped into two categories: the first takes advantage of the natural autogenous self-healing properties of cementitious matrix, whereas the second is termed autonomic self-healing and relies on the use of embedded repair agents; both are explained in the sections below.

2.2.1. AUTOGENIC SELF-HEALING OF CEMENTITIOUS MATERIALS

The self-healing process is termed autogenic when the recovery process uses components that could otherwise be present when not specifically designed for self-healing (Rooij et al., 2013). The mechanism of autogenic self-healing can be attributed to physical, chemical and mechanical

processes, as shown in Figure 2.2 (Reinhardt et al., 2013). In a physical process, the absorption of water near the crack faces results in the swelling of hydrated cement paste, consequently closing the crack. In the mechanical processes the crack can be closed by spalling-off loose concrete particles and/or impurities in the water, but these processes have minor importance to the autogenic self-healing. Alternatively, the chemical processes could rely on (i) the secondary hydration of the unhydrated cement particles and (ii) the precipitation of calcium carbonate. In the former, the reaction between unhydrated cement particles in early age concrete and water leads to the formation of hydration products resulting in the healing of the crack.

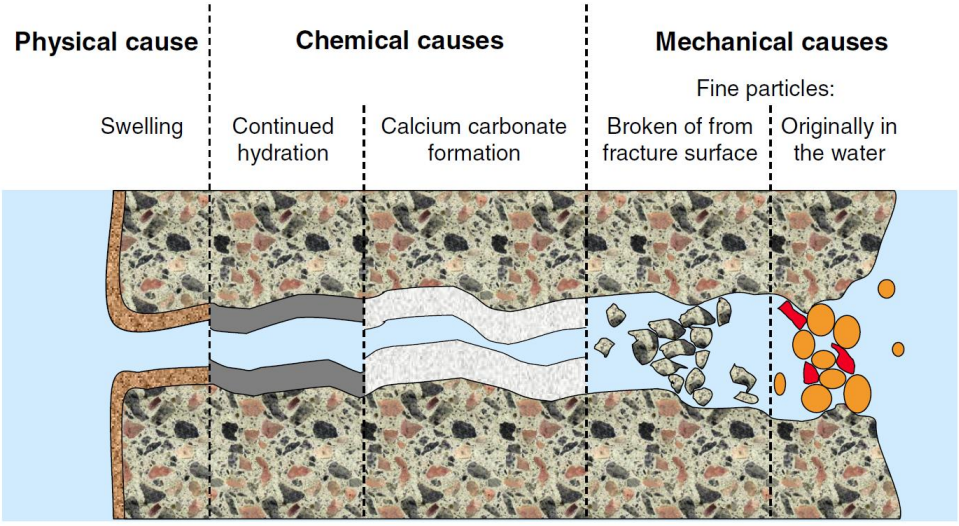

Figure 2.2 - Schematic representation of the mechanisms of autogenic self-healing (Reinhardt et al., 2013).

The healing efficiency depends on the age of the concrete, the water to cement ratio (w/c) and the available water in the cracks. The mechanism of the chemical autogenous healing relies on the presence of anhydrous cement particles that, in contact with water, yield new hydration products. In parallel, calcium hydroxide is leached from the hydrated cement matrix and reacts with carbon dioxide forming crystals which precipitate and fill the space of the crack. The following chemical equations represent the process:

$$H_2O + CO_2 \leftrightharpoons H_2CO_3 \leftrightharpoons H^+ + HCO_3^- \leftrightharpoons 2H^+ + CO_3^- \quad \text{Equation 2.1}$$

$$Ca^{2+} + CO_3^{2-} \leftrightharpoons CaCO_3 \downarrow \quad \text{Equation 2.2}$$

$$Ca^{2+} + HCO_3^- \leftrightharpoons CaCO_3 \downarrow + H^+ \quad \text{Equation 2.3}$$

According to the literature, the crystallisation of calcium carbonate is the most important mechanism of autogenous self-healing in mature concrete (Edvardsen 1999). The precipitated

crystalline products observed in the opening of the cracks have been used as confirmation of autogenous self-healing and it has been attributed as carbonate precipitation. Extended ongoing hydration can also be promoted by replacing part of the cement by fly ash or blast furnace slag, since high amounts of both materials remain unhydrated even at later age (Qian et al. 2009; Sahmaran et al. 2013; Huang et al. 2014a). As both materials are industrial by-products, their use as replacement in concrete structures also reduces the CO_2-emissions caused by cement manufacture. Nonetheless, the autogenous self-healing is limited by the size of the crack; a crack width below 150 µm, and preferably below 50 µm, is critical to the self-healing of any cementitious system (Li and Yang 2007; Fan and Li 2015).

2.2.2. Autonomic self-healing of cementitious materials

The engineered addition of materials or components capable of promoting self-healing in cementitious material characterises autonomic self-healing, since the recovery process uses components that wouldn't otherwise be found in the material (de Rooij et al. 2013). In general, autonomic self-healing materials could be classified broadly into three groups: stimulated intrinsic healing materials, vascular-based healing materials and capsule-based healing materials, as shown in Figure 2.3.

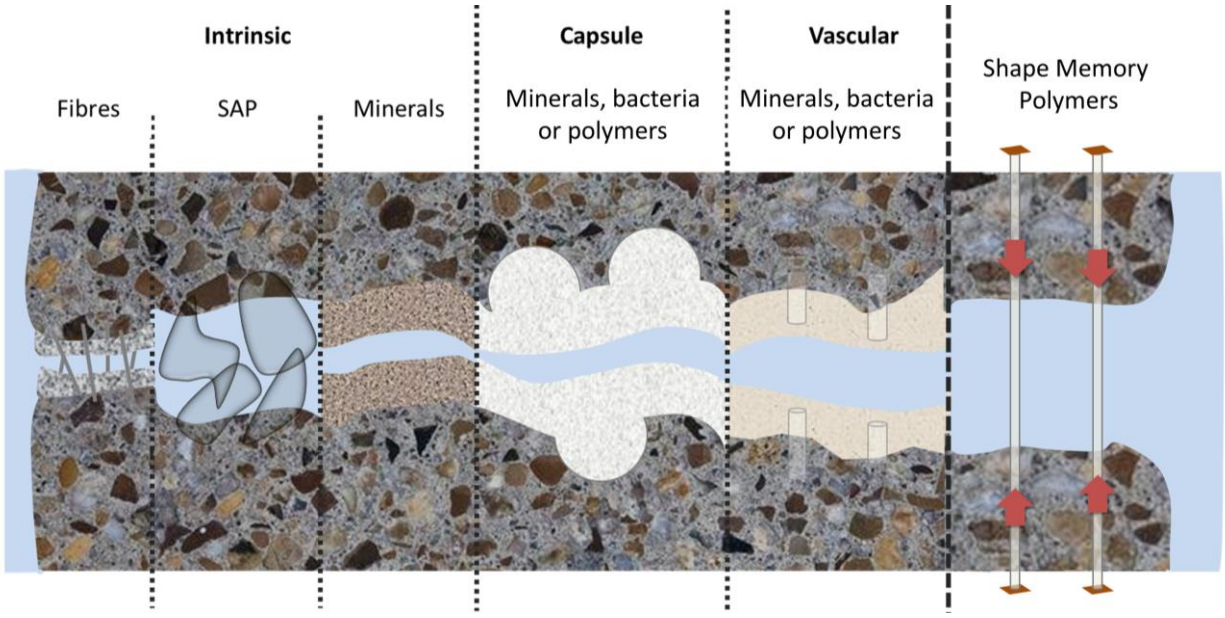

Figure 2.3 – Schematic representation of the mechanisms of autonomic self-healing.

The mechanism of the healing agent is the main difference between the different classifications of autonomic self-healing. In addition, it dictates the extent of the damage that could be healed, the repeatability of the healing and the recovery rate for each approach. Each group will be briefly presented in the following sections.

2.2.2.1. STIMULATED INTRINSIC SELF-HEALING

Intrinsic self-healing in cementitious material is based on the latent healing functionality of composites added to the matrix and it is triggered by damage. Commonly, the materials added are designed to enhance the autogenous healing and a wide array of materials has been used for these purposes, e.g., fibres, polymers, minerals, which are directly added during the mixing process. The material healing functionality remains latent until the crack formation and contact with water which together promote the improved autogenous healing.

Since the presence of water and tight cracks are regarded as the two most important criteria to enhance autogenous self-healing (de Rooij et al. 2013), several materials have been investigated to favour these conditions. For instance, the addition of fibres to the cementitious materials help reduce the crack width to the values needed to ensure maximum efficiency of autogenous healing (Li and Yang 2007; de Rooij et al. 2013); similarly, the use of shrinkable polymer tendons have been demonstrated to close macro-cracks upon heat activation (Jefferson et al. 2010). The reduced crack width has been demonstrated to promote self-healing due to continued hydration and pozzolanic reaction and enable the recovery of mechanical and transport properties (Fan and Li 2015). Additionally, super absorbent polymers (SAPs) have been used to provide additional water for the development of autogenous and autonomic self-healing (de Rooij et al. 2013; Snoeck et al. 2014). SAPs have the ability to absorb water from the surrounding environment and to retain the liquid within their structure (Snoeck et al. 2014). Hence, when the water enters the crack, SAPs along the crack faces will swell, block the crack and use the retained water to promote autogenous healing (Snoeck et al. 2012; Mignon et al. 2017). The main concern regarding using SAPs is the macropores present in the matrix after the water is released, which negatively influence the strength (Mignon et al. 2017).

The addition of mineral admixtures has also been considered to enhance the autogenous healing of cementitious materials. Upon crack formation, these admixtures can expand (Ahn and Kishi 2010; Sisomphon et al. 2012; Qureshi and Al-Tabbaa 2016; Ahn et al. 2016), swell (Ahn and Kishi 2010; Jiang et al. 2015), and promote crystallization (Sisomphon et al. 2012; Jiang et al. 2015; Roig-Flores et al. 2015; Roig-Flores et al. 2016; Ahn et al. 2016) and/or pozzolanic reaction (Jiang et al. 2015) in the crack surface. The properties of the different materials are generally combined to maximise the self-healing performance. A typical example of this approach reported the addition of expansive agents, geo-materials and carbonates to Portland cement, resulting in almost the healing of a crack of 0.2 mm after 28 days (Ahn and Kishi 2010). The geo-material is composed of SiO_2 and sodium aluminosilicate hydroxide, but also contains montmorillonite, which swells in the presence of water. The process of self-healing occurs after the contact with water, essentially due to three factors: (i)

the swelling of clay; (ii) the expansion effect; and (iii) the formation of re-hydration products, which are mainly composed of fibrous phases and calcite. Similarly, the addition of MgO resulted in the sealing of cracks up to 500 μm after 28 days (Qureshi and Al-Tabbaa 2016). The main issues regarding the addition of mineral admixtures for promoting self-healing is their reactivity; since the material is sensitive to water, it promptly starts to react when they are added during the mixing of concrete and thus it is consumed before the crack formation (Huang et al. 2016). In the case of expansive agents, the expansion in the interior of the matrix may lead to further cracks. Therefore, encapsulation is suggested prior to the addition of the minerals in the matrix to minimise contact with water.

2.2.2.2. VASCULAR BASED SELF-HEALING

Vascular self-healing is based on the storage of the healing agent in a network in the form of capillaries or hollow channels, which may be interconnected in one, two, or three-dimensions. The system uses tubes to encapsulate the material and when the crack occurs in the matrix, it triggers the release of the healing agent. Although both vascular and capsule based systems rely on the storage of the healing agent, only the vascular system allows the refilling using an external source and therefore the occurrence of multiple local healings (White et al. 2014). Dry and co-workers pioneered the use of this system, proposing the use of glass tubes loaded with cyanoacrylate, silicon based adhesive, separated two-part epoxy system (Dry 2001) and a multi-component methylmethacrylate system (Dry and McMillan 1996). The dual system offers more stability, since it is activated *in situ*, just when the crack occurs. Joseph and co-workers proposed that single-agent cyanoacrylate offers the greatest chance of flowing into the crack, mainly attributable to its low-viscosity (Lark et al. 2010). Alternatively, smooth-surface bars were embedded inside the concrete matrix during casting and after curing the bars are pulled out creating canals. By connecting multiple canals, a network is formed where epoxy can be pumped resulting in self-healing and structural regain, without the need of water (Pareek et al. 2014). The use of vascular systems is appealing when the aim is to address large cracks (White et al. 2014; Huang et al. 2014b), when the water is not available and for multiple events. However, it presents significant drawbacks, such as the prior planning and introduction of the vascular system and the negative influence on mechanical properties of the cementitious matrix (Huang et al. 2014b).

2.2.2.3. CAPSULE BASED SELF-HEALING

The capsule-based self-healing is the most promising technique for the autonomous healing of cracks larger than 200 μm. Capsules containing healing agent can be easily added during the mixing of cementitious materials and they have been reported to heal cracks up to 1 mm (Wang et al. 2014). The overall autonomous process is illustrated in Figure 2.4, where the capsules act as a reservoir of healing agent inside of the matrix. When the shell is damaged due to cracks or chemical

variations in the matrix, the healing agent is available to fill the crack. Then, the healing agents react with the matrix, moisture or additional components, resulting in solidified healing products.

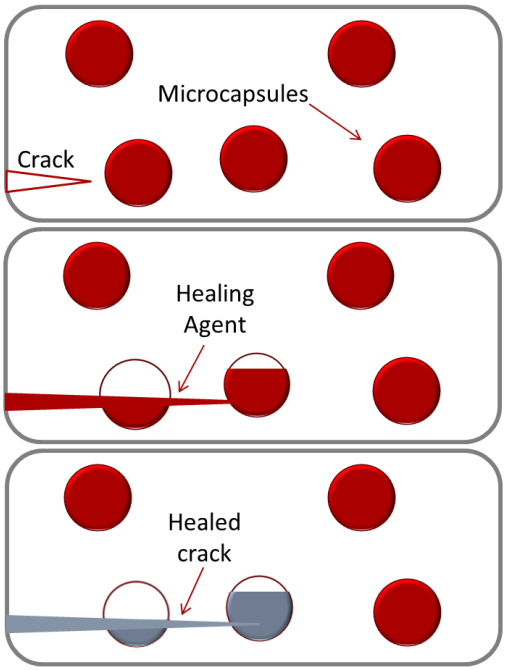

Figure 2.4 – Concept of autonomic capsule based self-healing.

Although a considerable amount of literature has been published on capsule based self-healing showing promising results, there is still no optimised methodology for the encapsulation of healing agents. The challenge lies in the complex design cycle for the capsule-based self-healing, which is divided in five steps: development, integration, mechanical characterisation, triggering, and healing evaluation (Blaiszik et al. 2010). For the **development** of the microcapsules, the first step is to choose a healing agent and the encapsulation method, since the latter is closely associated with the properties of the shell material. Once the material is encapsulated, the shell properties determine whether the capsules survive **integration** process and also whether they respond to external **triggering** and release the healing agent. Furthermore, the combination of the healing agent and shell properties, as well as size and volume of added microcapsules, is responsible for the effect on the **mechanical properties** of the matrix and also for the **self-healing performance**. Once self-healing is achieved, the properties of the healing agent and the shell can be tuned to optimise the performance, according to the application. As a result, the design cycle of the microcapsules may be resumed, considering an optimised healing agent and the encapsulation method. In this setting, the choice of the healing agent is the cornerstone, typically being the first and last topic considered during the design of autonomic capsule-based self-healing. These active ingredients can be grouped into three categories according to their properties, and labelled mineral, biological and polymeric healing agent.

The healing agent must have some intrinsic properties to guarantee the cure efficiency. Ideally, these materials should be **expansive, stable and with suitable viscosity** (Van Tittelboom and De Belie 2013). The expansion of the healing agent ensures that the volume of healed material is sufficient to fill the crack and the original volume of the microcapsule, minimising the water permeability. Bacterial spores, polyurethane prepolymer and MgO are examples of healing agents capable of producing reaction products which occupy larger volume than the healing agent. On the other hand, polymers like epoxy, cyanoacrylates and some minerals may not be capable of filling the entire crack, indicating the water could still permeate through it. It is also desirable that the healing agent would be active for several years inside of the microcapsule. However, this can be challenging since one-component healing agents usually react upon contact with moisture or air and could polymerise inside the capsule (Hilloulin et al. 2015). To enhance the stability over time, the use of a two- or three-component healing agent is preferred, where both components are separated, minimising the risk of premature hardening (Van Tittelboom and De Belie 2013). For example, the microbiological induced precipitation is triggered only in the presence of three components – spores, water and nutrients. However, if two or more phases are encapsulated, the main concern is that the crack will not reach both phases and the healing will not take place. This limitation can be mitigated by encapsulating only one-component, while the second-component is dispersed in the matrix. For example, amines used as hardener to assure the polymerisation of epoxy have been dispersed in the cement matrix (Li et al. 2013). Last, the viscosity of the healing agent controls its spread and hence the healing efficiency, particularly in the case of liquid healing agents. If the material is too viscous, it may not flow out the capsules and fill the crack. On the other hand, if the healing agent viscosity is too low, it could drip away from the crack and be absorbed by the matrix.

In addition, the choice of the healing agent also needs to consider the potential applications. In this case, the **service conditions** of the concrete structures need to be considered, as well as **cost**. For example, the continuous presence of water supply needs to be considered for the autonomic self-healing based on minerals and bacteria. Therefore, the material can be encapsulated in solid form and rely on water to dissolve the core and act as reaction medium. This is only possible because the material is less reactive and the process of precipitation and crystallization of healing products takes several hours to days (Van Tittelboom and De Belie 2013). In this case, encapsulated minerals and spores are suitable for applications where water is continuously available, such as structures under water, under wetting-drying cycles or underground (Huang et al. 2016). Alternatively, autonomic self-healing based on polymers can occur in the absence of water or in the presence of only moisture. Since the water is not present, the material must be liquid and with suitable viscosity to flow out the capsule. Furthermore, certain polymeric materials have a fast curing time,

typically less than 1 hour (Van Tittelboom and De Belie 2013). In this scenario, the technique would be applied in concrete structure in open air and indoors (Huang et al. 2016). As for costs, the healing agent is the main reason behind the additional price of the self-healing, although this is typically not considered in early stage research. However, it is necessary to bear in mind the viability of the healing agent is associated with its price, since the construction industry is highly cost-sensitive and use large volumes of materials. This is particularly important when considering the high cost of polymeric materials, as well as the nutrients for bacteria. For example, dicyclopentadiene (DCPD) is unlikely to be used as healing agent for cementitious materials due to the elevated cost of the Grubbs catalyst used to polymerise the material. Alternatively, the use of minerals can provide a low-cost healing performance, because the price of mineral admixtures is close to that of cement.

Then, to compare their performance for self-healing, three properties are usually assessed: healed crack width, permeability and recovery in mechanical properties. Table 2.1 summarises the performance of some biological, mineral and polymeric healing agents. Commonly, the first approach is visual observation of the width of the healed crack using optical and/or scanning electron microscope (Muhammad et al. 2016). However, the extent of crack closure depends on the crack dimensions and healing may occur just near the surface. Thus, to demonstrate in-depth crack healing, X-ray computed microtomography (Snoeck et al. 2015; Van Tittelboom et al. 2016) and ultrasonic measurements (Alghamri et al. 2016; Kanellopoulos et al. 2016) have been used. Once the crack is healed, tests to quantify the matrix permeability can be performed, including chloride (Maes et al. 2014; Dong et al. 2017), methanol gas (Yang et al. 2011; Kanellopoulos et al. 2015; Qureshi and Al-Tabbaa 2016) and water permeability (Van Tittelboom et al. 2011; Wang et al. 2014), as well as water sorptivity (Kanellopoulos et al. 2015; Alghamri et al. 2016; Giannaros et al. 2016). The reduction in permeability due to healing is crucial since the ingress of moisture and ions that react with reinforcement in concrete can create expansive stress and lead to spalling. Biological, sodium silicate and polyurethane healing agents have shown to be effective in reducing the crack permeability to a similar value of the uncracked samples (Wang et al. 2014; Maes et al. 2014; Alghamri et al. 2016). The reduction in permeability without recovering the mechanical properties is termed sealing and it is suitable for applications when the water percolation due to the crack needs to be reduced (Wiktor and Jonkers 2015; Phillips et al. 2016). To achieve self-healing, however, the healed crack needs to not only reduce the permeability but also provide recovery in mechanical properties. Typical tests to assess the mechanical recovery induce the load regain during flexural test of healed samples. Bacterial and mineral healing agents, for example, have shown up to 80% strength regain, indicating good performance (Wang et al. 2012; Alghamri et al. 2016).

Table 2.1 – Service conditions, self-healing mechanism and healing performance of healing agents with potential to be used in liquid form.

Service conditions	Healing agent	Expansion	Mechanism of reaction	Healing performance	Reference
Continuous water supply	Bacteria	yes	Microbiologically induced precipitation of calcite in the presence of yeast and nutrients	Healed width: 970 μm Permeability: 100%↓ Load regain: 80-100%↑	(Wang et al. 2012; Sierra-Beltran et al. 2014; Wang et al. 2014; Qian et al. 2015)
	Sodium silicate	no	React with calcium hydroxide in the presence of water to produce calcium silicate hydrate	Healed crack width: 400 μm Permeability: 90%↓ Load regain: 20-80%↑	(Formia et al. 2015; Kanellopoulos et al. 2015; Alghamri et al. 2016; Kanellopoulos et al. 2016; Giannaros et al. 2016; Formia et al. 2016)
	Colloidal silica	no	React with calcium hydroxide in the presence of water to produce calcium silicate hydrate	Healed crack width: 250 μm Permeability: 43%↓ Load regain: 17%↑	(Kanellopoulos et al. 2015; Tan et al. 2016)
Non continuous water supply	Epoxy	no	Polymerise when in contact with amines	Crack size:- Permeability: 12-46%↓ Load regain: -	(Yang et al. 2011; Dong et al. 2017; García Calvo et al. 2017)
	Polyurethane	yes	Polymerise when in contact with moisture	Crack size: - Permeability: 100%↓ Load regain: 35-80%↑	(Van Tittelboom et al. 2011; Van Tittelboom et al. 2012; Maes et al. 2014; Feiteira et al. 2016)

Once a healing agent is selected, its healing performance can be investigated via external intervention and/or autonomous healing. In early stage research, the material can be manually applied to the crack surface to investigate the healing process. However, to investigate a more autonomous healing mechanism, the material had to be encapsulated in vials/tubes to act as container of the healing (Van Tittelboom et al. 2011; Wang et al. 2012; Hilloulin et al. 2015; Formia et al. 2015; Kanellopoulos et al. 2015; Qureshi et al. 2016). The use of vials allows a simple route to prevent the healing agent from unwanted reaction prior damage. In addition, it also enables a simple, but time-consuming, encapsulation of reactive cores such as sodium silicate and polyurethanes. However, the tubes cannot be mixed with concrete mixer, thus they are placed nearby the rebar and this time-consuming step prevents large-scale applications (Van Tittelboom et al. 2014). Furthermore, it is important to consider the large amounts of healing agent provided using glass vials and manual application of the healing may not be comparable with the amount of material released from dispersed microcapsules. For example, using manual application of polyurethane pre-polymer resulted in a strength regain as high as 80% (Van Tittelboom et al. 2012). However, more recent studies with smaller vials indicated maximum of 35% load regain with polyurethane (Feiteira et al. 2016), and no study has been performed so far using microcapsules. Thus, to investigate a realistic autonomous self-healing, the material is encapsulated using the methods described in the following section.

2.3. Encapsulation process for capsule based self-healing

Encapsulation addresses the challenge of protecting the core material from undesired reactions, followed by delivery of the core material at precise time and place. The role of the capsules for cargo storage and targeted release is of considerable importance in many sectors such as agriculture (Trenkel 1997), food industry (Dias et al. 2015), drug delivery and cosmetics (Martins et al. 2014). Additionally, the use of encapsulated materials is a growing field, with applications for the capture of CO_2 from coal-fired power plants (Vericella et al. 2015) and catalysis (Nam et al. 2016). Although the use of microcapsules is a new concept for self-healing of cementitious materials, phase-change materials (Shannaq and Farid 2015) encapsulated for use in thermal insulation have been largely used in the construction industry (Boh et al. 2008). As the field of application of encapsulated material expands, new methods of encapsulation are also explored, particularly relevant for industrial applications (Andrade et al. 2015). Within the several processes of encapsulation available, properties of the core and the shell are important, as well as efficiency, costs, carbon footprint, final mechanical properties and scalability. For self-healing, the size of the capsules ranges between a few micrometres in diameter, named microcapsules, up to a few millimetres, called capsules. Thus, different techniques have been applied for producing macro- and

microcapsules, as shown in Figure 2.5. The following sections cover these different techniques, starting with macroencapsulation of solid cores through pan-coating, followed by the production of capsules (or vials) to retain liquid materials using co-extrusion. Then, the routes to produce microcapsules with liquid core are presented, where an emulsion is used as template to form a core-shell structure through coacervation, *in situ* polymerisation or sol-gel reactions.

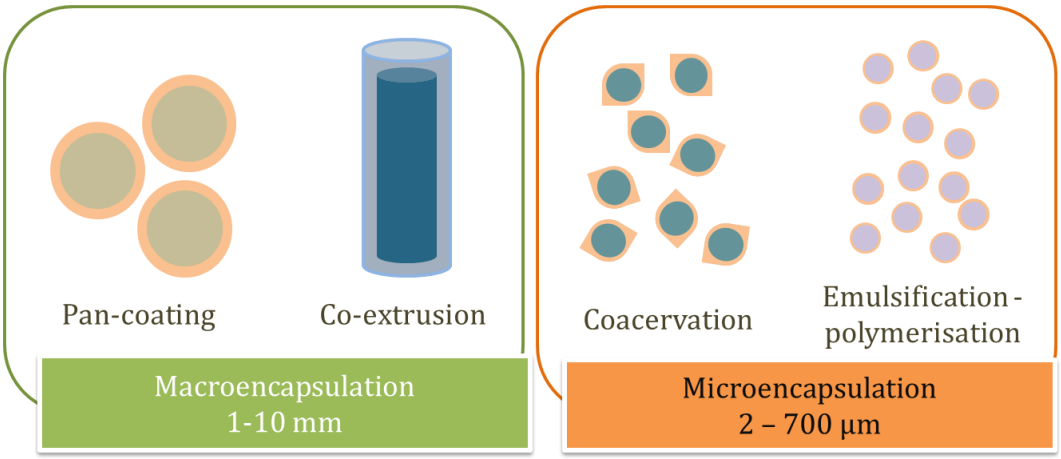

Figure 2.5 – Macro- and microencapsulation processes used for capsule-based self-healing of cementitious materials.

2.3.1. MACROENCAPSULATION METHODS

2.3.1.1. ENCAPSULATION OF SOLID CORES

The pan coating process is among the oldest industrial encapsulation processes for producing coated particles between 0.5 to 2 mm. During the process, the core material is in the form of pellets and the coating material is gradually sprayed on the pellets tumbling in the vessel, as shown Figure 2.6.

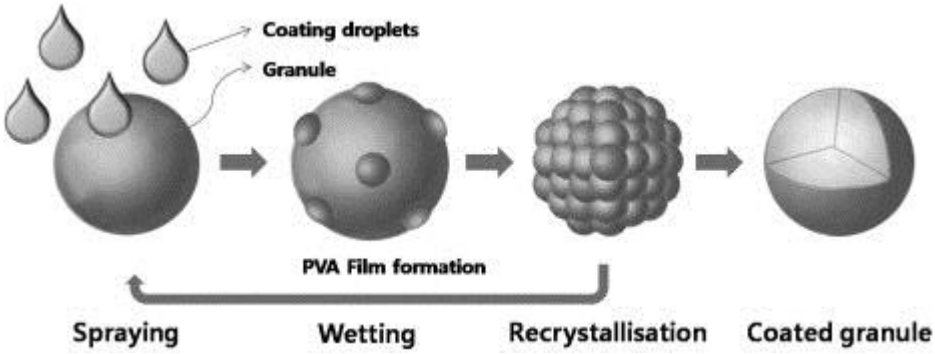

Figure 2.6 – Schematics of pan-coating process used to encapsulate pellets (Lee and Ryou 2014).

Thus, the development of the process has two crucial steps: firstly, the pelletisation, also known as granulation, where fine powder is agglomerated into pellets or granules. During this step, the powder undergoes moistening followed by consolidation and growth of the granules and then it is submitted to attrition and breakage, commonly in the granulator (Iveson et al. 2001). The second step aims at achieving a thin and uniform coating covering the pellets. This is attained by applying or spraying a coating solution on the pellets rotating in the pan while warm air is blown to hasten the drying. Alternatively, the material can be oven dried. This method has been scaled-up and is well-established in the pharmaceuticals' and food industry (sugar coatings) where preference is given to the coating of large solid particles (greater than 500 μm).

The technique has been used to produce capsules with solid cores to be used in the self-healing of cementitious materials, particularly focusing on the encapsulation of minerals. Poly(vinyl alcohol) (PVA) has been used as coating material to encapsulate calcium suphoaluminate (Lee and Ryou 2014; Lee and Ryou 2016) and lightweight aggregate impregnated with sodium silicate (Alghamri et al. 2016). The aqueous solution containing the dissolved PVA was sprayed onto the surface of the granules and the PVA shell was formed by evaporating the water. Alternatively, to minimise the hydration of the core material, non-aqueous based coating can also be used. Polylactic acid (PLA) was used to coat moisture sensitive cores such as calcium oxide-based expansive additives (Wang et al. 2016). Similarly, polystyrene (PS) resin and talc powder dissolved in chloroform were used to form a film around pellets of sodium monofluorophosphate (Na_2PO_3F) mixed with microcrystalline cellulose (Dong et al. 2014a; Dong et al. 2014b). The resultant capsules have a diameter between 400 μm and 1200 μm (Dong et al. 2014b), as shown in Figure 2.7. The method can also be used to produce shells to be chemically triggered, such as the CaO pellets encapsulated using a pH-sensitive ethyl cellulose shell (Wang et al. 2015). Furthermore, CO_2-sensitive shells were produced using a cement layer to cover expanded clay embedded with monofluorophosphate (Sisomphon et al. 2011).

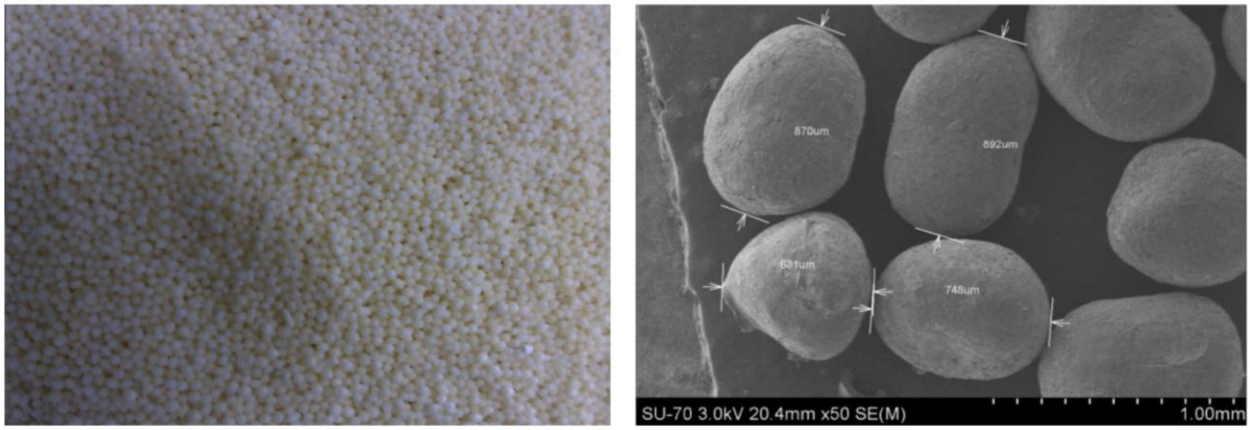

Figure 2.7 – Capsules containing Na_2PO_3F coated with polystyrene and talc. (left) Optical microscopy showing the macro-morphology and (right) micro-morphology of capsules (Dong et al. 2014a).

The use of coated pellets or impregnated materials for autonomic self-healing is attractive due to relative simplicity and low cost. However, minor limitations of the technique still need to be addressed, such as preventing the agglomeration of pellets during coating process and improving the homogeneity of the shell thickness.

2.3.1.2. ENCAPSULATION OF LIQUID CORES

In the co-extrusion, a dual fluid stream core and shell liquid material is pumped through a concentric tube, forming droplets in the nozzle by gravitational forces or vibration, as shown in Figure 2.8. Different co-extrusion technologies are used aiming to create smaller capsules, narrower size distribution or higher production rates, e.g., stationary nozzle, centrifugal nozzle, vibrating nozzle and submerged nozzle (Oxley 2012). Once the droplet is formed, the outer liquid is hardened into a shell via solidification of melted materials, gelation or precipitation. Natural or semisynthetic polymers such as alginates, gellan gum, chitosan, pectin and carboxymethyl cellulose have been widely used for the encapsulation of materials using this technique (Patil et al. 2012). The ionotropic gelation is particularly relevant for this method, and relies on the monomers crosslinking in the presence of dissolved ions, forming hydrogel. For the use in cementitious materials, the technique has been used for the production of encapsulated phase change materials (Liang et al. 2014), due to the reproducibility of the method, simplicity, speed and cost-effectiveness.

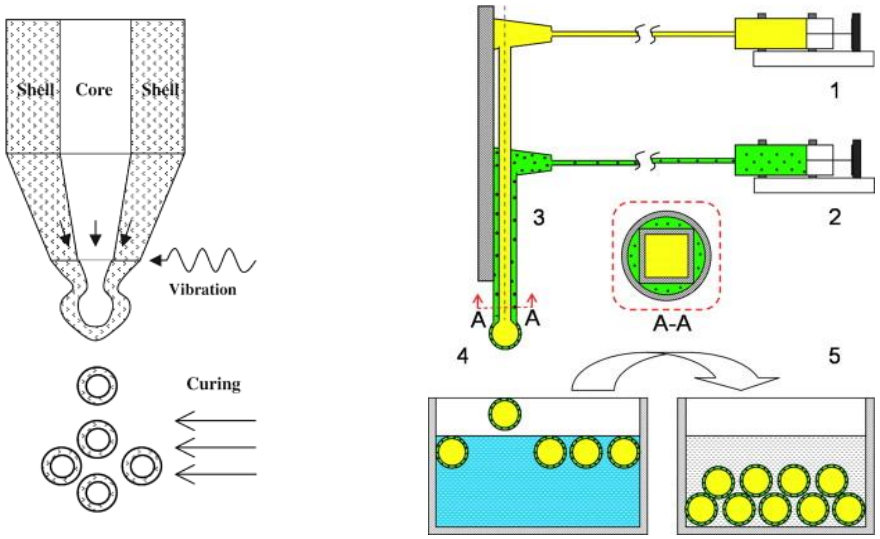

Figure 2.8 - Schematic presentation of the co-extrusion process (left) and apparatus used to produce Ca-alginate capsules (right). Adapted from (Ghosh 2006; Wang et al. 2011).

The technique provides a flexible route to produce beads, capsules and vials. This is achieved by controlling the extrusion of one of two fluids, and the breakage of the fluid which controls the length of the product. A single flow of alginate containing bacteria and mineral precursor compounds was used to produce calcium alginate beads of ~1000 μm (Palin et al. 2016). The method was also used to produce silver alginate beads ~2500 μm (Xiong et al. 2015), which can act as chloride sensitive shells. To produce polymeric tubes, three different polymers were investigated: poly(lactic acid) (PLA), polystyrene (PS) and poly(methyl methacrylate/n-butyl methacrylate) (P(MMA/n-BMA)) (Hilloulin et al. 2015). Using an extruder at temperatures above 120°C to assure the melting of the polymer, hollow tubes with length of 1 m were produced, and then cut into small ones, with 5 or 10 cm length. The outer diameter of PLA ranged between 1.9 and 5.2 mm, PMMA ranged between 6 and 6.8 mm and PS was 7.2 mm. The tubes were manually filled with the healing agent (polyurethane precursor) and the sides were sealed with MMA glue.

The flexibility of the method also enabled the production of cementitious hollow tubes, as shown in Figure 2.9. Two types of tubes were produced, with the external diameter of 5 mm and an internal opening of 2 mm (Figure 2.9a) and with a diameter of 10 mm and an internal opening of 7.5 mm (Figure 2.9b). To enhance the durability of both the core and the shell material, two layers of coating were applied: sodium silicate on the internal and external surfaces of the extruded elements, plus a more compact layer of polyester resin, applied only to the external surface. Then, the tubes were sealed with wax and an aqueous solution of sodium silicate as core material was added with a syringe. The tube kept the sodium silicate liquid for 4 weeks which demonstrates the waterproofing.

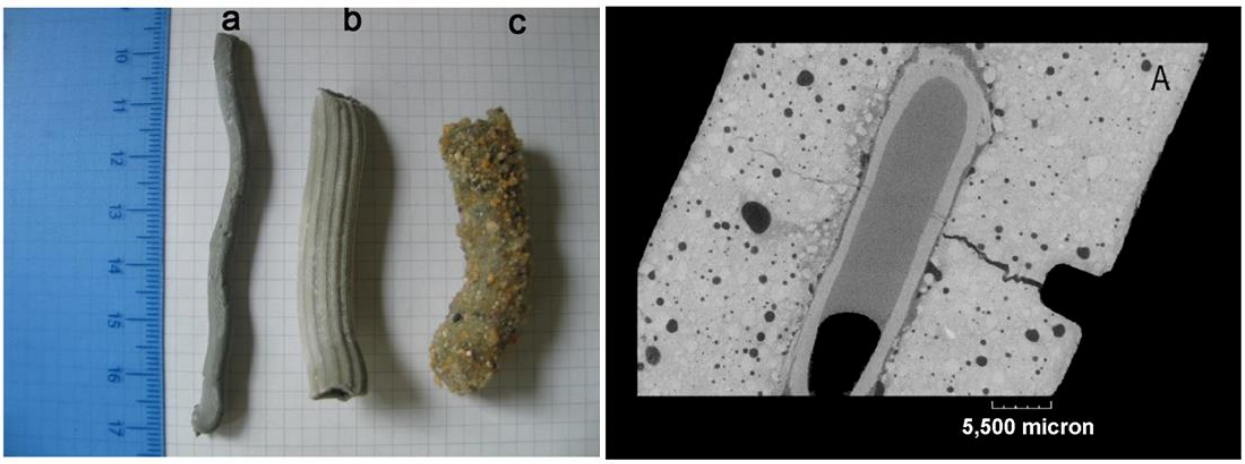

Figure 2.9 - Hollow tubes achieved by the extrusion of the cement paste (left) and XCT showing cracks crossing the cementitious matrix and the maccherone tube (right) (Formia et al. 2015; Formia et al. 2016).

Co-extrusion is still in the early development as a technique to produce capsules for self-healing. The production of alginate beads is promising, but its effect on mechanical properties still needs to be considered. Up to date, the co-extrusion has not been applied to produce spherical capsules for self-healing, although good results have been achieved from phase change materials. Despite the technique being useful to investigate different shell materials for cylindrical capsules, the time-consuming preparation and filling of the tubes is the main drawback of the technique (Van Tittelboom et al. 2016). Hence, a protocol to produce bulk quantities of capsules that can be easily added to the cement mix is still necessary.

2.3.2. Microencapsulation methods

Microencapsulation methods are typically used to produce core-shell structures containing a liquid healing agent. The microencapsulation of liquid cores is attained by producing an emulsion, followed by the formation of a solid shell around the droplets of the emulsion. Emulsions are made out of **two immiscible fluids**, one being dispersed in the other in the form of droplets, in the presence of **surface active agents**. The droplets are termed **dispersed phase**, while the liquid around the droplet is named **continuous phase**. Since the liquids are immiscible, their dissolution into each other is minimal; as a result the imbalance of attraction-repulsion forces in the surface of the liquid causes an interfacial tension. Alternatively, if they were miscible, they would dissolve into one another, to form a single phase, like the ethanol in water. Since the interfacial energy is much larger than the favourable entropic distribution, the emulsification process is not spontaneous. To **form an emulsion**, an energy input is needed such as vigorous stirring of an oil/water system. This approach leads to an emulsion with a broad size distribution, between few micrometres to 1000 μm. Alternatively, membranes have been investigated for the production of monodisperse emulsions, where the dispersed phase is forced through a membrane having a uniform size distribution (Leal-Calderon et al. 2007; Liu et al. 2011). To increase the stability of the emulsion, surface active substances, also known as **surfactants** are added. Surfactants are molecules or particles with amphiphilic properties, i.e., they contain one part that is hydrophobic (hates water) linked to another part that is hydrophilic (likes water). As a result, they are solvated in both the hydrophilic and hydrophobic phases of the emulsion, reducing the interfacial tension and preventing coalescence.

Once formed, the water-in-oil (w/o) or oil-in-water (o/w) emulsions act as a template where the shell is formed in the oil-water interface, encapsulating the dispersed phase. As a result, w/o emulsions are used to produce microcapsules with hydrophilic cores, while o/w emulsions are used to encapsulate hydrophobic cores. Four methodologies have been explored to microencapsulate active agents for self-healing of cementitious materials: coacervation, which is a

physical-chemical process; and *in situ* polymerisation, *in situ* interfacial polymerisation and sol-gel reactions, which are chemical processes. Table 2.2 presents the microcapsules for self-healing of cementitious materials produced via each methodology, along with the emulsion template, materials used as shell and core, diameter and shell thickness. Interrogation marks indicate lack of clarity in the description of the formed emulsion, and n.m. stands for not mentioned.

Table 2.2 – Reported methodologies to produce microcapsules with liquid core for self-healing of cementitious materials.

Method	Emulsion	Shell	Core	Shell size (µm)	Average size (µm)	Reference
Coacervation	o/w	gelatine/gum acacia	42% Sodium Silicate solution in 54% Mineral Oil and 4% Emulsifier	n.m.	290	(Kanellopoulos et al. 2016)
	o/w	gelatine/gum acacia	liquid sodium silicate solution dispersed in mineral oil	n.m.	500	(Giannaros et al. 2016)
	o/w	gelatine/gum acacia	liquid sodium silicate solution dispersed in mineral oil	5 - 20	200-700	(Kanellopoulos et al. 2017)
***in situ* polymerisation**	o/w	Poly(urea formaldehyde)	Epoxy resin in butyl glycidyl ether	4 – 8	166	(Wang et al. 2013)
	o/w	Poly(urea formaldehyde)	Epoxy resin in butyl glycidyl ether (ratio of 100:17.5)	n.m.	132 - 230	(Dong et al. 2016)
	o/w	Poly(urea formaldehyde)	Epoxy resin in butyl glycidyl ether (ratio of 100:17.5)	n.m.	132 - 230	(Dong et al. 2017)
	o/w	Melamine-based	Organic-based containing bacteria	n.m.	2 - 5	(Wang, Soens, et al. 2014)
	o/w	Poly(melamine urea-formaldehyde)	17.5 % wt of epoxy resin n-butyl glycidyl ether	1.1 - 2.4	10 – 100	(Li, Zhu, et al. 2016)
	o/w	poly(phenol-formaldehyde)	DCPD	n.m.	100 - 650	(Lv, Yang, et al. 2016)
	o/w	poly(phenol-formaldehyde	DCPD	8 - 45	25 - 500	(Lv, Schlangen, et al. 2016)
	w/o	Poly(urea formaldehyde)	aqueous calcium nitrate	0.6 - 1.3	45 - 110	(Hassan et al. 2016)

Method	Emulsion	Shell	Core	Shell size (µm)	Average size (µm)	Reference
***in situ* polymerisation (cont.)**	w/o	Poly(urea formaldehyde)	aqueous calcium nitrate	0.9	51	(Al-Ansari et al. 2017)
	w/o	Poly(urea formaldehyde)	aqueous calcium nitrate	n.m.	45 - 92	(Milla et al. 2016)
	w/o	Poly(urea formaldehyde)	aqueous calcium nitrate	n.m.	45 - 92	(Arce et al. 2017)
	o/w	Poly(urea formaldehyde)	DCPD	0.2	80 - 600	(Gilford III et al. 2014)
	w/w (??)	Poly(urea formaldehyde)	sodium silicate (?)	0.4-0.7	400 - 700	(Gilford III et al. 2014)
	o/w (??)	Poly(urethane/urea-formaldehyde)	sodium silicate liquid with toluene (?)	n.m.	n.m.	(Mostavi et al. 2015)
***in situ* interfacial polymerisation**	w/o	polyurea	Solid Sodium Silicate	n.m.	130	(Giannaros et al. 2016)
	w/o	poly(urea-urethane)	aqueous colloidal silica (50% w/w)	n.m.	60–120	(Tan et al. 2016)
	w/o	Polyurethane	Water (?)	n.m.	40-800	(Pelletier et al. 2011)
	w/o	Polyurethane	MMA	n.m.	0.3	(Litina et al. 2014)
Sol-gel	o/w	Silica	methyl- methacrylate & triethylborane	n.m.	4.15	(Yang et al. 2010)
	w/o	Silica	MMA	2	3.5	(Litina et al. 2014)
	o/w	Silica	Epoxy (Epothin®)	2	70	(Perez, Erkizia, et al. 2015)
	o/w	Silica	Epoxy (Epothin®)	n.m.	5 - 180	(Perez, Erkizia, et al. 2015)

The volume of produced emulsion is the key factor governing the amount of synthesised material. Conveniently, emulsification is a well-established industrial process, and lab protocols (usually in beakers smaller than 1L) can be scaled-up to batches of 80 L of emulsion (Benita 2006). The size of the microcapsules depends on the size of the droplets formed in the emulsion, which in turn depend on the properties of the emulsified liquids and the stirring rate. Although the properties of the liquids (e.g., viscosity, density and interfacial tension) may vary between different emulsions, it is typically observed that the size of the emulsion droplets decrease with the increase of the stirring rate. This is illustrated in Figure 2.10 where the size distribution of microcapsules produced through coacervation and emulsification polymerisation is related to agitation speed; with a broaded size distribution at low stirring rates, as observed at 400 rpm (Figure 2.10a,b). At 600 rpm, a mean diameter of 121 μm was achieved for PUF shells (Wang et al. 2017). However, the same speed rate used during coacervation would result in microcapsules with increased size, due to the differences in the liquids properties.

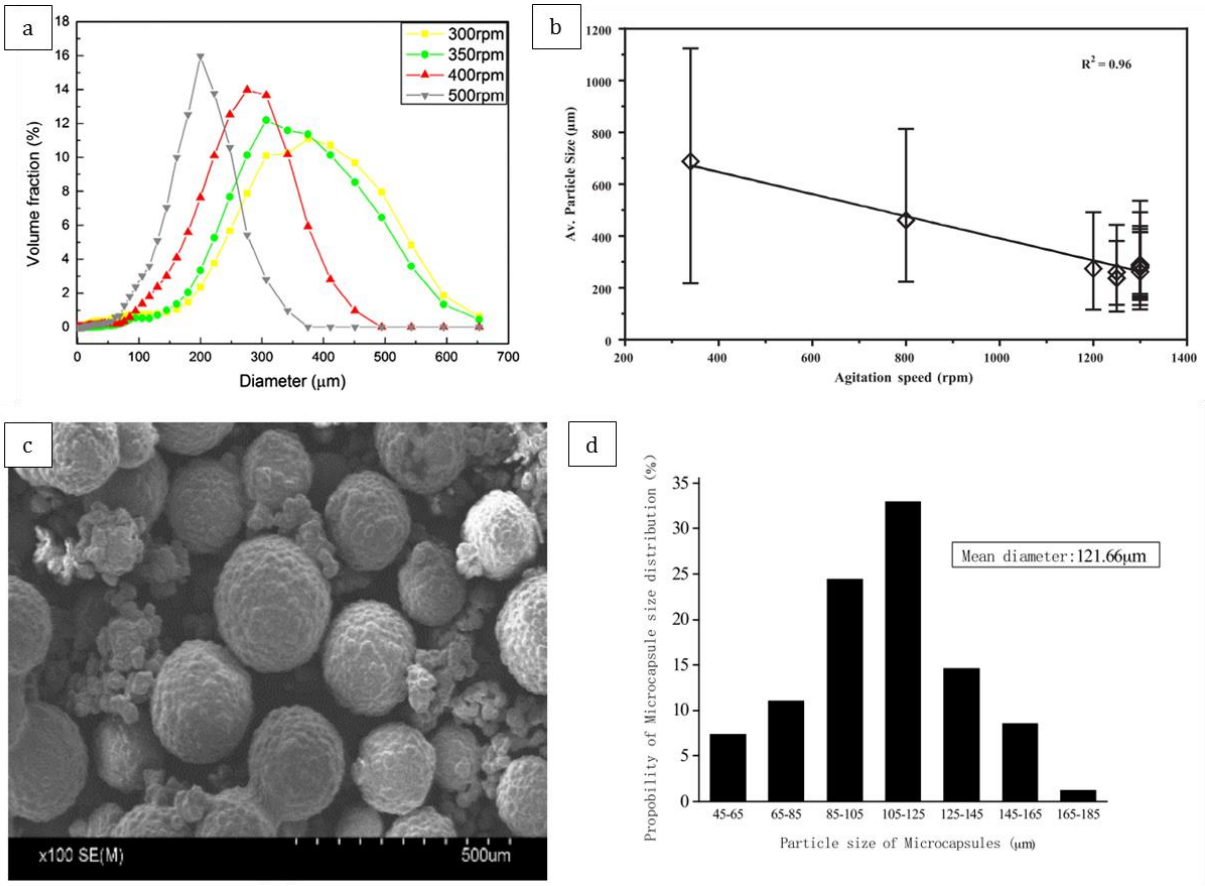

Figure 2.10 – Size distribution of microcapsules formed after emulsification. a) Size distribution of the poly(phenol-formaldehyde) microcapsules at various stirring rates (300, 350, 400 and 500 rpm) (Lv et al. 2016b); b) Average size of gelatine microcapsules with increasing agitation speed (Kanellopoulos et al. 2017); (c, d) Size distribution of polyurea formaldehyde (PUF) capsules produced at 600 rpm (Wang et al. 2017).

The following sections discuss the mechanism of shell formation for each methodology, as well as the limitations associated with reaction conditions.

2.3.2.1. COACERVATION

Coacervation is the process during which a macromolecular lump (coacervate) forms as a result of phase separation. In complex coacervation, the coacervate is formed when two oppositely charged polymers in aqueous solution interact forming a new polymer-rich phase. The formed coacervates gradually migrate to the interface of the droplets to form the microcapsule shell. Coacervation was recently proposed as a methodology for producing capsules for self-healing of cementitious materials (Kanellopoulos et al. 2016; Giannaros et al. 2016; Kanellopoulos et al. 2017). The method uses environmentally friendly materials and results in an organic based core encapsulated by a hydrophilic shell. The encapsulation consists of three stages (Ghosh 2006): (i) preparation of an oil-in-water emulsion, (ii) encapsulation of the core and (iii) stabilisation of encapsulated particles, as schematically illustrated in the Figure 2.11.

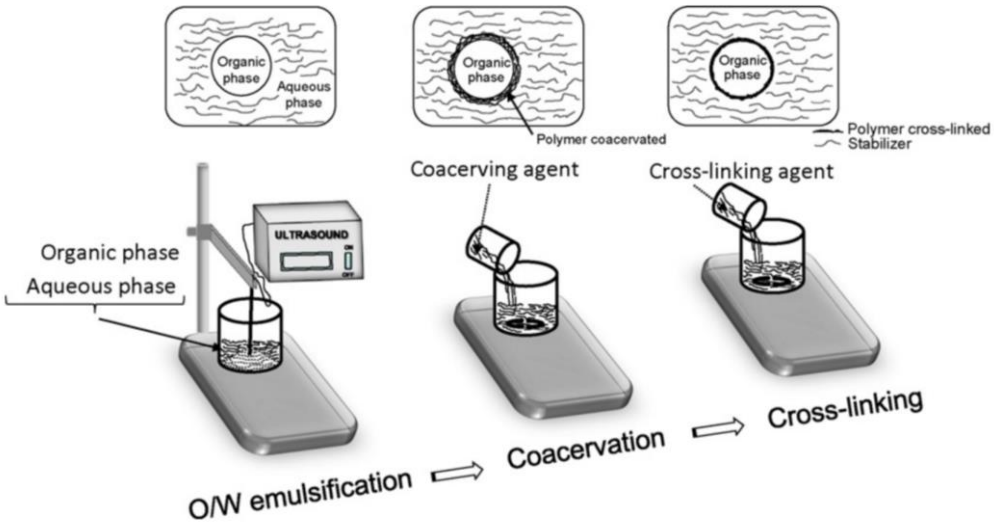

Figure 2.11 - Schematic representation of the preparation of capsules by the emulsion-coacervation method (Mora-Huertas et al. 2010).

Although there are several materials with potential to be used as shell, the most studied system is the complex coacervation of gelatine/gum acacia (Gouin 2004). In this system, an oil-in-water emulsion is produced with the gelatine and gum acacia (i.e., gum arabic) dissolved in the water phase at a 2-4 wt % of each polymer. Under agitation and at temperatures above 35°C, which is the gelation temperature of gelatine, the pH is adjusted from neutral to ~4, where the net charge between the gelatine and gum Arabic becomes equal (Zuidam and Shimoni 2010). The charge neutralization leads to the formation of hydrophilic polymer-rich phase (coacervates) which deposits on the emulsion surface because of interfacial adsorption (Heath 1981; Zuidam and

Shimoni 2010). The process is termed physico-chemical because the shell is formed upon cooling bellow 35°C, where the deposited gelatine solidifies and can be crosslinked by glutaraldehyde. Using complex coacervation, microcapsules with a diameter ranging between 10-800 μm can be achieved, with an outstanding payload of up to 90% (Zuidam and Shimoni 2010).

Since the process relies on an o/w emulsion, the encapsulation of hydrophilic cores is only possible through the emulsification in an organic phase. For example, the water-based sodium silicate solution was emulsified in mineral oil, resulting in an overall hydrophobic core which prevented the contact of the alkaline sodium silicate with the oil/water interface (Kanellopoulos et al. 2016; Giannaros et al. 2016; Kanellopoulos et al. 2017). As a result, a core-shell structure was formed, containing sodium silicate in mineral oil as core and gelatine as shell, as shown in Figure 2.12a. The diameter of the microcapsules ranged between 200-700 μm, and 5-20 μm of shell thickness. SEM-EDX analysis performed in ruptured microcapsules in mortar (Figure 2.12b) indicated the presence of sodium, thus confirming the encapsulation of sodium silicate.

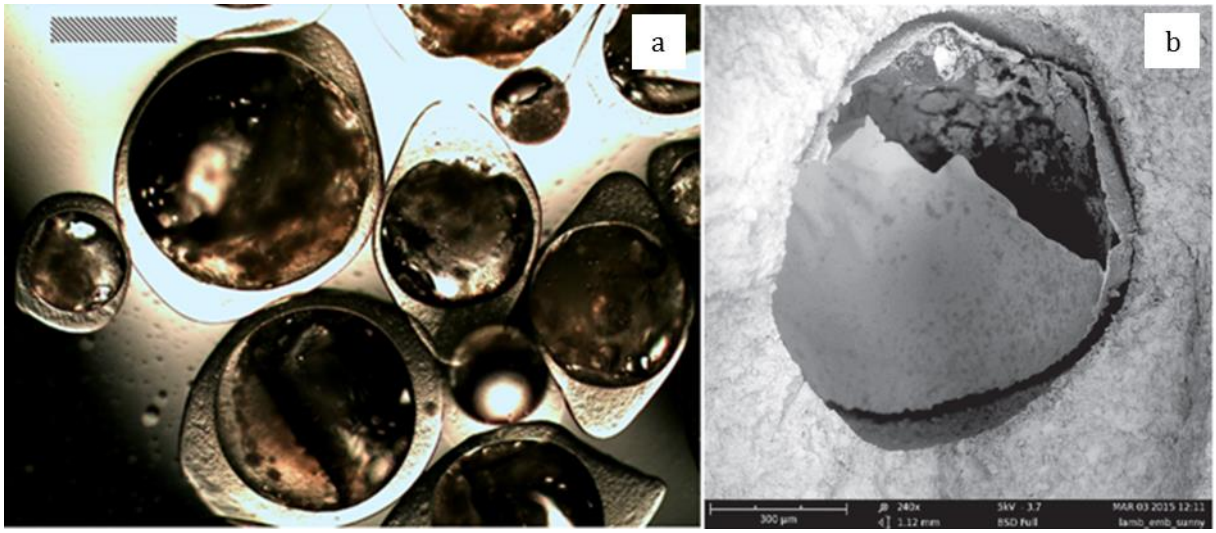

Figure 2.12 – Microcapsules produced through coacervation. (a) Optical microscopy of core-shell structure showing the retention of organic core (Kanellopoulos et al. 2017); (b) SEM of ruptured capsule in mortar (Giannaros et al. 2016).

2.3.2.1. *IN SITU* POLYMERISATION

Up to date, the most investigated methodology for the encapsulation of organic-core microcapsules for self-healing is the *in situ* polymerisation. In this case, the precursor of the shell material is dispersed in the continuous phase, and the shell is formed *in situ*, surrounding the droplets of the emulsion. The encapsulation is based on a well-known procedure in which the shell polymerisation is triggered by a slight increase in the temperature in acidic conditions (Brown et al. 2003). In this protocol, an oil-in-water emulsion was formed, containing dicyclopentadiene (DCPD) as dispersed phase to be encapsulated. The aqueous continuous phase contains urea, ammonium chloride and

resorcinol in a pH adjusted at 3.5. The formation of the shell was triggered by the addition of formaldehyde at 55°C and it was developed by stirring the emulsion for 4 hours. In these conditions, a high molecular weight water-insoluble prepolymer was formed and it deposited on the oil/water interface. Ultimately the shell became cross-linked poly(urea formaldehyde)(PUF) and encapsulated the core material (Brown et al. 2003; Jian-ping Wang et al. 2004; Fan et al. 2013). As a result, microcapsules with a diameter varying between 10-1000 μm were produced, and the shell ranged between 160-220 nm (Brown et al. 2003). Since then, several authors investigated the production of microcapsules to be used in cementitious materials with the PUF-based shell. To encapsulate epoxy, an adapted protocol was proposed where the oil-in-water emulsion was prepared containing urea and formaldehyde in the dispersed phase. By acidifying the solution to pH 2-3 at 60°C, the PUF shell was formed and the curing took place during 2 h of stirring (Wang et al. 2013; Dong et al. 2016; Dong et al. 2017).

Different formaldehyde-based shells can be formed by varying the monomers in the continuous phase. This enables the formation of shells via polycondensation. The addition of melamine in the dispersed phase, for example, resulted in the encapsulation of epoxy with poly(melamine urea-formaldehyde) shell (Li et al. 2016b). Interestingly, the amine present in the melamine shell can enable the addition of reactive functional group to provide covalent bonding within the concrete (Soens et al. 2014). Poly(phenol–formaldehyde) shells have also been investigated aiming at increased control over shell thickness, stiffness and brittleness (Lv et al. 2016b; Lv et al. 2016a). In this case, phenol and formaldehyde were added to the continuous phase and encapsulated DCPD. By adjusting the pH to 1, and keeping the solution stirring at 90°C for 3.5h, the shell was formed. The resultant microcapsules presented a diameter of 25-500 μm and a shell thickness of 8-45 μm.

Organic cores were not the only ones encapsulated using *in situ* polymerisation. Recently, an interesting adapted protocol was proposed to encapsulate water-based core material containing minerals (Hassan et al. 2016; Milla et al. 2016). In this case, hexane containing dodecylbenzenesulfonic acid was used as continuous phase and the acid was responsible for lowering the pH. The continuous phase was stirred at 40-50°C, while the aqueous solution containing calcium nitrate, resorcinol, urea, ammonium chloride, and formalin was added dropwise. The reaction time to form the shell varied between 1 to 3h, and resulted in the encapsulation of an aqueous solution of calcium nitrate. The conditions of the reaction slightly affect the dimensions of the microcapsules, which varied between 45 – 110 μm of diameter and 0.6-1.3 μm of shell thickness, as shown in Figure 2.13. The yield was reported to be higher than 95% - as a result, every batch of production results in more than 50 g of capsules.

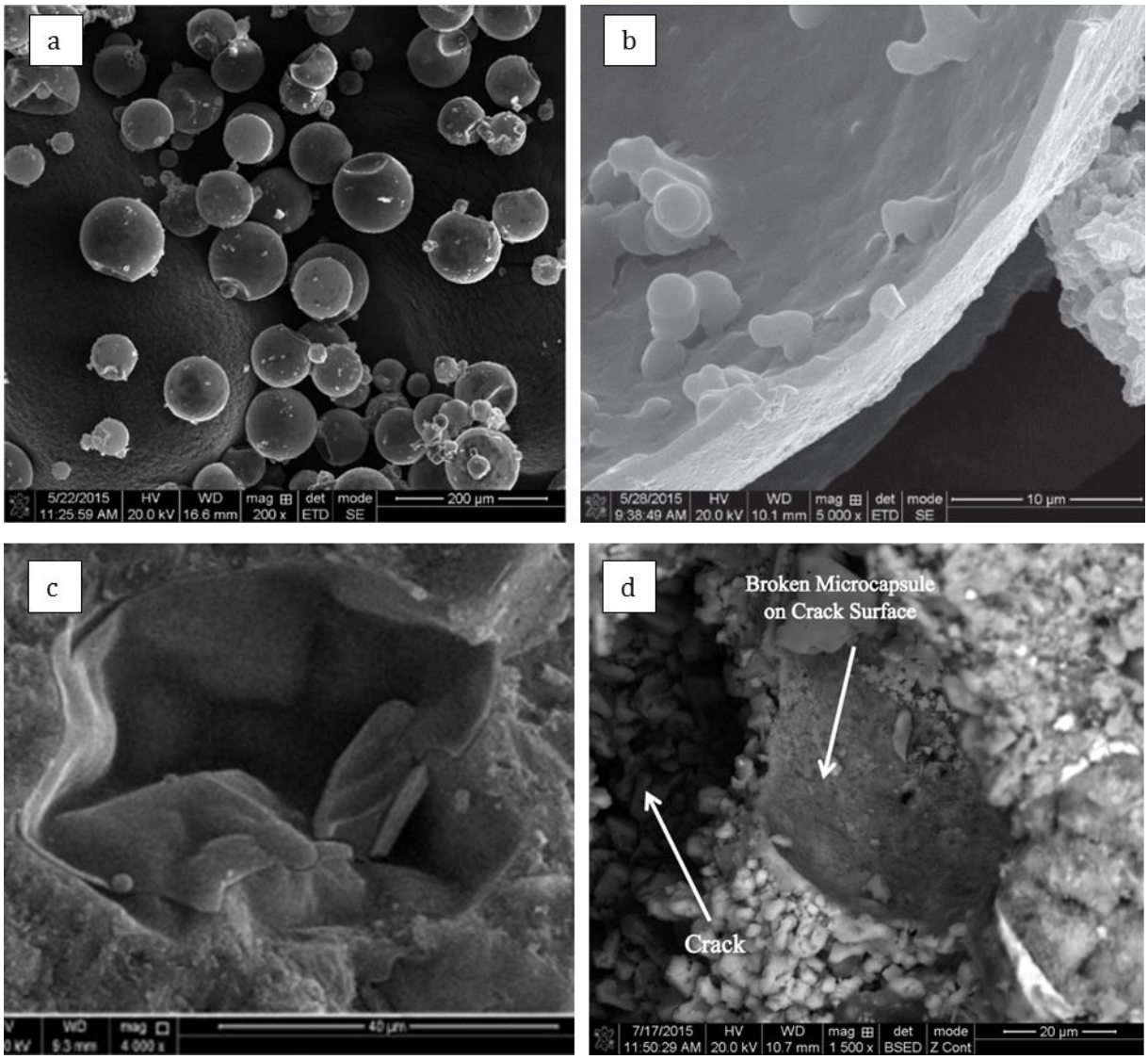

Figure 2.13 – SEM of microcapsules with calcium nitrate core and PUF shell. (a) microcapsules surface; (b) PUF shell; (c,d) ruptured microcapsule shell on mortar. Adapted from Ref. (Hassan et al. 2016; Al-Ansari et al. 2017; Arce et al. 2017).

Difficulties arise, however, when investigating the encapsulation of alkaline aqueous solution as it may prevent the acid triggered polymerisation of the shell. This is a severe limitation since typical water-based minerals with potential to be used for self-healing are dissolved in water and present high pH, such as colloidal silica (pH 9) and sodium silicate (pH 12.5) (Kanellopoulos et al. 2015). Considering this inherent constraint of the method, studies reporting the encapsulation of sodium silicate with PUF shell need to be critically examined. Gilford III et al. (2014) investigated the encapsulation of sodium silicate but did not define the composition of the emulsion. From the protocol, it is implied that the sodium silicate solution was emulsified in another aqueous phase containing the precursor of the PUF shell. However, they do not explain how the water-in-water emulsion was formed, how the sodium silicate behaved in an acidic solution and if the shell was

deposited. The lack of clarity was also noticed in the work of Mostavi et al (2015), where liquid sodium silicate with the polyurethane prepolymer was used as core and dispersed in an aqueous phase. Once more, the formation of the emulsion of water-in-water seems to be the goal and the authors did not explain how they prevent a simple dissolution of the core in the aqueous phase. Both studies would have been more relevant if the protocol was more clearly explained and the formation of the core-shell structure had been demonstrated.

2.3.2.1. *IN SITU* INTERFACIAL POLYMERISATION

In situ interfacial polymerisation offers a protocol less limited by pH to encapsulate hydrophilic cores with a urea-based shell. The protocol is based in the work of Saihi et al. (2006) and relies on the formation of a water-in-oil emulsion stabilized with Span 85 as surfactant. Followed by the addition of a diisocyanate monomer (diphenyl methylene diisocyanate) to the oil phase, the shell formation is triggered by a catalyst (dibutyl tin dilaureate) and the membrane developed by stirring the solution at 63 °C for 4 hours (Saihi et al. 2006). The shell is formed from the reaction between diisocyanate and water to form urea groups and from the reaction between diisocyanate and Span 85 to form urethane groups, as shown in Figure 2.14. The produced microcapsules presented an average diameter of 13.35 μm.

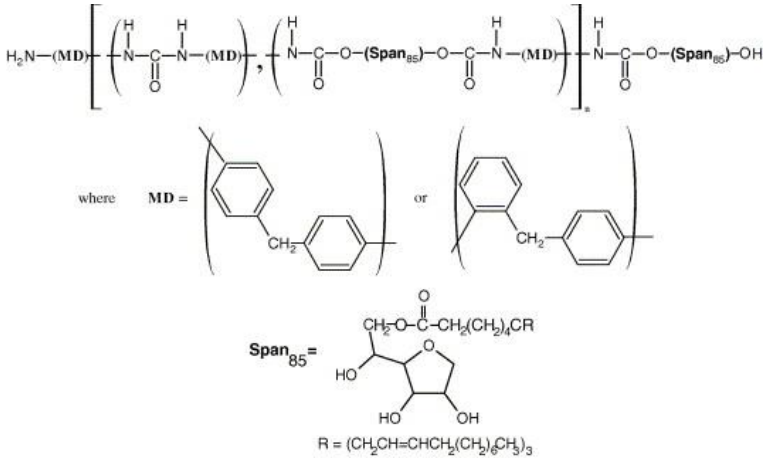

Figure 2.14 – Chemical structure of polyurethane shell according to Saihi et al. (2006).

This protocol was used to investigate the production of microcapsules for cementitious materials, containing aqueous sodium silicate (Pelletier et al. 2011) and methyl methacrylate (Litina et al. 2014) as core materials. Furthermore, the encapsulation of aqueous colloidal silica was investigated using poly(urea-urethane) (Tan et al. 2016), as shown in Figure 2.15. However, in the three above-mentioned studies, the authors did not demonstrate the formation of core-shell structure or investigated core-retention. Recently, Giannaros et al. (2016) investigated the performance of poly(urea) shells encapsulating sodium silicate, and the core-shell structure of the

microcapsule is shown in Figure 2.15d. Nonetheless, due to the highly acidic conditions encountered during production, the encapsulated sodium silicate polycondenses to a semi-crystalline state inside of the shell (Giannaros 2017).

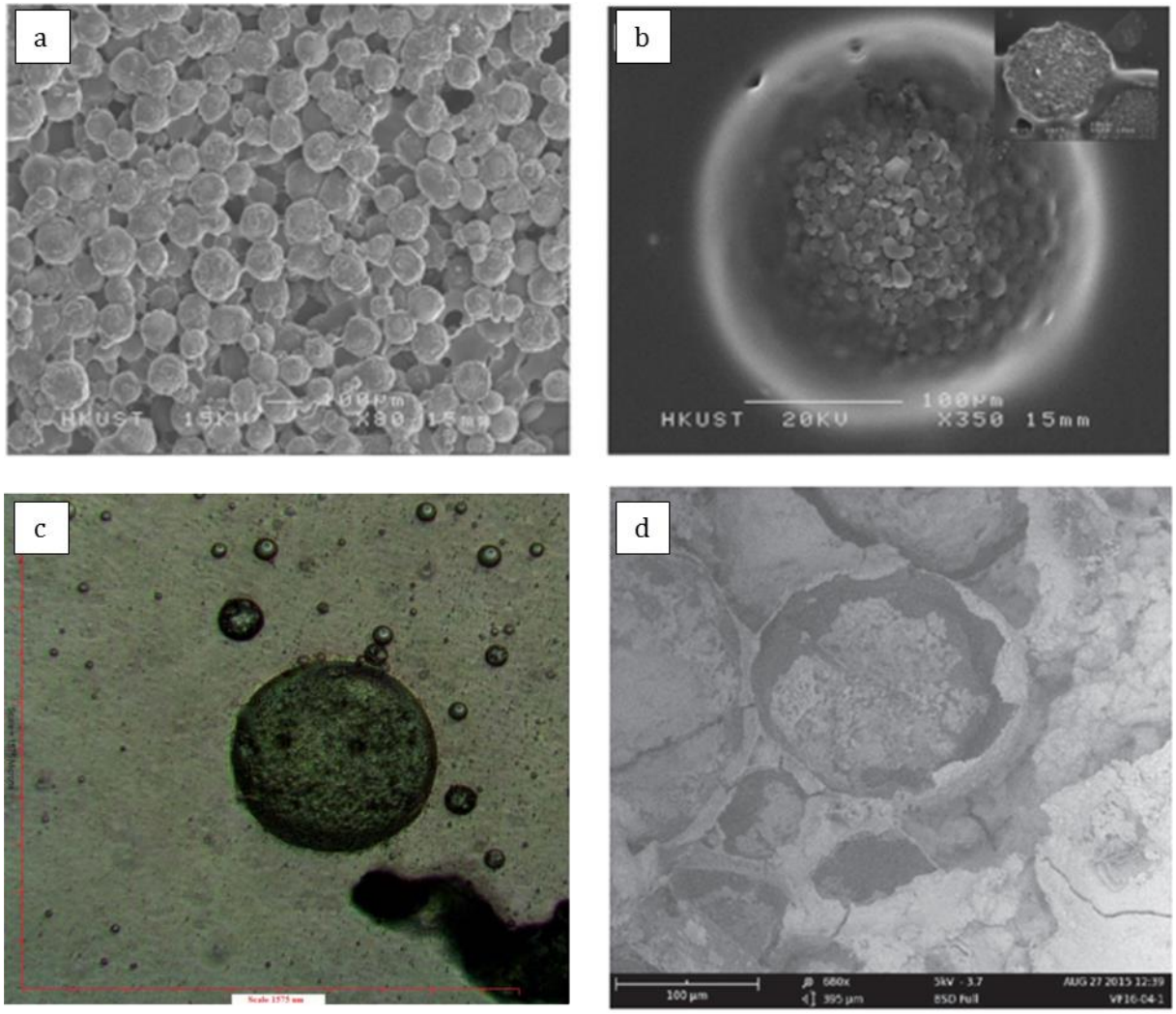

Figure 2.15 – Microcapsules with poly(urea-urethane) shells. (a,b) SEM of colloidal silica as core (Tan et al. 2016); (c) Optical microscopy of sodium silicate (Pelletier et al., 2001); (d) SEM of core-shell structure of capsule containing sodium silicate (Giannaros et al. 2016).

2.3.2.1. SOL-GEL

To produce microcapsules with organic core and silica shell the sol-gel process was used. The production of silica shell is suitable for self-healing, as the silica shell presents a better interfacial bonding with the cementitious materials compared with the other polymeric shells (Perez et al. 2015b). The process has been used to encapsulate epoxy using an oil-in-water emulsion, with a hydrolysed tetraethoxysilane (TEOS) dissolved in the dispersed phase. The shell formation is triggered by adding ammonium hydroxide solution (NH_4OH) until the pH was ~10. The suspension of microcapsules was left aging for an hour and yielded ~2 g. The resulting microcapsules with

diameter varying between 5 to 180 μm and a shell thickness of 2 μm are shown in Figure 2.16 (Perez et al. 2015a). A similar protocol also based in oil-in-water emulsion to synthesise a silica shell through hydrolysis and condensation of TEOS was put forward by (Yang et al. 2010). However, the work did not detail the dissolution of hydrophilic methylmethacrylate in hydrophobic hexane and no characterisation of core-shell formation or core retention was performed.

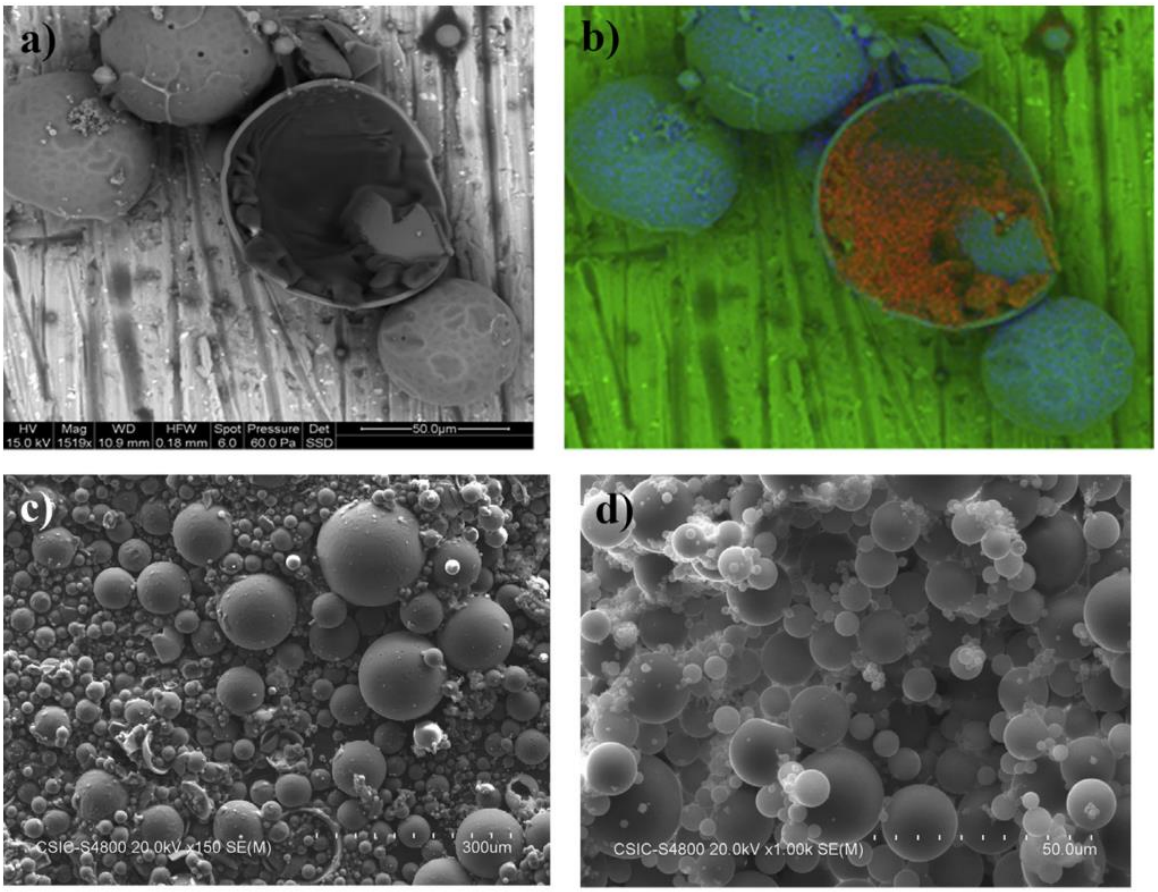

Figure 2.16 – Images of silica microcapsules containing an epoxy compound obtained by scanning electron microscopy (SEM) and elemental analysis by X-ray microanalysis. The red colour indicates the epoxy compounds (Perez et al. 2015a).

In summary, methods to produce macro and microcapsules have been successfully applied for encapsulation of healing agents for capsule-based self-healing. Furthermore, the production of capsules through pancoating or microcapsules via emulsification can be scaled-up to produce large quantities of material to be used in civil construction. Overall, the encapsulation method is chosen based on the size of the capsules and the nature of the core material: if the core is liquid or solid, hydrophobic or hydrophilic. And the encapsulation method determines the material used as shell and therefore the properties of the shell. As a result, the encapsulation method will also govern some of the key parameters for self-healing, as it will be discussed in next section.

2.4. Shell parameters for capsule-based self-healing

To achieve the best possible performance for self-healing, it is necessary to optimise the material, size and volume of added capsules. From the design point of view, it is very interesting to focus on survival during the integration process and triggering stimulus, as the self-healing cannot take place without it. In this scenario, the shell material is crucial as it is the interface between the healing agent and the cement matrix, protecting the core material during mixing and releasing it upon triggering. Thus, during the capsule design, fine-tuning the mechanical properties of the shell material is needed to ensure survival during mixing and release of core content upon external stimuli. Furthermore, the shell material also plays a fundamental role in the retention of the core material, maintaining it active inside of the capsule. Regarding the size and volume of capsules added for self-healing, optimisation is also required, particularly considering the effect on the overall mechanical properties of the cementitious matrix. Hence, the following sections cover these key parameters necessary to ensure integration survival, minimal effect on the matrix, triggering mechanism and core retention.

2.4.1. Mechanical properties

The greatest advantage of using capsule-based self-healing is the convenience of simply adding it during the mixing of the cementitious matrix. However, the capsules need to survive the strong alkalinity, the high shear during mixing and the temperatures ranging from 35 to 80°C during the cement hydration and setting processes. The survival in these conditions may be difficult. Glass capsules, for example, cannot resist concrete mixing due to their brittleness (Van Tittelboom et al. 2014). One possible way of improving the survival of the capsules is to increase the shell thickness, making the material more resistant during mixing. However, the increase in shell thickness would also decrease the payload of core material and may hinder the physical triggering.

Alternatively, the survival of the capsules can be improved by taking advantage of the inherent water sensitivity of some materials. Because of the wet conditions during mixing, the shell can react with water and change its behaviour. For example, the presence of water during the mixing enables the use of a shell material that has a soft and ‘rubbery’ behaviour when hydrated and a stiff and ‘glassy’ behaviour when dried. Gelatine shells are suitable for this approach and have been used to produce capsules via coacervation, encapsulating sodium silicate emulsion (Kanellopoulos et al. 2017). The mechanical transition is attributed to the presence of water trapped in the gelatin shell, increasing the compliance of the hydrated sample. As a result, the material is more likely to survive mixing and still rupture upon crack formation. The presence of water was also investigated to tune the brittleness of extruded ethyl cellulose tubes containing plasticizers. In this case, the tubes are

flexible during mixing, but as the plasticizer leaches out during mixing, it results in brittle shell for the mechanical triggering (Gruyaert et al. 2016).

Additionally, the tuning of mechanical properties of the shell has been investigated, focusing on producing a ductile shell capable of resisting mixing. Hilloulin et al. (2015) looked at the production of vials via co-extrusion made of polymeric materials with low glass transition temperature (T_g). Three polymers with different T_g were studied: Poly(lactic acid) (PLA) (Tg = 59 °C), Polystyrene (PS) (Tg = 102 °C) and Poly(methyl methacrylate/n-butyl methacrylate) (P(MMA/n-BMA)) (Tg = 59 °C). Heating the vials prior to mixing with other components shifted the mechanical properties from a brittle to a rubbery state, thus increasing the survival ratio (Hilloulin et al. 2015). In both cases of extruded tubes, the premature curing of the healing agent was noticed, preventing the healing process. Furthermore, the high tensile strength of the shell (e.g., PLA ~60 N/mm^2) combined with the thick shells may also prevent the breakage of the vial.

Although a more ductile shell material is desirable during mixing, stiff capsules are preferred after setting of the cementitious materials. This is because of the effect of microcapsules on the mechanical properties of the matrix and, consequently, on the feasibility of a capsule-based self-healing. The key parameters influencing the effect on the mechanical properties are the elastic properties, size and shell thickness of the microcapsules, as well as the volume fraction of added capsules. Typically, the microcapsules used for self-healing present values of Young's modulus around 3 GPa (Keller and Sottos 2006; Lee et al. 2012; Ghorbanzadeh Ahangari et al. 2014; Su et al. 2015; Lv et al. 2016a), which is 1/10 of the modulus of concrete (~25-38 GPa). As a result, the microcapsules have lower strength than the cementitious materials and they act as weak points during mechanical testing. As a general behaviour, the compressive strength of the cementitious material decreases when the volume of the microcapsules increases (Wang et al. 2013; Wang et al. 2014; Perez et al. 2015b; Kanellopoulos et al. 2016; Milla et al. 2016; Wang et al. 2017). However, a small amount of microcapsules have a negligible effect or even lead to a slight increase in strength (Wang et al. 2013; Kanellopoulos et al. 2016). Kanellopoulous et al. (2016) added microcapsules with pig gelatin shell (average size of 290 μm) to the mortar and measured the compressive strength and Young's modulus for different volume fraction of the microcapsules, as shown in Figure 2.17. The incorporation of up to 8% of volume fraction, V_f (1.6% by weight of cement, bwoc) had a negligible effect on compressive strength. However, the optimum self-healing performance was observed with 16 % V_f (3 % bwoc), which resulted in a 25% reduction in the compressive strength of mortar (Figure 2.17).

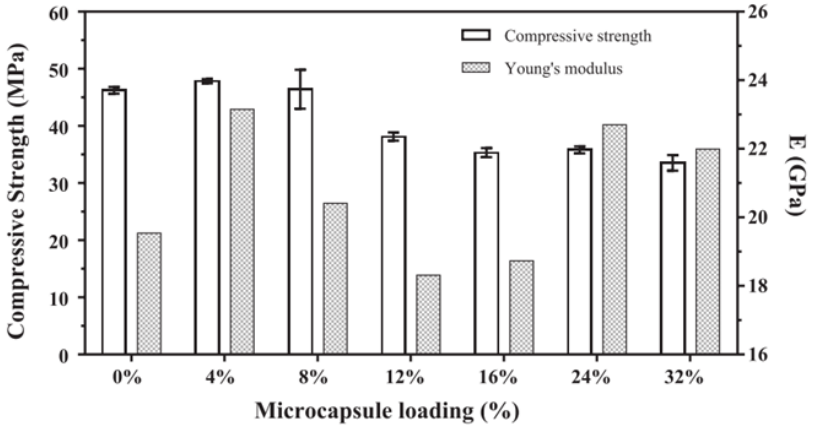

Figure 2.17 – Compressive strength and Young's modulus variation with increasing volume fraction of the microcapsules (Kanellopoulos et al. 2016).

The choice of capsule diameter and dosage is the result of a compromise: if the dosage is too large, a decrease in compressive strength of the matrix is likely to occur, limiting applicability; conversely, if the dosage is too low, the self-healing performance may be insufficient. However, estimating the amount of capsules needed to efficiently promote self-healing is a complex calculus, mainly because of the mechanism of healing where the material may or not expand. Thus, the volume of healing products needs to be taken into account, together with volume of the crack to heal, size and percentage of microcapsules. For example, an X-ray computed tomography of a matrix containing 5 % bwoc of microcapsules filled with epoxy showed that the cracks cannot be completely filled, and indicates the concentration of the capsules should be much higher (García Calvo et al. 2017). This is partially attributed to the non-expansive nature of epoxy, which cannot fill the entire crack. However, the addition of more microcapsules to promote the self-healing performance may compromise the compressive strength, limiting the applicability. For instance, Wang et al. (2014) restricted the addition of microcapsules to 3% bwoc to limit the decrease in compressive strength to ~30%. Theoretical analyses also reported the trend of a diminishing Young's modulus as the volumetric fraction of the microcapsules increases. In fact, the microcapsule content should be below 4 V_f % to ensure that at least 90% of the Young's modulus of the matrix is retained (Li et al. 2016a).

2.4.2. Triggering mechanism

Once the microcapsules survived mixing and affected minimally the overall mechanical properties of the matrix, the triggering of self-healing can be investigated. A wide array of external stimuli can be used to trigger the release of capsule materials (Esser-Kahn et al. 2011). For cementitious self-healing, they are grouped into chemical triggering, defined as a trigger that causes chemical

reactions with a shell wall material, and physical triggering, in which physical force is used to trigger the capsule rupture.

2.4.2.1. PHYSICAL TRIGGERING

The physical rupture of the capsules induced by cracking of the cementitious matrix is the most common external stimuli used to trigger the release of the healing agent. In this case, the stress concentrated at the crack tip is transferred to the wall of the capsule, leading to the rupture and release of the healing agent. The fracture of the microcapsules depends on the properties of the shell, namely, (i) elastic properties; (ii) fracture strength; (iii) fracture energy and (iv) interfacial properties (Ponnusami et al. 2015). Consequently, the shell properties may lead to capsule rupture, i.e., mechanical triggering, but also undesirable interfacial debonding or crack deflection may occur, as shown in Figure 2.18. In the latter two cases, the healing agent remains inside the capsule and prevents self-healing.

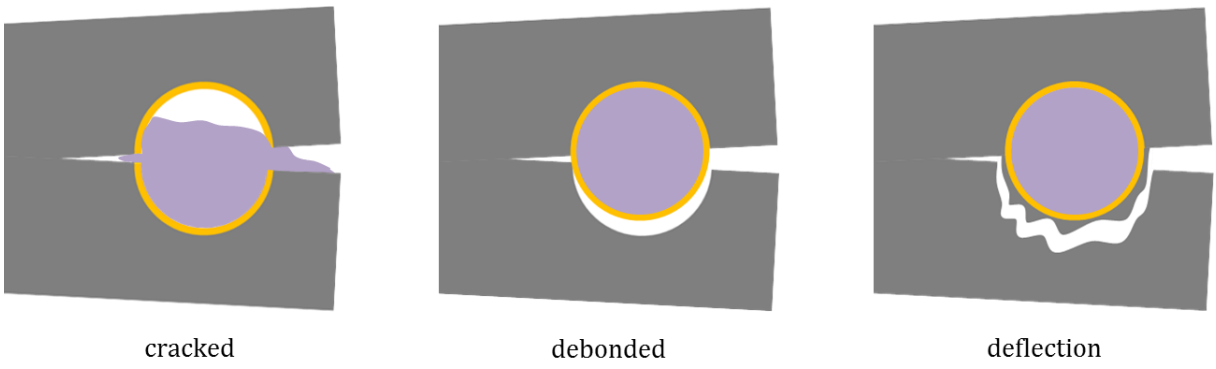

Figure 2.18 – Schematics of the three possible fracture mechanism of cementitious matrix containing microcapsules.

The mismatch between the elastic properties of the cementitious matrix and the microcapsules favours the capsule fracture, as the general trend is that fracture is more likely to occur in softer particles (Ponnusami et al. 2015). This is demonstrated in Figure 2.19(left); when the stress field is in the vicinity of the crack tip, a tendency of deflecting the crack away from stiffer inclusions can be observed ($E^* = E_{sphere}/E_{matrix} = 3$). Alternatively, the inclusion of a more compliant sphere ($E^*=1/3$) attracted the crack towards the inclusion, which is necessary for the rupture of the capsule and triggering of self-healing (Figure 2.19 right). As elastic modulus of microcapsules is ~ 1/10 of the modulus of concrete, the crack is attracted towards the microcapsules. In addition, according to numerical analyses, the elastic mismatch also plays a role in the minimum bonding strength required to prevent debonding (Gilabert et al. 2014). Thus, a capsule with Young's modulus of 5 GPa would have a 10-fold increase in the minimum bonding strength between the shell and the matrix when compared with a capsule with elastic modulus of 1 GPa.

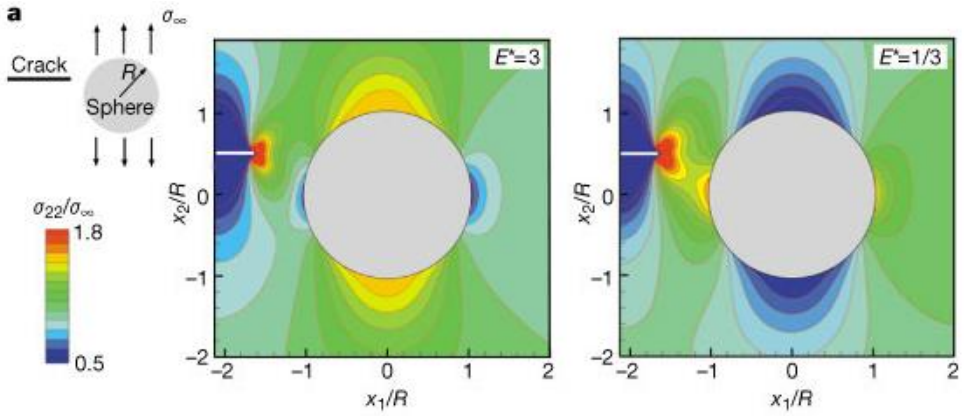

Figure 2.19 - Stress state in the vicinity of a crack as it approaches a spherical inclusion embedded in a matrix. The left and right figures correspond to an inclusion three times stiffer and three times more compliant, respectively. Adapted from Ref. (White et al. 2001).

Once the crack is attracted towards the capsule, interfacial debonding may occur instead of capsule rupture. In this case, the fracture mechanism is mainly determined by the tensile strength of the shell and the interfacial bonding between the shell and the matrix. The higher the tensile strength of the shell, the higher the interfacial bonding needs to be to prevent debonding. This is a limitation of using microcapsules, given the low tensile strength of concrete (2-6 MPa) when compared with polymers; for example, the urea-formaldehyde (PUF) shell has a tensile strength of 55 MPa (Gilabert et al. 2017a). The high tensile strength of the PUF shell may result in the capsules being pulled out during fracture without rupture, as shown in Figure 2.20a (Wang et al. 2013). When the high tensile strength is combined with an increase in shell thickness, it may preclude the physical triggering, as noticed for the PMF shells (Li et al. 2016b).

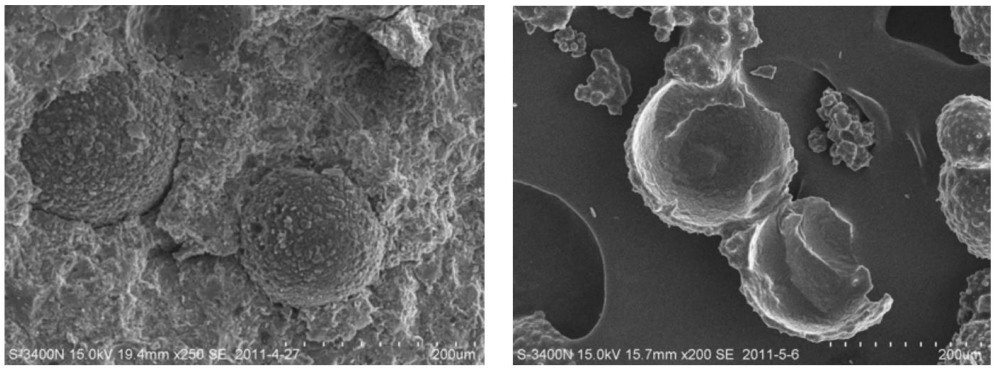

(a) (b)

Figure 2.20 – SEM images of PUF microcapsules embedded in the surface of mortar specimens showing (a) debonded and (b) ruptured microcapsules (Wang et al. 2013).

Thus, an increased interfacial bonding is necessary to prevent debonding of microcapsules. A good interfacial bonding between a polymeric material and the cementitious matrix is ensured by the

presence of hydrophilic groups, which are compatible with the water-based cement paste (Li et al. 2002; Peled et al. 2008; Pakravan et al. 2012; Halvaei et al. 2014). A similar example is the reduced wettability of hydrophobic fibres which results in a low chemical affinity with the cement matrix. This may lead to the formation of a gap between the fibre and the matrix (Pakravan et al. 2012), as observed in Figure 2.21a. On the other hand, when hydrophilic acrylic fibres are used, a chemical adhesion occurs and the fibre is surrounded entirely by compact cement matrix (Figure 2.21b). Thus, the functionalisation of hydrophobic polymeric fibres has been investigated to assure a good interfacial bonding (Hernández-Cruz et al. 2014). While the average bond strength between hydrophobic propylene fibres and cement is ~1 MPa, treated propylene fibres present values ~3MPa (Peled et al. 2008).

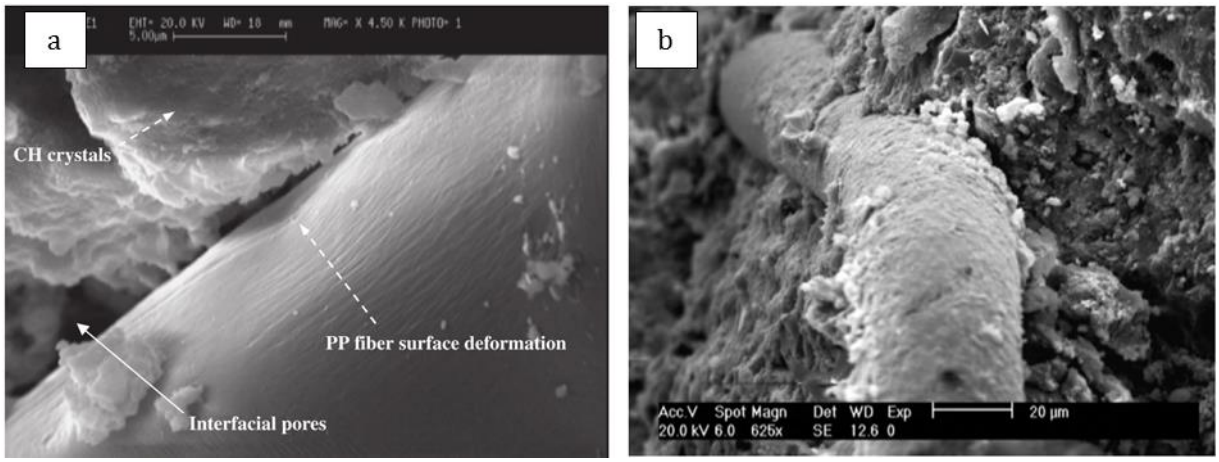

Figure 2.21 - SEM images of fibres in cement composite. a) hydrophobic polypropylene fibre and b) hydrophilic acrylic fibre. Adapted from (Pakravan et al. 2012).

However, as discussed earlier, the choice of encapsulation process can affect the shell surface and thus the interfacial bonding strength. Microcapsules produced using *in situ* and interfacial polymerisation may present poor interfacial bonding with the cementitious matrix and easily debond upon crack. This is because the *in situ* polymerisation relies in the formation of a water-insoluble prepolymer phase which deposits in the oil/water interface. The formation of PUF shell, for example, was attributed to the coalescence of a colloidal sol which precipitates when the molecular weight increases (lyophobic) (Brown et al. 2003; Jian-ping Wang et al. 2004; Fan et al. 2013). Furthermore, the use of nonpolar material such as melamine increases the hydrophobic nature of the shell surface (Tong et al. 2010). For the *in situ* interfacial polymerisation, when a non-polar group is used as surfactant, it will be added to the polymeric shell, resulting in nonpolar groups dangling from the backbone of the main chain (Saihi et al. 2006). Likewise, shell prepared with nonpolar phenol-formaldehyde groups presented poor interfacial bonding with the cement matrix and resulted in the debonding of the capsule during crack formation, instead of rupture (Lv

et al. 2016a). Using X-ray computed tomography (XCT), the rupture behaviour of phenol-formaldehyde microcapsules along the crack zone was investigated (Figure 2.22), where the microcapsules were mostly debonded. For large size microcapsules (400–600 μm) embedded in cement paste only 8 % of those microcapsules were triggered on the path of crack. With the decrease of diameter from large size to medium size (200–400 μm), the trigger ratio of microcapsules increased to 20% (Lv et al. 2016a).

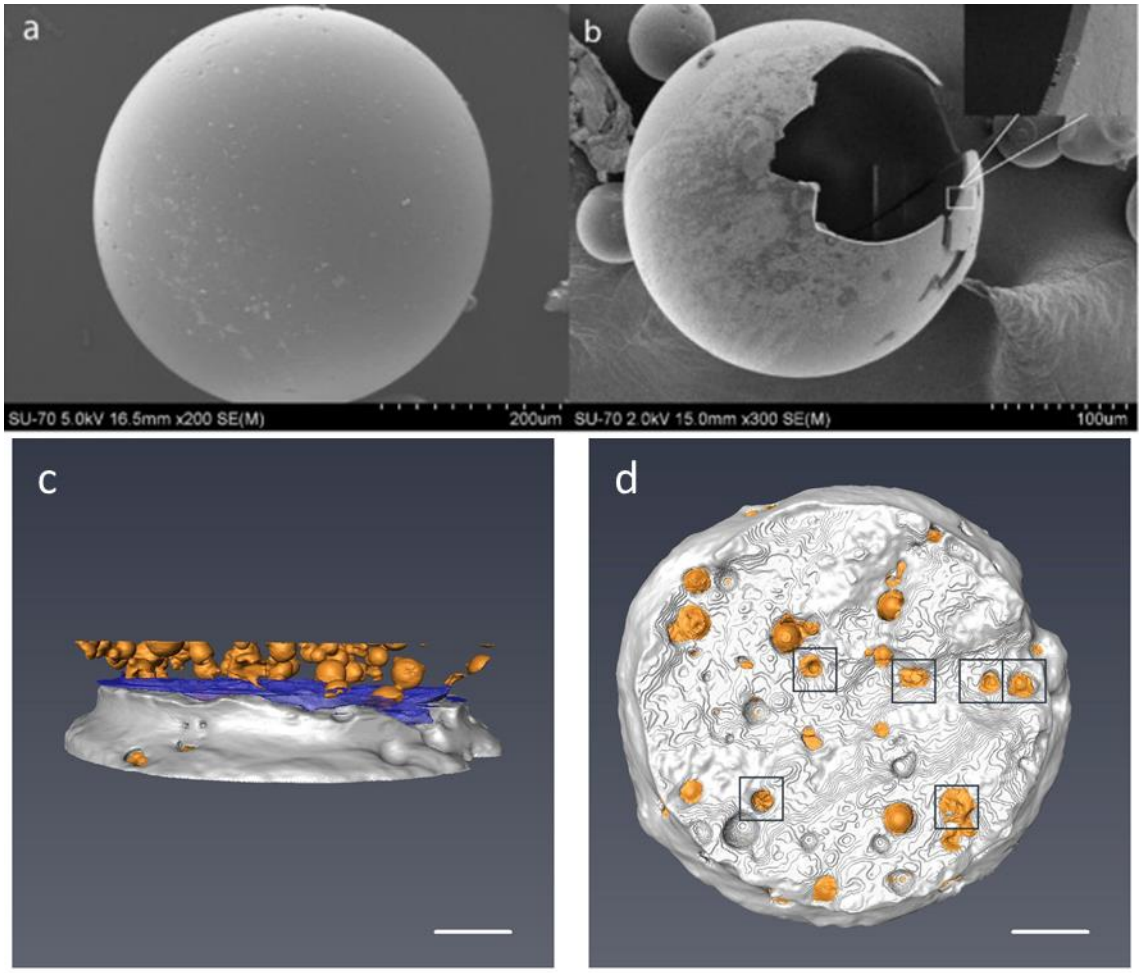

Figure 2.22 – Images of phenol-formaldehyde microcapsules. (a) surface morphology; (b) core-shell structure of a ruptured microcapsule; (c) 3D reconstructed images showing the crack (blue), microcapsules (yellow) and cement (grey); (d) a top-down view of crack surface, indicating the ruptured microcapsules with a black square box. The scale bar is 1 mm. Adapted from Ref. (Lv et al. 2016b) and (Lv et al. 2016a).

In summary, the interfacial bonding between the shell and the matrix relies on the chemical interaction, which is possible when hydrophilic groups are present in the shell. However, most of the *in situ* polymerisation techniques yield hydrophobic shell materials, as shown in Figure 2.23. Therefore, a poor interfacial bonding between these materials and the cementitious matrix is expected, and it may lead to debonding, precluding the physical triggering.

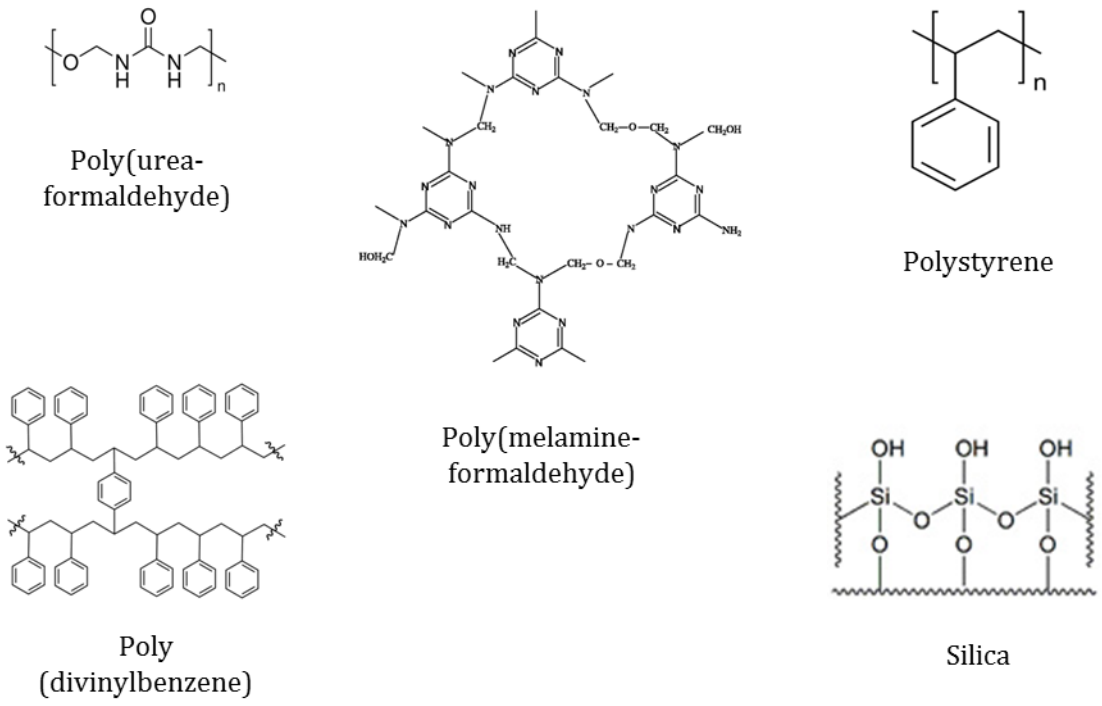

Figure 2.23 - Structure of main shell materials proposed for the fabrication of physically triggered microcapsules.

Alternatively, pan-coating, coacervation and sol-gel reactions offer alternative routes to the production of hydrophilic shell materials. The hydrophilic gelatine shell formed during coacervation resulted in a good interfacial bonding, favoured by the occurrence of cement hydration. This was confirmed by elemental analysis of the interface between the gelatine microcapsules, showing the presence of ettringite and calcium silicate hydrates (C-S-H) (Kanellopoulos et al. 2016). Similarly, EDX analysis suggested a chemical reaction between the silica capsules' shell with the matrix, resulting in a tight interface (Perez et al. 2015b). When a hydrophilic material as PVA is sprayed on the pellets to form the shell, the pan-coating will also result in hydrophilic shell material. And the average bond strength between PVA and the cementitious matrix can be as high as 4.4 MPa (Peled et al. 2008). Alternatively, the bonding strength of 1 MPa was determined for the glass-concrete interface (Gilabert et al. 2017b). Considering the tensile strength of concrete to be 3 MPa (Gilabert et al. 2017b), the interfacial bonding between the microcapsule shell and the concrete matrix should be around 3 N/mm^2 to favour physical triggering.

2.4.2.2. CHEMICAL TRIGGERING

The release of the encapsulated material can also be triggered by chemical changes in the matrix, which react with the shell and induce the disassembly of the capsule. An example of chemical change used for chemical triggering is caused by the ingress of water and aggressive compounds

due to the occurrence of crack. The ingress of chloride and carbon dioxide (CO_2) are special matter of concern since they are the two major collaborators for the corrosion of rebar. For instance, the diffusion of CO_2 leads to the consumption of $Ca(OH)_2$ and hence an overall decrease in the alkalinity, deactivating the oxide film layer in the rebar and facilitating the corrosion. Likewise, the ingress of chloride leads to an attack of the protective film on the reinforcement in alkaline concrete, subsequently giving place to the localised corrosion attack of rebar (Bertolini et al. 2013). Therefore, the development of shell sensitive to changes in pH, CO_2 or chloride concentration can increase the anticorrosion properties of self-healing concrete. For example, Xiong et al. (2015) proposed a capsule-based self-recovery system triggered by the chloride ions (Xiong et al. 2015). The shell is based on a silver alginate hydrogel, which collapses in the presence of chloride due to the precipitation of AgCl. The results indicate that the capsules were entirely collapsed at a very low concentration of chloride ions (0.1 % wt), as shown in Figure 2.24b,d. The capsules were produced with an average size of 2500 μm, which may indicate a significant effect on the mechanical properties of the matrix.

Since the changes in pH are directly associated with damage in the matrix, the tailoring of pH-sensitive shells requires special attention when considering the smart release material for the self-healing of concrete. Ethyl cellulose was proposed as shell material, since the material disintegrates in pH lower than 12 and releases the calcium hydroxide core thus increasing the pH (Wang et al. 2015). Dong et al. (2015) used polystyrene as shell material to encapsulated monofluorophosphate (Na_2FPO_3) and studied the release of the core material in different pH, using $Ca(OH)_2$ solutions to simulate concrete environment (Dong et al. 2014b). The swelling of polystyrene in the presence of water damages the shell, consequently releasing the core material, and this process depends on the thickness of the polymeric shell. However, for both ethyl cellulose and the polystyrene, the studies were performed using simulate concrete pore solution. Hence, the effectiveness of the process when immersed in the actual concrete still needs to be demonstrated.

CO_2-sensitive shells were developed by Sisomphon and coworkers (2011) using a cement layer to cover expanded clay embedded with monofluorophosphate. The mechanism of the triggering relies on the carbonation attack in the shell, increasing the porosity and subsequently allowing the permeability of the monofluorophosphate solution. As a consequence, the formation of denser and stronger apatite products, improve the microstructure of concrete, preventing further diffusion of CO_2.

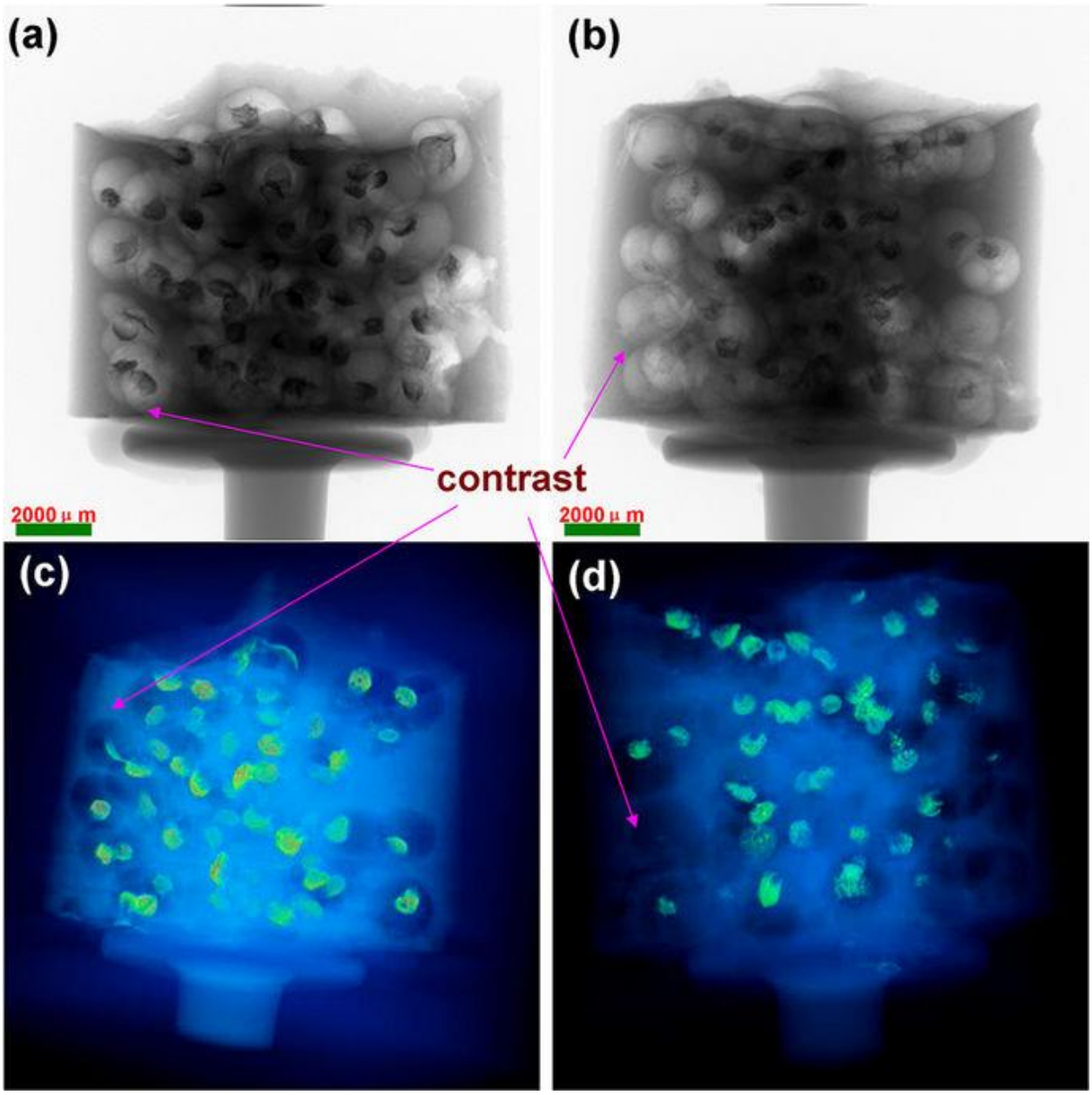

Figure 2.24 – X-ray CT of pH-sensitive shells in concrete (a,c) concrete specimen containing the shells; (b,d) concrete specimen soaked into NaCl solution(Xiong et al. 2015).

2.4.3. Permeability

The effectiveness of using microcapsules for storage of the healing agent and target release is essential for self-healing. Although several shell materials capable of potentially responding to chemical and physical triggering have been developed, the leakage of healing agent may prevent its use. However, the **permeability** of the shell to the core material is traditionally overshadowed by investigations in performance of self-healing. Thus, although the shell permeability to water is a well discussed topic in microfluidics, this topic is scarcely discussed during the encapsulation of cargos for self-healing of cementitious materials. For example, the encapsulation of sodium silicate

using emulsification polymerisation has been reported by Pelletier et al., (2011), Gilford III et al. (2014) and Mostavi et al. (2015). Typically, the sodium silicate solution is encapsulated by a solid shell formed in the droplet interface, as discussed in section 2.3. However, if the water was encapsulated inside the capsule, its retention was not discussed. Similarly, the encapsulation of silica sol has been also reported, but no characterisation of water retention was performed (Tan et al. 2016). The encapsulation of water for self-healing was investigated using paraffin wax as shell and co-extrusion as method of encapsulation (Janssen 2011). As a result, a core shell structure was formed, with diameter of 900 μm, shell thickness ranging between 110 and 190 μm. However, 60-90% of the water retained inside the microcapsule was lost after 6 days in a chamber with 90% of relative humidity. The paraffin shell was reported to buckle in the process while the water permeated through the shell.

Recently, the encapsulation of calcium nitrate in water by the urea-formaldehyde shell was also investigated, resulting in microcapsules ~40-110 μm of diameter and ~1 μm of shell thickness (Hassan et al. 2016; Milla et al. 2016; Al-Ansari et al. 2017; Arce et al. 2017). The core-shell structure of the microcapsule was observed in the SEM (Hassan et al. 2016; Arce et al. 2017), and it is shown in Figure 2.25.

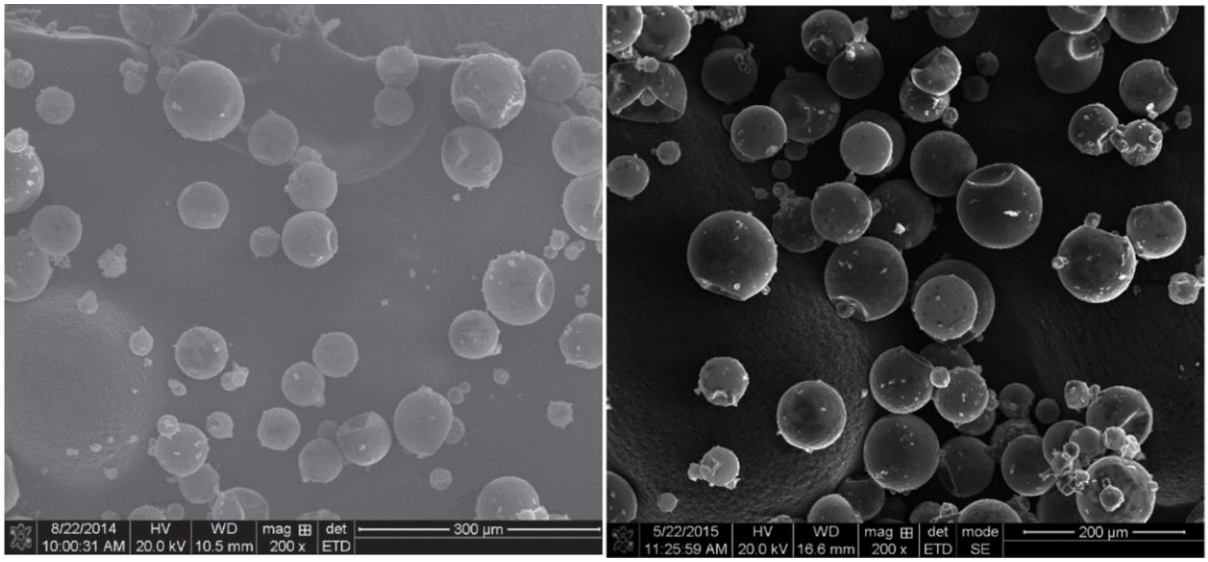

Figure 2.25 - SEM of buckled microcapsules with calcium nitrate core and PUF shell. Adapted from Ref. (Hassan et al. 2016; Al-Ansari et al. 2017; Arce et al. 2017).

Considering that the calcium nitrate solution was encapsulated, the indication of water loss is observed by the buckled shells Figure 2.25. Nonetheless, the authors did not report the water retention over time, and the effect of water loss on the microcapsules shape. Once the microcapsules are mixed with mortar and ruptured under crack, the surface of the shell is deformed (Figure 2.13c), indicating the material could have been buckled during the drying.

Alternatively, the encapsulation of cargo material with low vapour pressure may preclude the cargo leakage. This has been performed for the encapsulation of emulsified sodium silicate (Kanellopoulos et al. 2016; Kanellopoulos et al. 2017), bacteria (Wang et al. 2014), and healing agents such as epoxy (Perez et al. 2015b; Perez et al. 2015a) and DCPD (Lv et al. 2016b; Lv et al. 2016a). Giannaros et al. (2016) visually observed the release of oil core after rupture of the shell, indicating retention and triggered release of the core material, as observed in Figure 2.26.

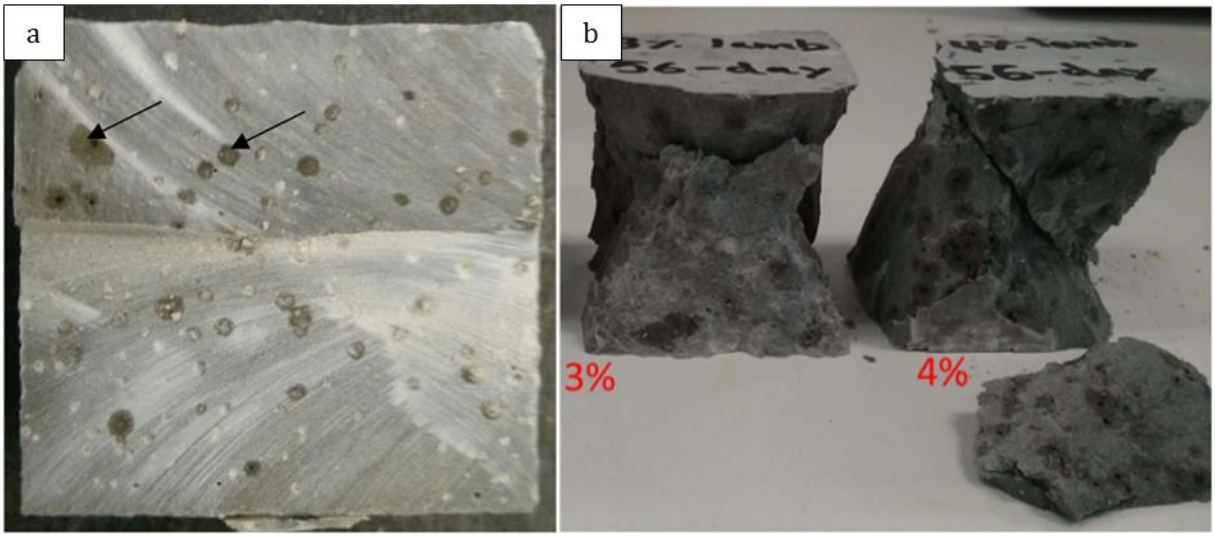

Figure 2.26 – Release of liquid cargo material comprised of sodium silicate in mineral oil. a) cross section of hardened cement paste; b) crushed cement cubes containing 3–4% V_f of microcapsules after 56 days. Adapted from Giannaros et al., 2016.

The permeability of the shell is also associated with stability of cores that are moisture and air sensitive. For example, the encapsulation of polyurethane prepolymer in extruded tubes resulted in the early hardening of the polymer within 10 days (Hilloulin et al. 2015). This was attributed to the permeability of the studied polymeric capsules or a possible reaction between the pre-polymer and the capsule. A longer shelf-life of polyurethane prepolymer was observed in microcapsules after 6 months storage at ambient temperature where 9 wt % reduction in core material was observed (Yang et al. 2008). However, when the microcapsules containing polyurethane prepolymer were immersed in water, the core reduced steadily due to the reaction with diffused water, and after 48 h the entire core was solidified (Huang and Yang 2011), as shown in Figure 2.27.

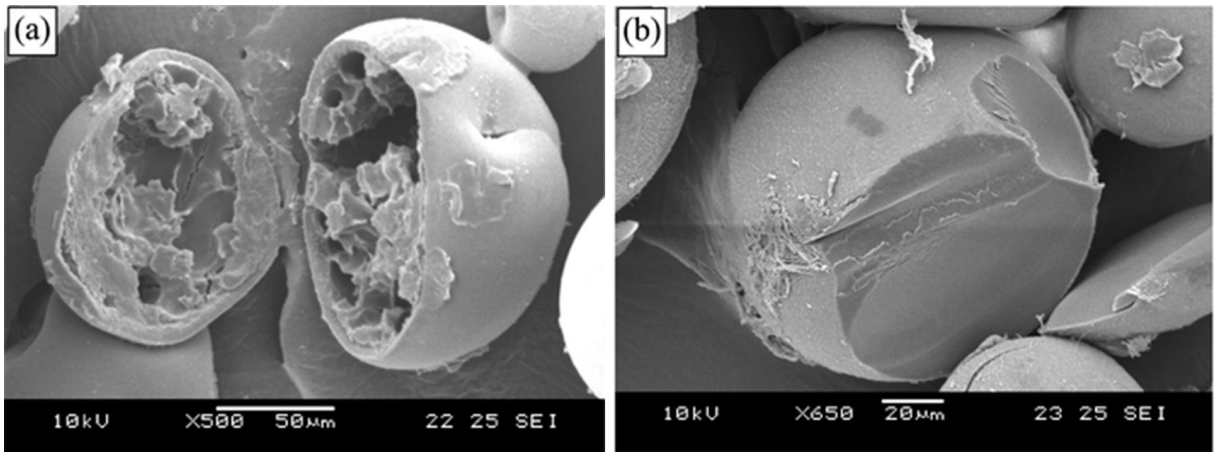

Figure 2.27 - SEM images of microcapsules with polyurethane shell containing moisture sensitive core after (a) 24 h and (b) 48 h immersion in aqueous solution (Huang and Yang 2011).

2.5. Design of microcapsules using microfluidics

The techniques used to produce microcapsules containing liquid core, such as coacervation, *in situ* polymerisation, *in situ* interfacial polymerisation and sol-gel reactions, rely on the formation of the emulsion template for the production of core-shell structures. These emulsions are made by dispersing droplets of the core phase in the dispersed phase are typically highly polydisperse, resulting in microcapsule with varied size and shell thickness. The variations in size and shell thickness prevent a systematic investigation of the influence of these parameters in the survival during mixing, effect on overall mechanical properties of the matrix and mechanical triggering. Furthermore, *in situ* polymerisation typically results in hydrophobic shells, favouring the debonding of the microcapsules, instead of rupturing, and thus preventing self-healing.

Microfluidics, on the other hand, use microchannels to manipulate small amounts of fluids, resulting in a controlled environment for the production of monodisperse emulsions. One area of particular interest is the generation of multiple emulsions systems, such as the double emulsion comprised of droplets inside another droplet. This double emulsion system can be used as template for the formation of the microcapsules, where the inner droplets stand as cargo material and the outer droplet can be solidified, generating the shell. Consequently, the diameter and shell thickness of the microcapsules produced using microfluidics can be precisely controlled, resulting in narrow size distribution, high cargo loading efficiency and a wide range of combination of shell and core material. Thus, the use of microfluidic devices to produce microcapsules stand as a very promising technology, still unexplored for the production of microcapsules for the self-healing of cementitious materials. The following sections explore the use of microfluidics to produce emulsions, the mechanisms of polymerisation to form the microcapsules. Furthermore, a brief description of

different designs of core-shell material is explored, particularly focusing on mechanical properties, permeability and triggering mechanism, since they are essential for self-healing.

2.5.1. MICROFLUIDIC PRODUCTION OF DOUBLE EMULSION

Microfluidic devices involve the flow of fluids in channels with typical dimensions of hundreds of micrometers; at such small length scales the inertial forces are virtually negligible and the interactions are based mainly on the viscous forces. This leads to predictable, reproducible and controllable flow regimes that can be used with great advantage to manipulate materials for practical applications or studying natural phenomena. The three most common geometries for microfluidics devices to produce droplets are the coaxial, flow-focusing and T-junction designs, illustrated in Figure 2.28.

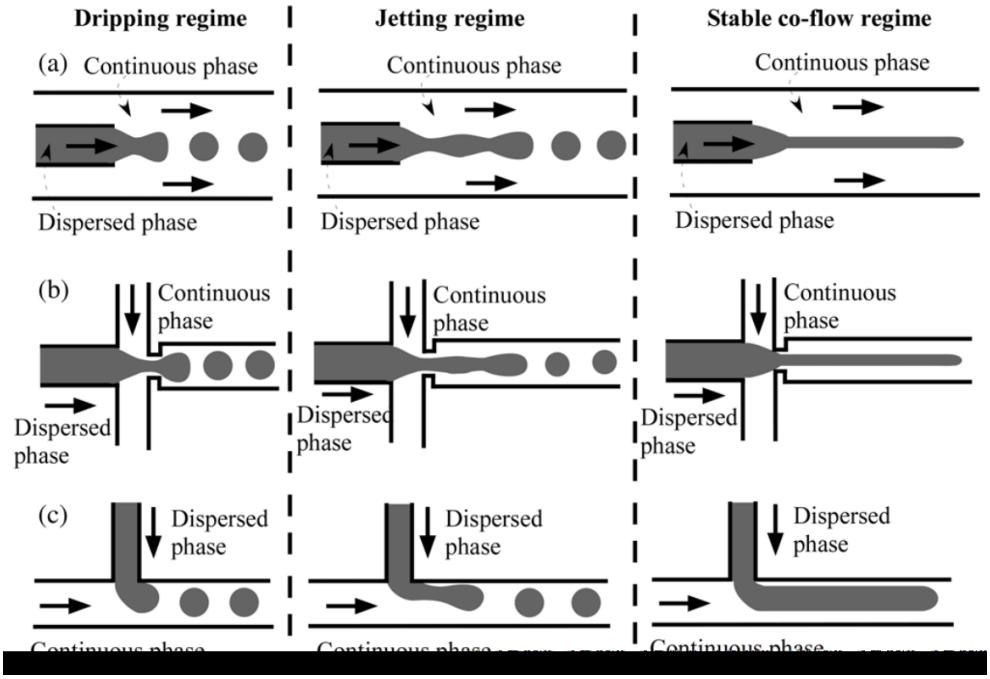

Figure 2.28 - Schematic of different flow regimes in (a) coaxial, (b) flow-focusing and (c) T-junction microfluidic devices (Nunes et al. 2013).

In the coaxial geometry, also referred as co-flow, the inner dispersed phase fluid is driven in the same direction as the outer continuous phase fluid, inside concentric channels. The capillary device is the most used device with the coaxial geometry and it is comprised of two tapered cylindrical capillaries inserted into the opposite ends of a square capillary (Utada et al. 2005). Alternatively, soft lithography is typically used for the production of devices to be used in the flow-focusing (Anna et al. 2003) and T-junction devices (Okushima et al. 2004). The flow-focusing geometry is comprised of the dispersed phase flowing through the central channel with the continuous phase flowing in two parallel side channels, as shown in Figure 2.28b. When the fluids meet at the cross-

junction, droplets or jets are formed and carried to the main collector channel. T-junction devices typically have the continuous phase flowing through a straight main channel, with the dispersed phase entering the main channel through a cross flowing side channel (Figure 2.28c). The size of the droplets formed in each device depends on several factors such as the flowing regimes, viscosities, interfacial tension, and dimensions of the devices. To make the production less dependent on the liquid properties, a new device has been proposed which used a triangular nozzle with its cross-section gradually increasing until it reaches a step where the channel height abruptly changes (Amstad et al. 2016). The goal of this device is to present parallelised channels to increase the throughput and a robust set-up, making the droplet size dependent solely on the geometry of the device.

Droplets are formed when the disperse fluid breaks in the dripping or jetting regime, depending on the individual fluids' flow rates, as shown in Figure 2.28; on the other hand, the stable co-flow regime can be used for the production of microfibers and microtubes (Choi et al. 2011). Different mechanisms have been proposed to explain the droplets formation, varying mainly device's geometry and the flow regime. In a T-junction, fluids typically meet at an angle of 90°, and droplet formation arises from the pressure drop in the continuous phase and squeezing of the dispersible phase (Silva et al. 2016). Regarding the co-flowing and flow-focusing geometries, in the dripping regime the droplet experiences two competing forces: (i) the viscous drag pulling it downstream and (ii) forces due to surface tension holding it to the tip. The balance between the two forces is given by the capillary number, $Ca = \eta\nu/\gamma$, which is a function of the viscosity (η), flow speed (ν) and interfacial tension (γ). The critical capillary number (Ca_c), which sets the crossover between capillary and viscosity-dominated flows for the flow-focusing device, is around 10^{-1}.

Figure 2.29 shows the transition between the dripping jetting and co-flow regime according to the capillary number of the dispersed phase (Ca_1) and the continuous phase (Ca_2). When Ca_2 is roughly between 10^{-2} and 10^{-1} and Ca_1 is around 1, a stable co-flow is observed. This is illustrated in Figure 2.29a, where the dispersed phase is focused and encapsulated by the continuous phase. By decreasing Ca_2 and Ca_1, the jetting regime is formed where the thread breaks up into an array of droplets due to the Rayleigh instability (Figure 2.29b). When the Ca_1 decreases even further and it is smaller than 10^{-1}, the dripping regime is achieved where the droplets are formed in the tip, as demonstrated in Figure 2.29c. This diagram illustrates the importance of the two fluids' properties when the regime is being established; by tuning the flow rate, interfacial tension and viscosity of the continuous and the dispersed phase, different regimes are achieved and thus, different droplet sizes. For example, variation in the flow rate will result in different capillary number and, consequently, different flow regimes. Interestingly, the formation of droplets is preferred in the

dripping regime, where the droplets are more uniform; however, the jetting regime is commonly formed by the increase of the flow rate and consequently, increases the output.

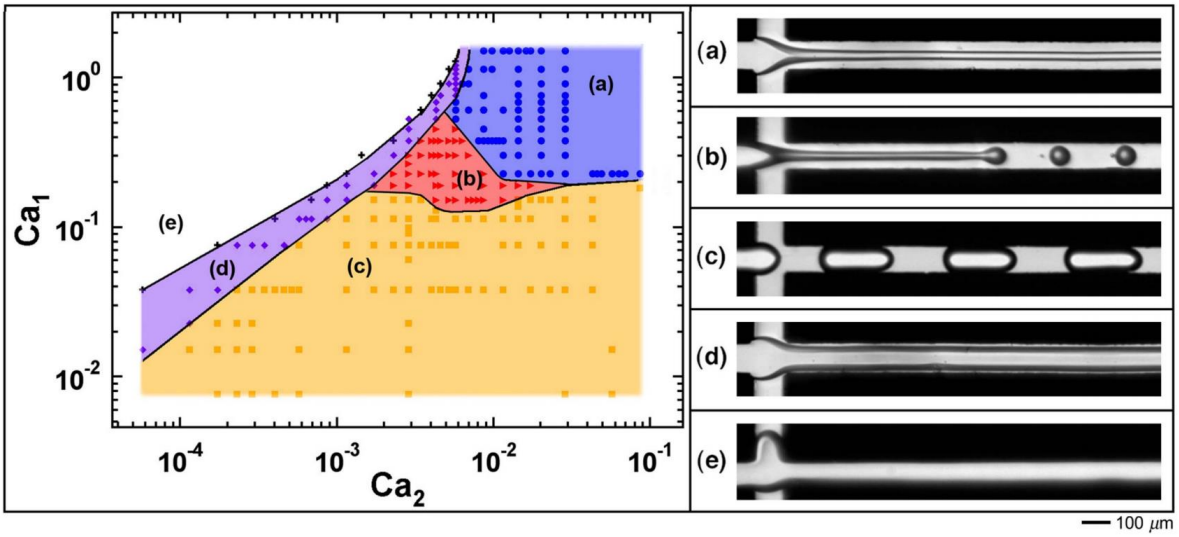

Figure 2.29 – Typical flow map based on the capillary number (Cubaud and Mason 2008).

To produce multiple emulsions, such as the double, triple or higher order emulsion, different techniques can be used, such as sequential or one-step emulsification (Lee et al. 2016c). In the sequential emulsification, the drops are prepared with a series of drop-makers: the innermost drops are prepared at the first drop maker, and are then inserted into the second level of drop maker and so on (Figure 2.30, right). In this case, the level of hierarchy of the multiple emulsions is governed by the number of the drop makers in series. Typically, the drop-makers are T-shape or cross-junction prepared by soft lithography, and the cross-shaped junction provides better control over drop size and formation frequency, thus being more popular (Lee et al. 2016c). Alternatively, multiple emulsions can be formed in a single-step by the simultaneous break up of two or more coaxial flows. This is achieved by using a flow-focusing device designed to form coaxial jet of the inner and middle phases embedded in an outer fluid (Figure 2.30, left)(Nie et al. 2005). By manipulating the flow rates, the size and thickness of the double emulsion is controlled; notably, the same protocol can be used to produce microtubes, when the jet forms a co-flow (Choi et al. 2011). Glass capillary devices are also used for the formation of double, triple and higher order emulsions in just one step (Utada et al. 2005; Choi et al. 2016) .

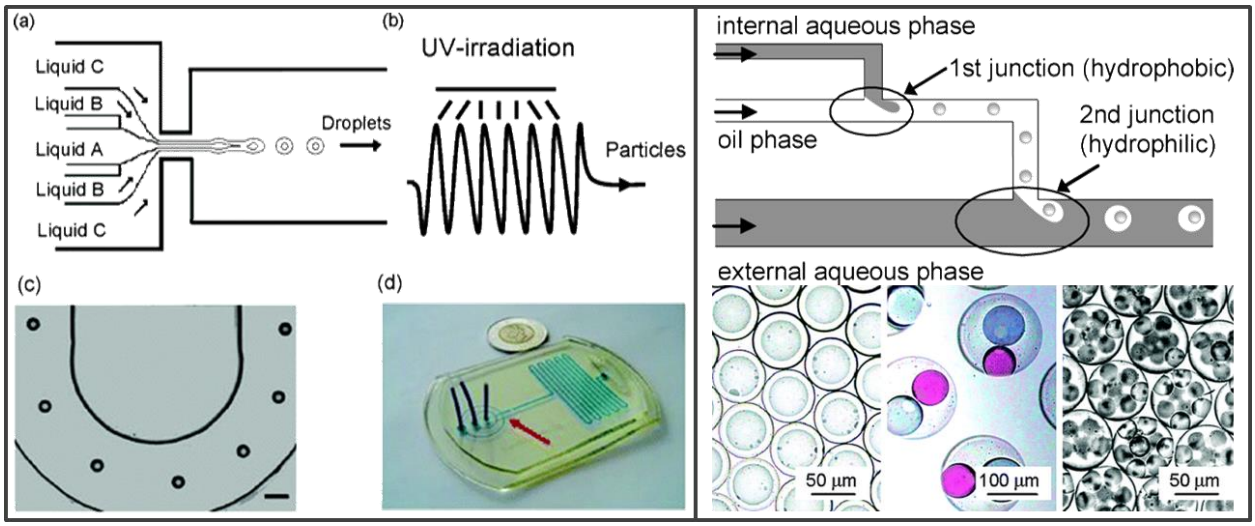

Figure 2.30 – (left) (a,b) Schematic of production of microcapsules in flow-focusing device (c) Optical microscopy image of core–shell droplets flowing in the wavy channel used for *in situ* monomer photopolymerisation. (d) Photograph of a polyurethane microfluidic system (Nie et al. 2005). (right) Schematic of production of droplets in T-juctions and double emulsions (W/O/W) produced with the device (Okushima et al. 2004).

An important aspect to be considered during the design of the device to be used for the production of single and double emulsions is the wettability of the channels. In order to prevent the droplet adhesion on the walls, the channel should have a higher affinity to the continuous phase than with the dispersed phase. For example, to produced water-in-oil droplets, the collector channel surface needs to be hydrophobic, whereas oil-in-water droplets need hydrophilic collection channels (Lee et al. 2016c). Thus, when a series of drop makers are used for the production of multiple-emulsions, different regions have different wettabilities. For example, to produce water-in-oil-in-water (w/o/w) emulsions, w/o are generated in the first hydrophobic junctions and then used to the formation of w/o/w and transferred to a hydrophilic channel (Okushima et al. 2004). Likewise, the production of w/o/w double-emulsion in a single step using capillary devices requires a hydrophobic emitter capillary to facilitate the inner droplet to be engulfed by the outer one.

2.5.2. Solidification of double emulsion and microcapsule formation

Once the emulsion is produced using the microfluidic device, the formation of a solid shell is necessary to produce microcapsules. During the decision on the shell material it is paramount to take into account the polymerisation technique used to solidify the emulsion template into core-shell structure. When a single emulsion is produced, interfacial polymerisation can be applied to form monodisperse polyurea microcapsules shells (Polenz et al. 2014). More interestingly, when a double emulsion is produced, the selected polymerisation of the middle layer can take place. This enables the fine tuning of the shell thickness and the production of a wide range of shell materials. There are several techniques used for selected polymerisation of the double emulsion, such as free-

radical polymerisation (photo and thermally-induced), interfacial polymerisation, ionic cross-linking, solvent extraction and cooling, among others. The choice of the methodology depends on factors such as properties of the precursor liquid, desirable shell composition, physical properties and triggering release; furthermore, the stability of the formed emulsion needs to be considered, since the droplets may coalesce or dissolve prior to solidification of the shell. Comprehensive reviews on the different solidification techniques used to produce micrometric particles, capsules, fibers and tubes using microfluidics are available in the literature (Nunes et al. 2013; Lee et al. 2016c). Figure 2.31 shows microcapsules obtained through different solidification techniques.

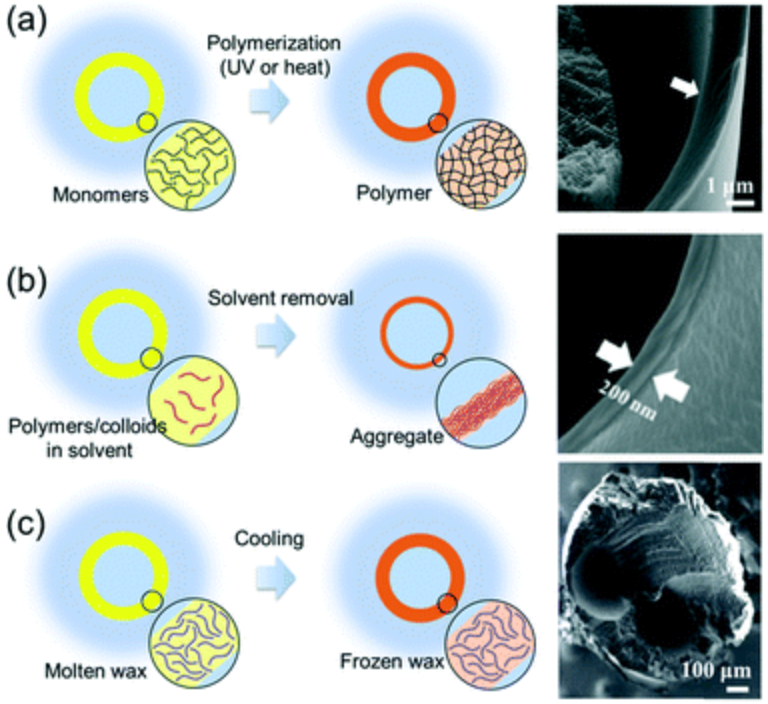

Figure 2.31 - Schematic and scanning electron microscopy (SEM) image showing the process of shell solidification and resulting shells: (a) radical polymerisation, (b) consolidation and (c) cooling. Adapted from (Lee et al. 2016c).

The free radical polymerisation is frequently used for solidifying microfluidic produced emulsions due to the cost-efficiency, fast polymerisation and solvent-free technology. In the radical polymerisation, the initiation step of the polymerisation is triggered by a radical attacking a monomer, subsequently propagating the radical reaction throughout the system. The radical is formed due to decomposition of a molecule (initiator) and it can be achieved via thermal process, photolysis and/or redox reactions. Typically photopolymerisation is used to start the solidification of the shell and the photoinitiator is added to the middle layer of the double emulsion. In this case, the main chemicals polymerised by radical polymerisation are silicone, acrylates and acrylamides, thus a wide range of functional groups can be altered to achieve suitable properties. For example, the technique is widely explored for the solidification of complex-shaped microparticles via

microfluidics, such as lens (Nisisako et al. 2014), Janus (Nisisako et al. 2006) and barcodes (Zhao et al. 2015) particles. Furthermore, by taking advantage of the confinement provided by the channels, different microparticles shapes can be explored: when the volume of the droplet exceed the largest sphere which could be accommodated in a channel, the droplet is deformed into a disk or an ellipsoid (Xu et al. 2005). The photopolymerisation has also been used for the formation of microfibers and microtubes, taking advantage of the 3D laminar flow and "on the fly" polymerisation (Jeong et al. 2004).

Focusing on microcapsules, the fast speed polymerisation of the droplets allows the encapsulation of reactive cores which are difficult to encapsulate via emulsification polymerisation. In addition, the prompt photopolymerisation may hinder the coalescence of the core material (Lee et al. 2014). Focusing on self-healing, photopolymerisation was used to encapsulate reactive cores as triethylenetetramine (TETA) and diethylenetriamine (DETA), two common hardeners of epoxy resin (Chen et al. 2014b). Due to the stability under the flow conditions, the reactive amines were successfully polymerised into capsules with a yield of almost 100% and the rate of production of 1 g/h, as shown in Figure 2.32a. The middle layer of the double emulsion was comprised of a solution of 1,6-hexanediol diacrylate (HDDA) and bisphenol A glycerolate dimethacrylate (BisGMA) containing hydroxy-2-methylpropiophenone as photoinitiator.

Another commonly used technique to produce the shell is the solvent evaporation, where the shell material is dispersed in a volatile solvent and used to form the middle phase; as this solvent evaporates, the shell material precipitates. The shell becomes thinner over the course of the evaporation process, while the core maintains its size; similarly, solvent evaporation has been used to tune the shell thickness of microcapsules (Chen et al. 2012). However, the solvent evaporation is slow relative to free radical polymerisation and requires a higher stability of the double emulsion to avoid coalescence (Lee et al. 2016c). In addition, due to the absence of covalent bonds, the shell may be less resistant than the photo-polymerised ones, and are unlikely to be used for cementitious self-healing. However, it can be used for the easier release of core material and tuning of shell properties. The technique was used to produce polystyrene microparticles with tuneable surface morphologies, due to the shrinkage of the particles after the evaporation of the solvents, as shown in Figure 2.32b (Liu et al. 2012). Polystyrene shells encapsulating air (Yoon et al. 2015) and water (Abbaspourrad et al. 2013a) were also produced using solvent evaporation; polystyrene is able to release the payload when in contact with hydrophobic oil and can be used for enhanced oil recovery and surfactant delivery (Abbaspourrad et al. 2013a). pH-sensitive shells consisting of acid-degradable poly(o-(α-methyl)vinylbenzaldehyde) (PMVB) were also investigated, providing acid-catalysed change in shell wall porosity while maintaining capsule structural integrity

(Grolman et al. 2015). Poly(lactic acid) (PLA) shells have also been produced via solvent extraction aiming at ultrathin and biodegradable shells (Kim et al. 2011).

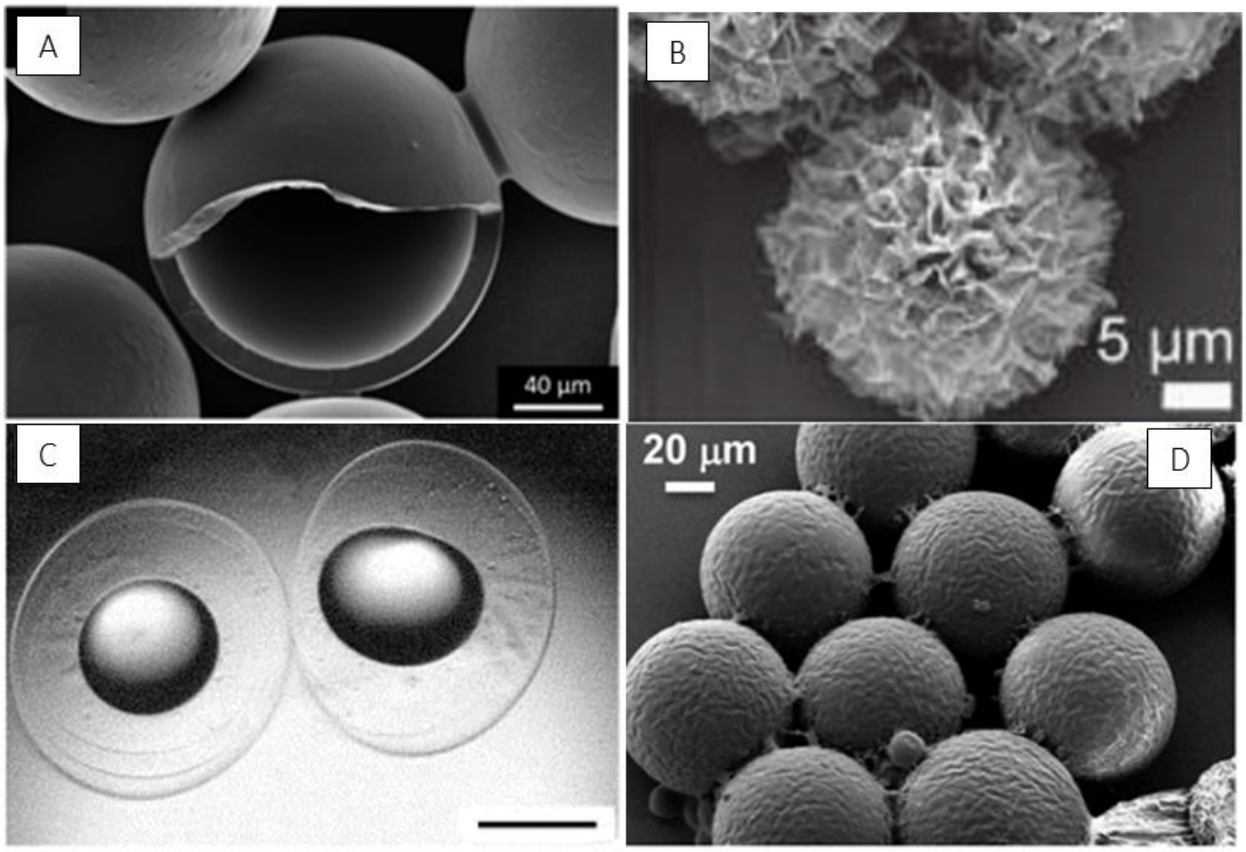

Figure 2.32 - Examples of microcapsules and microparticles produced via different solidification techniques. (a) SEM of core-shell microcapsule with acrylate formed via UV-polymerisation (Chen et al. 2014b). (b) solvent evaporation used to produce microparticles with controllable surface textures as shown via SEM (Liu et al. 2012) (c) alginate shell with organic core produced via ionic cross-linking (Ren et al. 2010). (d) SEM of polyurea microcapsules formed via interfacial polymerisation (Polenz et al. 2014).

Several other techniques and materials might be used for the formation of microcapsules from the emulsions: free radical polymerisation is also used for the formation of microcapsules and beads of poly(N-isopropylacrylamide) (pNIPAM) (Seiffert 2013); ionic cross-linking for the formation of alginate beads and microcapsules (Ren et al. 2010; Duarte et al. 2014), as shown in Figure 2.32c; condensation for the production of polyurea (Polenz et al. 2014) shells, presented in Figure 2.32d; cooling for the encapsulation of food actives with wax as shell (Comunian et al. 2014). However, these methodologies offer limitations such as the use of extra solvents, the use of toxic solvents for the condensation of polyurea and the soft nature of hydrogel and wax capsules. To be used in the capsule-based self-healing of cementitious materials, the radical polymerisation of the double

emulsion is the most suitable, enabling the encapsulation of reactive cores and suitable mechanical properties.

2.5.3. Mechanical Properties

Using the photopolymerisation, the mechanical properties of the shell can be precisely tuned, particularly to achieve suitable capsule size and shell thickness. The dimensions of the double emulsion template can be adjusted by controlling the flow rate of the different fluids. As shown in Figure 2.33a, the fine tuning of the outer droplet can be achieved by controlling the flow rate of the outer fluid (Chen et al. 2012). Similarly, the shell thickness can be predicted and controlled through the flow rate ratio of the middle and inner fluids, illustrated in Figure 2.33b (Hennequin et al. 2009; Chen et al. 2012). Thus, the size and shell thickness of the microcapsules can be controlled, resulting in monodisperse microcapsules with an outer diameter typically between 50-600 μm and minimum shell thickness of 1 μm (Figure 2.33c,d) (Chen et al. 2012; Kim et al. 2014b).

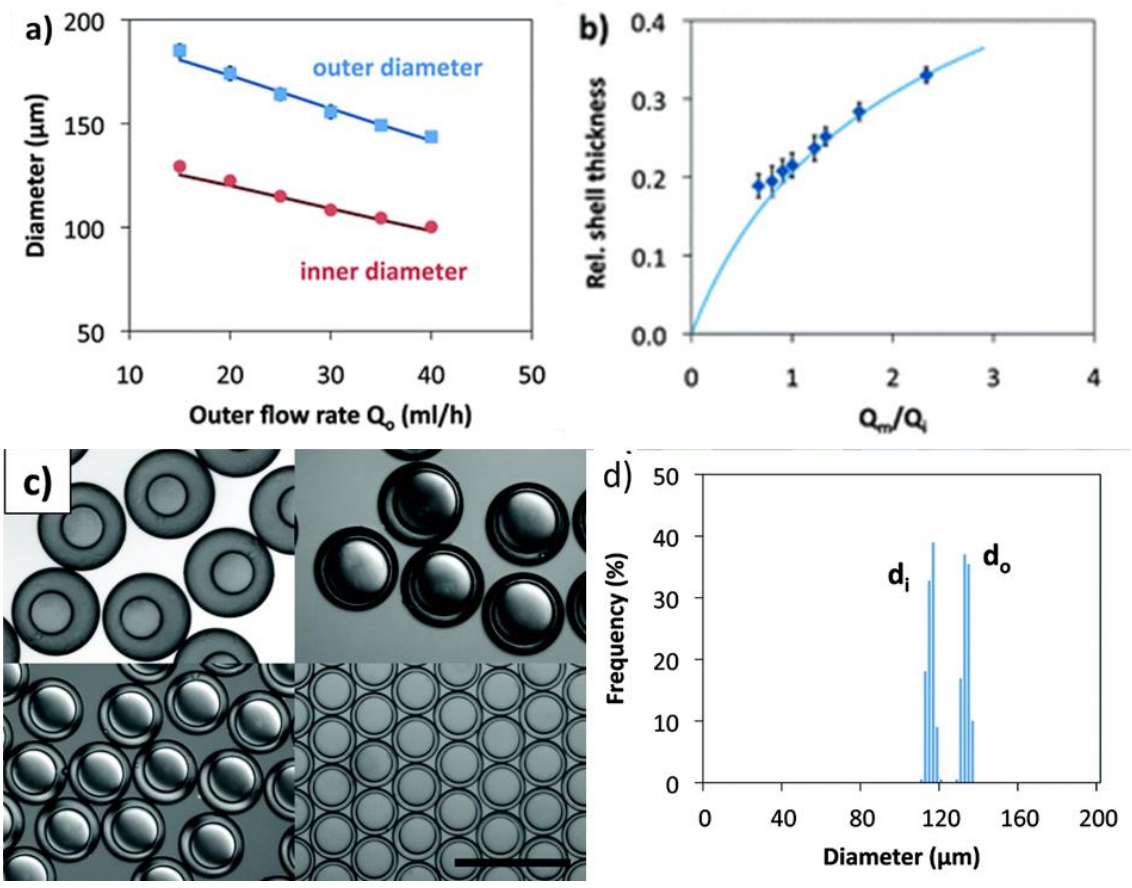

Figure 2.33 – Design microcapsules using microfluidics. (a) correlation between diameter and outer flow rate; b) correlation between shell thickness and inner and middle flow rates; (c) variations in size and shell thickness; and d) narrow size distribution. Adapted from (Chen et al. 2012).

The use of a double emulsion template also allows a broad spectrum of shell materials to be used, thus enabling the tailoring of shell properties. The different glass transition temperature (T_g) of the polymers can be explored to result in a brittle or elastomeric mechanical response of the shell. For example, poly(2-phenoxyethyl acrylate) (PEA, T_g = 5°C) and poly(isobornyl acrylate) (IBOA, Tg = 52°C) were used to study the mechanical properties of the capsules (Chen et al. 2012). Single compression tests were performed in three types of capsules: (i) an elastomeric capsule blend of PEA and IBOA 1:1; (ii) a brittle capsule comprised only of IBOA; and (iii) a brittle capsule containing 90 vol% IBOA and 10 vol% hydrophobised silica nanoparticles and the results are shown in Figure 2.34. During the compression of brittle capsules with 186 μm of diameter and 10 μm of shell thickness, failure was found to occur through the formation of longitudinal cracks around the load of 53 mN, as illustrated in Figure 2.34 (b-d) (Chen et al. 2014a). The characteristic failure load increases along the shell thickness and the size of the microcapsules, and for a same shell thickness, the larger capsules generally display larger rupture force.

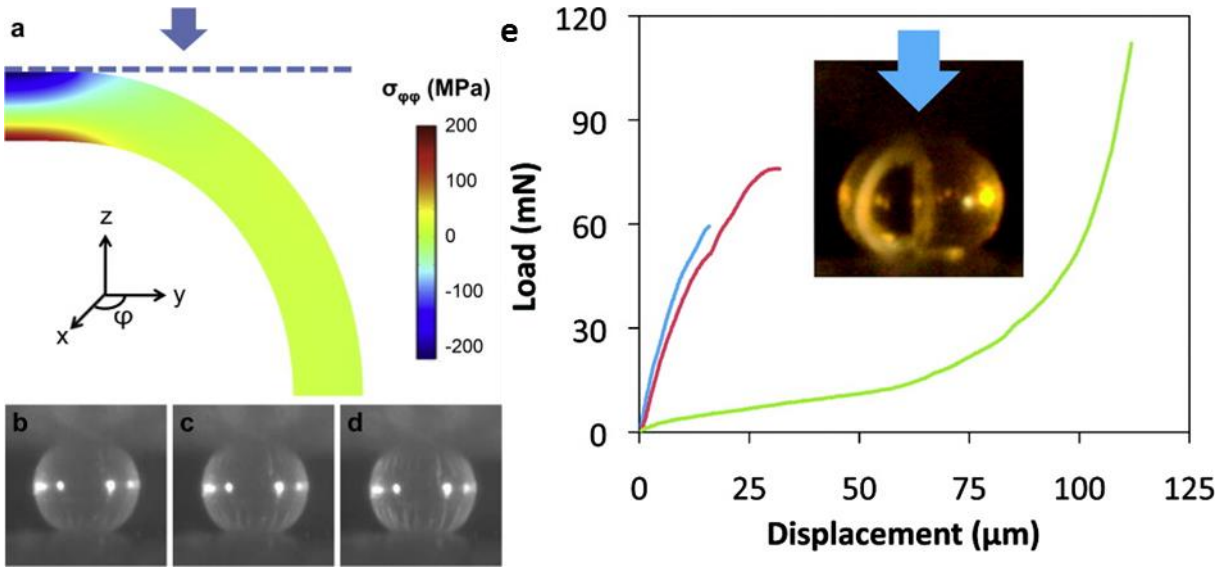

Figure 2.34 - (a) Distribution of circumferential stresses within the microcapsules, (b-d) formation of longitudinal cracks under increasing compression load and (e) typical load–displacement curves of brittle (red), rubbery (green), and particle-filled brittle (blue) capsules. Adapted from (Chen et al. 2012; Chen et al. 2014a).

Alternatively, microcapsules comprised of silicone shell (Vilanova et al. 2013; Fu et al. 2014) were also investigated due to its low glass transition temperature, thermal and chemical stability, high permeability to various organic solvents and gases and biocompatibility (Vilanova et al. 2013). In addition, the elastic properties of cross-linked silicones can be easily tuned by controlling either the structure or the degree of cross-linking of the network. While brittle acrylate microcapsules are easily ruptured when compression force is applied, silicone microcapsules expand without rupturing and recover back to their original morphology upon removal of the initial load (Lee et al.

2016a). This difference in mechanical response of microcapsules from being brittle to elastomeric directly implies that a broad spectrum of shell material can be utilised depending on the application needs. These results are particularly interesting bearing in mind the criteria to achieve suitable microcapsules of self-healing: unaffected through the mixing process and with good mechanical performance.

As discussed in section 2.4.2.1, the control over size, shell thickness and mechanical properties of the microcapsules is crucial to ensure physical triggering. Thus, microfluidics is a valuable tool, particularly when considering the tuning of brittle failure (Chen et al. 2012; Chen et al. 2014a). The physical triggering may be achieved by rupturing the microcapsule membrane due to the tensile force that appears during the crack formation, where the interfacial bonding is fundamental. Alternatively, the physical triggering may also be triggered in compression mode, when the capsules are exposed to a stress larger than their yield point. In both cases, the triggering depends on the elastic properties and shell needs to be designed to avoid deformation without rupture.

2.5.4. Permeability

Although several hydrophilic and hydrophobic core materials can be encapsulated using microfluidics, the retention of the core is an issue. Particularly the retention of water, which can permeate through the nanopores of the shells and lead to the loss of aqueous core. In general, the permeability of the microcapsule shell is dependent on the polymer crosslinking density, the surrounding solution, the polarity and the molecular weight of the core. For instance, isobornyl acrylate is a monoacrylate permeable to molecules with molecular weight around 400 g/mol (Chen et al. 2012) and ETPTA is a triacrylate impermeable for sodium and chloride ions and molecules with high molecular weight such as PVA (Kim et al. 2008). Aiming at densifying the shell and reducing the pore size of the polymeric network, crosslinkers and plasticizers can be added to the middle phase. The use of 1,6-hexanediol diacrylate (HDDA) as cross-linker and hexadecane as a plasticizer resulted in decreased permeability of the capsules, even when 0.3% of crosslinker is used (Chen et al. 2012). The polarity of the microcapsules also plays a key role in the shell permeability, and the use of the w/o/w template slows down the loss of water-soluble cargo material through the hydrophobic shell (Zieringer et al. 2015). To explore the importance of the polarity, crosslinkable perfluorinated monomers have been investigated, due to their chemical stability and concurrently hydrophobic and lipophobic properties (Zieringer et al. 2015). This shell is capable of retaining small ions such as Ca^{2+} and Cl^{-}, with loss of only 2% of core over a period of 4 weeks without osmotic stress; however, once the capsules are immersed in water, the osmotic stress enhances the loss of cargo.

Although water can be encapsulated, it cannot be retained and the loss of core material may lead to the buckling of the capsules (Kim et al. 2014a; Shang et al. 2016; Nabavi et al. 2016). This is because above a threshold pressure, the shrinkage is energetically prohibitive and the volume reduction leads to a localized indentation (Datta et al. 2012). The likelihood of buckling will depend on the elastic modulus, Poisson ratio, shell thickness and diameter of the microcapsule. For rubbery microcapsules made of silicone shell, it was noticed that the shell thickness to radius ratio (h) is the parameter controlling the buckling behaviour. For h $\geqslant$ 0.19, the capsules were stiff enough to retain their spherical shape after drying, while for h $\leqslant$ 0.06, all capsules exhibited an irreversible buckling. In between, for 0.19 $\geqslant$ h $\geqslant$ 0.06, there was a mixture of both types of capsules, as observed in Figure 2.35 (Vilanova et al. 2013). Similarly, for ETPTA with elastic modulus of 600 MPa, the buckling threshold was observed to be h = 0.14 (Abbaspourrad et al. 2013b).

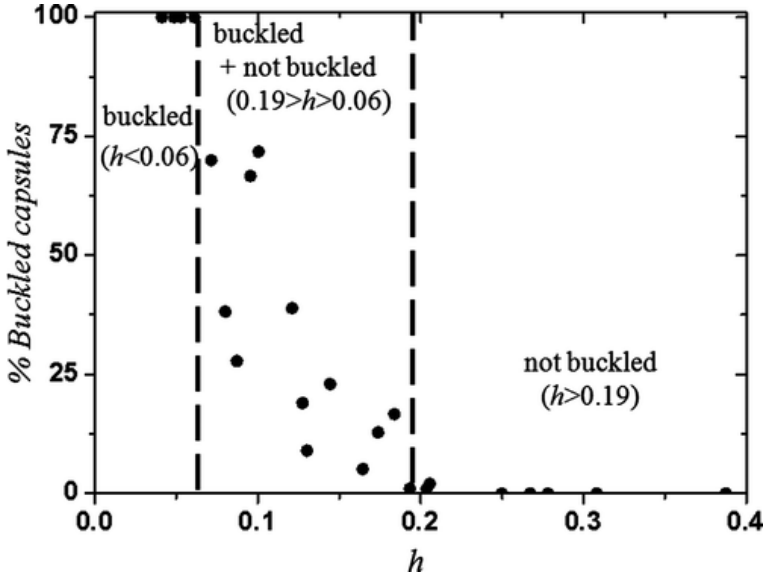

Figure 2.35 - Percentage of buckled microcapsules as a function of h (Vilanova et al. 2013).

To reduce the cargo loss, the cargo material can be emulsified, in which the dispersed phase acts as a barrier for the diffusion of the cargo (Lee et al. 2016b). Traditional bulk emulsification techniques can be used to produce a cargo in water emulsion which is pumped as inner phase to form a double emulsion. To prevent a biphasic separation due to the instability of the emulsion, PEG-diacrylate was used as dispersing phase. During the UV-polymerisation, PEG-diacrylate is also polymerised, resulting in a hydrogel network, locking the cargo material inside of the capsule. Instead of using an emulsion as core, the permeability of microcapsules shell was also explored by using triple emulsion comprised of a fluorocarbon oil (Lee et al. 2016a) and ultrathin hydrogel (Choi et al. 2016) layer surrounded by a photocurable oil phase (ETPTA). The quick photopolymerisation is necessary for the stability of the triple emulsion which could result in the destabilisation of the

structure prior to polymerisation. This system proved to improve the retention of polar and non-polar cargos in a single platform. The leakage of the hydrophobic model molecule through the ETPTA shell is showed in Figure 2.36.

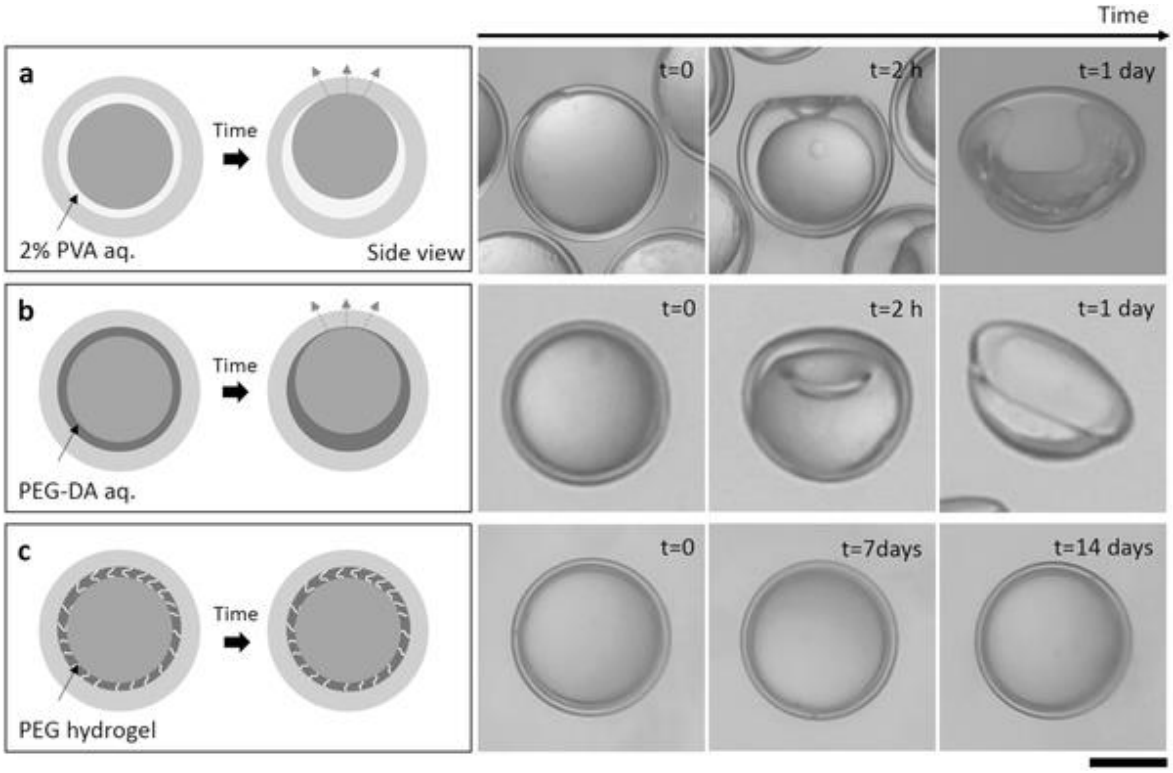

Figure 2.36 - Leakage of hydrophobic model fragrance (α-pinene) encapsulated in polymeric microcapsules, which is composed of ETPTA shell and a) 2% PVA aqueous solution, b) 15% PEG-DA aqueous solution, and c) PEG cross-linked hydrogel. The leakage behaviour is monitored in an aqueous solution. Scale bar represents 50 µm (Choi et al. 2016).

Figure 2.36a, shows a model fragrance α-pinene being encapsulated by a thin layer of water with PVA and then by a solid shell of ETPTA. The density mismatch between the water and the hydrophobic core results in the core rising and directly contacting the polymeric shell; the fragrance imbibes into the hydrophobic polymer, leading to a rapid leakage and hence limiting the long-term storage. To achieve long term storage of the fragrance, the ultrathin layer was rigidified by using PEG diacrylate. Figure 2.36b shows the PEG without the photoinitiator where the material still undergoes leakage due to the density mismatch as observed by the buckled shell. On the other hand, when PEG is photopolymerised into a hydrogel (Figure 2.36c), the hydrophilic layer is effective in retaining the hydrophobic cargo up to 14 days and the capsule maintains its structural integrity. The alter shows the microfluidics potential to tune crosslinking density, polarity and thickness of the shell in order to enhance the cargo retention.

2.5.5. Upscaling microcapsule production in microfluidic devices

The major drawback of using microfluidic devices for the production of microcapsules is the low rate of droplet production, typically less than 1mL/h, which limits the industrial application. Several studies report the investigation of scaling-up systems for the production of single emulsions with low dispersion, including parallelisation (Nisisako and Torii 2008), drop splitting(Abate and Weitz 2011) and 3D networks with ladder-like (Jeong et al. 2015) and tree-like (Conchouso et al. 2014) geometry. And the droplet production is escalating fast: while the parallel system (Romanowsky et al. 2012) produced droplets at a rate of 40 mL h^{-1}, the tree-like geometry (Conchouso et al. 2014) allows the production up to 1 L h^{-1}. Nonetheless, although the production of single emulsions has been explored, the scaling up of double emulsion production is a bigger challenge. The glass capillary devices (Utada et al. 2005) used to produce double emulsion in one-step are impractical to scale-up since it is manually produced. Alternatively, devices created through soft lithography are easier to produce and to parallelise. Soft lithography has been used to produce devices that are suitable for scaling up (Saeki et al. 2010; Arriaga et al. 2015) and can be used to parallel up to 15 double drop makers. This results in an inflow of core and shell at 24 mL h^{-1} and 30 mL h^{-1}, which running continuously for an entire day would result in 1.5 kg of microcapsules (Romanowsky et al. 2012). In this case, the control of wettabilities is an issue, since the devices for producing double emulsion consists of two drop making junctions in series, commonly the first one hydrophobic and the second one hydrophilic. Abate et al. (2011) reported the split of large double emulsion droplets into small drops using the splitting array (Abate and Weitz 2011), to increase the speed of double emulsion production. Recently, Eggersdorfer et al. (2017) proposed the use of tandem emulsification, where the single emulsion produced in one device is directly injected into a second device, to produce a double emulsion, as shown in Figure 2.37.

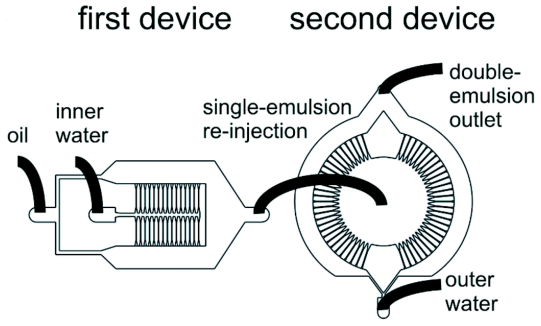

Figure 2.37 - Scale-up production of double emulsion via tandem emulsification (Eggersdorfer et al. 2017).

In the first parallelised device, the step-emulsification nozzles are arranged along a straight distribution channel. Then, the produced single emulsion is injected in a second device, where the nozzles are radially distributed around the inlet to achieve a homogenous encapsulation. This

approach circumvents the wettability issue, and presents one device for the formation of water-in-oil, and a second device for the formation of water-in-oil-in-water. Production rates of 60 mL h^{-1} were achieved and control over size and shell thickness was possible (Eggersdorfer et al. 2017).

2.6. Conclusion

Concrete is still the most used construction material and it is vital for driving economic growth, boosting productivity and raising living standards. However, the durability of concrete is impaired by the formation of cracks, resulting in the need for repair and maintenance actions and increasing the life-cycle cost of structures. To overcome these limitations, the concept of self-healing has been investigated, whereby materials have an in-built capability to repair inflicted damage. Intrinsically, cement-based materials possess a certain autogenous self-healing capability, which is effective in the presence of water and cracks below 0.15 mm and preferably lower than 0.05 mm (Li and Yang 2007; de Rooij et al. 2013; Fan and Li 2015). Furthermore, the autogenous healing can be stimulated by controlling the crack width, providing additional water and adding mineral admixtures to boost chemical autogenous healing. Alternatively, vascular and capsule based systems can be used to heal larger cracks, where the healing agent is isolated prior to damage. Although the vascular based self-healing offers several advantages, its installation in the matrix is still challenging and limits the application of the technique (Huang et al. 2014b; Huang et al. 2016). Capsule based self-healing, on the other hand, offers the advantage of easily adding the capsules during mixing and the encapsulation of a wide variety of healing agents.

The production of the capsules remains a challenge due to complex design cycle of capsule-based self-healing, thus offering several fronts of research. The design cycle of capsule-based self-healing is comprised of five stages, namely (Blaiszik et al. 2010): (i) the encapsulation of the healing agent, followed by (ii) the investigation of the survival during integration, (iii) the triggered release of the core material, (iv) the effect on the mechanical properties of the matrix, and the (v) self-healing performance for a certain application. In this cycle, the construction of the capsule, its evaluation and subsequent feedback to refine the design further are executed until a satisfactory design is achieved. In order to fill the crack, ideally the healing agents should also be expansive, stable and with suitable viscosity (Van Tittelboom and De Belie 2013). Furthermore, the service conditions of the concrete structures need also to be considered for the choice of healing agent, since the mechanism of self-healing may rely on the presence of water or moisture (Huang et al. 2016). Finally, to assess the healing performance, several tests are used to evaluate healed crack width and recovery in transport and mechanical properties (Muhammad et al. 2016). The healing performance can be used to select a suitable healing agent to be investigated in the design cycle, and thus to be encapsulated to perform autonomous self-healing.

Several encapsulation processes to protect the core material and deliver it at a precise time and place have been used to produce macro- and microcapsules with solid and liquid cores. For capsule-based self-healing of cementitious materials, the encapsulation of solid cores has been investigated using pan-coating, which offers a simple methodology to produce large quantities of material (Dong et al. 2014a; Lee and Ryou 2014; Alghamri et al. 2016). Alternatively, co-extrusion has been applied to produce beads containing the healing agent and hollow tubes with tuneable properties (Hilloulin et al. 2015; Formia et al. 2015; Formia et al. 2016). However, the inclusion of the liquid healing agent inside the hollow tubes is very labour intensive and the production of bulk quantities of encapsulated material remains a challenge (Van Tittelboom et al. 2016). On the other hand, microencapsulation techniques can be used to generate large quantities of capsules containing liquid cores. In this case, typically the core material is emulsified and the shell is formed in the interface of the droplets. Four methodologies have been used for this purpose: coacervation (Kanellopoulos et al. 2016; Giannaros et al. 2016; Kanellopoulos et al. 2017), *in situ* polymerisation (Milla et al. 2016; Lv et al. 2016b; Lv et al. 2016a; Wang et al. 2017), *in situ* interfacial polymerisation (Litina et al. 2014; Giannaros et al. 2016) and sol-gel reactions (Yang et al. 2010; Perez et al. 2015a). These conventional encapsulation techniques produce capsules with a wide range of sizes, shell thickness and structures, thus offering poor control of their release properties. Moreover, typically the process is used to encapsulate hydrophobic cores and shell formation is initiated by adjusting the pH, thus limiting cargo diversity and shell combinations that can be used.

The encapsulation process limit not only the materials used as core, but also the shells. And the shell properties are fundamental to attend the integration survival, minimal effect on the matrix properties, response to triggering and core retention. For example, survival and triggering can be ensured by designing water sensitive shells that are ductile during mixing and brittle shells after curing of cement matrix (Kanellopoulos et al. 2017). Furthermore, the optimisation of capsule stiffness, diameter and dosage to minimally affect the compressive strength of cementitious matrix is also necessary (Gilabert et al. 2017a). The addition of capsules with reduced elastic modulus when compared with the cementitious matrix contributes to attracting the crack towards the capsule, making it suitable for physically triggered self-healing (White et al. 2001; Ponnusami et al. 2015). To ensure the rupture upon crack, the shell thickness, tensile strength and interfacial bonding between the capsule and the matrix also need to be adjusted. This can be a challenge, particularly when considering that the *in situ* polymerisation may lead to the formation of hydrophobic shells, preventing a good interfacial bonding with the matrix (Wang et al. 2013; Lv et al. 2016a). The properties of the shell are also associated with the permeability of the shell which is important to retain the core material and to prevent unwanted reactions (Janssen 2011; Huang and Yang 2011).

A promising route to produce a wide range of core-shell structures with fine control over the shell properties is the use of the microfluidic device. In this process, controlled double emulsification is achieved by pumping an inner fluid into a middle fluid, which is in turn engulfed by an immiscible outer fluid (Nunes et al. 2013). Capsules are formed by consolidating the middle phase of the resultant double emulsions, which is typically achieved by photopolymerisation (Lee et al. 2016c). Double emulsion templating in microfluidic devices has been shown to enable the formation of emulsions independent of the pH, thus allowing the encapsulation of a wide range of core materials (Chen et al. 2014b). In addition, the double emulsion template enables fine tuning of template dimensions, thus offering superior control over size and shell thickness (Hennequin et al. 2009; Chen et al. 2012). A wide range of materials can be used as shell, enabling the tailoring of shell properties such as glass transition temperature, elastic modulus and tensile strength (Chen et al. 2012; Vilanova et al. 2013; Fu et al. 2014; Chen et al. 2014a; Nabavi et al. 2016). Building on the literature about core retention in microcapsules produced using microfluidics (Kim et al. 2008; Chen et al. 2012; Vilanova et al. 2013; Abbaspourrad et al. 2013b; Zieringer et al. 2015; Choi et al. 2016), the core retention of the typical healing agent can also be assessed. Thus, the objective of this research was to use microfluidic encapsulation protocol to synthesise microcapsules for autonomic self-healing in cementitious materials. Particularly, the research was focused on developing microcapsules to be physically triggered, thus investigating the integration, survival and design of chemical and physical properties of the shell to ensure rupture upon crack formation.

3. Materials and Experimental Methods

This chapter introduces the raw materials and their properties, sample preparation procedures and the experimental tests performed. The first part presents the chemicals used throughout the thesis and their properties. The second section presents the production of the microcapsules, including the preparation of the solutions, microfluidic set-up, the parameters influencing the formation of double emulsion and photopolymerisation. Also, the experimental protocol used to produce a capillary microfluidic device is described. Finally, the last part of the chapter describes the experimental procedures used to investigate the samples properties, including microscopy, TGA, casting, DMA, microindentation and tensile tests.

3.1. Materials

Six different acrylates were used for the production of the double emulsion and investigation of mechanical properties. Bisphenol A glycerolate dimethacrylate (BisGMA) and urethane diacrylate (MU3603, Miwon, Korea) were used to increase the viscosity of the acrylate solution, facilitating the formation of the double emulsion. To tune the viscosity and the properties of the fluids, the following monomers were used: 2-phenoxy ethyl acrylate (PEA), isobornyl acrylate (IBOA), 1,6-hexanediol diacrylate (HDDA) and trimethylolpropane ethoxylate triacrylate (ETMPTA). The structure and properties of the different acrylates is described in Table 3.1, based on the datasheets of Sigma Aldrich and from Miramer (Miwon Specialty Chemical Co.). The photoinitiator hydroxy-2-methylpropiophenone was used to initiate the photopolymerisation of the acrylates. Except by the urethane triacrylate, all the chemicals were purchased from Sigma Aldrich.

To tune the interfacial tension and the viscosity of the aqueous fluids, poly(vinyl alcohol) (PVA, MW 31000-50000, 98-98.8% hydrolyzed, Acros Organics, Belgium) was used as surfactant. To produce the double emulsion, typical concentrations ranged between 2-10% wt of PVA in water.

Different solutions were used as inner fluid in the pumps and resulted in different core materials inside the capsules. The colloidal silica (LUDOX HS-40, 40 wt% colloidal silica suspension in water, Sigma Aldrich, UK) used presented a density of 1.3 g/mL, viscosity of 35 cPs and pH of 9. The sodium silicate (Sigma Aldrich) presented a density of 1.39 g/mL, viscosity of 60 cPs and the pH of 12.5. To produce microcapsules with organic core, paraffin oil (SipMed 68, Brenntag UK) and mineral oil (light mineral oil, Sigma Aldrich, USA) were used. To produce the emulsion of healing agent dispersed in the continuous organic phase, sorbitan triolate (Span 85, Sigma Aldrich) was used for the stabilisation of colloidal silica and of sodium silicate.

Acrylic acid (Sigma Aldrich, UK) was used to functionalise the surface of the acrylate shell.

Table 3.1 – Characteristics of the acrylates monomers and photoinitiator used in this work.

Monomer	Structure	Molecular Weight (g/mol)	Viscosity (cps @25°C)	Glass transition temperature (°C)	Density (g/mL)
BisGMA	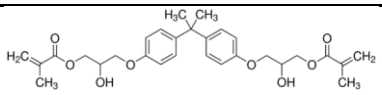	512.6	-	-	1.161
MU3603	Aromatic diacrylate	3300	4000 (60°C)	-	-
PEA	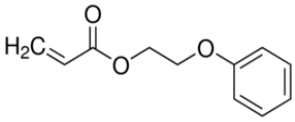	192.2	8-20	7	1.104
IBOA	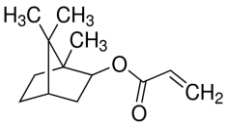	208.3	15	55	0.986
HDDA	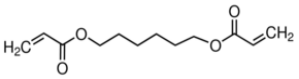	226.3	5-15	43	1.01
ETMPTA	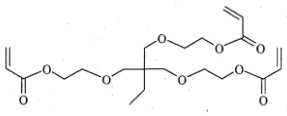	~428	50-70	40	1.11
2-hydroxy-2-methylpropiophenone	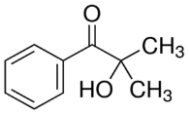	164.2	-	-	1.077

The cement used for the preparation of the cement paste was CEM I 52.5 N with a particle density of 2.7 – 3.2 g/cm3 and a specific surface area of 0.30 – 0.40 m2/g, supplied by Hanson UK. The chemical composition of the cement is presented in Table 3.2.

Table 3.2 - Chemical composition of cement as provided by the manufacturer.

Materials	Composition (%)						
	CaO	SiO_2	Al_2O_3	Fe_2O_3	MgO	SO_3	LOI

Cement	63.6	19.5	4.9	3.1	0.9	3.3	2.1

Five types of acrylate admixtures were selected to investigate the mechanical properties of copolymers with potential to be used as shell and they are described in Table 3.3. The preparation of the copolymers was the same as the one described in section 3.3.1.1. However, to polymerise larger quantities of material to investigate the properties of the bulk material, the oxygen inhibition effect and the exothermic reaction was taken into consideration.

Table 3.3 - Composition of the copolymers used to investigate shell properties.

Copolymer name	Oligomer	Monomer	Photoinitiator
BP	50% wt of BisGMA	50% wt of PEA	1% wt of hydroxy-2-methylpropiophenone
BI	50% wt of BisGMA	50% wt of IBOA	1% wt of hydroxy-2-methylpropiophenone
BH	50% wt of BisGMA	50% wt of HDDA	1% wt of hydroxy-2-methylpropiophenone
BT	50% wt of BisGMA	50% wt of ETMPTA	1% wt of hydroxy-2-methylpropiophenone
UH	50% wt of MU3603	50% wt of HDDA	0.8% wt of hydroxy-2-methylpropiophenone

3.2. Production of microcapsules

3.2.1. Production of the solutions

3.2.1.1. Shell material

Five different shell materials were used in this work and its composition is reported in Table 3.4. The BisGMA was stored at 5°C which increased the viscosity of the acrylate. Thus, to produce the copolymers, the BisGMA bottle was placed in a water bath at ~60°C where the viscosity of the polymer was sufficiently decreased to enable the sampling. Typically, 15g of BisGMA was added to a beaker and magnetically stirred with 15g of the monomers for 1 h using hot plate at ~60°C . Then, 1% wt of the total solution (0.3g) of photoinitiator was added and mixed for 1 min. Alternatively, the MU3603 acrylate was kept at room temperature and directly mixed with the monomers for 1h, without the water bath or the hot plate. Considering the high molar weight of the urethane acrylate

(~3300 g/mol), the concentration of photoinitiator was decreased to 0.77% wt. Hence, for 30 g of a mixture 1:1 of MU3603 and HDDA, 216 μL of photoinitiator was added and magnetically stirred for 1 min. To prevent unwanted polymerisation, the produced copolymers were transferred to a 50 mL centrifuge tube which was covered with aluminium foil.

Table 3.4 – Composition of the copolymers used as shell material.

Copolymer name	Oligomer	Monomer	Photoinitiator
BH	50% wt of BisGMA	50% wt of HDDA	1% wt of hydroxy-2-methylpropiophenone
BIH	50% wt of BisGMA	40% wt of IBOA 10% wt of HDDA	1% wt of hydroxy-2-methylpropiophenone
BI	50% wt of BisGMA	50% wt of IBOA	1% wt of hydroxy-2-methylpropiophenone
20BE	20% wt of BisGMA	80% wt of ETMPTA	1% wt of hydroxy-2-methylpropiophenone
UH	50% wt of MU3603	50% wt of HDDA	0.8% wt of hydroxy-2-methylpropiophenone

3.2.1.1. CORE MATERIAL AND OUTER SOLUTION

PVA was used as surfactant to adjust the interfacial tensions and prevent phase separation. To prepare the PVA solution, typically 10g of PVA was magnetically stirred with 90g of water in an Erlenmeyer for 1 h, at ~100°C. When the solution became homogenous due to the dissolution of PVA crystals, the material was cooled down and dissolved to produce 2 or 5% wt solutions. The solution produced was consumed within a week; after this time, the formation of precipitates was observed.

To encapsulate colloidal silica in water, a mixture of 1:1 in volume of colloidal silica suspension and PVA 10% wt. solution was prepared. Since the material is miscible, the solutions were hand shaken in a centrifuge tube. As a result, the aqueous solution consisted of 20% wt of colloidal silica and 5% wt of PVA.

To encapsulate sodium silicate and colloidal silica in oil, the mineral oil was mixed with Span 85 and then the mineral healing agent was added. A detail description is presented in section 4.5.2.

To functionalise the shell surface, a solution of 1% of acrylic acid in the outer solution of PVA was produced.

3.2.2. Production of double emulsion

In order to produce the emulsion template, a flow-focusing microfluidic device (Dolomite Microfluidics, United Kingdom) was purchased and it is depicted in Figure 3.1. The chip is made using hydrofluoric acid (HF) etching on glass, combined with thermal bonding of the fused silica capillary (Dolomite Centre). Two fluidic junctions are present in the chip – the lower is used for producing single emulsions while the upper is used for double emulsions. In the upper junction, the hydrophilic glass microchannels are used to transport the middle and outer fluid, and the droplets are formed in the confluence of those channels. A glass capillary tube is used to carry the inner fluid, and the outer part of this capillary tube is coated with a fluorophilic coating. This coating is used to reduce the interfacial tension between the acrylate (middle phase) and the device's walls, consequently facilitating the formation of the double emulsion. At the junction, the channel cross-section is comprised of channels with 100 μm depth and 105 μm width, and all the other channels have 100 μm depth and 300 μm width. The total dimensions of the chip are 15 x 11.25 x 4 mm (W x L x D).

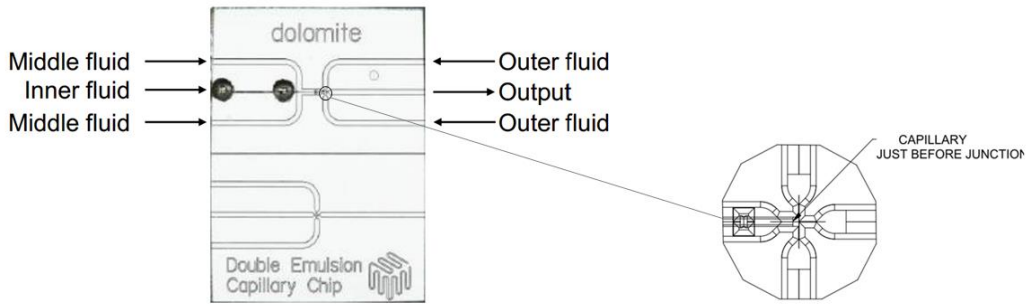

Figure 3.1 – Dolomite double emulsion chip and amplified schematic representation of the junction.

The chip was placed in a H-interface (Dolomite, UK), a 7-way linear connector (Multiflux-2 Linear Connectors 7-way, Dolomite, UK), as shown in Figure 3.2a. To connect the multiple inflows, a 7-way FKM rubber seal (Dolomite, UK) was used, as shown in Figure 3.2b. The system is designed to provide a fast and reliable connection of 0.8 mm outer diameter tubing with the microchannels in the glass microfluidic chip (Figure 3.2d). Furthermore, the in-built tube restraint mechanism holds tubes securely in place preventing unwanted displacement and assuring a more robust operation. It is worth mentioning that the FKM rubber seal is sensitive to acetone, thus when acetone is used to

clean the chip the rubber swells and blocks the flow. For this reason, typically water and ethanol are used as cleansing fluids for the chip.

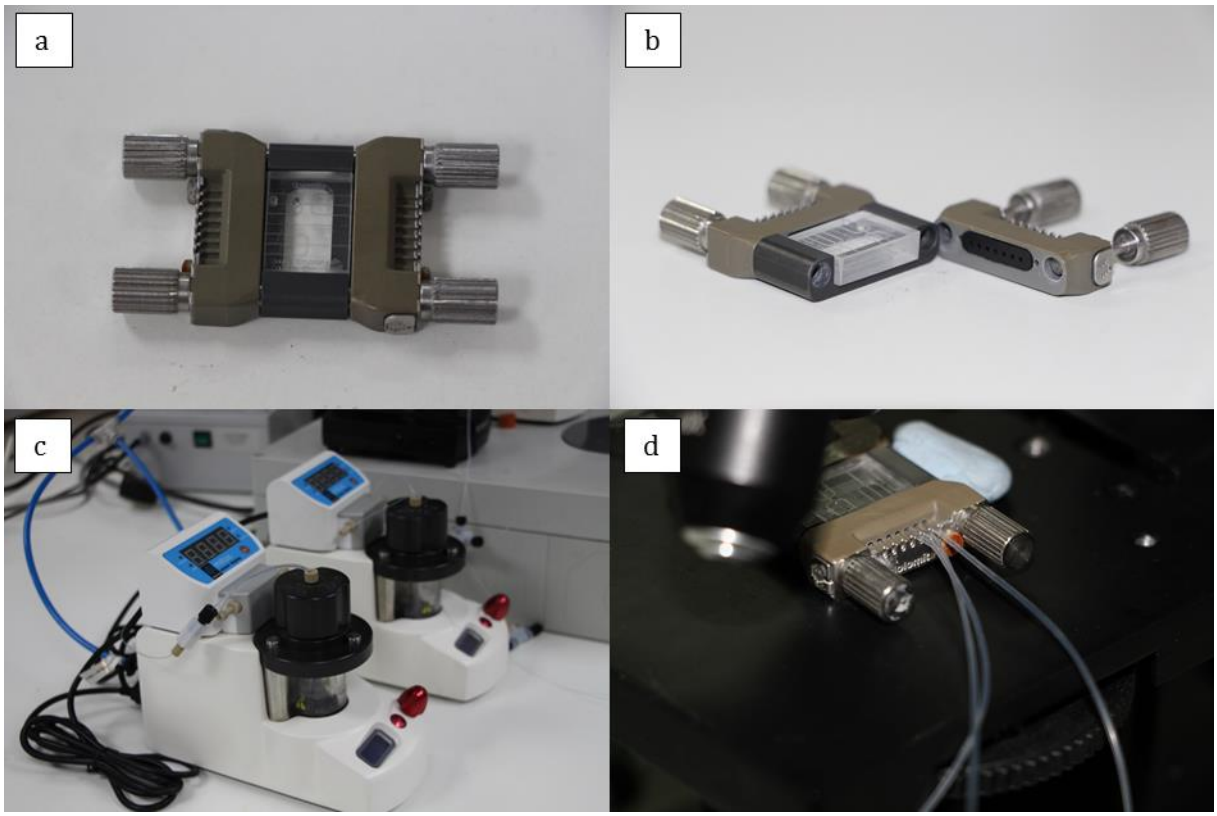

Figure 3.2 – Set-up for the microfluidic production of double emulsion: a) Double emulsion device placed in the H-interface; b) Detail of the interface of the device and the 7-way rubber seal; c) pressure pumps; and d) detail of the connected tubing.

Pressure pumps shown in Figure 3.2c were used (Mitos P-Pump, Dolomite, UK) to pump the fluids inside of the device. The pressure pump was selected due to the pulseless liquid flow with a precise pressure driven pumping mechanism. The design features a lockable pressure chamber for safety, which accommodates a wide range of fluid vessels and a twist-and-click knob. In the tests, a glass vial with maximum capacity of 30 mL was used. The pumps were used with air supply with a maximum pressure of 5 mbar. A flow rate sensor (Mitos Sensor Display, Dolomite, UK) was used to measure and display the flow rate with high precision due to the thermal sensor technology (Dolomite Centre). The flow rate sensors are calibrated in a flow rate range of 0.4 - 7µL/min for the inner and middle fluids and 30-1000 µL/min for the outer fluid. After coming out of the flow rate sensors, the middle and outer fluid were split in two using a T-connector (0.5 mm inner diameter and 1.6 mm outer diameter).

Preliminary experiments to investigate the formation of double emulsions used a Graseby™ 3150 syringe pump (Smiths Medical, Smiths Group PLC, UK). The minimum and maximum flow rates allowed in these pumps were 0.1 and 30 mL/h, respectively.

3.2.3. Parameters affecting the production of double emulsion

When the flowing thread comprised of the inner and middle fluids arrives at the cross junction, it is immersed into the continuous fluid. The different properties of the dispersed and continuous phase such as viscosity (μ), density (ρ), interfacial tension (γ), flow rate (Q) and channel dimensions (w and h) will contribute for the different forces governing the fluid. The four main forces acting upon the system are (Kumacheva and Garstecki 2011): (i) the surface tension attempting to minimise the interfacial area of contact; (ii) the viscous forces suppressing the growth of deformations that could lead to the pinch off; (iii) inertial forces, promoting the formation of a long fluid thread; and (iv) gravitational forces, deforming the shape of the sphere. In order to assess the relative importance of the different forces, non-dimensional numbers are commonly used in fluid mechanics, as shown in the Figure 3.3.

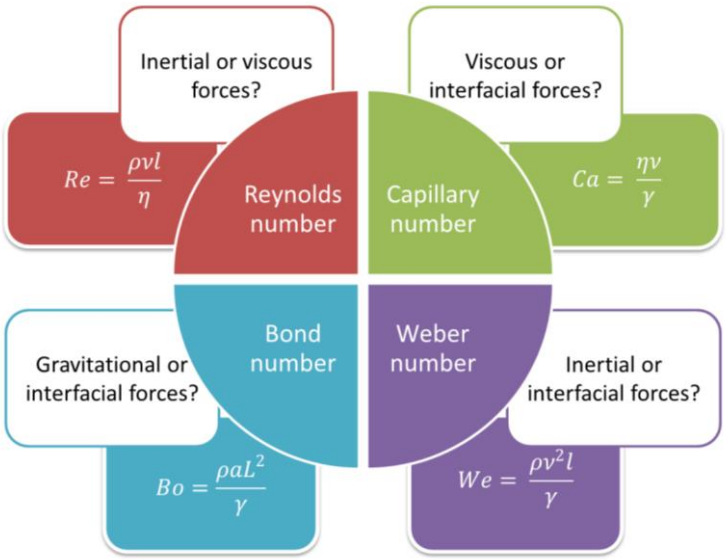

Figure 3.3 – Non-dimensional numbers used to analyse the relative importance of the main forces acting upon the microfluidic system.

The Reynolds number (Re) assesses the relative importance between the inertial and viscous forces in a particular flow. The Re is defined as:

$$Re = \frac{\rho v L}{\eta} \qquad \text{Equation 3.1}$$

where ρ is the density of the flow, ν stands for the magnitude of speed, L is the diameter of the flow and η is the dynamic viscosity. To illustrate, one can consider the formation of water-in-oil droplets using a flow-focusing geometry with a channel width and height of 100 μm. Considering a solution of 2% polyvinyl alcohol as the dispersed phase, (PVA, ρ = 1000 kg/m^3, η= 1.95 mPa s)(Nisisako et al. 2004), a flow of 0.4 mL/h (0.01 m/s) and the droplet diameter of 100 μm:

$$Re = \frac{\frac{1000\ kg}{m^3}.\frac{0.01m}{s}.10^{-4}m}{\frac{1.95x10^{-3}kg}{m.s}} = 0.5 \qquad \text{Equation 3.2}$$

This low value of Reynolds number is coherent with the typical values reported in microfluidic devices, and indicates that the viscous forces are dominant and the flow is completely laminar, i.e., no turbulence occurs. The laminar-turbulent transition occurs when the Reynolds number is around 1000.

The Bond number (Bo) characterises the relative importance of gravitational forces and interfacial tension, and is given by

$$Bo = \frac{\rho a L^3}{\gamma} \qquad \text{Equation 3.3}$$

being ρaL^3 the approximated gravitational force acting on the fluid, where ρ is the mass density, a is the gravitational acceleration, L represents the diameter of a jet or a droplet and the interfacial forces given by γ. For example, we can still assess the formation of water-in-oil droplets using a flow-focusing geometry, using the parameters described previously. As the continuous phase, we can consider the 1,6-Hexanediol diacrylate (HDDA, ρ = 1020 kg/m^3; η=6.71 mPa s; γ=11.2 mN/m) (Nisisako et al. 2004; Erb et al. 2011):

$$Bo = \frac{1000\ {}^{kg}/_{m^3}\ 9.81\ {}^{m}/_{s^2}\ (10^{-4}m)^3}{11x10^{-3}\ {}^{N}/_{m}} = 0.009 \qquad \text{Equation 3.4}$$

In this example, Bo equals 0.009, guaranteeing that the interfacial forces dominates and the gravitational forces can be neglected in the analysis of the dynamic of the system. In other words, the diameter of the droplet is so small (10^{-4} m) that the interfacial tension is higher than gravity and the droplet is perfectly spherical.

Up to now, the main forces that dictate the regime in microfluidics are the viscous and interfacial forces. The dimensionless number comparing the viscous stresses and the interfacial forces is the capillary number (Ca) which plays a key role in the droplet formation:

$$Ca = \frac{\eta v}{\gamma} = \frac{\frac{1.95x10^{-3}kg}{m.s} \cdot \frac{0.01m}{s}}{11x10^{-3}\,{}^{N}/_{m}} = 0.002 \qquad \text{Equation 3.5}$$

Where η is the dynamic viscosity, ν denotes the magnitude of speed and γ interfacial tension. Still taking into account the formation of water-in-oil droplets using PVA and HDDA as the continuous and dispersed phase, respectively, the capillary number for the dispersed phase is 0.002. This means that the capillary forces dominate and the drops have the spherical shape imposed by the interactions with the surface.

The interplay between the viscous and interfacial forces is the main responsible for the formation of emulsions using microfluidics. If there was no interfacial tension and both middle and outer fluid were miscible, the two liquids would flow along the output channel. However, interfacial tension acts to reduce the interfacial area, and the viscous stresses act to extend and drag the interface downstream (Squires and Quake 2005; Nunes et al. 2013). These stresses destabilise the interface (Rayleigh-Plateau instability) and cause droplets to be formed to minimise the fluid surface. Typically the droplets are formed when a critical capillary number of 0.1 is achieved (Cubaud and Mason 2008). With the increase of the viscous stresses, i.e., typically increasing the flow rate, dragging forces also increase and larger droplets could be produced. To assure the double emulsion formation, a minimum threshold of dynamic viscosity needs to be achieved and typically the viscosity of the middle phase was increased using BisGMA or MU3603.

Last, when inertial and the interfacial forces are more important than the viscous stress to break up the droplet, the Weber (We) number is used. We is the product of Reynolds number and the capillary number and judges the relative importance of inertial and interfacial forces:

$$We = \frac{\rho v^2 L}{\gamma} \qquad \text{Equation 3.6}$$

where ρ is the density of the flow, ν denotes the superficial velocity of the dispersed phase, L the characteristic dimension in the system and γ the interfacial tension. The number can be derived from the ratio between kinetic energy ($\rho v^2 L^3$) and the energy added by the Laplace pressure (γL^2). When the inertia of the dispersed phase and the viscous forces of the continuous phase begin to take effect, jetting regime appears (Utada et al. 2007). In the water-in-oil example, the Weber number would be 0.009.

3.2.4. Polymerisation of the shell

Once the double emulsion template was formed, the middle layer of the emulsion was polymerised to form the solid shells. The free radical polymerisation was initiated with the absorption of UV

energy by the photoinitiator hydroxy-2-methylpropiophenone. Figure 3.4 shows the photocleavage of this molecule, resulting in a benzoyl and an α-hydroxyalkyl radical, both of which are capable to react with the acrylate double bond (Decker et al. 2001).

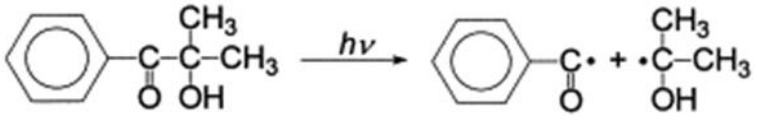

Figure 3.4 – Photocleavage of hydroxy-2-methylpropiophenone molecule (Decker et al. 2001).

To produce free radicals, the photoinitiator first absorbs energy from the light source. The photoinitiator hydroxy-2-methylpropiophenone presents a peak of absorbance for cleavage at 244 nm (Segurola et al. 1999). This wavelength is at the UVC range, which is commonly used as germicidal. Thus, the UV-lamp Sylvania, BL350 was used to initiate the photopolymerisation. Once the radicals are formed, it attacks the monomer, as depicted in Figure 3.5 and the chain polymerisation is initiated.

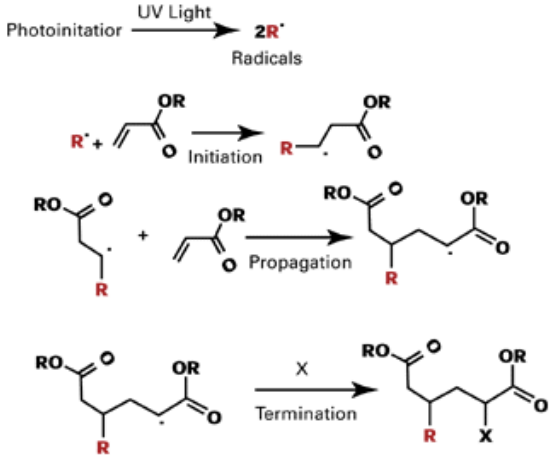

Figure 3.5 – Mechanism of free radical polymerisation of the acrylates (PCI 2000).

The radicals attack the β-carbon, leaving the α-carbon with the formed radical to propagate the reaction. Although the reactivity of α-carbon of acrylates and methacrylates are different, the co-polymers were uniformly formed. The polymerisation is intrinsically vulnerable to inhibition by molecular oxygen, which results in incomplete or failure to cure. The presence of oxygen may quench the excited state of the photoinitiator. Alternatively, it may react with the radicals to form the form peroxyl radicals (ROO•), which are not energetically favorable toward propagating the polymerisation (Ligon et al. 2014). The oxygen inhibition was not a major concern for the polymerisation of the double emulsion since the material was polymerised in water. However, the production of bulky materials was more sensitive to this limitation.

As discussed in section 4.2.2, the difference in density between the inner and middle phase led to the formation of spatially varying shell thickness. Since the gravitational forces are time-dependent, the polymerisation of the acrylate shell was performed as soon as possible. The shortest distance between the formation of the double emulsion and the UV-light to initiate the polymerisation was established by safety reasons, since the UV-light needed to be covered while on. Thus, typically 30 cm tubing was used to carry the double emulsion to the UV-light exposure, as shown in Figure 3.6a. To prevent the coalescence of the droplets, the outlet tube containing the double emulsion was immersed in a collection solution present in a petri dish, as demonstrated in Figure 3.6b. To further minimise the coalescence, a PVA 10% wt solution was used to collect the double emulsion and prevent the formation of agglomerations of microcapsules.

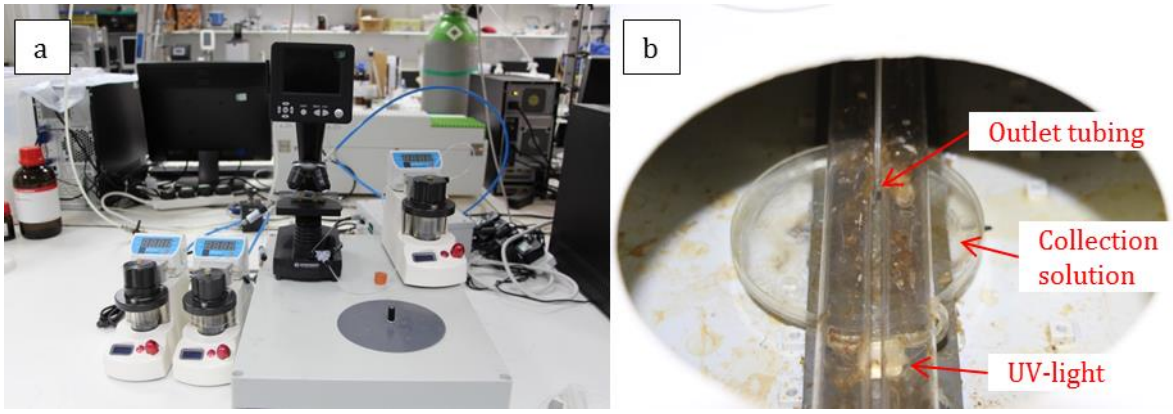

Figure 3.6 – Microfluidic station for the production of the double emulsion and polymerisation of the shell. (a) set-up with the outlet tube inserted in the UV-light box; (b) detail of the tubing inside the UV-light box.

To dry the microcapsules, the collection solution was filtered using a Whatman n º1 filter paper, washed with 20 mL of water and dried at room temperature.

To remove the PVA from the collection solution while still keeping the capsules in water, a pipette was carefully used to remove the PVA solution while water was added.

3.2.5. Progression of work

During initial stages of this research, the encapsulation of aqueous based core was investigated. Water is important during autogenous and some autonomic processes of self-healing, however its microencapsulation for cementitious materials has not been demonstrated yet. The microfluidic device allowed the encapsulation of water-based core containing PVA (BH-82/12, BH-88/7), colloidal silica (BHCS-88/9, UHCS-125/8) and sodium silicate (BH-SS). However, the water is not retained inside of the capsule, leading to two possible outcomes: either the capsule has a thin shell

and deforms during the loss of water core or the capsule has a thick shell and do not deform, but also cannot be physically triggered.

Thus, mineral oil was also encapsulated in order to demonstrate the retention of an organic-based core material. Furthermore, the use of oil-in-oil-in-water (o/o/w) double emulsion resulted in a thinner shell, which facilitate the physical triggering (BIMO-110/2). As a result, the capsule retained its structural integrity during the hardening of the cement paste and some capsules were physically triggered. In addition, emulsions of mineral oil containing sodium silicate (BIMO-SS) and colloidal silica (BIMO-CS) as healing agent were also demonstrated. However, most capsules debonded upon crack formation which was attributed to the poor interfacial bonding between the hydrophobic acrylate shell and the cementitious matrix.

A new methodology was proposed to improve the interfacial bonding between the microcapsules and the cementitious matrix. The capsules were functionalised with hydrophilic groups which are easily bonded with the water-based cementitious matrix. This resulted in a substantial increase of the interfacial bonding, particularly for highly functionalised acrylates. However, capsules with aqueous core still deform during hardening of cement and preclude physical triggering (BH-A, UH-A). On the other hand, capsules with organic core were physically triggered due to the good interfacial bonding and the thin shell of the microcapsules (BIAMO-110/2, BIAMO-140/2). The results obtained during the progression of the work are summarized in Table 3.5.

Table 3.5 – Summary of the microcapsules produced during this work and comparison between the four main parameters investigated in this thesis.

	Sample name	Core material	Core retention	Deformation after drying	Interfacial bonding	Physical triggering
hydrophobic shell	**BH-82/12**	PVA2%	no	no	no	no
	BH-88/7	PVA2%	no	yes	no	no
	BH-CS-88/9	colloidal silica	partially	no	n.m.	no
	BH-SS	sodium silicate	partially	yes	n.m.	n.m.
	UH-CS-125/8	colloidal silica	partially	yes	no	no
	BIMO-110/2	mineral oil	yes	no	no	yes
	BIMO-SS	mineral oil w/ sodium silicate	yes	no	n.m.	n.m.
	BIMO-CS	mineral oil w/ colloidal silica	yes	no	n.m.	n.m.
hydrophilic shell	**20BE-86/14**	PVA10%	no	no	no	no
	BH-A	PVA2%	no	no	yes	no
	UH-A	PVA10%	no	yes	yes	no
	BIAMO-110/2	mineral oil	yes	no	yes	yes
	BIAMO-140/2	mineral oil	yes	no	yes	yes

3.2.6. Fabrication of microfluidic devices

In order to learn how to produce the microfluidic devices, I visited the group of Prof. André Studart at ETH Zurich; Prof. André worked with Prof. David A. Weitz at Harvard University and he has several publications exploring the use of microfluidics for the production of microcapsules. The fabrication of the microfluidic devices is shown in Figure 3.7, and it is based on the publication of Utada et al. (2005) (Utada et al. 2005). The fluidic device consists of cylindrical glass capillary tubes nested within a square glass tube. By ensuring that the outer diameter of the round tubes is the same as the inner dimension of the square tube, a good alignment is achieved to form a coaxial geometry.

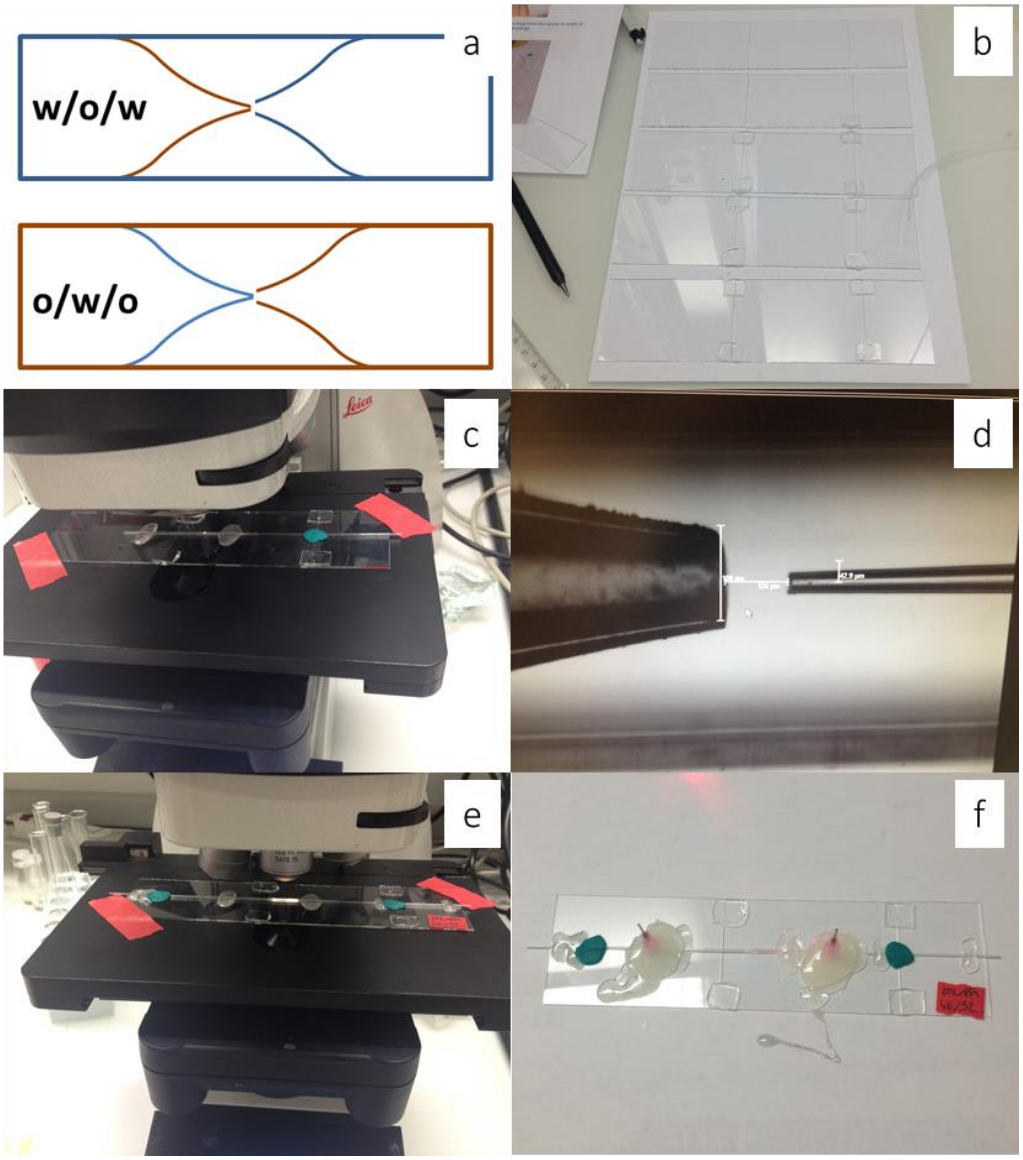

Figure 3.7 – Fabrication of capillary microfluidic devices. (a) schematics of the hydrophobic capillary (in brown) and the hydrophilic capillary (in blue) for the production of double emulsion; (b) glued glass plaques to be used as support; (c) square capillary glued on top of

the glass plaque; (d) alignment of the tubes and adjustment of the distance between the emitter (right) and collector (left) tubes; (e) gluing the emitter and capillary tubes with epoxy; and (f) final device with the needle hub glued over the ends of the square capillary to act as tube connectors for the continuous and dispersed phase.

One end of the inner capillaries was shaped into a tapering orifice with an inner diameter ranging between 30 and 70 μm. To achieve the tapered tube, a flaming micropipette puller (P-97, Sutter Instrument) was used to produce an elongated capillary. Then, to cut the edge of the capillary, the other half capillary tube was used to score the tapered end without break, followed by a smooth and continuous push above the scored location, resulting in the formation of the flat tip. The orifice diameter was then smoothened and/or increased by sanding the tip against abrasive paper. The capillary was cleaned with air to remove any glass debris and the emitter capillary was immersed in a solution of toluene with 10% of Trimethoxy(octadecyl)silane (ODTMS) and 1% of n-butylamine for 2 hours. Next, the inner tapered capillary was washed with ethanol and dried at room temperature. For the production of double emulsion of water-in-oil-in-water (w/o/w), the emitter capillary needs a hydrophobic coating, as shown in Figure 3.7a. Alternatively, for the production of double emulsion of oil-in-water-in-oil (o/w/o) the collector tube and the square external capillary must be hydrophobic. This hydrophobisation facilitates the flow of the oil phase around the emitter tube, and consequently the engulfing of the inner droplet; it also make sure that the outer phase of the double emulsion have little to no interaction with the collection tube.

The treated round capillary was partly inserted into the square capillary (Figure 3.7c) and a microscope was used to align the capillaries and also to adjust the distance between the collector and the emitter, commonly between 120 and 180 μm (Figure 3.7d). Then, the capillaries were in position using epoxy resin adhesive (5-Minute Epoxy®, Devcon), as shown in Figure 3.7e. Hypodermic needles with polypropylene hub (BD Precisionglide®, Sigma–Aldrich, UK) were dented and allocated over the ends of the square capillary to act as tube connectors for the continuous and dispersed phase and then glued in this position. After glued, the needle shaft can be used to connect the tubings and pump the liquids within the device; the end of the capillaries can also be connected with the tubings to pump the inner fluid and collect the formed double emulsion. The innermost fluid is pumped through a tapered cylindrical capillary tube, and the middle fluid is pumped through the outer coaxial region, which forms a coaxial flow at the exit of the tapered tube. The outermost fluid is pumped through the outer coaxial region from the opposite direction, and all fluids are forced through the exit orifice formed by the remaining inner tube.

Although the produced devices provided a straightforward formation of the double emulsion, the flow-focusing microfluidic device was selected to be used in the thesis. The capillary device is cheaper, but more time consuming to produce and, more importantly, if the hydrophobisation step

is not carefully done, the double emulsion is not formed. Also, if the tubes are not perfectly aligned and trimmed it precludes the formation of the double emulsion. Lastly, the main problem was the blockage of the emitter tube because of dust and debris. Since this tube had a small end, ~30-70 μm, it was easily clogged, and very difficult to unclog it, mainly because the amount of fluids that can go inside such a small tube is reduced.

3.3. Testing procedures

3.3.1. Microscopy Images

To manipulate the microfluidic device and observe the formation of different flow regimes, Bresser LCD microscope was used.

To observe and measure the formed double emulsion, an optical microscope (OM) (DM 2700 M, Leica, Germany) was used. To confirm the formation of core-shell structure and investigate the morphology of the microcapsules, a scanning electronic microscope (SEM, Phenom, Pro G2, Netherlands) was used. Before being inserted in the SEM, the microcapsules with aqueous core were dried at room temperature for 1 day and then cut with a razor blade on the SEM stubs. The microcapsules with oil core were ruptured between two glass slides, washed with ethanol to remove the mineral oil, and vacuum dried as preparation for SEM.

The SEM was also used to investigate the mechanical triggering and interfacial bonding of the microcapsules embedded in the cement paste. Cement paste was produced by hand-mixing 20g of Portland cement (CEMI 52.5N) with 9g water (water-to-cement ratio of 0.45) and ~0.7g of microcapsules. Next, the cement paste was casted for 24h in the mould shown in Figure 3.8a. After casting, the prisms (10x10x100 mm) were demolded (Figure 3.8b), a small portion was fractured for SEM observation. The rest of the cement/microcapsules prisms were submerged for further hydration and SEM observations took place at 1, 7, 14, 28 and 64 days, unless specified otherwise.

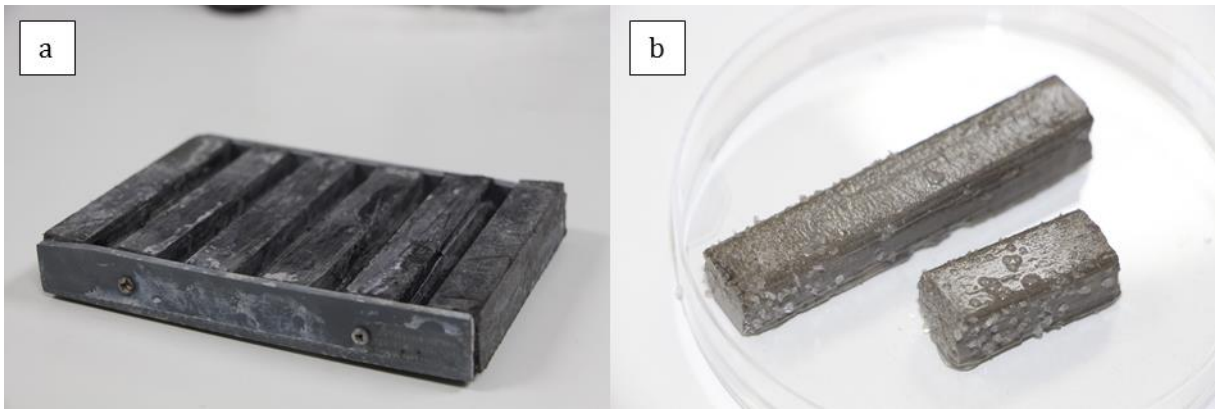

Figure 3.8 - Integration of capsules in the cement paste: (a) mould used to cast the samples; (b) produced sample broken after immersion in water.

Before being observed in the SEM, the cement sample was dried at room temperature for at least 1 day. Then, the sample was attached to the stub using a carbon tape, blasted with an air duster and vacuumed.

3.3.2. SEM-EDX ANALYSIS

To investigate the retention of colloidal silica inside the microcapsules, SEM-EDX analysis was performed using a Nova nanoSEM 450 equipped with a Bruker Quantax Xflash 6/100 EDX detector. Dry microcapsules were placed in the stub, a razor blade randomly cut the microcapsules and the sample was examined under a 10 kV accelerating voltage.

3.3.3. THERMOGRAVIMETRIC ANALYSIS

Thermogravimetric analysis (TGA) was performed to characterise the thermal properties and stability of the microcapsules, the shell and core materials. To investigate the shell, the microfluidic device was used to produce single emulsion which was polymerised into acrylate beads. To investigate the core, a single droplet (< 1 mL) of aqueous solution or mineral oil was added to the crucible. To investigate the microcapsules, ~5 mg of material was used. The TGA was performed under air atmosphere, between 100 and 700°C at a rate of 5°C/min, using PerkinElmer STA6000 and alumina crucible. To assess the thermal stability and water content, the microcapsules were dried at room temperature for 1 day before analysis, unless specified.

3.3.4. DYNAMIC MECHANICAL ANALYSER

To analyse the glass transition temperature of the acrylates BI and UH, a dynamic mechanical analysis (DMA) was used. In a DMA, an oscillating force is applied to the sample, causing a sinusoidal stress to be applied to the sample, generating a strain. The representation of the equipment used in this thesis and the resulting sine waves is shown in Figure 3.9. As shown in Figure 3.9 (left), the DMA applies an oscillatory force, causing a sinusoidal stress to be applied to the sample, generating a strain. By measuring both the amplitude of the deformation at the peak of the sine wave and the lag between the stress and strain sine waves (Figure 3.9, right), quantities like storage modulus, viscosity and the damping can be calculated. Hence, the elastic modulus can be obtained each time a sine wave is applied, enabling the record of the modulus as a function of temperature and thus the glass transition temperature. The modulus measured in DMA is, however, not exactly the same as the Young's modulus of the classic stress-strain curve. Young's modulus is the slope of a stress-strain curve in the initial linear region. In DMA, a complex modulus (E*), the

storage modulus (E') and an imaginary (loss) modulus (E'') are calculated from the material response to the sine wave.

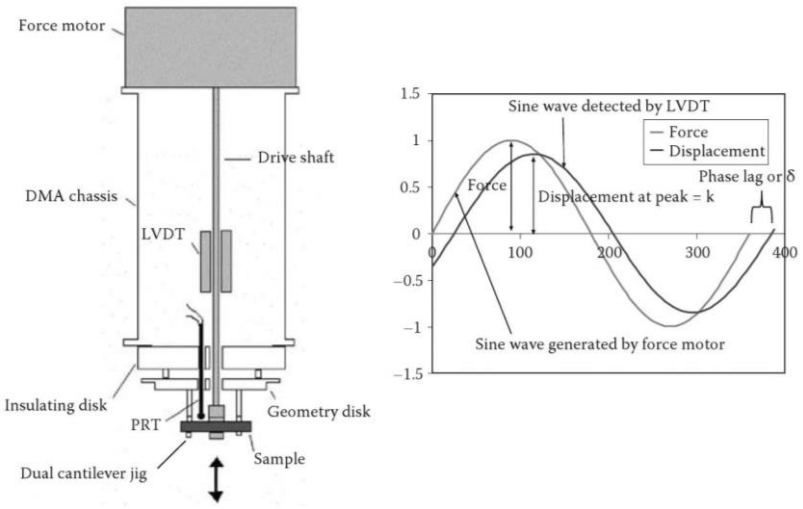

Figure 3.9 – Representation of dynamic mechanical analysis (DMA): (left) schematic of the equipment and (right) applied stress-strain curve indicating the phase lag.

DMA measurements were performed on a DMA 8000 apparatus (PerkinElmer, Waltham, MA, USA) operated in tension mode. The samples (~25 × 6.5 × 0.3 mm) were placed in a dual cantilever jig and subjected to a frequency of 1 Hz at a heating rate of 5 °C min^{-1} from −60 to 120 °C. In this way, the storage modulus (E′), loss modulus (E″) and loss factor (tan δ) can be achieved; the glass transition temperature was considered based on tan δ peak.

To prepare the sample for the DMA, ~2 mL of acrylate copolymer was poured in a petri dish and carefully covered with a PVA 10% wt solution. The aqueous solution was used to minimise the contact with oxygen and to disperse the heat of the exothermic polymerisation reaction. Then, the sample was placed on top of the UV-lamp and polymerised for 10 min. To assure the entire polymer was polymerised, after 2 min the sample was turned. After the polymerisation, the sample was washed with ethanol to remove any unpolymerised monomer and the PVA solution. The flat disc of polymerised acrylate was cut into small samples to perform the test.

3.3.5. Microindentation

A microindententor was used to calculate the hardness and Young's modulus. The microindentation test was performed by applying and removing a load to a sample in a controlled manner with a geometrically well-defined probe to induce local surface deformation. The response of interest is the load–displacement curve (often called the P–h curve, Figure 3.10), which is used to calculate the micromechanical properties of a sample. The global shape of the P–h curve differs between materials, and these variations typically reflect the different mechanical properties. As seen at the

Figure 3.10, the maximum load (P_{max}), maximum penetration depth (h_{max}), contact depth (h_c), and final depth (h_f) measured during microindentation test were observed in the load–displacement curve.

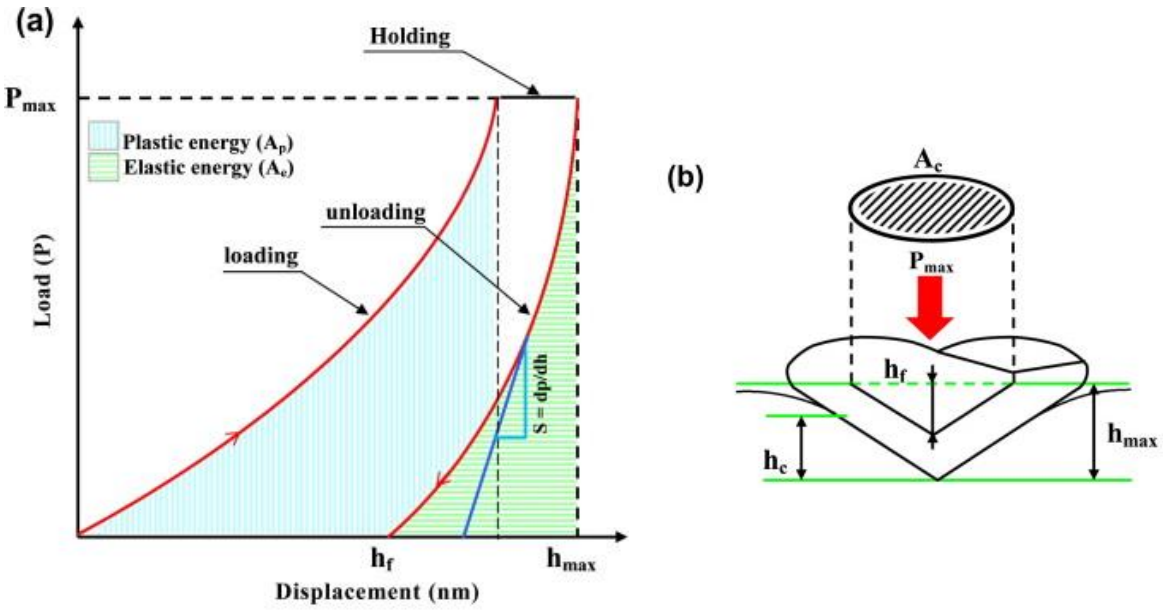

Figure 3.10 - Schematic representation of the principle of microindentation (a) a typical load–displacement curve and (b) the interaction between the tip of the indenter and the sample during the indentation test (P_{max} = maximum applied load; h_{max} = maximum penetration depth; h_c = contact depth. Adapted from (Ghorbanzadeh Ahangari et al. 2014)

The mechanical properties of the material, such as elastic modulus and hardness, can be calculated by using the equations based on elastic contact theory. The contact stiffness (S), which is defined as the slope at the beginning of the unloading curve, is given by

$$S = \frac{dP}{dh} \qquad \text{Equation 3.7}$$

where p is the indentation load and h is the indentation depth for the determination of the slope. The parameters between the tip of the indenter and the specimen that are used for analyzing the data during the indentation process are shown in Figure 3.10. The elastic modulus (E) and hardness (H) were measured by the Oliver and Pharr method (Oliver and Pharr 1992), which states that the hardness and elastic modulus can be measured by analysing the unloading part of the load–displacement curve. If the indenter is considered to be much stiffer than the probed material, the hardness is defined as the maximum load divided by the contact area of the indenter at the maximum load (A_c)

$$H = \frac{P_{max}}{A_c}$$ Equation 3.8

The maximum value of 1000 mN was chosen in order to achieve a deeper penetration of the indenter over the meniscus area with a more uniform response. The reduced modulus (E_r), also called indentation modulus (EIT), can be calculated from the slope of the linear portion, dP/dh upon unloading

$$E_r = \frac{\sqrt{\pi}}{2}\frac{dP}{dh}\frac{1}{A_c}$$ Equation 3.9

And E_r is related to the elastic modulus (E) of the sample and the elastic modulus of the indenter by the following equation:

$$\frac{1}{E_r} = \frac{1-\nu^2}{E} + \frac{1-\nu_i^2}{E_i}$$ Equation 3.10

where E and ν are the elastic modulus and the Poisson's ratio of the specimen, respectively. The elastic modulus (E_i) and the Poisson's ratio (ν_i) of the diamond indenter are 1141 GPa and 0.07, respectively (Anton Paar 2014). In addition, ν was considered as 0.35 based on the Poisson ratio of acrylates (Chen et al. 2014a).

The preparation of the samples for the microindentation test is shown in Figure 3.11. Approximately 4 mL of each acrylate solution was poured in a cylindrical recipient (Figure 3.11a), covered with 5 mL of PVA 10% wt to avoid the intrusion of oxygen and to disperse the heat of the highly exothermic polymerisation reaction. The solution was placed over a UV-lamp for 10 minutes, followed for 10 minutes of lateral exposure. Once the material was polymerised, the disc was demoulded (Figure 3.11c), and washed with ethanol solution to remove reminiscent PVA and unreacted acrylates. The formed polyacrylate disc was washed with ethanol and the meniscus formed at the bottom of the sample removed using a disc cutter (Presi Mecatome T255/300, France). To obtain a smooth surface for the indentation, the top surface was carefully wet ground with 1200, 2500 and 4000 grit SiC paper (MetPrep, UK), followed by final polishing using 0.3 micron alumina suspension (MetPrep, UK) on a Mecapol P225 (Presi, France). The resultant disc was 32 mm diameter and 10 mm thickness and the indentation was performed on the polished top surface one day after the polymerisation (Figure 3.11d).

The instrumented indentation platform (MHT, Anton Paar, Switzerland, Figure 3.11b) was used with a Vickers diamond indenter. The samples were loaded at a rate of 400 mN/min until a peak of 1000 mN when the maximum load was kept constant for 20s and then the samples were unloaded

at the same rate. For each sample, at least 15 indentations were performed at different points on the surface.

Microindenation was also used to measure the Young's modulus of single microcapsules. The microcapsules were carefully dispersed over a steel stub coated with a thin layer of glue. A flat punch indenter (200 μm diameter) was used to obtain the load-displacement curve used for the calculation of the Young's modulus. Three microcapsules were loaded at a rate of 30 mN/min until a peak of 30 mN when the load was kept constant for 10s and then the samples were unloaded at the same rate.

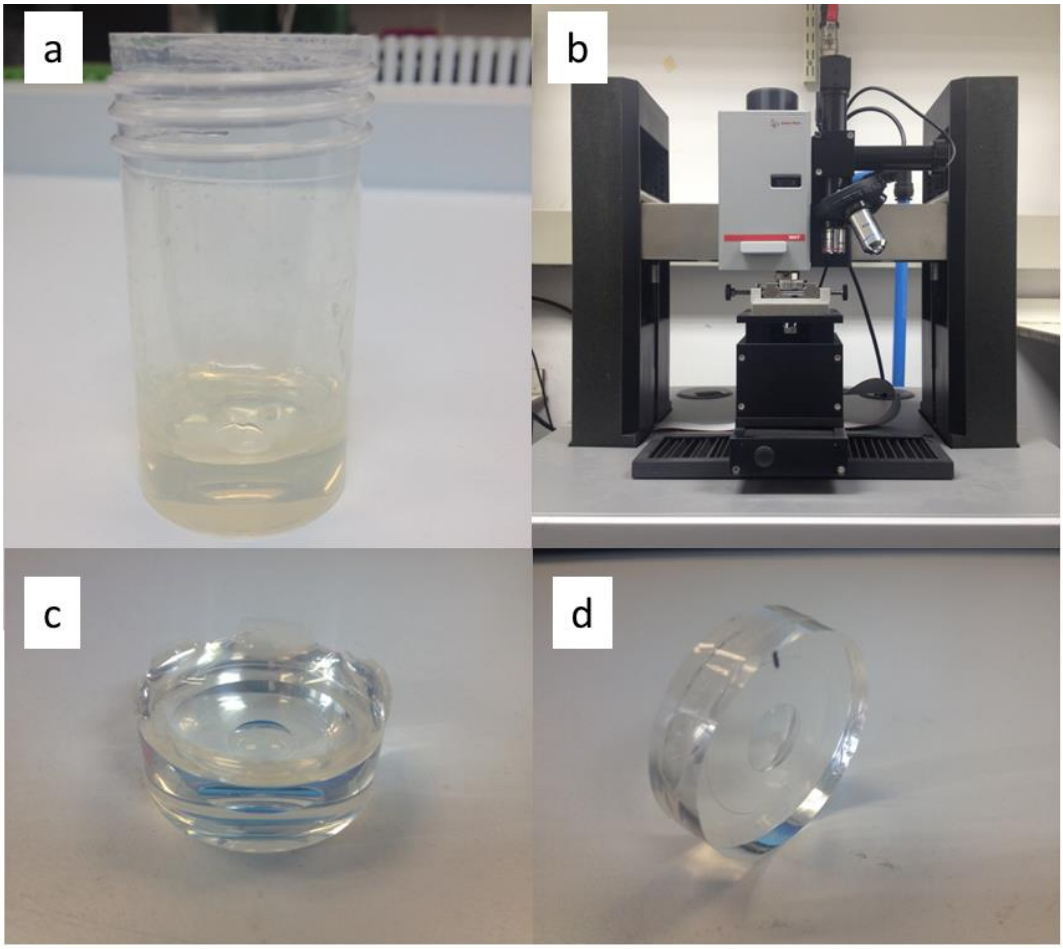

Figure 3.11 - Preparation of the sample for the microindentation test: (a) cylindrical mould, (b) instrumented indentation platform, (c) demoulded disc after the polymerisation and (d) final disc for indentation after the removing the polymerised meniscus.

3.3.6. TENSILE STRENGTH

To investigate the tensile properties, an electromechanical universal testing machine was used (model 1011, Intron Corporation Ltd, USA). To prepare the sample, approximately 1 mL of acrylate was poured and spread in a plastic petri dish. Then, the solution was covered with PVA 10% to

avoid the intrusion of oxygen and to disperse the heat of the exothermic polymerisation reaction. The petri dish was placed over a UV-lamp for 5 minutes; after the polymerisation, the acrylate sheet was demoulded and washed with ethanol solution to remove reminiscent PVA and unreacted acrylates. The sheet was then cut into small plaques (8 x 0.4 mm) to perform tensile tests. This procedure was carried out shortly after the polymerisation to prevent the formation of small cracks during cutting. The tests were performed in the Instron machine with maximum load of 250 N, crosshead speed of 1 mm min^{-1} and the gauge length was 20 mm. The tests were carried out at 20 ± 2 °C. The tensile stress is expressed in MPa, this being calculated by dividing the load (in Newtons) at break by the cross-sectional area of the plaque (in mm^2). The strain (in %) was calculated by dividing change in length of the specimen by the original length.

4. SYNTHESIS OF MICROCAPSULES USING MICROFLUIDICS

How can microfluidics be employed to produce microcapsules? Can these microcapsules encapsulate common mineral healing agents for the self-healing of cementitious materials? What can be learnt about the limitations of using microfluidics capsule-based self-healing? These are the main questions which inspired the work presented in this chapter, providing a comprehensive understanding of microfluidic encapsulation of liquid healing agents. The initial part of this chapter looks at the experimental protocol for the production of fully closed microcapsules: the use of the microfluidic device for the assembly of the double emulsion, the solidification of shell via photopolymerisation and the formation of fully closed shells. Subsequently, the different flow regimes used for the production of double emulsion were investigated as well as the control over size and shell thickness of the capsules. The established protocol and the tuning of the shell properties were used to encapsulate aqueous core materials, including water, colloidal silica and sodium silicate. Furthermore, the use of different epoxy and urethane-based acrylate as shells was also explored. The retention of the core material was investigated using TGA and EDX and indicated that the water was not retained inside the microcapsules and the mineral healing agent remained solid inside the shell. Hence, to investigate the production of microcapsules capable of retaining a liquid material, organic core was also investigated. Furthermore as proof-of-concept, the encapsulation of emulsified sodium silicate and colloidal silica was demonstrated.

4.1. SETTING-UP A MICROFLUIDIC STATION

Microencapsulation using microfluidics relies on two steps: the use of the microfluidics device to produce the emulsion template and the solidification of a shell to produce the microcapsule (Figure 4.1). Several factors influence both stages of the process, such as the fluid dynamics inside the microchip, the physicochemical properties of the liquids and the assembly during the photopolymerisation stage. The literature describing these factors is abundant, ranging from the theoretical aspects of fluid dynamics to the applications of produced microcapsules in a wide range of fields. However, the experimental details and procedural set-up are not as prolifically reported, mostly because the research groups have already developed the expertise to deal with the microencapsulation using microfluidics. Thus, a preliminary investigation was necessary to tackle a variety of challenges arising from setting-up a protocol to produce fully closed microcapsules. Predominantly, this section deals with the initial investigation for the production of the double emulsion and for the polymerisation of the shell.

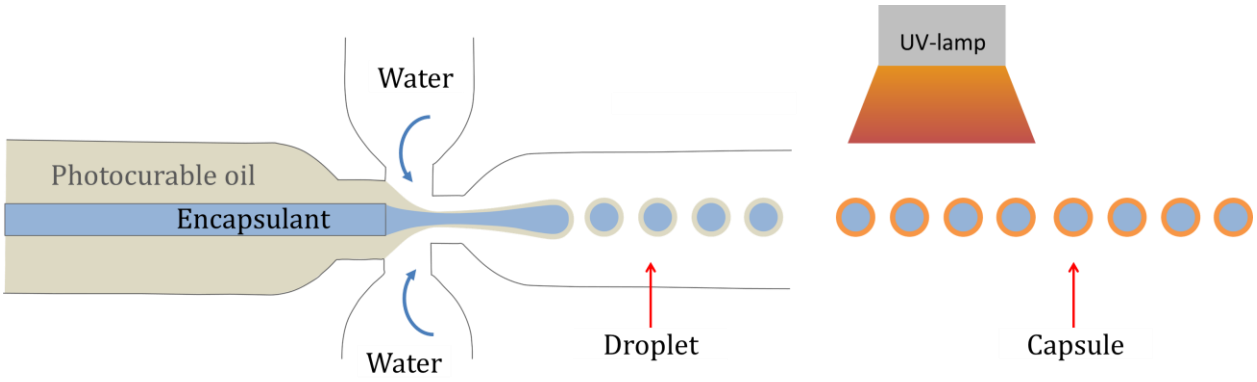

Figure 4.1 – Schematic representation of the microencapsulation using microfluidics in which the double emulsion is produced in the microfluidic device, followed by the photopolymerisation of the shell using a UV-light.

4.1.1. Production of double emulsion

To set up a microfluidic station, a commercial flow-focusing microfluidic device was chosen to overcome the challenges associated with producing a device. The devices were purchased from Dolomite, cost ~£600 and last for approximately 6 months, depending on the conditions of use. Once the devices were in the laboratory, the initial challenge was to properly connect the tubings to the device. The 0.8 mm tubing was first connected to the rubber seal inside the H-interface (Figure 3.2) and then the H-interface was screwed around the microchip. In this step, it was necessary to develop a certain skill to sense if the H-interface is properly attached: if the screwing is too loose, there would be leakage; if the screwing is too tight, it would block the fluids' flow to inside the channels of the device.

When the microchip was connected to the tubings, the syringe pumps were used to pump the inner, middle and outer phases inside the device. Initial tests to use the microchip were performed using syringe pumps capable of pumping liquids at a minimum flow rate of 0.05 mL/h. BH, a mixture of HDDA and BisGMA, was selected as shell because of its stability during the encapsulation of amines for self-healing of polymers (Chen et al. 2014b). To adjust the interfacial tensions and also prevent the coalescence of the double emulsion, an aqueous solution of 2% wt. poly(vinyl alcohol) (PVA) was used. The efficient stabilisation of droplets with PVA is due to steric hindrance imposed by the polymer adsorbed at the liquid interface, which prevents close approximation between adjacent droplets (Chen et al. 2012).

In the first attempts to use the microfluidic device, the goal was the production of a simple o/w single emulsion. BH was used as middle phase and PVA2% as outer phase and different flow ranges were explored. However, the single emulsion was not formed. At low values of middle and outer flow rate, a biphasic system would be formed in the outlet tubing of the microchip, as shown in

Figure 4.2a. When the BH flow rate was increased to 0.5 mL/h, the dispersed phase was focused and encapsulated by the continuous phase PVA2%. This co-flow system would be stable, independent of the outer flow rate as shown in Figure 4.2b,c,d. When the outer flow was 15 mL/h, the middle flow would start to counterflow.

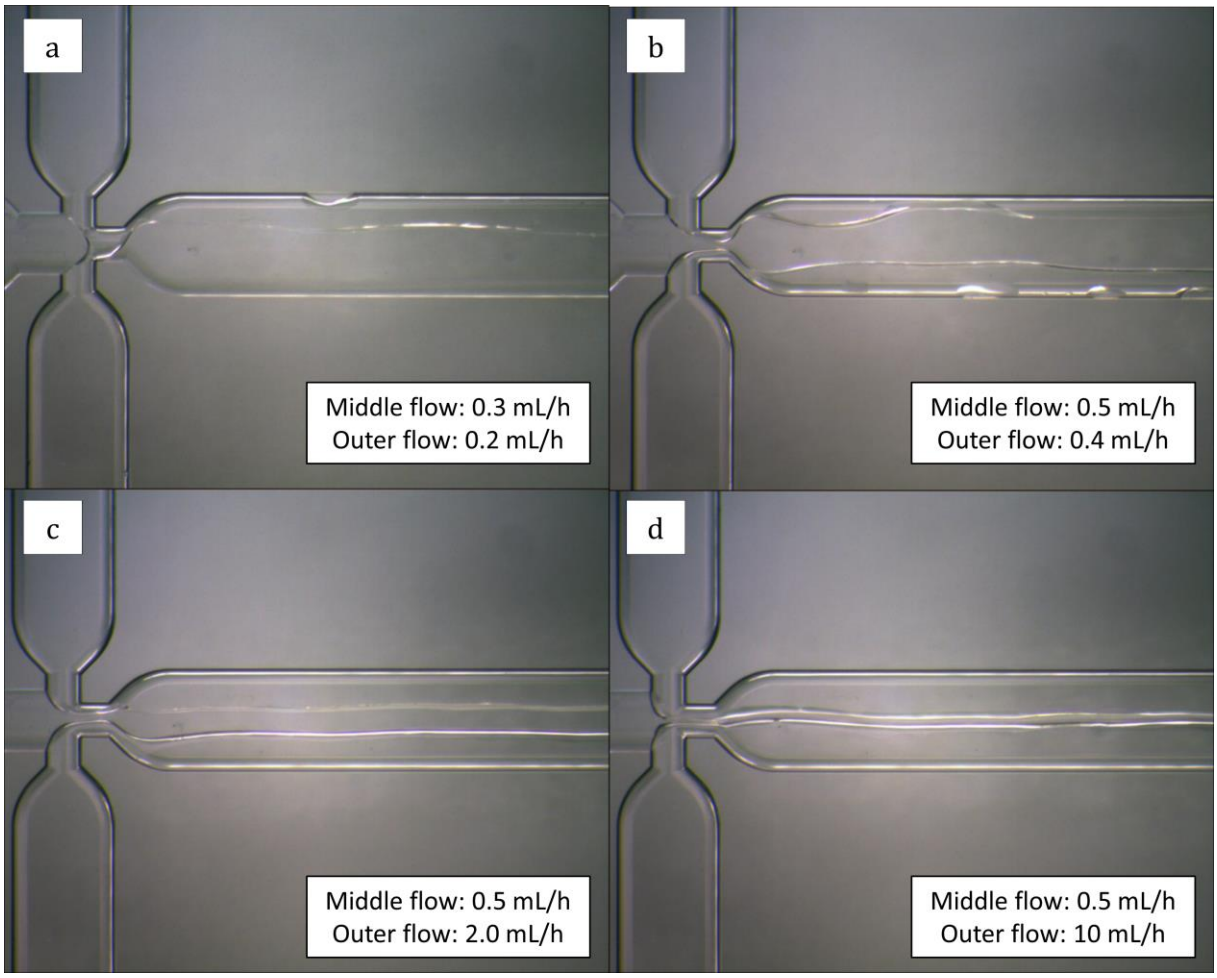

Figure 4.2 – Optical microscope image of the microfluidic device during the attempt to produce a single emulsion.

To produce an emulsion at the flow rates provided by the syringe pump, the inner phase was also used, as shown in Figure 4.3. The successful formation of the double emulsion is very sensitive to variations in the flow rate, as illustrated in Figure 4.3 (bottom) where the inner flow rates was varied between 0.9 and 0.4 mL/h. When the inner flow was higher than 0.4 mL/h, just the single emulsion was formed and an increase in size dispersion of the single emulsion was also observed. However, the difficulty in forming the double emulsion with an increase of the flow rate indicated that there is an upper limit of core-to-shell ratio. Furthermore, the flow regime was also sensitive to the flow rates: when the outer flow rate was increased, the middle phase was squeezed and commonly just adhered to the walls of the device, instead of staying in the middle. At lower flow

rates of the outer fluids, the pressure of the middle phase was overwhelming and just pumped outer fluid in a counterflow. Thus, the drops were produced in the jetting regime and in a small window of flow rate which was challenging to vary while still succeeding in producing a double emulsion. Additionally, despite the syringe pumps being capable of pumping fluids in order to produce the double emulsion, they were not fit to be used in the microfluidic device. In a syringe pump, an electrical engine sets an endless screw in motion and sets motion to the syringe's piston. At low flow rates, closer to the low limit of the syringe, the step-by-step operation of the electrical engine was noticeable because the syringe pump's piston had to move very slowly to deliver the required flow rate. As a result, oscillations in the flow rate were observed and the fluid flow was not uniform over time. Thus, to use the microfluidic device, pumps working at a lower flow rate range were necessary. Furthermore, the reduced control over the flow rates using the syringe pump resulted in the impractical regulation over the shell thickness and size of the double emulsion through the flow rate.

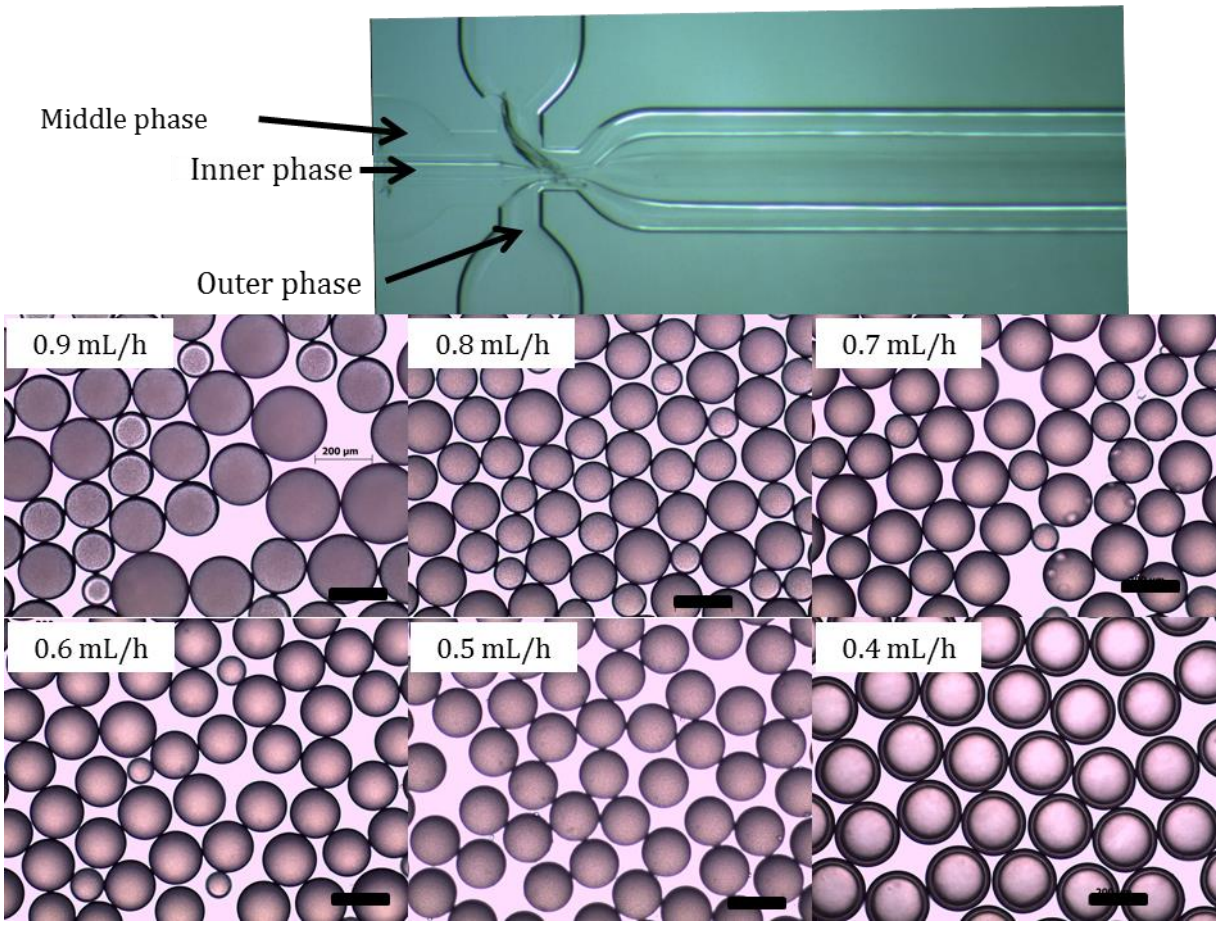

Figure 4.3 – Optical microscope image of the device used for the formation of the double emulsion (top) and variations in the formation of the single and double emulsion according to the inner flow rate (bottom). All the emulsions were formed using an middle flow rate of 0.4 mL/h and an outer flow rate of 4 mL/h. Scale bar indicates 200 µm.

Nonetheless, the interfacial tension between the hydrophobic middle phase and the hydrophilic outer phase and the viscous forces of the fluids resulted in the formation of the double emulsion. At the flow rate of 0.4, 0.4 and 4 mL/h for inner, middle and outer fluids, the system was similar to a tubing regime, where the middle phase would continuously flow and squeeze the outer fluids in the walls of the collection tube in the microfluidic device (Figure 4.3top). This protocol resulted in the production of double emulsion of water-in-oil-in-water (w/o/w) with 225 μm of outer diameter and 26 μm of middle layer thickness. The order of initiating the pumping of the fluids inside the device was extremely important and if the fluids were not carefully introduced, the double emulsion would not form. First, the middle fluid was pumped, followed by the careful pumping of the outer fluids, initially at low velocities to assure that the aqueous solution was touching the collection tube walls and surrounding the middle phase, but without squeezing the middle fluid in the cross-junction. Last, when the system was stable, the inner fluid was pumped; since the inner flow was not being pumped during the stabilisation of the middle and outer flow, typically the capillary tune was also used as an outlet tube. Thus, when the inner fluid was pumped, the initial flow would be the middle phase and then the inner fluid would be inserted in the device. The main issue with this approach was that the initial insertion of the middle fluid resulted in a contact with the collection tube of the device and the FEP tubing and made it less hydrophilic. As a result, the coalescence of the double emulsion was more likely and the system would have to be washed with ethanol and started again.

4.1.2. Polymerisation of the shell

To form the microcapsules, the double emulsion produced using the microfluidic device was used as template for the photopolymerisation of the shell. In this protocol, the acrylate middle layer contained a photoinitiator, namely 2-hydroxy-2-methylpropiophenone, which forms radicals in the presence of UV-light. These radicals initiate the polymerisation reaction of the acrylate and result in the solidification of the middle layer and the formation of the core-shell structure. Figure 4.4a shows the flow regime for the formation of the double emulsion using BH as acrylate middle fluid, with PVA 2% being used as the inner and outer fluids and with the flow rate of 0.5, 0.4 and 4 mL/h for the inner, middle and outer fluid, respectively. The high flow rates for the middle and inner fluids caused a more turbulent flow (Figure 4.4a), and resulted in the formation of double emulsion with different sizes (Figure 4.4b). Following the production of the double emulsion, the first attempt to consolidate the acrylate was performed in batch synthesis. The produced solution w/o/w double emulsion was collected for 1 hour in a small vial and then the vial was placed above a UV-lamp. The polymerisation of the shell was quickly confirmed by the observation of the solid shapes of the shell in an optical microscope (Figure 4.4c and d). This resulted in the core-shell structure encapsulating the aqueous solution containing 2% PVA. However, the microcapsules

were not uniformly polymerised and it was common to observe the formation of just polymerised beads (Figure 4.4c). Furthermore, the zoom in the formed shell (Figure 4.4d) shows the formation of black sports, possibly due to the formation of nanopores during the photopolymerisation.

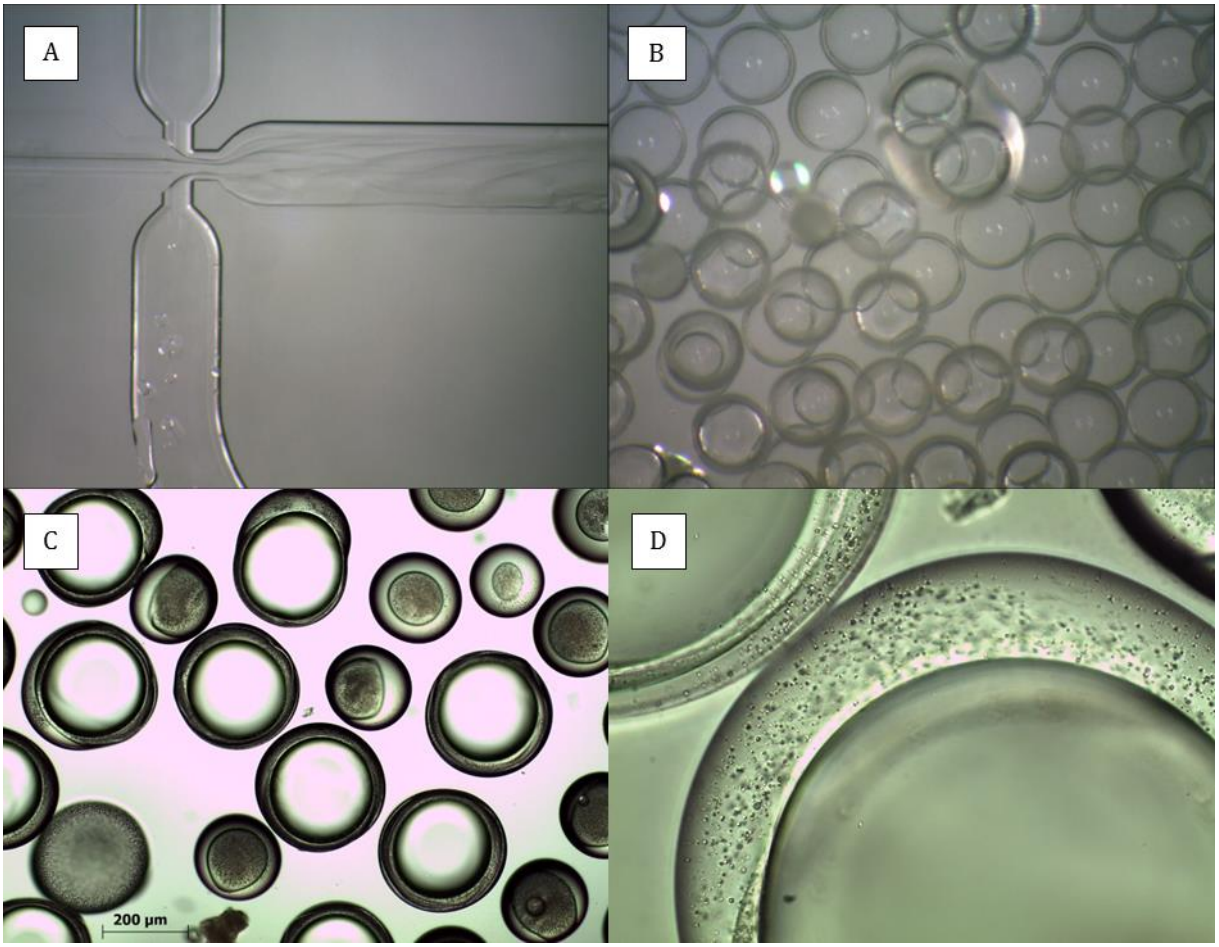

Figure 4.4 – Optical microscope images of the initial attempt to produce microcapsules. (a) the turbulent flow occurring in the microfluidic device; (b) the double emulsion produced; (c) and (d) images of the microcapsules in water shortly after polymerisation.

The microcapsules were observed in a scanning electron microscope (SEM) to investigate the formation of the core-shell structure and the morphology and structure of the shell. The produced microcapsules were first washed with water to remove the outer solution containing PVA, filtered and dried in air for 24h. The shell material had a smooth aspect and no visible pores were observed (Figure 4.5) and a core space was observed, indicating the formation of the core-shell structure. However, the microcapsules presented large holes in the shell, some of which had a uniform shape and appeared to be formed during the polymerisation (Figure 4.5a). Interestingly, a capsule with a ripped shell was also observed (Figure 4.5b) indicating that the hole was formed after the polymerisation of the shell. In both cases, the formation of the holes prevented core retention and was detrimental for the microencapsulation of healing agents.

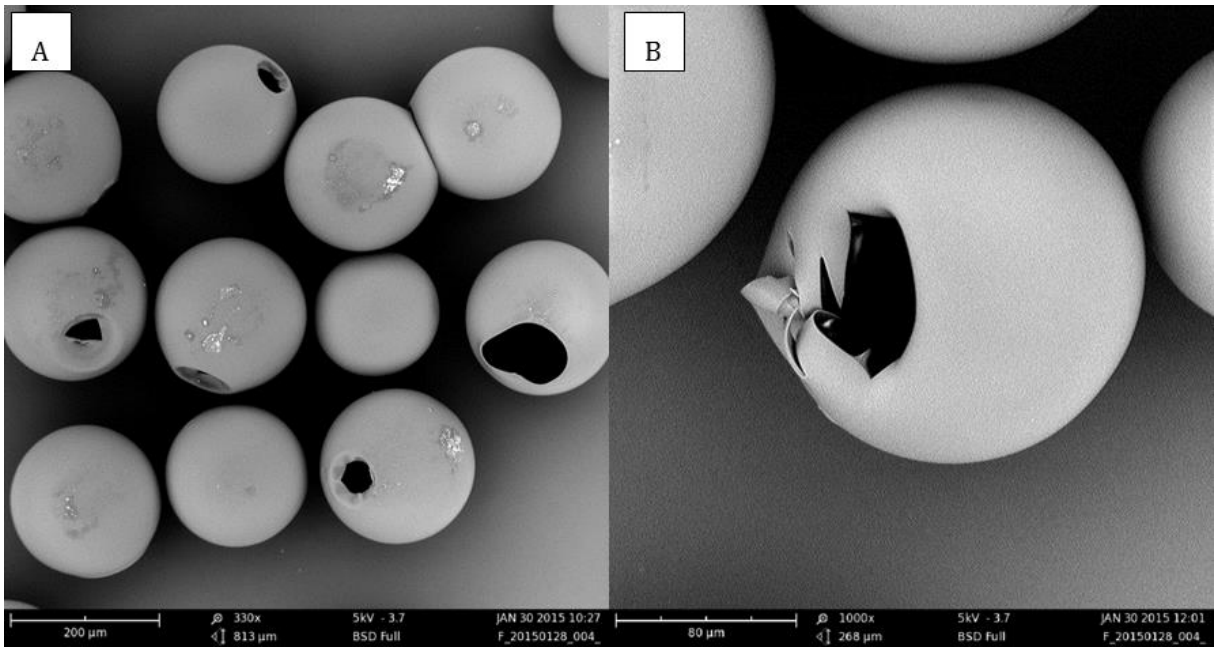

Figure 4.5 - SEM images of the microcapsules with BH as shell and PVA 2% as core material (a) formed capsules with holes and (b) ripped shell resulting in the hole.

To investigate the microcapsules formed with different materials, a mix of 50 % BisGMA, 40% IBOA and 10% HDDA, named BIH was used as precursor of the shell, and presented in section 3.3.2. As reported in the literature, HDDA shrinks during the polymerisation by ~16% (Ji et al. 2013), thus IBOA was investigated due its lower shrinkage. The BisGMA was used to increase the viscosity of the middle phase, IBOA, due to the reduced shrinkage and HDDA due to its crosslinking properties. The ripped shell of BH hinted that the formed holes could be due to the shrinkage of the shell during polymerisation. The double emulsion was formed in the tubing regime with 0.3, 0.4 and 5 mL/h as inner, middle and outer flow rates, respectively and PVA 2% as inner and outer phases. The double emulsion was collected for one hour prior to photopolymerisation. SEM on the dried microcapsules showed that the shells had also holes. Furthermore, the capsules had a buckled shape, in which the shell curved inwardly in the capsule (Figure 4.6a). The broken shell shows a spatially varying shell thickness, in which the bottom is thicker than the top (Figure 4.6b). A negative pressure in the thin part of the shell leads to the buckling in Figure 4.6a and could rupture the shell as in Figure 4.5b. This indicates that the HDDA shrinkage was not the main factor governing the hole formation, but the spatially varying shell thickness.

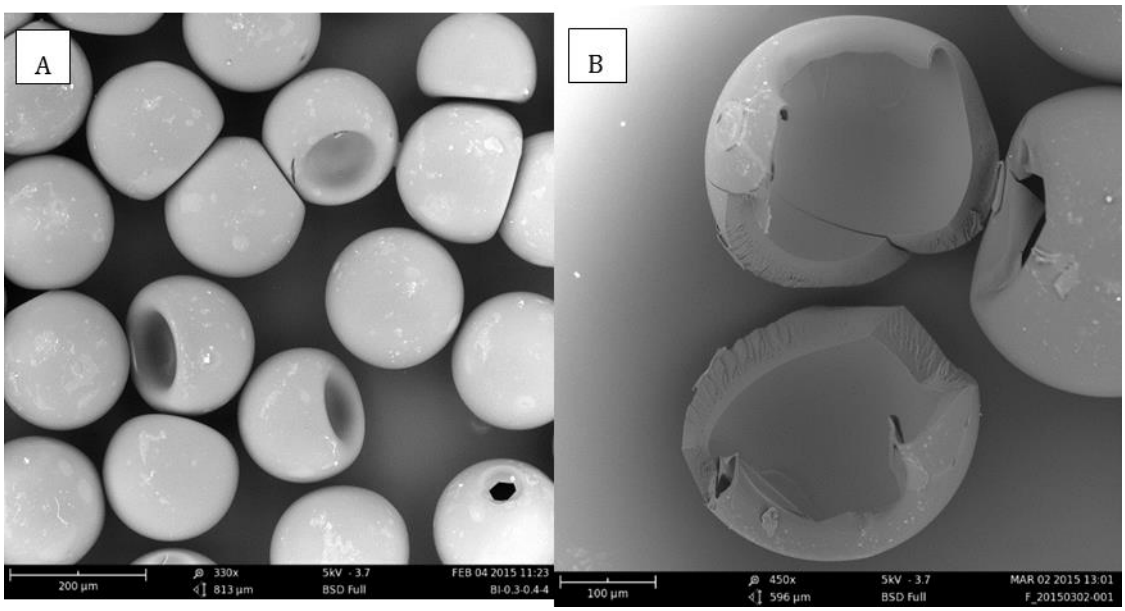

Figure 4.6 – SEM images of microcapsules with BIH as shell and PVA 2% as core material (a) the formed buckled capsules and (b) spatially varied shell thickness.

The spatially varying shell thickness arises from the microcapsule fabrication process. The difference in density between the polyvinyl alcohol solution used as inner droplet and the acrylate used as outer droplet resulted in the gradual rise of the lighter inner droplet after the collection (Datta et al. 2012). The oil layer is gradually thinner on the topside of each droplet and thicker on the bottom, as shown schematically in Figure 4.7.

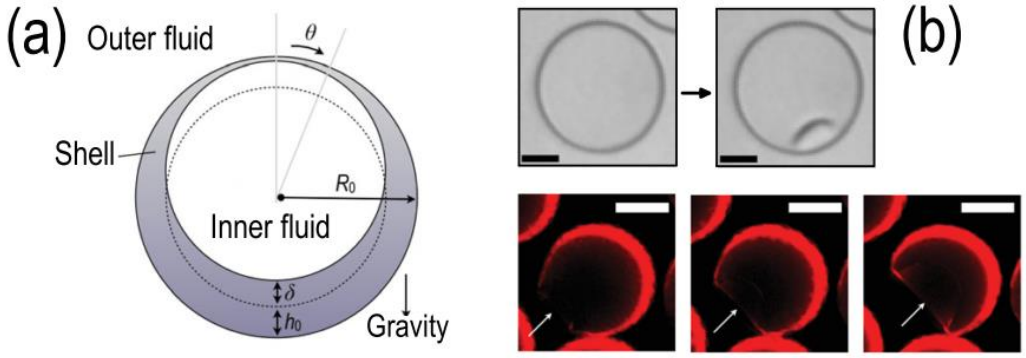

Figure 4.7 – Formation and buckling of inhomogeneous microcapsules. (a) Schematic showing the geometry of inhomogeneous double emulsion-templated microcapsules and (b) Images of buckling beginning at the thinnest part of the microcapsule shell - scale bars 50 µm. Adapted from (Datta et al. 2014).

The gravitational settling caused by the density mismatch of the inner and middle fluids resulted in the formation of inhomogeneous double emulsion templates, and, consequently, non-uniform capsules. Furthermore, combined with variations in the interfacial tension between the core and

the shell, the core may have escaped during the polymerisation, leading to the formation of fishbowl shaped microcapsules. Figure 4.8 shows the buckling process of the capsules where the capsules had an off-centred core, and consequently, an inhomogeneous shell with the capsule still submersed in water. After 13 minutes, the surrounding solution was dried and the core-shell structure was no longer observed. Nonetheless, the region with the thinner part of the shell was no longer curved, but formed a plateau. After 20 min, all the surrounding and inner solution evaporated, resulting in the buckling of the capsule at the thinnest part. This process resulted in buckled capsules similar to the ones illustrated in Figure 4.6a.

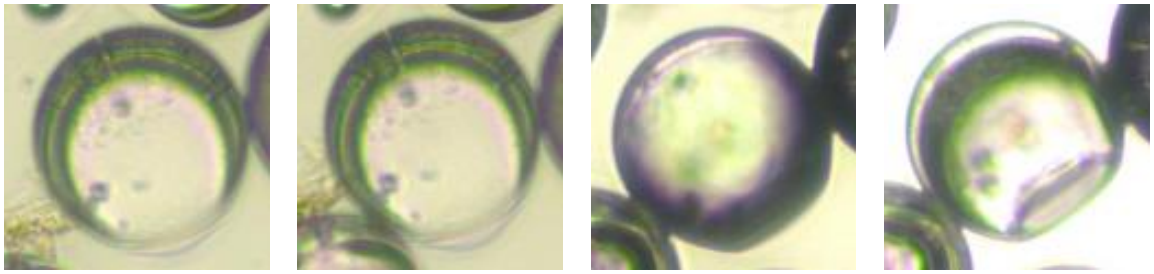

0 5 min 13 min 20 min

Figure 4.8 – Optical images of the buckling of the microcapsules during the drying process.

4.1.3. THERMAL STABILITY

In order to evaluate the chemical composition and thermal stability of the produced microcapsules, TGA analysis of the samples was conducted. The thermal stability of microcapsules is a vital factor, as it is desirable that the microcapsules are stable over a wide range of relevant temperatures. Additionally, the TGA can assist in the identification of the different groups present in the shell and core material and give further indication of the synthesis process and core retention. Figure 4.9 shows the curves of thermogravimetric analysis corresponding to BH bulk material (grey curve), whereas the black curve corresponds to the sample BH-0.5-0.4-4 (Figure 4.5a). The comparison between the shell and bulk material is useful to indicate core retention and encapsulation efficiency. To produce the bulk material, the microfluidic device was used without the inner phase, resulting in the formation of a single emulsion which was subsequently polymerised into beads. The curves for the bulk BH and the microcapsules with BH shell are similar up to 300°C. This indicates no water was retained inside of the microcapsules, as the water would evaporate below 100°C. Thus, this hints that the holes formed in the shell prevented the retention of the water. Around 450°C, there is a sudden drop in the curve due to mass loss and it is hypothesised that this loss is associated with the abrupt loss of PVA trapped within some fully closed microcapsule. Although the core material curve is not plotted, the PVA degrades between 200 and 600°C. Thus, potentially the material which was contained inside the microcapsule suddenly burst the shell at ~450°C. This results in the

weight loss, since the material is ejected out of the crucible. Similarly, the sample BIH-0.3-0.4-4 (Figure 4.6c) presented no weight loss below 100°C, indicating no presence of water. The 20% weight loss below 200°C is associated with the decomposition of IBOA, whereas the weight loss between 250 and 550°C is likely to be due to the oxidation of the acrylate shell and the PVA inside the microcapsules. It is possible that the shell decomposition of BIH prior 250°C enabled the increase in the porosity of the shell and the degradation of the encapsulated PVA, consequently no indications of burst capsules was observed.

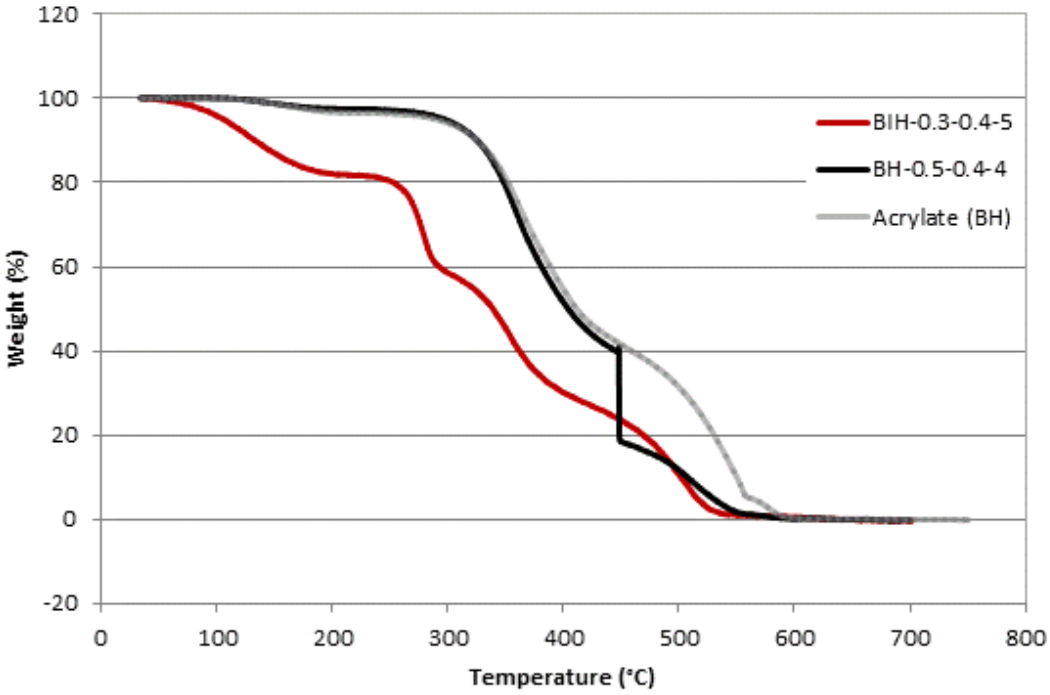

Figure 4.9 - TGA curves of dried microcapsules with BH and BIH as shell materials where the grey line indicates the TGA curve of only the shell material (BH as bulk material).

In the light of the results of the preliminary investigation, a new methodology was established for the production of the double emulsion and microcapsules. The objective of this methodology was to obtain fully closed microcapsules, without holes, and with precise control over size and shell thickness. New pressure pumps providing pulseless liquid flow with a precise pressure driven mechanism were used. The pressure pumps also worked in the range of 0.4-7µL/min for the inner and middle fluids and between 30-1000 µL/min for the outer fluid. Hence, other flow regimes could be explored more effectively due to the lower limit of flow rates and better dispersion of microcapsules size could be achieved. To boost the core retention and the formation of fully closed microcapsules, the batch synthesis polymerisation was substituted by *in situ* polymerisation. Since the formation of inhomogeneous shell thickness due to the density mismatch is time-dependent, the polymerisation of the shell shortly after the formation of the double emulsion would lead to

more homogenous shells. Instead of collecting the solution in a vial and then placing the vial above a UV-lamp, the UV-lamp was placed on top of the outlet tube coming from the microchip. The final set-up used for the production of the microcapsules with pressure pumps, the microfluidic device, optical pressure and the box containing the UV-lamp is shown in Figure 4.10.

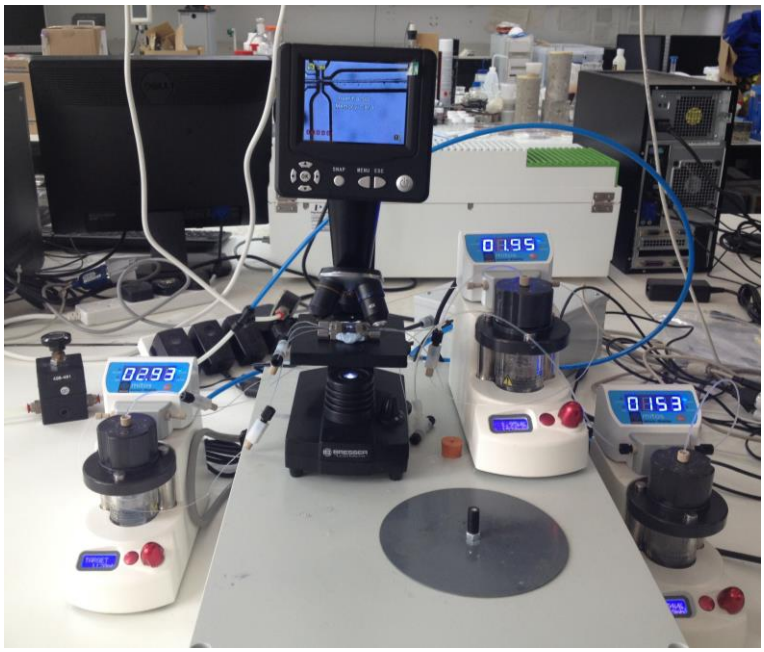

Figure 4.10 - Production of microcapsules showing the pressure pumps and the grey box containing the UV-lamp for *in situ* polymerisation.

4.2. Adjusting size and shell thickness of the microcapsules

After a set-up protocol was established to produce fully closed microcapsules, the tuning of size and shell thickness of the double emulsion was investigated. The tuning of the dimensions of the capsules is relevant since it enables the tuning of permeability, mechanical properties and payload of core material. To tune these properties using microfluidics, the flow rate and thus the flow regime used to produce the double emulsion plays a key role, and it is discussed in the initial part of the section. Then, the equations used to predict the shell thickness of the double emulsion were investigated. The main objective of this section is to deepen the understanding of the mechanism of formation of the double emulsion, as well as the main parameters governing the size and shell thickness.

4.2.1. Flow regime

To produce the double emulsion using the microfluidic device, three pressure pumps were used for the inner, middle and outer fluid. Each pump was connected to a flow rate sensor with a thermal sensor technology which is calibrated to water and oil phases. The microfluidic device was used for

the formation of the double emulsion, where the water-in-oil-in-water (w/o/w) droplets are stabilised by the presence of surfactants. By varying the flow rates, it is possible to vary between the different regimes for the formation of the double emulsion (Cubaud and Mason 2008; Nunes et al. 2013), as illustrated in Figure 4.11 and Figure 4.12. To illustrate the different flowing regimes, PVA 2% was used as inner and outer fluids, and BH was used as middle fluid.

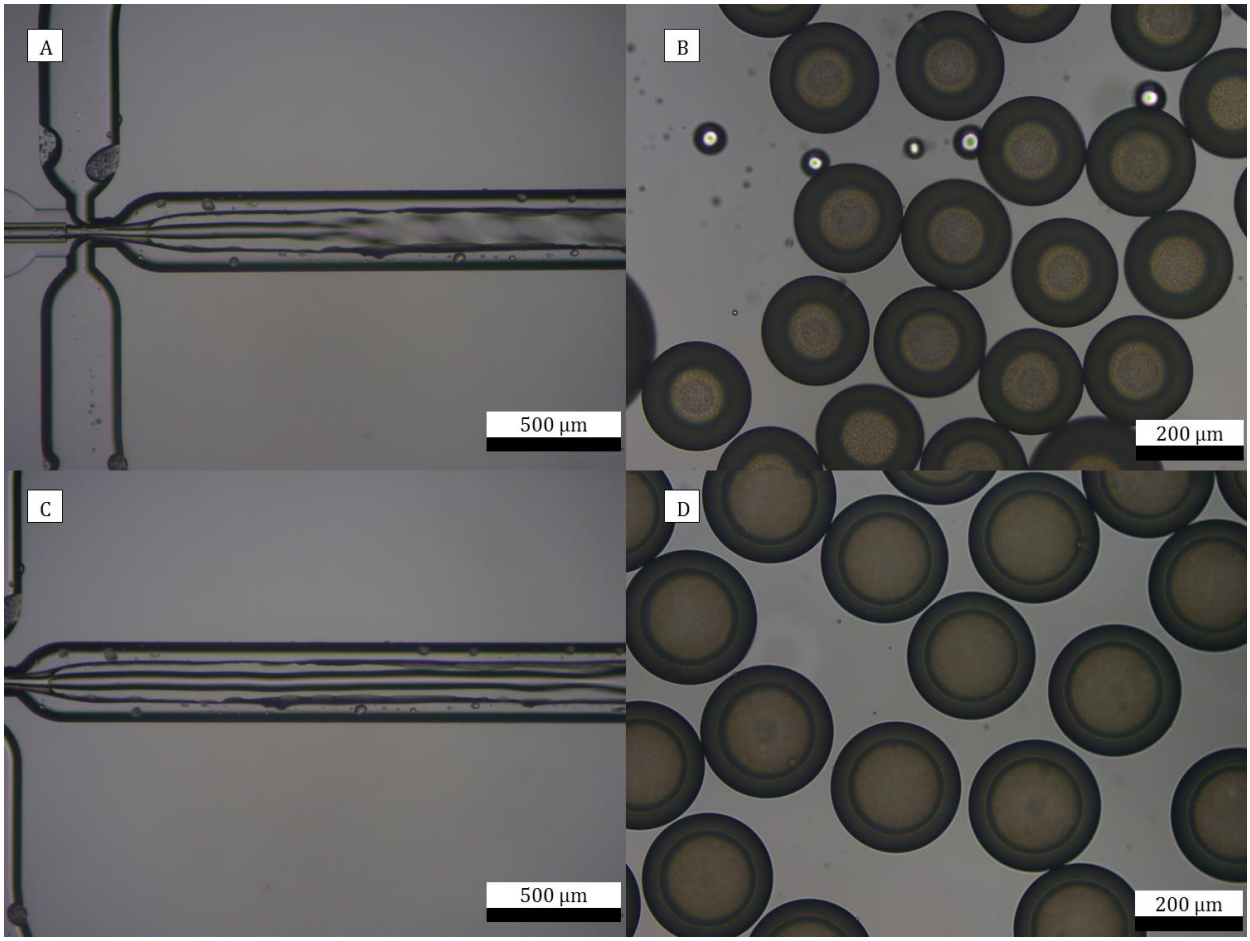

Figure 4.11 - Optical microscope images of the tubing regime and the resulting microcapsules. (a) tubing regime breaking into double emulsion in the middle of the channel, (b) double emulsion produced in the regime depicted in (a); (c) tubing regime breaking into double emulsion in the end of the channel, (d) double emulsion produced in the regime depicted in (c);

At high flow rates, similar to the ones used with a syringe pump, the middle fluid fills almost the entire outlet channel's cross-section and the outer fluid flows nearly entirely in the corners of the outlet microchannel (Figure 4.11a and c). In this system, the inner fluid is pumped in jetting regime inside of the middle fluid and downstream the jet destabilises and eventually breaks into drops, in what is called tubing regime (Cubaud and Mason 2008). Since the water-based inner fluid is immiscible in the organic based middle fluid, the jet instability is caused by surface tension forces seeking to minimise the interfacial area (Rayleigh– Plateau instability). Opposing this action are

viscous forces which suppress the growth of deformations of the jet and it is the balance of these forces that determine whether droplets or jets will be formed. Due to the high velocity of the process, the double emulsion formation could not be observed without a high speed camera, but the shadows of the emulsion were observed (Figure 4.11a). With the increase of the inner flow rate (Figure 4.11c), the inner flow forms a jet until almost at the end of the collection tube in the microfluidic device. By the very end of the tube, the neck formation characteristic of fluid instability was observed, resulting in the formation of the droplets. Due to the increase in the inner flow rate, the core-to-shell ratio also increased, resulting in larger double emulsion with thinner shells. As a result, the double emulsion observed in Figure 4.11b have smaller size and thicker middle layer than the ones observed in Figure 4.11d. The system was stable when the outer flow was ~70 μL/min and the middle flow was 7 μL/min or higher. To achieve these flow rates, a high pressure was necessary, typically ~1000 mbar for each pump. This could cause a problem since after a certain pressure value, the middle and inner phase will form a counterflow. On the other hand, if the outer flow is too high, ~100 μL/min, the middle flow is squeezed in the walls of the outlet tube and the system would be unstable. Thus, there is a window of flow rate values in which the double emulsion would formed. Regarding the inner flow, at low flow rates, ~3-8 μL/min, the system was stable and resulted in the formation of double emulsion with low core-to-shell ratio. However, when the inner flow was increased, the flow was likely to adhere to the walls of the tube and destabilise the system. Typically the tubing regimes would form less uniform size distribution, but the higher flow rates yielded higher production rates. In this regime, microcapsules were produced in a range ~1.1g/h assuming 100% yield.

With the decrease of the inner and the middle flow rate, the regime transfers to a jetting regime, as shown in Figure 4.12a. In the jetting regime, the inner and middle fluids streamed inside the collection tube as a single thread or jet until the jet destabilised and droplets were formed in the tip. This resulted in the cap formed by the inner and middle flow rate staying in the middle of the outlet tube after the breakup. This fluid was less stable than the dripping regime, and the flow might have adhered to the walls of the collection tube. Furthermore, the capsules formed in this regime were less monodisperse than those produced in the dripping regime. Regardless of this, it was possible to produce the capsules in a size range between 140 and 180 μm. Since this flow regime was not as stable as the tubing of dripping, it was rarely used for the production of double emulsion in this work.

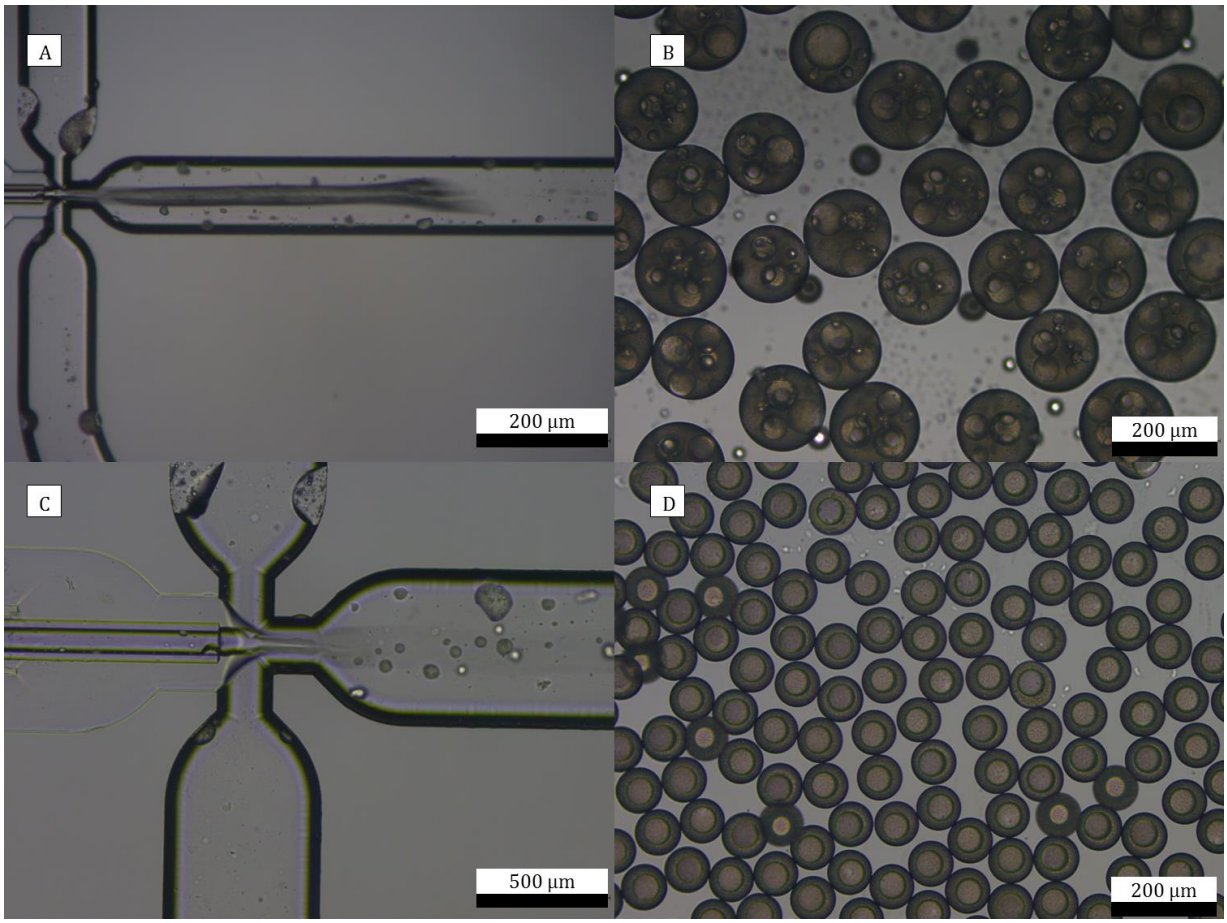

Figure 4.12 – Optical microscope images of the jetting and dripping regime, and the resulting double emulsion. (a) jetting regime breaking into double emulsion in the middle of the channel, (b) double emulsion produced in the regime depicted in (a); (c) dripping regime breaking into double emulsion in the cross-junction, (d) double emulsion produced in the regime depicted in (c).

At low flow rates of the dispersed phase, typically with inner and middle flow <5 µL/min each and outer flow ~100 µL/min, double emulsions are formed in a dripping regime. In this regime, the cap formed by the inner and middle flow stayed in the junction after the breakup. The rate of droplet formation was ~2500 double emulsion/min and the breakup mechanism could not be observed due to its fast speed. Nonetheless, a shadow of the formed capsules was observed in the collecting tube Figure 4.12c. Furthermore, this regime is the most commonly reported for the formation of double emulsion and known for the high uniformity of the produced droplets. Despite being suitable for the production of double emulsion, there are difficulties associated with the use of this flowing regime using the Dolomite microfluidics device. Although, the dripping regime was stable once established, it was difficult to create – typically, the tubing regime was formed and the flow was decreased until the dripping was formed. Moreover, after some time of use, the emitter capillary partially lost its hydrophobic coating and the inner fluid then easily connected with the walls of the device and with the outer fluid. Thus, the poorly hydrophobic emitter precluded the

formation of the double emulsion. With the decrease of flow rates, the production of double emulsion and thus the microcapsules also decreased to ~0.5g/h assuming 100% yield. Typical flow rates used to produce double emulsion in the dripping regime are presented in Figure 4.13.

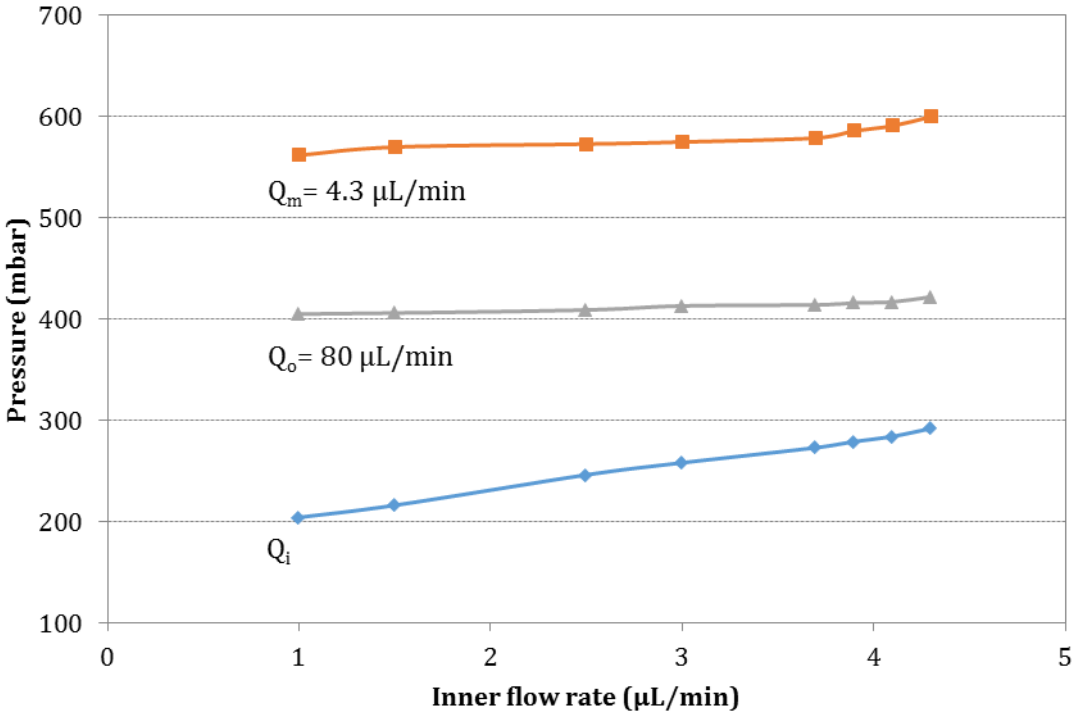

Figure 4.13 – Pressure values used for the inner (Q_i), middle (Q_m) and outer (Q_o) flows while the middle and outer flow rates were kept constant at 4.3 and 80 µL/min, respectively and the inner flow was varied.

The outer and middle flow rates were kept constant at 80 and 4.3 µL/min, and the inner fluid was varied between 4.3 and 1 µL/min and the respective pressure used in each pump to generate these flow rates is also shown in Figure 4.13. The pumps offer an option to control of the flow rates or the pressure, so commonly, the flow regime is established controlling the pressure. This is convenient when the flow rates are above the ones calibrated for the pump, particularly in the case of the tubing regime. When the dripping regime is established, the system is then controlled by the flow, similarly to a traditional syringe pump. In this option, the flow rate of each fluid was kept constant, regardless of variations in the pressure. This is useful since the outer flow is very stable, but the inner and middle are likely to vary the flow rate for the same pressure. Furthermore, the control of the flow rate allows the easy variations of a single fluid while the two others are kept constant. For example, in Figure 4.13 the inner fluid varied between 1 and 4.3 µL/min, by varying the pressure of the pumps. With the decrease of the pressure of emitter capillary, the pressure of the middle and outer fluids was also decreased to keep the flow rate constant at 4.3 and 80 µL/min, respectively. The flow was easily clogged by the presence of dust, fibres, or just the misplacing of the inlet tube in

the device. Therefore, the values of the pressure can act as a guideline if more or less pressure is necessary to pump the same flow rate, and thus if the channels are clogged.

4.2.2. Size control

The outer diameter of the double emulsion and consequently the capsule size can be varied within a broad range by changing the flow conditions in the dripping and tubing regimes. Figure 4.14 shows the variation of outer diameter of the double emulsion as a function of the inner and middle flow rates and thus the flowing regime.

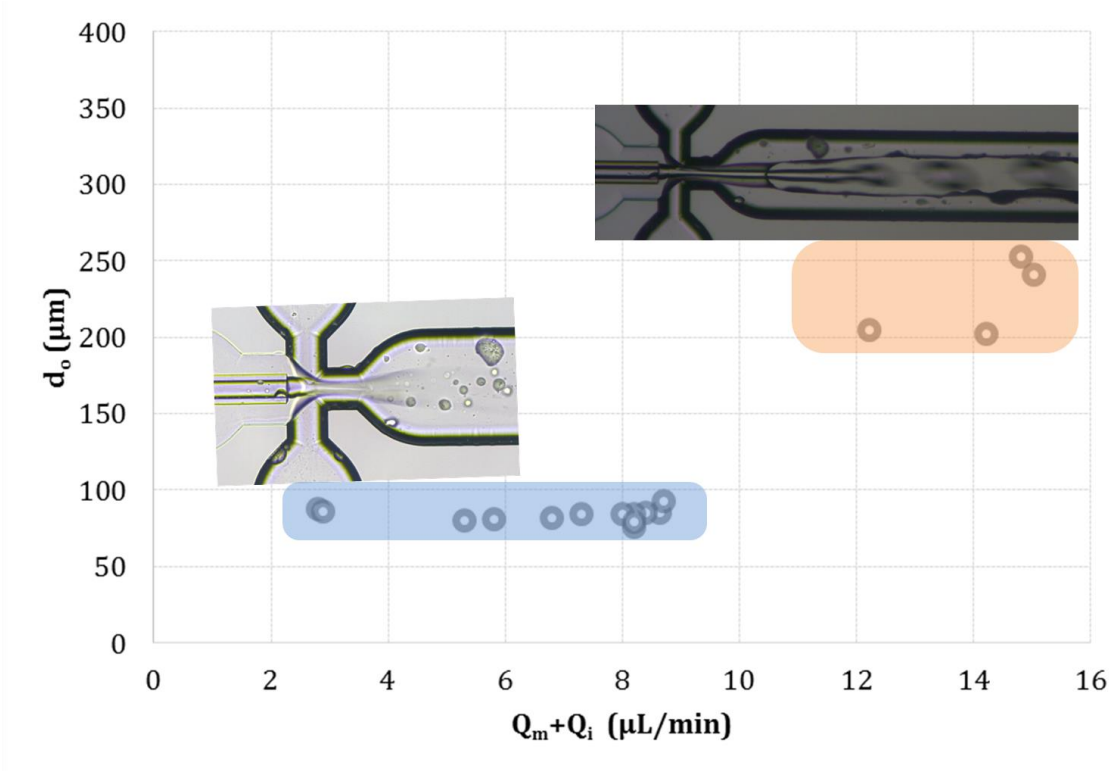

Figure 4.14 – The outer diameter of the double emulsion as a function of variations of the sum of inner and middle flow rates - the blue box indicates the double emulsion produced in the dripping regime, and the orange box the double emulsion produced in the tubing regime.

In the tubing regime, larger double emulsions are formed, typically with an outer diameter ranging between 190 and 250 µm, because of the higher flow rates used. The orange box in Figure 4.14 shows the flow rates associated with the outer diameter of the double emulsion. The outer flow rate can be used to fine tune the size for a given flow rate of the inner and middle fluid, as indicated by the variations of size for a singular $Q_i + Q_m$. With the decrease of the middle and inner flow rates, double emulsion are formed in the dripping regime, typically 3-5 µL/min for the middle fluid and 0.8-5 µL/min for the inner fluid. This results in monodisperse capsules with outer diameter ranging between 65 and 100 µm, as indicated by the blue box in Figure 4.14. The low flow rates result in a lower value for the capillary numbers $Ca = \eta\nu/\gamma$, where η is a fluid viscosity, ν a typical velocity, and

γ an interfacial tension. In this work, the fluid viscosity and the interfacial tension was not estimated for the mixture of acrylates, thus the capillary number was not determined. However, for the formation of double emulsion in the dripping regime, Ca_{crit} =0.1 has been traditionally reported (Hennequin et al. 2009; Chen et al. 2012), in which excellent size control can be achieved. Figure 4.15 shows the double emulsion formed in the dripping regime and the size distribution of inner and outer diameter. Using the optical microscope, the inner and outer diameter of at least 20 double emulsions was measured. The coefficient of variation was 0.7 and 1.8% for the outer and inner diameter, respectively, which is slightly below the values reported in the literature (Chen et al. 2012; Chen et al. 2014b; Polenz et al. 2014) and indicates excellent reproducibility.

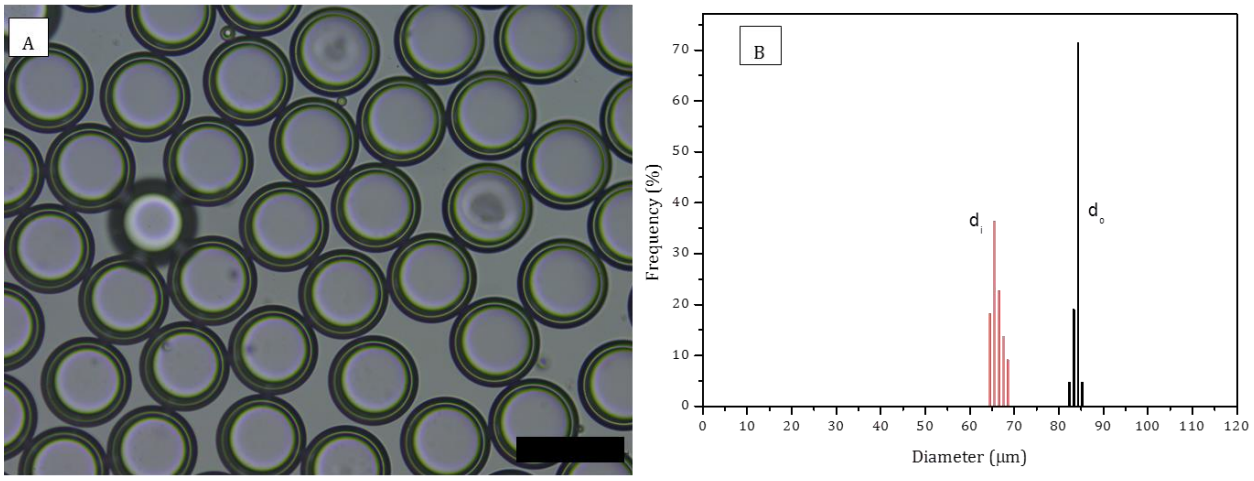

Figure 4.15 – Double emulsion formed in the dripping regime (a) double emulsion produced using the inner middle and flow rates of 3.7, 4.3 and 80 µL/min (scale bar represents 100 µm) and (b) Size distribution for the inner and outer diameters of a representative batch of microcapsules.

4.2.3. Shell thickness control

While the diameter d_o is determined by shear and interfacial forces acting on the outer droplet, the size of the inner droplets of the double emulsion is governed by the flow rate of the inner and middle fluid. Assuming that all middle and inner flows are used for the formation of the double emulsion, the ratio of volumetric inner and outer flow rates is equal the volume ratio of inner and outer material due to mass conservation, hence:

$$\frac{Q_i}{Q_m} = \frac{\frac{4}{3}\pi\frac{d_i^3}{8}}{\frac{4}{3}\pi\frac{d_o^3}{8} - \frac{4}{3}\pi\frac{d_i^3}{8}} \qquad \text{Equation 4.1}$$

where Q_i and Q_m are the inner and middle volumetric flow rates, d_i the internal diameter and d_o the measured external diameter. Hence, the predicted internal diameter is given by:

$$\frac{d_o}{d_i} = \sqrt[3]{1 + \frac{Q_m}{Q_i}} \qquad \text{Equation 4.2}$$

As a result, the inner diameter can be predicted when the outer diameter of the double emulsion, the inner and the middle flow rate are known. This is illustrated in Figure 4.16 where the outer diameter of the double emulsion is observed as a function of the inner flow rate between 1 and 4.3 µL/min while keeping the middle and outer flow constant at 4.3 and 80 µL/min, respectively.

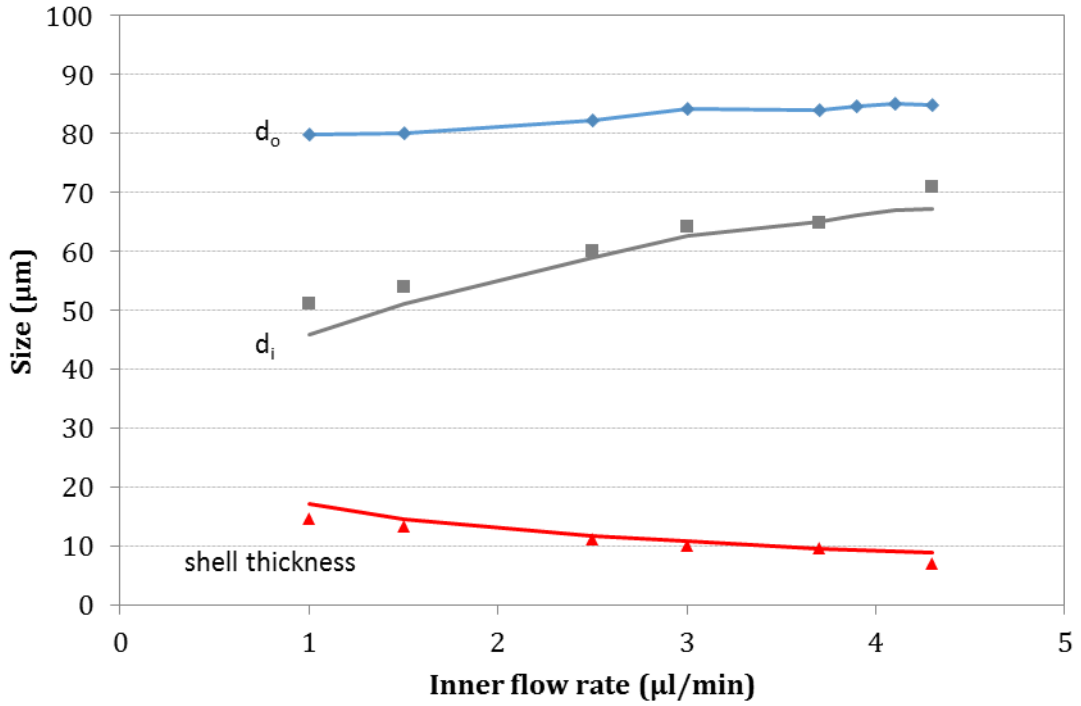

Figure 4.16 – Shell thickness, inner and outer diameter of the double emulsions in function of the inner flow rate. The middle and outer flow rate were kept constant at 4.3 and 80 µL/min, respectively. The solid grey and red lines represent the predicted size for inner diameter and shell thickness, respectively.

The inner diameter of the double emulsion can be predicted using Equation 4.2 and it is compared in Figure 4.16 with the values measured in the microscope. The difference between the measured and predicted values of the inner diameter of the double emulsion can be attributed to the difficulties in reading it using the optical microscope – while the outer border of the double emulsion is clear, it is hard to exactly determine the inner diameter of the double emulsion. Thus, small variations are also observed with the measured and estimated shell thickness of the microcapsules, determined by the difference between d_i and d_o divided by two. Furthermore, although the sensors used to measure the flow rate are calibrated for water and oil, when they were used to PVA solution and acrylate as oil the results were not as precise. Thus small variations were

expected from the measured values and the actual flow. The shell to radius ratio, h, can be predicted by rearranging the Equation 4.2, resulting in the corresponding theoretical formula:

$$h = \frac{d_o - d_i}{d_o} = 1 - \left(1 + \frac{Q_m}{Q_i}\right)^{-1/3} \qquad \text{Equation 4.3}$$

Figure 4.17 shows the relative shell thickness of the double emulsion as a function of the flow rate ratio Q_m/Q_i with theoretical and experimental results.

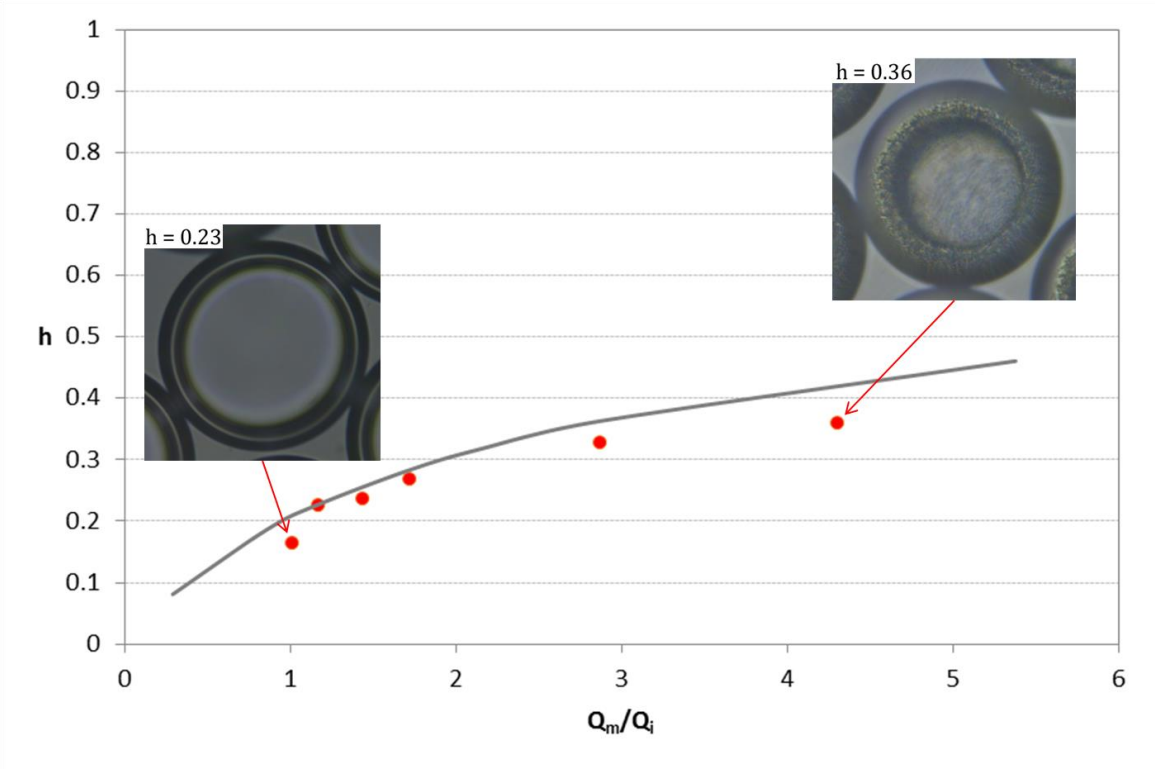

Figure 4.17 - Relative shell thickness h against ratio Q_m/Q_i. The solid line was inferred from mass conservation constraint. The circles were obtained at constant middle and outer flow of 4.3 and 80 µL/min, respectively.

Although the curve can be used for estimating the shell thickness, the predicted values were slightly higher than the measured values, and not as exact as reported in the literature (Hennequin et al. 2009; Chen et al. 2012). Nonetheless, the predicted inner diameter corresponded to 90-100% of the actual values, and the equation can be used as a guideline for predicting the shell thickness. Again, the difference between the predicted and experimental values was attributed to calibration of the pumps and technical difficulties in reading the inner droplet diameter. Large values of h can be easily obtained at low flow rates of the inner phase, but they are not useful for self-healing, due to the small payload of core material. On the other hand, small values of h are challenging using BH as middle layer – the minimum values obtained in this work for w/o/w systems were approximately

0.15. Interestingly, the production of microcapsules with ultra-thin shells using different shell materials has been reported in the literature (Kim et al. 2011; Lee et al. 2014; Arriaga et al. 2015), thus microcapsules with higher payload can be obtained using microfluidics and different shells.

4.3. Production of microcapsules with aqueous core

4.3.1. Encapsulating water

The encapsulation of water is desirable for the self-healing of cementitious materials because water is fundamental for autonomic and autogenous healing. The water is necessary during the crystallisation of calcium carbonate for autogenous self-healing and it is also important during autogenic healing using minerals(Kanellopoulos et al. 2015) and bacteria (Wiktor and Jonkers 2016). Despite its importance, there is surprisingly little research in the encapsulation of water to be used in cementitious materials. Furthermore, when encapsulated water was reported (Cailleux and Pollet 2009; Hassan et al. 2016; Milla et al. 2016), the focus was on the application of the capsules for self-healing and provided little insight on the characterisation of water encapsulation and retention. Thus, little is known about how long the water is retained inside of the capsules embedded in cement and whether the encapsulated water participates in self-healing. Hence, this section addresses these issues, and in particular examines the water encapsulation using microfluidics and its retention over time. Double emulsions of w/o/w were achieved under the conditions described in Table 4.1, using a solution of PVA 2% as inner and outer material, and BH as precursor of the acrylate shell. By varying the ratio of inner flow to middle flow (Q_i/Q_m) different shell thickness could be obtained, whereas the ratio of inner plus middle flow to the outer flow governs the size of the microcapsules (Q_i+Q_m/Q_o) (Chen et al. 2012). By varying the flow rates, two resultant samples were obtained: BH-82/12, with shell thickness of 12 μm and diameter of 82 μm, shown in Figure 4.18; and BH-88/7 with shell thickness of 7 μm and diameter of 88 μm, shown in Figure 4.19.

Table 4.1 – Flow rate (μL/min) and dimensions of microcapsule samples. Q_o, Q_m and Q_i are the outer, middle and inner flow rates, respectively; D_o is the outer diameter; t is the shell thickness.

Sample name	Q_o	Q_m	Q_i	D_o (μm)	t (μm)
BH-82/12	75	3.5	1.9-2.5	82	11.7 ± 1.5
BH-88/7	60	3.2	4.3-4.5	88	7.4 ± 0.7

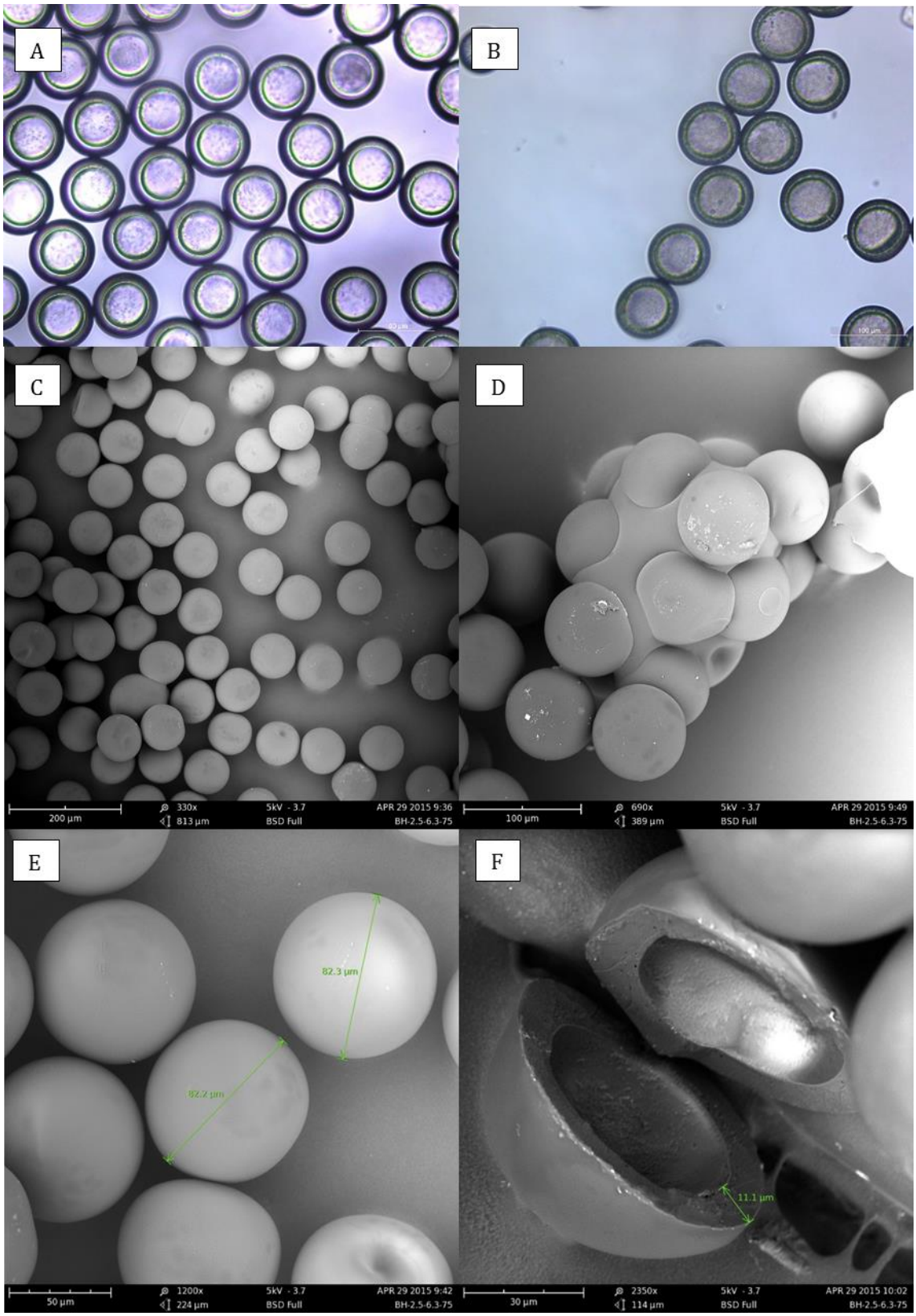

Figure 4.18 – Images of the capsules BH-82/12 (a) Double emulsion template before the polymerisation; (b) Capsules obtained after polymerising the shell and filtering the material, (c & d) general view of the obtained capsules, (e) diameter of the capsule using SEM and (f) a sliced microcapsule showing the shell thickness.

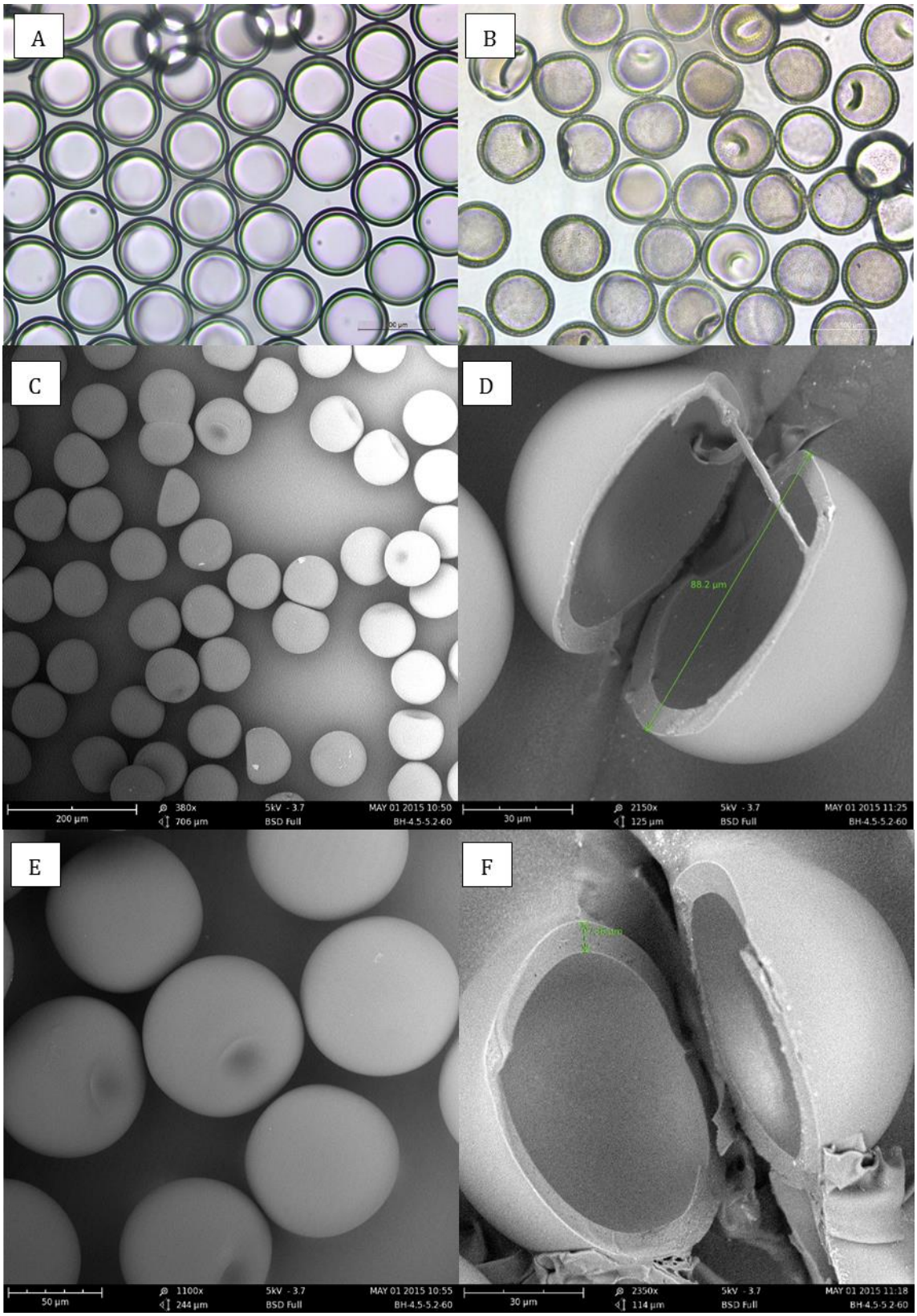

Figure 4.19 - Images of the capsules BH-88/7 (a) Double emulsion template before the polymerisation; (b) Capsules obtained after polymerising the shell and filtering the material, (c & d) general image of the obtained capsules, (e) diameter of the capsule using SEM and (f) sliced shell showing the thickness of the microcapsule.

Figure 4.18a shows the optical image of the double emulsion formed for the sample BH-82/12, presenting the efficiency of the PVA solution on preventing the coalescence of the emulsion by decreasing the superficial tension. After the exposition under the UV-light, the acrylate was selectively polymerised forming a fully closed microcapsule (Figure 4.18b, c and e). Figure 4.18e shows a microcapsule cut into two halves, were the core-shell structure is clearly observed. Furthermore, the shell is smooth and nanopores can be observed in the shell. Unfortunately, the acrylate coalesced during the polymerisation, resulting in the formation of clusters of microcapsules (Figure 4.18d). One possible explanation for the microcapsules agglomeration was that the double emulsion was not stable enough, which resulted in the coalescence of the acrylates. To prevent it, the concentration of surfactants in the collection solution was increased, aiming at increasing the stability of the double emulsion. The capsules were subsequently collected in a solution of PVA 10%. Figure 4.19 shows the double emulsion and the capsules formed for the sample BH-88/7.

The increase of the inner flow rate and the decreasing on the middle flow rate was effective to produce capsules with a thinner layer of acrylate in the double emulsion for the sample BH-88/7 (Figure 4.19a). The optical micrograph and the SEM images show the formation of fully closed microcapsules, with an average diameter of 88 μm and a shell thickness of 7.4 μm (Figure 4.19b, e, f). No agglomeration of the microcapsules was observed, showing that collecting solution with PVA 10% is efficient on preventing the coalescence of acrylate. After the polymerisation, the microcapsules were washed with water to remove the outer PVA solution and filtered.

The images of the dried microcapsules show the formation of dimples (Figure 4.19b, c and e) which are associated with the permeability of the polyacrylate shell. During the water evaporation through the nanopores of the shell, the internal pressure decreases and may lead to buckling (Shang et al. 2016; Nabavi et al. 2016). Several authors have reported shells permeable to water, whereas it can be impermeable to ions and molecules with high molecular weight such as PVA. For example, microcapsules made with ETPTA shell (5 μm thickness) showed complete water evaporation after 2 hours with buckled shell during the evaporation (Kim et al. 2008). Alternatively, in thick shelled microcapsules (15 μm) the evaporation is slower and the microcapsules retain the spherical shape. These results indicate that the thinner shells can be deformed with much greater ease by a decrease in the internal pressure during evaporation compared with same size microcapsules with thick shells.

The likelihood of buckling is also due to the evaporation of the aqueous core and the evaporation of the water surrounding the microcapsules. Abbasppourrad et al. (2013) hypothesised that, as the water evaporates, tiny menisci are formed in the pores of the cross-linked polymeric shell (Abbaspourrad et al. 2013b), which results in a uniform externally imposed pressure. If this pressure is sufficiently small, a homogeneous shell of uniform thickness supports a compressive stress, and it shrinks uniformly. Above a threshold pressure, however, the strain energy required to shrink the shell becomes larger than the energy required to form a localised, circular indentation in its surface; consequently, the shell buckles. The capillary pressure across the shell was estimated as

$$P_c \approx \frac{2\gamma}{r_p} \qquad \text{Equation 4.4}$$

where γ is the surface tension between the outer fluid and air (70 mN/m for water(Datta et al. 2012) and 44.7 mN/m for PVA) and r_p is the typical radius of a pore (~10 nm for ETPTA (Datta et al. 2012)). For a capsule shell to buckle, P_c must exceed a threshold buckling pressure of a thin walled shell given by

$$P_{buckling} = \frac{2E}{\sqrt{3(1-\nu^2)}}\left(\frac{t}{R}\right)^2 \qquad \text{Equation 4.5}$$

where E and ν are the Young's modulus and Poisson's ratio of the shell material and R is the radius of the capsule and t is the shell thickness (Datta et al. 2012; Datta et al. 2014; Neubauer et al. 2014). Considering the Young's modulus of BH as 2.6 GPa and ν ≈ 0.35, the values of buckling pressure for the two capsules produced are shown in Figure 4.20. For microcapsules BH-82/12 with the shell thickness of 12 μm and the diameter of 82 μm, no buckling was observed. In fact, according to Equation 4.4 the required pressure to buckle such capsules would be 279 MPa and this pressure is not achieved during the evaporation of the water. However, for microcapsule BH-88/7, several buckled microcapsules were observed and according to Equation 4.4, the pressure to achieve such buckling would be 82 MPa. This value is higher than the critical capillary pressure of 14 MPa found for the ETPTA microcapsules because of the increase in the Young's modulus of BH (ETPTA = 600MPa). The relative shell thickness h is key for the control of buckling and capsules with h ≥ 0.19 have been observed to retain their spherical shape after drying (Vilanova et al. 2013). For BH-82/12, h = 0.29 and the capsules are stiff enough to remain spherical whereas BH-88/7 presented h = 0.17 and the capsules are partially buckled. Furthermore, for the microcapsule to start to buckle due to externally imposed pressure, the water inside the capsule needs to escape (Datta et al. 2014). Thus the buckling occurs due to a combination of evaporation of the surrounding liquid and evaporation of the water within the shell.

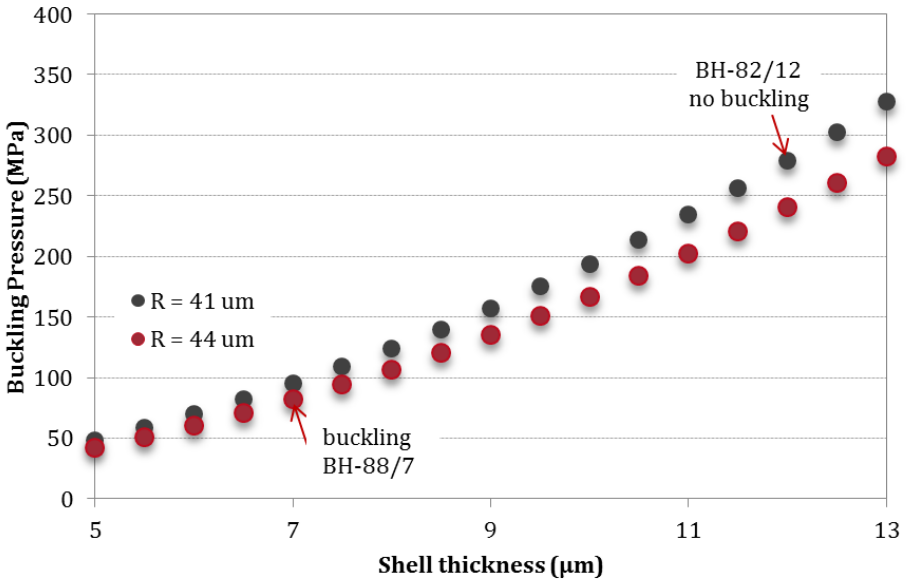

Figure 4.20 – Buckling pressure in function of the shell thickness for the microcapsules with a diameter of 82 µm (black lines) and 88µm (red lines).

This model is valid for microcapsules with uniform shell thickness; if the shell is not uniform, the buckling is likely to occur in the thinnest part of non-homogenous shells. Applying shell theory to the inhomogenous shell thickness led to equations to predict the pressure buckling which is proportional to the thinnest part of the shell (Datta et al. 2012). As discussed before, when the inner phase of the double emulsion templates is less dense than the middle phase, the inner drop will gradually rise. As a result, microcapsules with spatially varying shell thicknesses are produced, according to the time the capsule takes to be polymerised (Datta et al. 2012). To increase the shell symmetry, the capsules were polymerised shortly after formation of the double emulsion. Nonetheless, the off-centeredness of the double emulsion due to the mismatch of inner and middle fluid density has been reported for in-situ polymerisation (Chen et al. 2012). Thus, to minimise even further the formation of inhomogenous shells, colloidal silica was encapsulated as core material, decreasing the density mismatch.

4.3.2. Encapsulating colloidal silica

To prevent the formation of non-homogenous shell characterised by spatially varying thicknesses, the density of the inner liquid was increased with the aim of reducing the density mismatch. The choice of colloidal silica as densifying aqueous fluid was also based on its potential as self-healing agent. Nanoparticles of SiO_2 can react with the portlandite present in cement generating a surplus of calcium silicate hydrates (CSH) capable of sealing cracks (Kanellopoulos et al. 2015), as shown in Equation 4.6 and Equation 4.7.

$$CaO + H_2O \rightarrow Ca(OH)_2$$ Equation 4.6

$$SiO_2 + Ca(OH)_2 \rightarrow x(CaO.SiO_2).yH_2O$$ Equation 4.7

The encapsulation with colloidal silica and water is suitable for self-healing, since the presence of water is important for the formation of healing products in the crack (Kanellopoulos et al. 2015) and it is also important for the diffusion of the mineral compounds. To examine the impact of a denser core solution, an inner aqueous solution comprising of a mixture of 2% wt of PVA and 40% in volume of a solution of colloidal silica was used, as described in the experimental section. BH was used as middle fluid and PVA 2% as outer fluids at a flow rate of 2.5, 6.4 and 75 μL/min (pressure of 200, 840 and 400 mbar) for inner, middle and outer fluid, respectively. The microcapsules encapsulating colloidal silica as core material were named BHCS-88/9 and are shown in Figure 4.21.

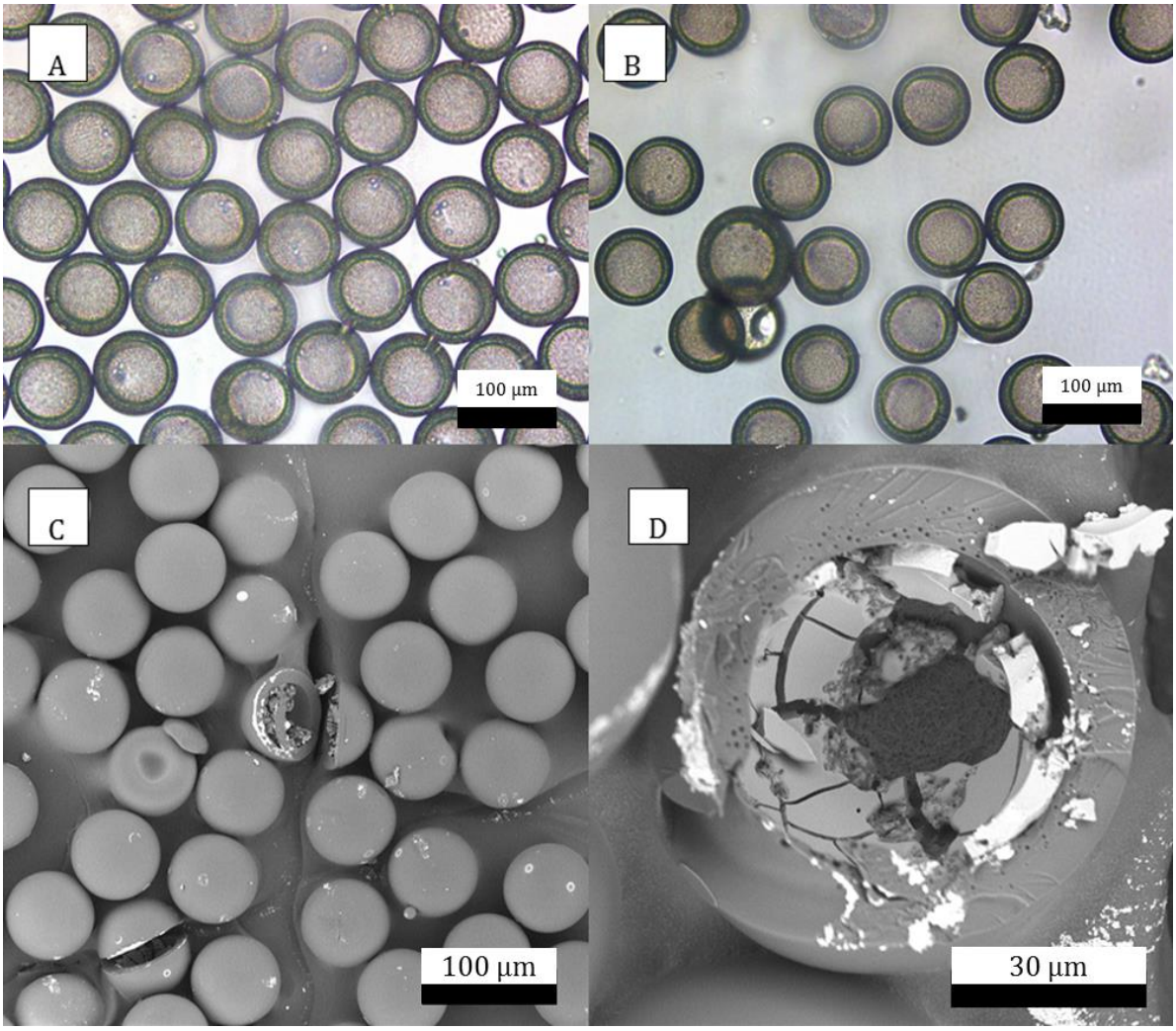

Figure 4.21 – Optical microscopy and SEM images of capsules BH-CS-88/9 encapsulating colloidal silica (a) Double emulsion template before the polymerisation;(b) Capsules obtained after polymerising the shell, (c) general SEM image of the obtained capsules and (b) SEM image of a sliced shell showing the shell thickness and the core.

As shown in Figure 4.21, the double emulsion containing colloidal silica was successfully formed and the 2% wt of PVA was enough to maintain its stability, preventing the coalescence of the solutions. After the polymerisation, Figure 4.21b, the capsules presented uniform shells with fewer dimples when compared to capsules BH-88/9 (Figure 4.21b). The SEM images (Figure 4.21c and d) of the material after drying show microcapsules formed with a uniform shell and containing dried colloidal silica and PVA as cargo material. Furthermore, no dimples were observed, indicating that the presence of colloidal silica was effective to produce more uniform shells. EDX of the microcapsules shell and core material were performed and Figure 4.22 shows the SEM image of the microcapsules and the scan across the core and the shell material. At point 1, located inside a cut microcapsule, the signal of silicon, oxygen and carbon are clearly visible. The peaks of silicon and oxygen indicate the presence of colloidal silica inside of the microcapsule. Conversely, at point 6 where just the shell is analysed, only the peak for carbon and a weaker signal of oxygen can be detected. Thus, the results indicate that the capsule shell is efficient in retaining the colloidal silica and its use as core material prevents the buckling due to inhomogenous shells.

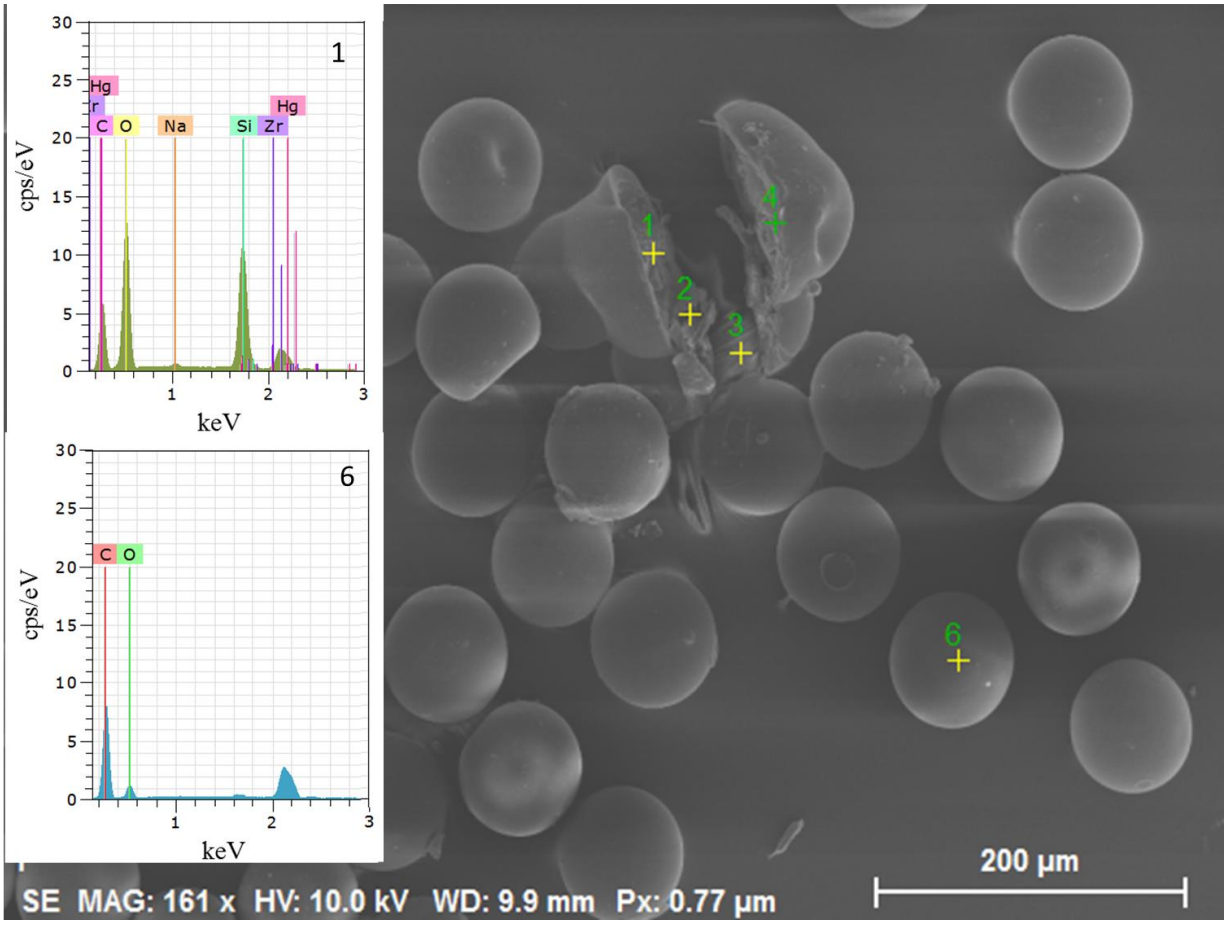

Figure 4.22 - SEM micrograph of the cut and non-cut microcapsules. On the left are the representative EDX spectra of point 1 (inside the microcapsule) and point 6 (microcapsule shell).

4.3.3. Encapsulating sodium silicate

Sodium silicate is another promising mineral healing agent to be used for self-healing of cementitious materials. The silicate reacts with portlandite present in the cement-based matrices, to form a surplus of calcium silicate hydrate (CSH). CSH is the main reaction product of cement hydration and provides the mechanical strength of the cementitious materials (Fan and Li 2015), resulting in denser and more durable self-healing. However, the encapsulation of sodium silicate is a challenge given the reactive alkaline nature of the sodium silicate. The hydrolysis of sodium silicate (Na_2SiO_3) results in the formation of the weak acid $HSiO_3^+$ and thus the dissolution of Na^+ and hydroxyl groups, increasing the pH. Bearing in mind the pH-sensitive nature of emulsification polymerisation, it is possible to understand the difficulty in using sodium silicate as dispersed phase and to expect the deposition of the polymeric shell in the interface. Although some authors did report the encapsulation of sodium silicate, the full characterisation of core-shell was not performed, indicating that the material may not have been encapsulated. Microfluidics, on the other hand, provides a suitable reactor for the formation of microcapsules containing sodium silicate. Using the device, the hydrophobic middle phase quickly surrounds the inner phase, and does not allow the sodium silicate solution to dissolve in water. Furthermore, the photopolymerisation is not affected by variations in pH, as conventional emulsification polymerisation techniques are. Thus, using the microfluidic device, the formation of double emulsion of sodium silicate solution in the acrylate monomer was explored, and, subsequently, we photopolymerised the shell. Figure 4.23 shows optical microscope images of the double emulsion and the SEM of the microcapsules.

To form the double emulsion, PVA 2% was used as outer solution and BH as middle phase, at a flow of 4 and 0.6mL/h, respectively. These results were obtained before the arrival of the new pressure pumps, so the syringe pumps and their protocol were used. First, the microfluidic device was set to produce the double emulsion using PVA 2% as inner phase; the goal was to make sure that the outer and middle flow were stable enough before the addition of the sodium silicate and thus minimise the chance of the sodium silicate being in contact with the device walls. This parameter was particularly important taking into consideration the capillary tube of the inner phase is coated to make the material hydrophobic. This coating was not guaranteed as stable at high pH provided by the sodium silicate solution. When the device was stable producing double emulsion containing PVA 2% as inner and outer phase, the inner fluid syringe was quickly exchanged, and the sodium silicate solution was pumped into the device. Due to the high viscosity of the sodium silicate solution, the material offered resistance to being pumped and the syringe pumps repeatedly reported clogging of the material. As a consequence, the flow rate was slower than what was reported at the syringe pump (0.1mL/h). When the sodium silicate arrived at the cross-section of the microfluidic device, the inner flow was in a dripping regime; the middle phase was in a thread

regime, and the combination of those two regimes resulted in the formation monodisperse droplets containing the sodium silicate. Since the sodium silicate dripping, it resulted in low payload of core material and very thick layer of acrylate, as observed in Figure 4.23a and b. Furthermore, several single emulsions were observed, where the core had escaped and just droplets comprised only of acrylate had been formed. This was due to the lack of surface active substances in the inner core: due to the reactive nature of sodium silicate, when the material was mixed with PVA, the high pH resulted in phase separation and precipitation of the PVA. Thus, for this experiment, the inner phase was inserted without any surfactant, but it still produced double emulsion, more likely due to the low interfacial tension between the sodium silicate and the acrylate monomers.

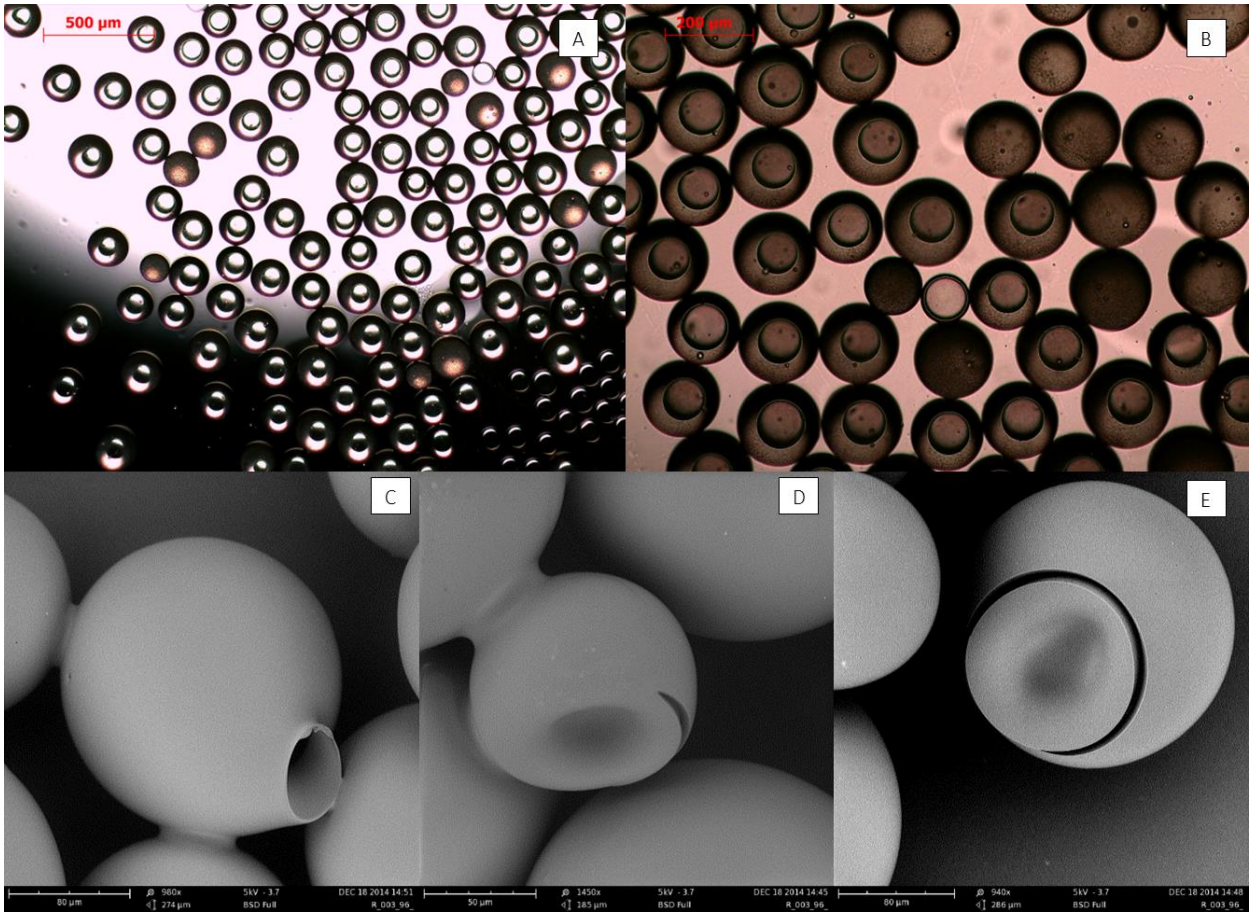

Figure 4.23 – Double emulsion and microcapsules containing sodium silicate as core. (a and b) Optical microscope image of the double emulsion template before the polymerisation and (c, d and e) SEM of microcapsules obtained after polymerising the shell and filtering the material.

After the formation of the double emulsion, the material was collected for one hour and then polymerised by placing it on top of UV-lamp. Due to the time spent between the formation of the double emulsion and the photopolymerisation, the density mismatch between the sodium silicate and the acrylate monomers led to the asymmetric double emulsion. As a result, the formation of

solid polyacrylates beads was observed. Furthermore, the photopolymerisation resulted in shapes such as the one observed in Figure 4.23c, where the acrylate polymerised while the core was escaping, resulting in a mouth-like shape. The encapsulation of sodium silicate was achieved, but during the drying process prior to SEM observation, the water evaporated through the shell, resulting in the buckling of the capsules, as observed in Figure 4.23d and e. Furthermore, the buckling also resulted in the breakage of the shell, partially (Figure 4.23d) and totally (Figure 4.23e). Thus, even though the sodium silicate solution was encapsulated, the water left the core when the microcapsules were dried. What was left behind was the solid deposition of Na_2SiO_3 and in order to be used as healing agent the water needs to dissolve the material. Furthermore, the buckling and breakage of the shell is not desirable for the capsules, as the bond with the cement matrix would diminish.

4.3.4. Urethane shell and colloidal silica as core

The versatility of the microfluidic device as platform to produce microcapsules with a wide range of materials was also explored for different shells. Using a mixture of HDDA and BisGMA (BH) or a mixture of IBOA, HDDA and BisGMA (BIH), the different shrinkage properties of the acrylate shells were explored. Additionally, urethane triacrylate (MU3603, Miwon, Korea) can also be used as oligomer to provide the suitable viscosity for shell formation, instead of BisGMA. Triacrylate urethanes have been suggested to undergo a low shrinkage, due to high molecular volume and multiple functionality (Chen et al. 2008). Furthermore, urethane acrylate has a tensile strength ~3.4 MPa, elongation of ~32% and Young's modulus of ~12MPa, thus it could facilitate shell rupture under crack. Also, the glass transition temperature of polyurethane has been found to decrease significantly after immersion in water. This change takes place due to the hydrogen bond between N-H and C=O groups being weakened by the absorbed water; furthermore, the bonded water decreases the tensile strength(Yang et al. 2006). In this case, the microcapsules can be maintained in a water solution prior incorporation in the cement matrix, consequently, presenting a rubbery behaviour during mixing. Subsequently, when the concrete dries and absorb the bonded water, the capsule would also dry and present a more brittle behaviour.

To explore the production of microcapsules with urethane based shell, a mixture of urethane triacrylate and HDDA (UH) was used and the results are shown in Figure 4.24.

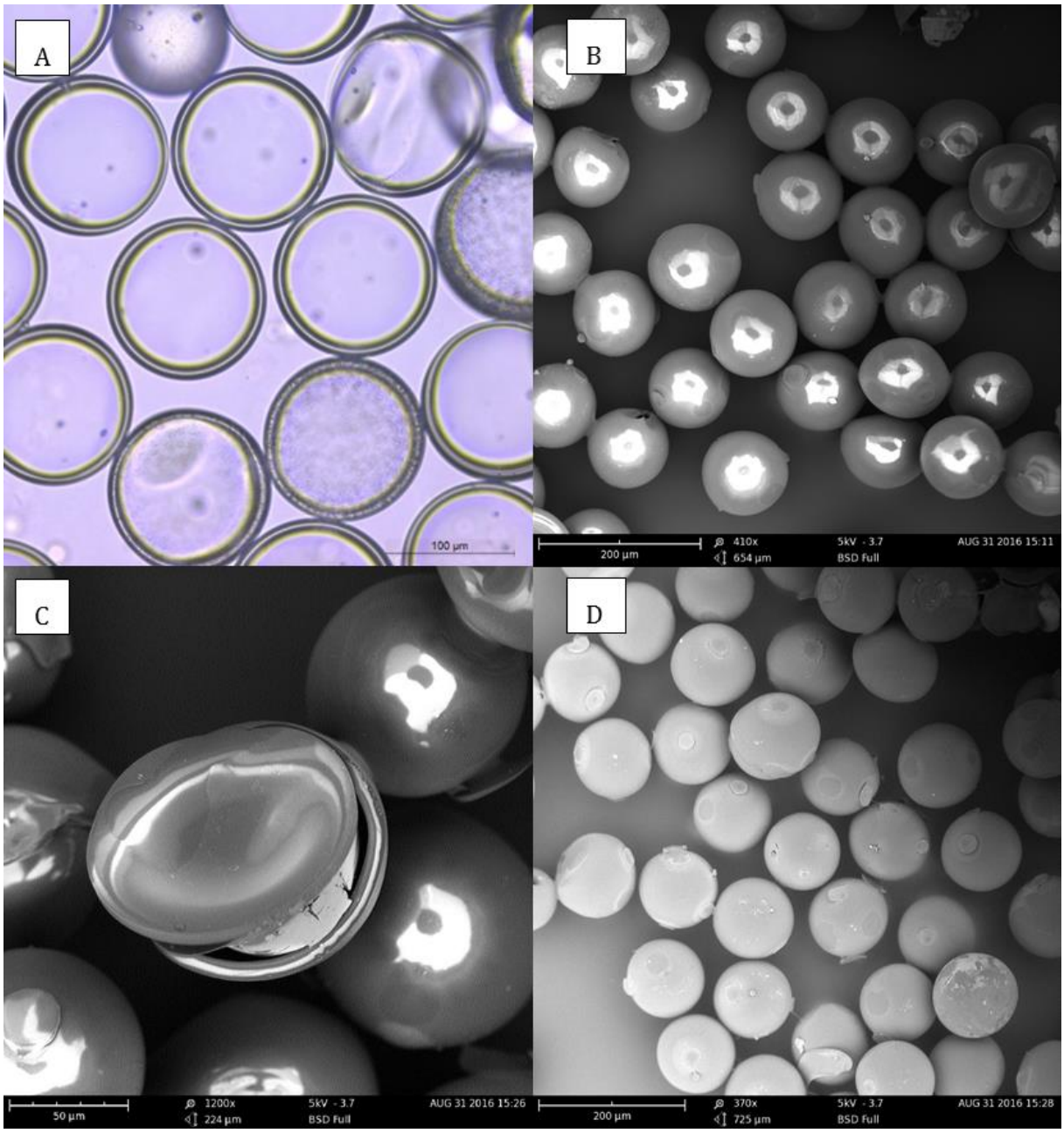

Figure 4.24 - Images of the capsules with UH shell and colloidal silica core: (a) Optical microscopy of the capsules in water after polymerising the shell and (b, c & d) SEM showing general aspect of the obtained capsules.

For the production of the double emulsion, an aqueous solution containing 20% of colloidal silica and 5% of PVA was used as inner solution, UH as middle and PVA 10% was used as outer solution. The flow rates were 6, 2 and 50 µL/min for the inner, middle and outer fluids, respectively. After the polymerisation, well centralised core-shell structures were produced, with 125µm of diameter and 7.5µm of shell thickness (Figure 4.24a). Due to the similar density for the core and shell material, the centre of the inner and the outer droplets are the same and the shell is homogenous. After drying, the microcapsules were observed using with monodisperse size distribution, fully

closed capsules and no observed holes. The colloidal silica was retained inside of the microcapsules after drying, as shown in Figure 4.24c where the white core material is shown inside the ruptured microcapsule. Remarkably, no buckled microcapsules were observed - despite having h = 0.12, the capsules retained the spherical shape observed in Figure 4.24b & d. In comparison, when BH microcapsules were produced with similar size and shape, as was shown in Figure 4.21, buckle microcapsules were easily observed in the optical microscope and the SEM. The retention of spherical shape was attributed to the formation of uniform shells due to the compatible densities of the inner and middle fluid.

To observe the drying process, microcapsules were produced with UH shell and colloidal silica in water as core and placed in a glass slide and observed in the optical microscope for 4 hours. The top of Figure 4.25 shows the recently produced microcapsules in water, whereas the bottom part of the picture shows the microcapsules after the evaporation of the surrounding water and also from the core material. The red arrow in the left points to an asymmetric capsule which folds inwardly during the drying process, as observed in the bottom left. Alternatively, the red arrow on the right points a symmetrical which during the drying process also folds inwardly. It is still not clear why the capsules observed in the Figure 4.24 did not buckle, but possibly is due to the evaporation speed.

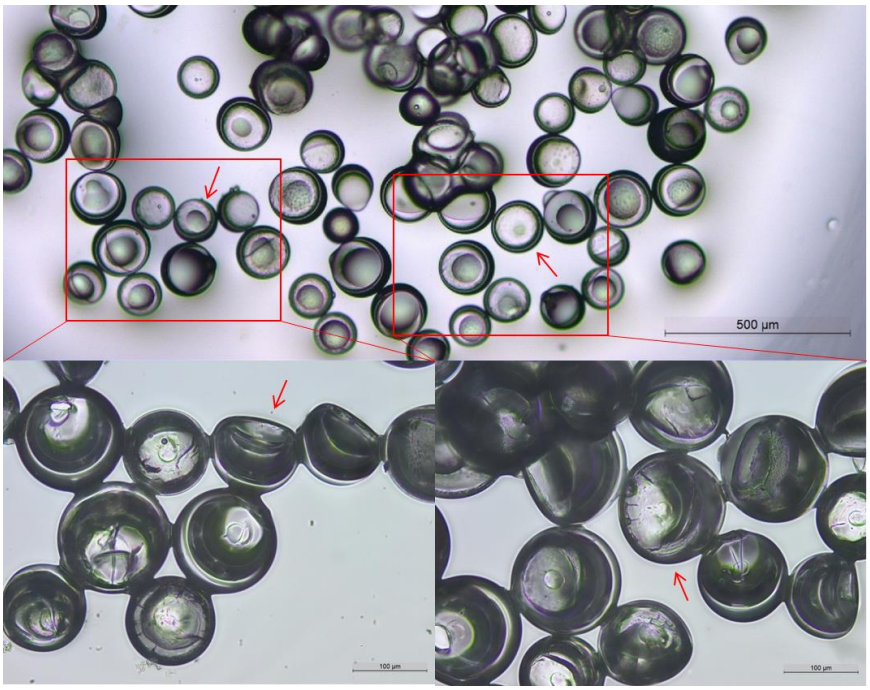

Figure 4.25 – Images of buckling of UH shell during the drying process. (top) UH-CS-4.5-2-50 microcapsules in water; (bottom) images of dried microcapsules after 4h showing the collapse due to loss of water.

To investigate the water loss during the drying process of the microcapsules, thermogravimetric analysis of the wet and dried microcapsules UH-CS-4.5-2-50 was performed. TGA was performed directly after removing the microcapsules from the water solution and after being exposed to air for 1 day. Also, the TGA of the core material was obtained. The curves are shown in Figure 4.26.

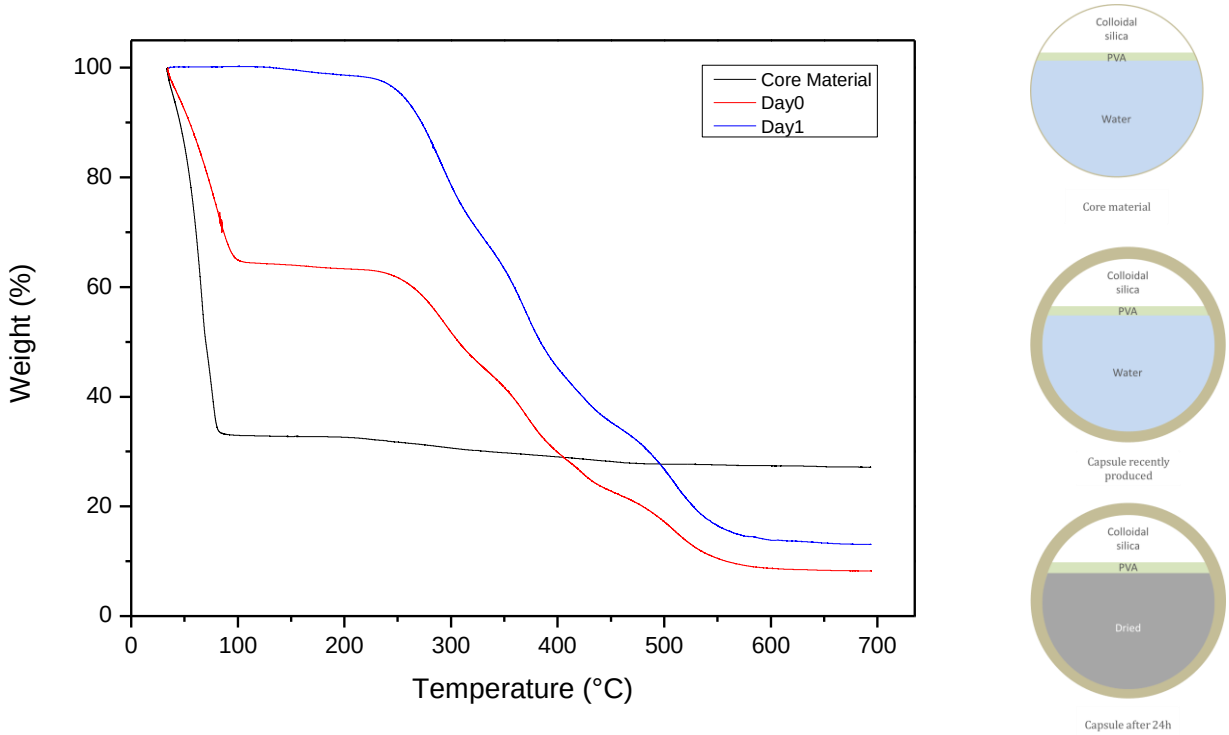

Figure 4.26 - TGA curves of wet (red) and dried (blue) microcapsules with UH as shell materials and colloidal silica in water as core, and the black line indicates the TGA curve of only the core material.

The core material is comprised of a solution of PVA 2% and colloidal silica 20% in water solution. The TGA results for the core material show a mass loss of 67.3% between 35 and 110°C due to the loss of water. Between 200 and 600°C, the material lost 5% of its weight due to the loss of PVA and, finally, the residual mass of 27.7% is due to the residual silica. When this core is encapsulated by the UH shell, the TGA of the resultant microcapsules shows a loss of water before 110°C corresponding to 35.5%. Considering the proportions of the TGA of just the core material, the total core weight of the microcapsules after can be estimated in 45.8%, i.e., 35.5% of water, 1.6% of PVA and 8.7% of colloidal silica. This estimation is supported by the amount of residual material after 600°C being around 8%, as observed in the red line results. This residual material is the colloidal silica and it plays the role of a tracer to estimate the amount of encapsulated core material. Since the decomposition of PVA happens at the same range of temperature as the shell, the PVA content was based on the content of residual silica. It is important to mention that the capsules were immersed in water just before the TGA, thus the initial water loss is not only from inside the microcapsules, but also from the water surrounding it. However, the presence of the colloidal silica

confirms the encapsulation of the core, otherwise the material would have been washed during the separation of the PVA prior to drying.

After 1 day of being exposed at the air atmosphere, the resultant microcapsules lost no water content between 35 and 110°C, indicating that all water was evaporated. Although the shell material is permeable to water, the permeability is not the same for colloidal silica. As result, the dispersed solid material remained inside of the microcapsule after the water was lost. Thus, the residual material was increased to 13.84% as the microcapsules were only comprised of UH shell, PVA and the colloidal silica. To conclude, the microfluidic device can be used to encapsulate water, but as soon as the produced microcapsules are dried, the water evaporates, leaving the core material inside. In this manner, water soluble materials can be encapsulated and deposit inside of the microcapsule once the water has evaporated; however, for the material to be used as healing agent, the ingress of water is required to dissolve and transfer the healing agent. This process would be similar to the use of pan-coated materials, where the water ingress dissolves the content of the capsules, but in this case, with lower payload. The literature of microcapsules containing water was scarce even for microcapsules produced by other techniques, and it is difficult to offer values of permeability, particularly under osmotic stress from different materials. Thus, oil can be used as carrier phase instead, preventing the need for water to promote self-healing, since the material can carry the healing agent to out of the microcapsules.

4.4. Production of microcapsules with organic core

4.4.1. Encapsulating oil

As discussed before, although the encapsulation of water is possible, the encapsulated water escaped through the nanopores of the membrane (Nabavi et al. 2016). Water core thin-shelled microcapsules shrank when immersed in a saturated medium, followed by the formation of dimples and microcapsule shell folding inwards and collapsing (Kim et al. 2014a; Shang et al. 2016). Thus, when these microcapsules are immersed in the cement paste, a similar process takes place and the collapsed microcapsules preclude the mechanical triggering of the self-healing. To overcome these problems, non-aqueous solvents can be used as core material as they are less likely to evaporate through the shell of the microcapsules. The vapour pressure of mineral oil is lower than water, and this relates to the tendency of particles to escape from the liquid. For example, at 20°C the vapour pressure of water is 2.3kPa while the value is lower than 0.1 kPa for mineral oil, indicating that the liquid evaporation rate of water is higher than of the mineral oil. Furthermore, due to the larger size of the oil molecule, it is less likely to pass through the nanopores of the acrylate membrane. These qualities of the organic core prevent the leakage of microcapsules, thus keeping their

structural integrity and supporting the mechanical triggering of the self-healing. As a result, a liquid core is retained and acts as a delivery vehicle solution, increasing the mobility of the healing agent and therefore maximising the surface area with potential to be healed.

Most of the literature for the production of double emulsion and microcapsules using microfluidics reports the use of double emulsion of w/o/w or o/w/o. However, the Dolomite microfluidic device has a hydrophobic coated capillary, enabling just the use of oil as middle phase. Thus, we decided to investigate the possibility of producing o/o/w double emulsion drops as templates using the flow-focusing device. The inner flow is comprised of mineral oil (without any surfactant), the middle phase UH stabilised by the outer solution containing 10% of PVA. Then, the double emulsion was exposed under the UV-light at the exit of the collection tube and the results are shown in Figure 4.27. The double emulsion of o/o/w was formed, as shown in Figure 4.27a, where the mineral oil was encapsulated by the UH solution. However, the polymerisation did not resulted in the formation of the core-shell structures, as shown in Figure 4.27b where the middle layer appears to have deformed during polymerisation. The reasons why the urethane acrylate did not polymerised around the mineral oil are unclear. Possibly, the heat released during the exothermic photopolymerisation was not dissipated in the oil as well as it was dissipated in the water core.

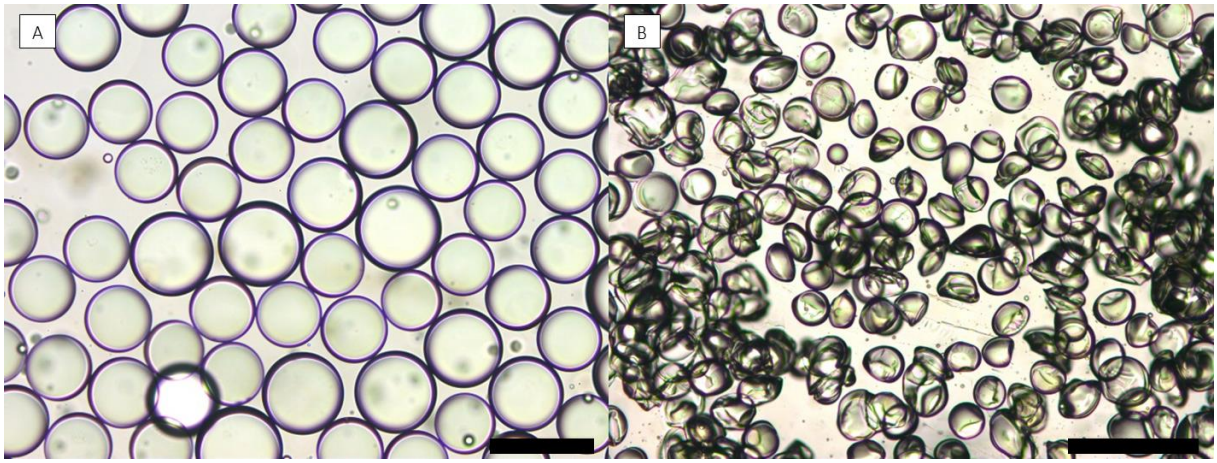

Figure 4.27 – Production of microcapsules with UH shell and oil core; (a) Optical microscope images of the double emulsion of o/o/w of mineral oil in UH; (b) cross-linked UH after the exposition under the UV-light. Scale of 200µm on the left and 500µm on the right.

Since the o/o/w double emulsion was formed using the microfluidic device, the formation of microcapsules was prevented only by the photopolymerisation of the shell. To verify if the acrylates used in this work would be suitable for encapsulating non-aqueous core, BI was investigated as middle phase while PVA 10% was the outer phase. Then the double emulsion was cross-linked and Figure 4.28a and b show the formed microcapsules in water just after polymerisation. Unlike the aqueous core double emulsion, where the shell can be easily observed, the shell of the organic core

microcapsules is almost not observed due to its reduced thickness. Due to decreased interfacial tension between the inner and middle phase in an o/o/w double emulsion, the template is more stable and allows the production of microcapsules with decreased shell thickness. In this way, thinner shells can be obtained, but the material can be tuned regarding shell thickness and size, similar to the w/o/w template. Some dimples can be observed in the capsules (Figure 4.28b), as well as the formation of microcapsules with spatially varying shell thickness. This hints to the fact that the density mismatch between the oil phase and the middle layer lead to the formation of non-uniform shell thickness. This is confirmed by SEM analysis of the microcapsules ruptured and washed with ethanol to remove the oil core. The microcapsules formed have a size of 110 µm and shell thickness around 2 µm, which varied along the shell as observed in Figure 4.28c and d. The core retention resulted in no buckling during the drying process, despite h = 0.04.

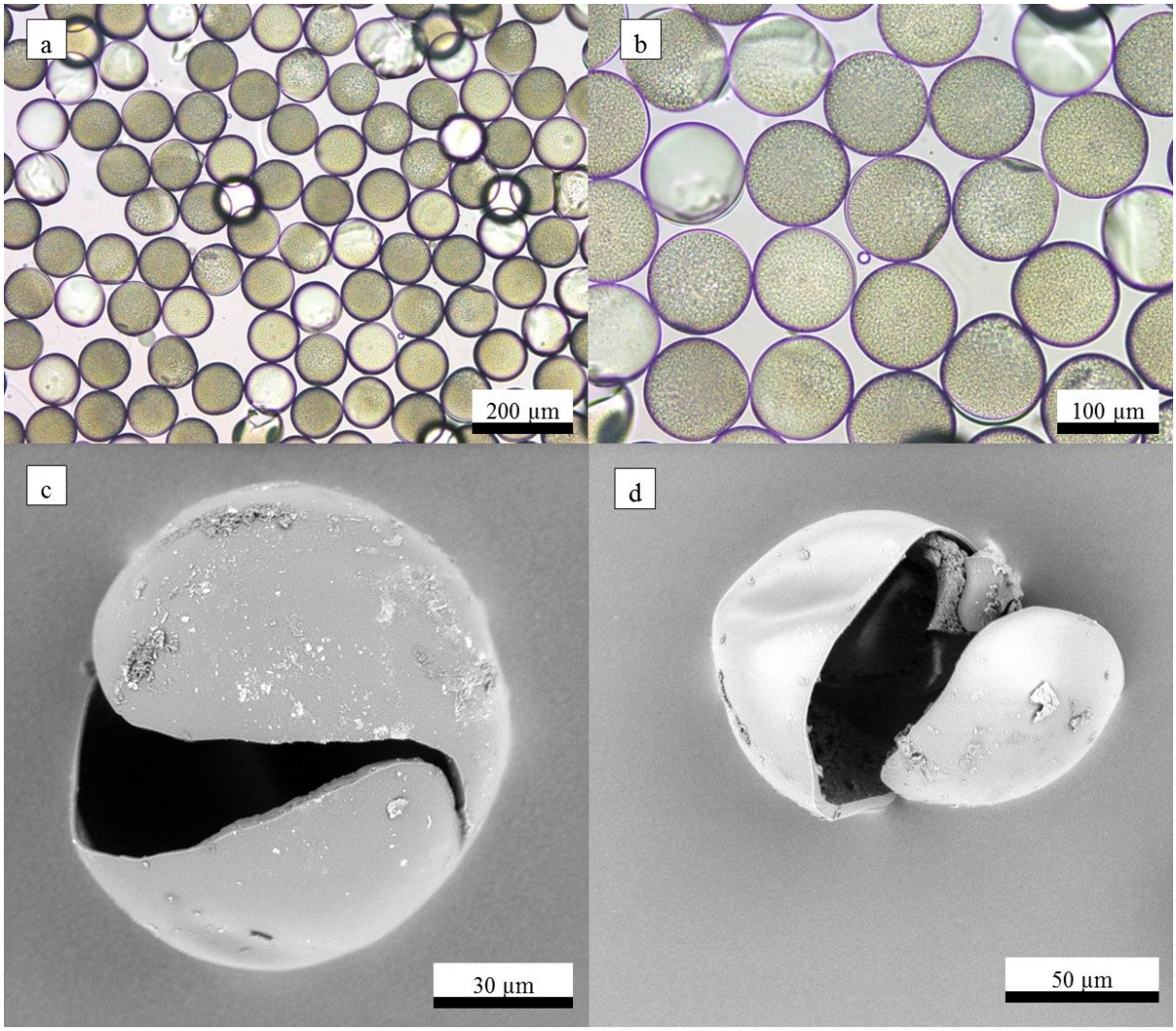

Figure 4.28 - Microcapsules BIMO-110/2. Optical microscope images of the monodisperse microcapsules (a) and (b). (c) and (d) SEM images of the dried and ruptured microcapsules.

Taking into account this dimensions, each microcapsule has 5 nL of core material and 0.6 nL of shell. Considering that the density of the shell is around 1.1 g/mL and the density of the core is approx.. 0.9 g/mL, the core content is 4.5 ng and the shell material is 0.6 ng. With this account, the shell represents 13% wt of the total material and the core material stands for 87% wt. To investigate these results, thermogravimetric analysis (TGA) of BIMO-110/2 dried capsules was performed and the results are shown in Figure 4.29. Between 150-300°C the degradation of the shell and of the mineral oil occurs simultaneously, as confirmed by the TGA of the bulk shell material and the neat mineral oil. By comparing the TGA of the microcapsules and the shell material at 400°C, the content of shell material was calculated to be 43%; thus, the mass balance of 57% was attributed to mineral oil as core. Based on the diameter and shell thickness of the double emulsion (110 and 2 μm, respectively), the expected core-to-shell volume ratio is 8.5:1, which corresponds to a theoretical weight fraction of mineral oil of 87% relative to the total capsule mass. Thus, the estimated encapsulation efficiency is 66% relative to the original mineral oil engulfed in the double emulsion. The loss of mineral oil can be attributed to the effects of gravitational settling due to the density mismatch of the mineral oil and acrylate phases. This led to the formation of spatially inhomogeneous emulsion and the escape of the mineral oil during the polymerisation, consequently reducing the encapsulation efficiency. This effect can be counteracted by the addition of healing agent to the organic carrier phase, potentially minimising the density mismatch and increasing the encapsulation efficiency.

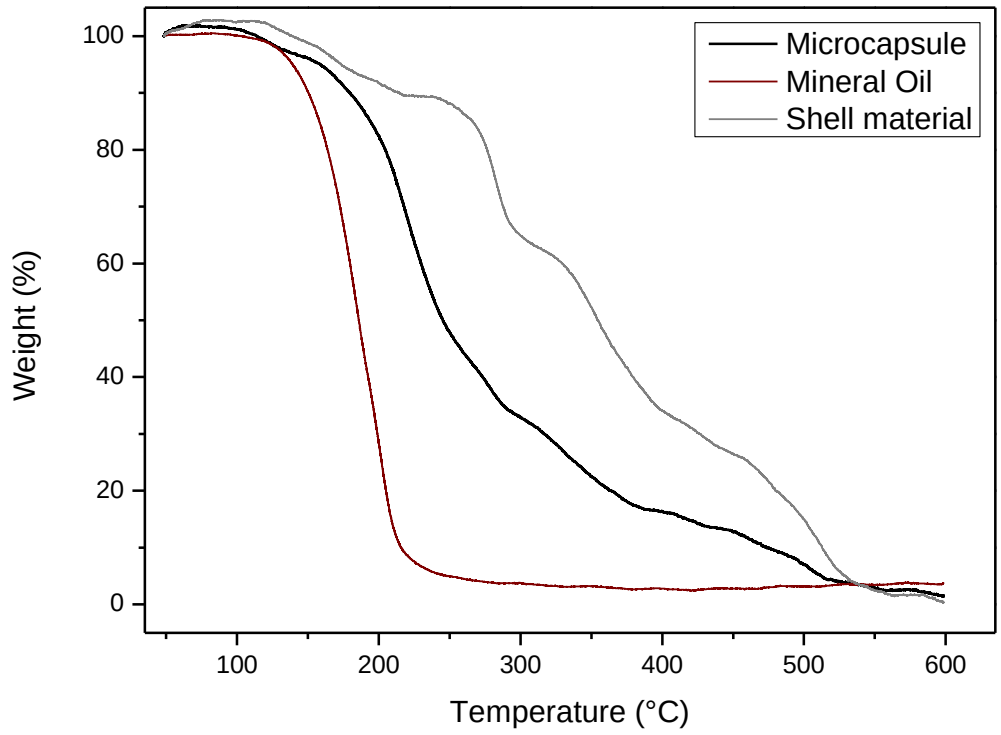

Figure 4.29. TGA curves of dried BIMO-110/2 microcapsules. Curves for the bulk shell material (grey) and mineral oil (red) are added for reference.

These results show that microcapsules containing non-aqueous core were successfully produced using the o/o/w template. The microcapsules are suitable to be used in capsule based self-healing due to the retention of the organic core which prevents the collapse of the capsule. Additionally, the thinner shell should favour the mechanically triggering self-healing. Although mineral oil does not participate directly in the self-healing process, its indirect use as vehicle has been explored in the encapsulation of bacteria (Wang et al. 2014) and emulsion of sodium silicate (Giannaros et al. 2016; Kanellopoulos et al. 2017). To produce organic core based microcapsules, microfluidics can be used for encapsulation of emulsions (Lee et al. 2016b), multiple component core (He et al. 2016) and a triple layered microcapsules (Choi et al. 2016; Lee et al. 2016a). Overall, the presence of oil was positive as it acted as an extra barrier in the microcapsule, increasing the retention of aqueous core (Lee et al. 2016b; Choi et al. 2016). The main disadvantage of using organic compound as core material is their easy absorption at the surface of mineral particles, and hence potentially decrease the cement hydration which is crucial for self-healing (Wang et al. 2014). But then again, the balance between conflicting solutions must be considered. Another disadvantage is the decrease in the payload – for instance, the content of sodium silica solution in the emulsion is ~20% (Kanellopoulos et al. 2016). However, accepting that the capsules are not capable of retaining the sodium silicate solution, the decreased payload in inevitable.

4.4.2. Encapsulating emulsions with mineral healing agent

As discussed before, typical mineral healing agents are water based and when the material is encapsulated the water leaks and the spherical integrity of the capsule is lost. Thus, an alternative option is to encapsulate an emulsion containing the healing agent – the oil is retained inside the microcapsule and prevents the structural failure. Furthermore, the oil works as a hydrophobic barrier and prevents the leakage of the water inside the containing the healing agent. Since the oil and the shell are hydrophobic, they work as a double barrier preventing the leakage of the core. To explore the potential of microcapsules containing organic core to encapsulate typical mineral healing agent, the production of an emulsion containing sodium silicate was investigated as shown in Figure 4.30.

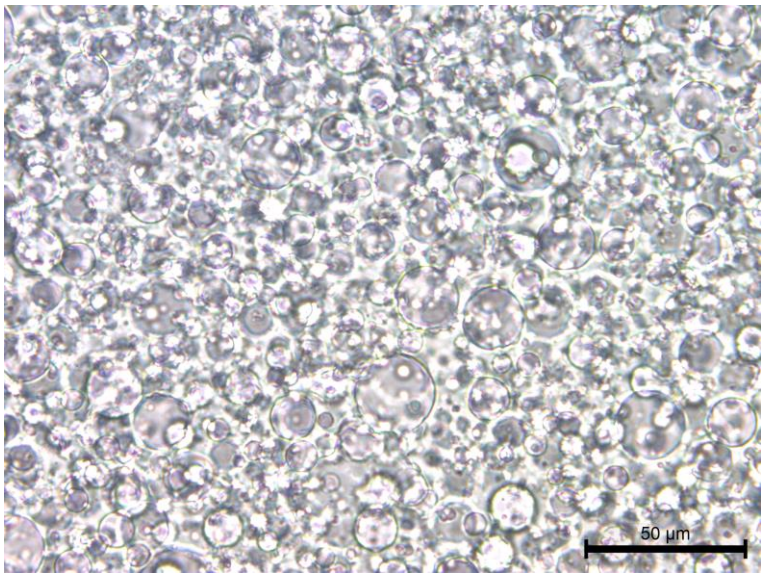

Figure 4.30 – Optical microscope image of the emulsion of sodium silicate in SIPMED oil shortly after the production.

The droplets of sodium silicate solution were homogenously dispersed in the continuous phase with maximum size around 20 µm. SIPMED 68 was used as continuous phase, Span 85 was used as surfactant and sodium silicate was used as dispersed phase. The SIPMED is a high purity, colourless and odourless oil which has been previously reported as continuous phase for the encapsulation of mineral healing agent (Kanellopoulos et al. 2017). Span 85, also known as sorbitan trioleate, is a sorbitol-based non-ionic surfactant comprised of a hydrophilic head-group linked to a hydrophobic alkyl chain. Span 85 is soluble in mineral oil but insoluble in water and it can be used as emulsifier in water-in-oil emulsions. Also, the hydrophilic-lipophilic balance (HLB), which expresses the relationship of hydrophilic and hydrophobic groups in a surfactant, is 1.8 for the Span 85. When the HLB is less than 10 this implies the surfactant is effective as water-in-oil emulsifier (Karsa 1999). The main concern during the production of the emulsion was the reaction of the sodium silicate solution with the surfactant. As discussed before, the high alkalinity of sodium silicate makes it highly reactive and it may result in reactions with the surfactants, e.g., the precipitation of PVA. Nonetheless, the emulsion was formed by mixing 6mL of SIPMED 68 with 300 µL of Span 85 and 1mL of sodium silicate using a magnetic stirrer for 10 min, as shown in Figure 4.30. The emulsion was still stable after 2 hours.

Next, as the emulsion was formed and stable without any visible phase separation due to reaction of sodium silicate and Span 85, another emulsion was formed for the production of the microcapsules. This time, 3 mL of SIPMED 68 was mixed with 120 µL of Span 85 and 1 mL of sodium silicate – in this case, the concentration of sodium silicate was 25% v/v, which is lower than the 40% of sodium silicate reported during the formation of emulsions (Kanellopoulos et al. 2016).

The emulsion was pumped inside the microfluidic device using BI as middle phase and PVA 10% as outer phase at flow rates of 0.73, 1.23 and 30 μL/min for inner, middle and outer flow, respectively. The produced microcapsules are shown in Figure 4.31.

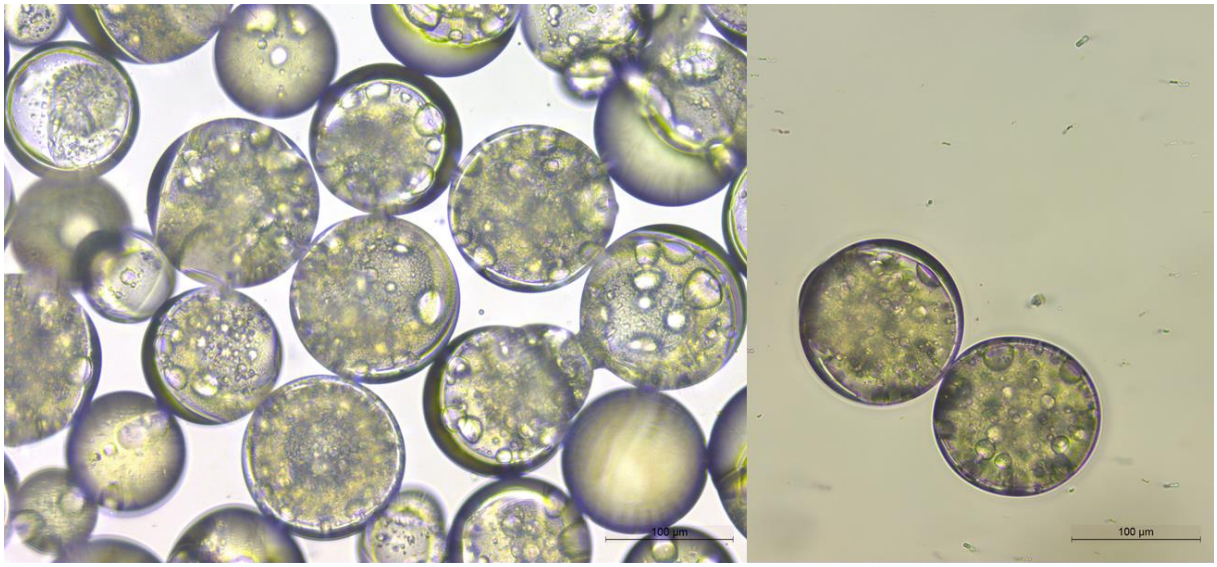

Figure 4.31 – Optical microscope images of the microcapsules with BI shell encapsulating an emulsion containing sodium silicate.

The microcapsules containing the emulsion can be observed in Figure 4.31, where the emulsion of sodium silicate in oil was encapsulated by the BI shell. These microcapsules were produced as proof-of-concept and more tests are necessary to investigate the formation of monodisperse microcapsules and minimum shell thickness of BI shell. Particularly, additional investigations looking at the maximum stable concentration of the sodium silicate in the dispersed phase are necessary. In this topic, special attention is necessary in the long term stability of the emulsion, outside and inside the microcapsule. For example, the emulsion containing 25% of sodium silicate used for the encapsulation was not stable for 2 hours, leading to phase separation of the oil and sodium silicate phases. However, when the material was encapsulated, no phase separation was observed.

The proof-of-concept of microcapsules containing emulsified colloidal silica was also investigated. The emulsion was formed by mixing 3 mL of mineral oil with 1 mL of Span 85 and 2mL of colloidal silica. In this case, the concentration of colloidal silica solution was 33% v/v and so, a higher concentration of surfactant was used to keep it stable. The resulting emulsion was not as uniformly dispersed as the emulsion of sodium silicate and black agglomerations were observed, indicating the phase separation of colloidal silica. Nonetheless, the material was stable to be used as inner phase in the microencapsulation using microfluidics and the results are shown in Figure 4.32.

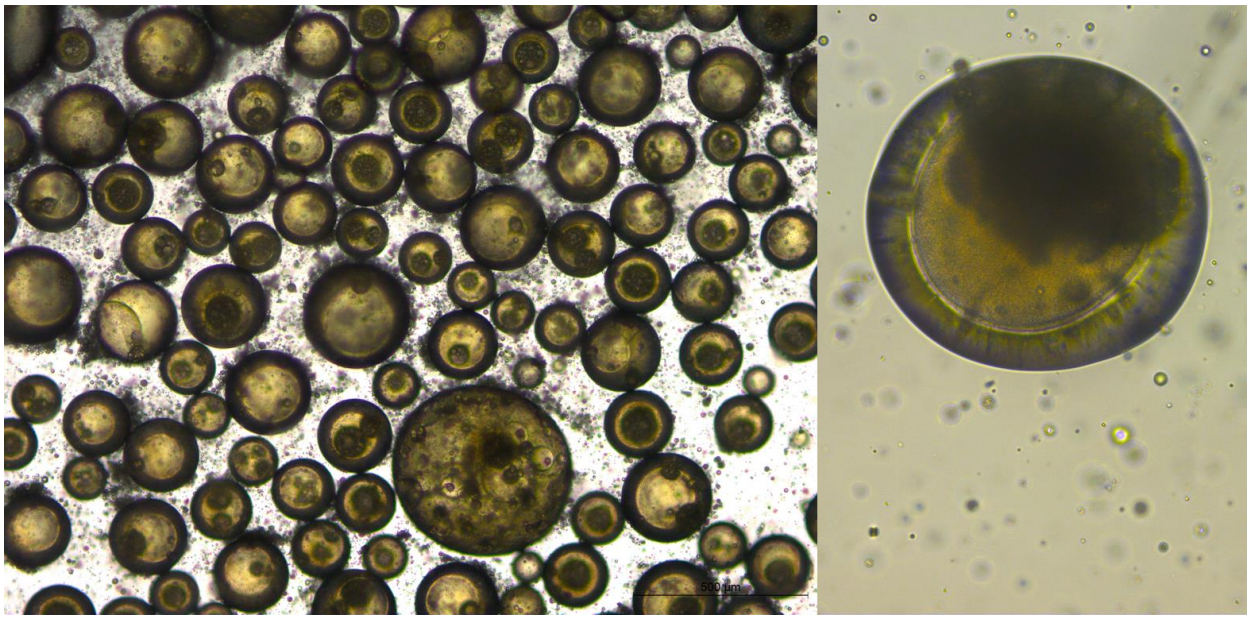

Figure 4.32 – Optical microscope image of the double emulsion (a) and the microcapsules (b) containing an emulsion with colloidal silica as dispersed phase.

The double emulsion was produced using a flow rate of 1.4, 2.4 and 60 μL/min, for inner, middle and outer flow rate, respectively. The flow rate was measured with the pumps calibrated for water with all the fluids, so the actual flow rate was higher and the microcapsules were produced in the tubing regime. This partially explains the variations of size of the formed double emulsion, as observed in Figure 4.32a. Some cloudy material was floating around the double emulsion, indicating that not all the colloidal silica was encapsulated. It is likely that the high concentration of colloidal silica in the mineral oil resulted in the poor stability of the emulsion. The phase separation explains the dark coloration of the core material in Figure 4.32b which can be attributed to the colloidal silica. Alternatively, the previous encapsulation of colloidal silica in water (Figure 4.21a) show no colour difference due to the colloidal silica inside the capsule. This indicates that more investigations are needed to adjust the maximum concentration of stable colloidal silica.

The stability of the formed emulsion containing the healing agent is of paramount importance for the formed microcapsule. While the emulsion can prevent the leakage of the core material, the density mismatch within the formed emulsion phase (e.g., $\rho_{oil} \sim 0.86$ and $\rho_{sodium\ silicate} \sim 1.5$ g/mL) can promote the phase separation due to buoyancy. When the core material is biphasic, the water is in direct contact with the shell and is free to permeate through the nanopores of the membrane leading to loss of structural integrity (Lee et al. 2016b). For example, Giannaros et al. (2017) reported the encapsulation of sodium silicate emulsified in SIPMED 68 using pig gelatine as shell (Kanellopoulos et al. 2017). In this case, the optical microscopy images of the capsules hint to phase separation inside the capsule (Figure 4.33), which could facilitate the loss of water through the

hydrophilic gelatine shell. Further studies are necessary to investigate the stability of emulsified core over time and if the loss of water would lead to the structural changes of the microcapsule. Also, the polymerisation of the continuous phase can be investigated as mechanism to prevent the phase separation and, thus, the leakage of the core (Lee et al. 2016b).

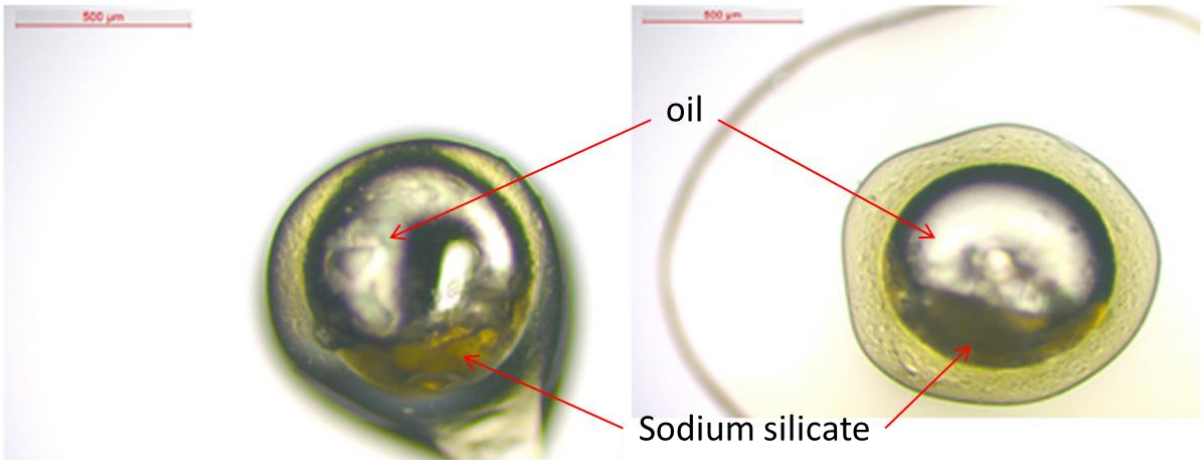

Figure 4.33 - Indication of phase separation inside of microcapsules containing emulsions with the healing agent. Adapted from (Kanellopoulos et al. 2017).

4.5. Conclusions

The production of microcapsules using microfluidics and the encapsulation of liquid mineral healing agents were detailed in this chapter. Microfluidics was successfully used to produce double emulsion templates which were subsequently polymerised into microcapsules under UV-light. Preliminary investigations of the methodology looked at the influence of the set-up in the production of fully closed microcapsules. Additionally, the effect of the flow rates at the flow regime and the mechanism of formation of the double emulsion were also explored. To investigate the production of microcapsules containing an aqueous core, double emulsion templates of water-in-oil-in-water (w/o/w) were produced and photopolymerised. By fine-tuning the inner, middle and outer flow, microcapsules containing an aqueous core with different shell and diameter were produced. The encapsulation of aqueous and organic based healing agents was demonstrated, as well as the use of four different shell materials (BH, BI, UH and BIH). The main outcomes of the research are summarised in Figure 4.34.

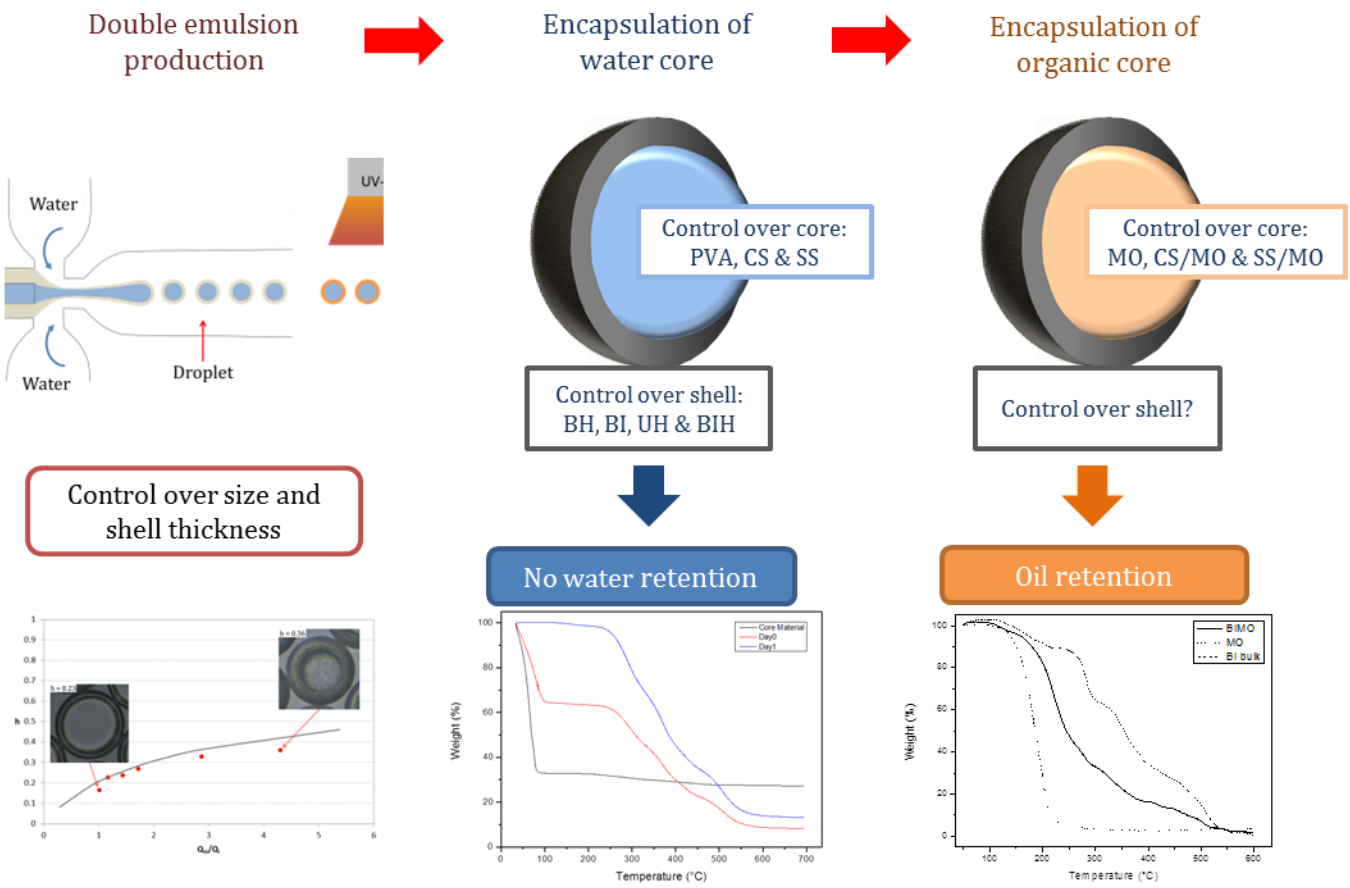

Figure 4.34 - Schematic representation summarising the outcomes of Chapter 4.

The water was encapsulated but, because of the permeability of the shell material, the water was not retained inside of the acrylate shell. Thus, although colloidal silica and sodium silicate aqueous solution were encapsulated, the loss of water during the drying process results in the retention of only the dried mineral inside the capsule. As a consequence of the loss of encapsulate water, the capsules are likely to shrink and/or buckle, depending on size of the capsules and mechanical properties, thickness and uniformity of the shell.

To produce microcapsules capable of retaining the core material, mineral oil was successfully encapsulated using an o/o/w template and the core retention was confirmed using TGA. However, the versatility of the double emulsion template was reduced and UH could not be used as shell material. Nonetheless, BI was used as shell and resulted in microcapsules with shell thickness ~2 µm. Furthermore, the encapsulation of emulsions containing colloidal silica and sodium silicate as healing agent has been demonstrated as proof-of-concept.

The integration of the microcapsules in the cementitious matrix and assessment of physical triggering is described in Chapter 5.

5. DESIGNING MICROCAPSULES FOR MECHANICAL TRIGGERING

The triggering mechanism for microcapsule-based self-healing is an important parameter for the assurance of the self-healing process. Microfluidics offer a route to explore a wide variety of shell materials, thus the mechanical properties can be tuned to boost the physical triggering. This chapter focuses on the development of mechanically triggered microcapsules produced using the microfluidic device. The preliminary investigation looked at the survival, dispersion and interfacial bonding of the microcapsules in the cement paste. The behaviour of aqueous and organic core microcapsules was also investigated. Then, five acrylate copolymers with potential for use as shell material were characterised using a DMA, microindenter, and tensile testing equipment to assess the glass transition temperature (T_g), Young's modulus and tensile strength. The adjustment of the glass transition temperature, Young's modulus, fracture toughness and strength can be used to boost the mechanical triggering. Furthermore, to overcome poor interfacial bonding between the cementitious matrix and the shell material, an easy and robust methodology to functionalise the microcapsule shell was proposed.

5.1. MICROCAPSULES' BEHAVIOUR IN THE CEMENTITIOUS MATRIX

To ensure the healing agent is released upon crack formation, the microcapsules need to survive the mixing process and be mechanically triggered by a crack. However, the survival can be challenging, due to the strong alkalinity of cementitious matrices (pH>12), the high shear during mixing and elevated temperatures ranging from 35 to 80°C during the cement hydration and setting processes. Additionally, the crack formation does not ensure mechanical triggering, and the microcapsules may debond or shrink during the integration in the cementitious matrix. Although several authors have reported the use of different shell materials to produce microcapsules for self-healing, this was the first time acrylates were used. Thus, a preliminary investigation of the behaviour of the microcapsules in the cementitious materials was necessary. Particularly, this section looks at the survival, dispersion and mechanical triggering of the acrylate microcapsules in the cement paste.

5.1.1. SURVIVAL, DISPERSION AND INTERFACIAL BONDING

In order to investigate the performance of microcapsules during integration in the cementitious matrix, the microcapsules with aqueous core were embedded in the cement paste. The microcapsules BH-82/12 with aqueous core were produced using a microfluidic double emulsion template, described in section 4.3.1 and dried at room temperature for 1 day prior to integration. Then, the microcapsules were hand mixed with the cement powder and water (water-to-cement ratio of 0.45) and cast for SEM observation after 1, 7, 14, 28 and 64 days (Figure 5.1). The

microcapsules were observed up to 64 days to investigate the variation of bond strength between the shell surface and the cement matrix overtime. SEM images revealed that the microcapsules with the acrylate shell survived the mixing and exposure to the alkaline cementitious environment. In an opposite scenario, the microcapsules would have not retained their characteristic spherical shape and excessive amount of ruptured shells and debris would have been observed. Microcapsule bunches or agglomerations formed during the polymerisation of sample BH-82/12 (Figure 4.18d) and remained together after the mixing process (Figure 5.1a). This agglomeration decreased the contact area between the cementitious matrix and the surface of the microcapsules, preventing its rupture. Although some sparse polymeric material was seen over the cracked surface of the cement, the first ruptured capsule was observed at 14 days after curing (Figure 5.1c).

Unfortunately, most of the microcapsules debonded upon the crack formation, indicating poor interfacial bonding between the shell and the matrix. In general, the interfacial bonding in the cementitious matrix results from a combination of mechanical interlock, physical bonding involving van der Waals's force and, possibly, chemical reactions (Mindess 1987). For example, the bond between concrete and steel reinforcement is primarily mechanical, whereas the interface between concrete and fibres can arise from chemical reactions. In the case of microcapsules, the formation of the double emulsion relied on the hydrophobic nature of the oil middle layer. Consequently, the shell was also hydrophobic and prevented the chemical bonding with the hydrophilic cement paste. In addition, the smooth shell surface formed due to the surface tension during the polymerisation hindered the physical interlock with the cementitious matrix. However, although the interfacial bonding between the shell and the matrix was initially low, the formation of chemical bonds increased over time. While the sample was submerged, the diffusion of the water-cement solution to the interface between the capsule and the matrix may have occurred, leading to the nucleation of $Ca(OH)_2$ crystals. As a result, a thin layer of cement was observed to be covering the microcapsules at 64 days (Figure 5.1f). Similar results were observed with hydrophobic fibres (Peled et al. 2008), where a gap developed between the hydrophobic fibre and the cement matrix due to the low chemical affinity. Alternatively, when hydrophilic fibres were used, the affinity between the matrix and the fibre resulted in chemical bonds, and no gap developed for the nucleation and growth of crystals. Nonetheless, even after the increase in the interfacial bonding, the microcapsules remained mostly unbroken due to debonding after 64 days.

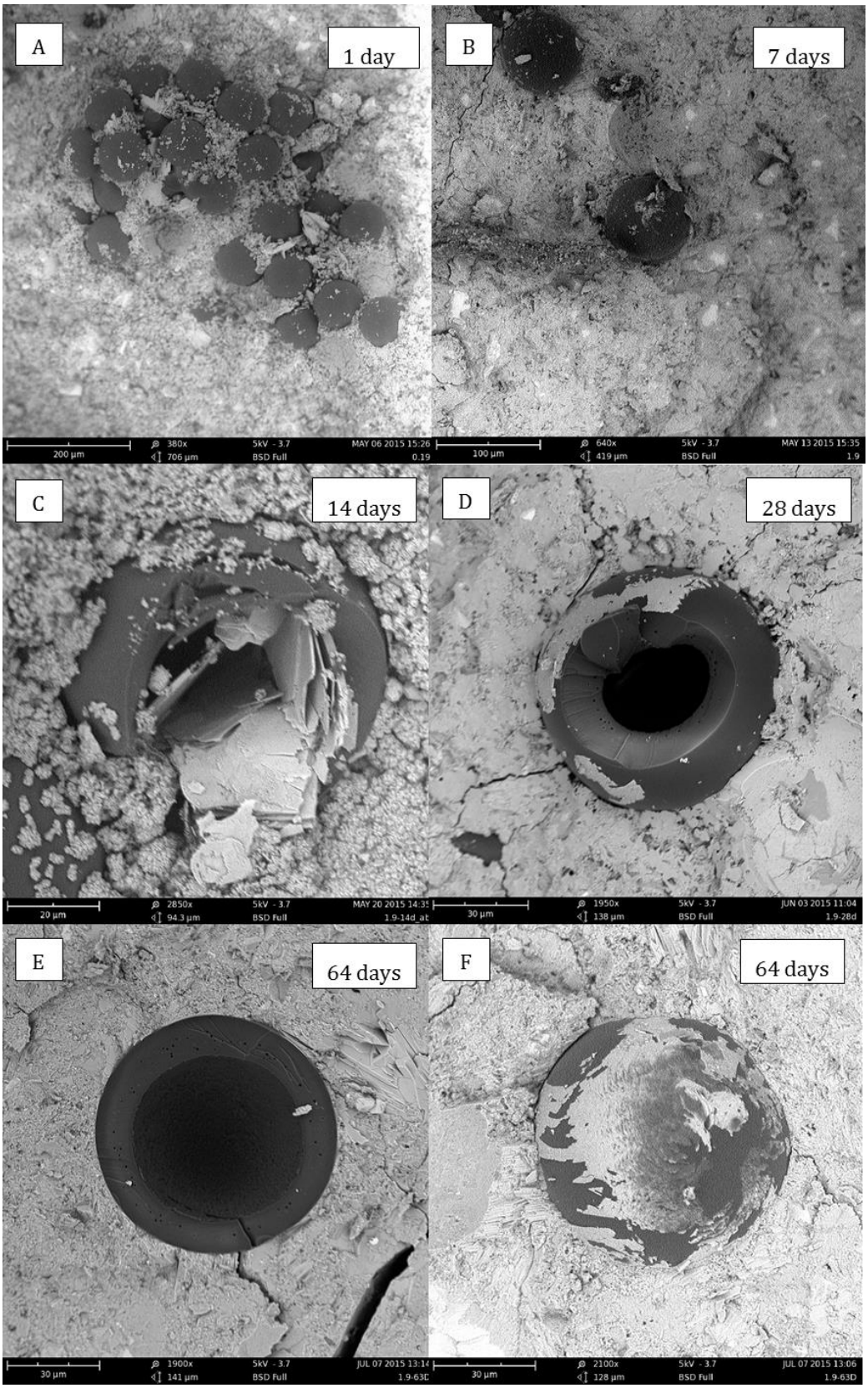

Figure 5.1 - SEM images of the microcapsules BH-82/12 embedded on cement paste after (a) 1 day, (b) 7 days, (c) 14 days, (d) 28 days, (e) and (f) 64 days.

5.1.2. Shell thickness

Another factor contributing to prevent the mechanical triggering of self-healing is the shell thickness. Microcapsules with thick shells present higher resistance against plastic deformation and higher stress is necessary to rupture the shell. Hence, to investigate the influence of shell thickness on the likelihood of mechanically triggering the microcapsules, sample BH-88/7 was also embedded in the cement paste. Commonly, the shell thickness of microcapsules used for self-healing of cementitious materials ranges between 0.6 and 45 μm, as shown in Table 2.2, depending on the diameter. Using microfluidics and the BH shell, microcapsules with 7 μm shell thickness were produced, as described in section 4.3.1, and named BH-88/7. These microcapsules were dried and hand mixed with the cement paste, and observed in the SEM after 1, 7, 14, 28 and 64 days (Figure 5.2). Sample BH-88/7 dispersed over the crack surface and no formation of debris was observed indicating good survival during the mixing. Because these microcapsules were collected in PVA 10% wt solution, the formation of bunches was prevented, favouring a more scattered distribution of the capsules. A broken capsule was observed at day 1, where the deposition of sheets of mineral (possibly $Ca(OH)_2$) inside the capsule was observed (Figure 5.2a). However, in the following days it was rare to observe ruptured microcapsules under crack.

A common feature observed for microcapsules BH-82/12 is the anisotropical shrinkage, as observed in the images at 14 days (Figure 5.2c) and 64 days (Figure 5.2f). As discussed previously (section 4.3.1), the capillary pressure caused by the evaporation of the surrounding water and the loss of water core may have caused the capsule to buckle. The likelihood of buckling is proportional to the shell thickness to radius ratio (Equation 4.5), thus, for the microcapsules BH-82/12 with the shell thickness of 12 μm, no buckling was observed. Alternatively, for the microcapsules with 7 μm shell thickness the deformation of their spherical shape, due to the loss of surrounding water during the drying of cement paste, was observed. Since the microcapsules were filtered and dried prior to mixing, partial evaporation of water had occurred resulting in the formation of dimples (Figure 4.19). When these capsules were mixed with the cement paste, the shape of the dimples was imprinted in the cement cavity, as observed in Figure 5.2c,f. However, after the hardening of the cement, the dimples deepened even further resulting in the formation of an empty space between the microcapsule and the matrix (Figure 5.2c). A similar process was observed in Figure 5.2f, where the microcapsules collapse inwardly causing the shell breakage into two parts. As a result, the gap between the microcapsule and the original cavity formed by the microcapsule during the hardening of the cement was wider. This gap offered a preferential and less energy intensive crack path, preventing the mechanical rupture of the shell.

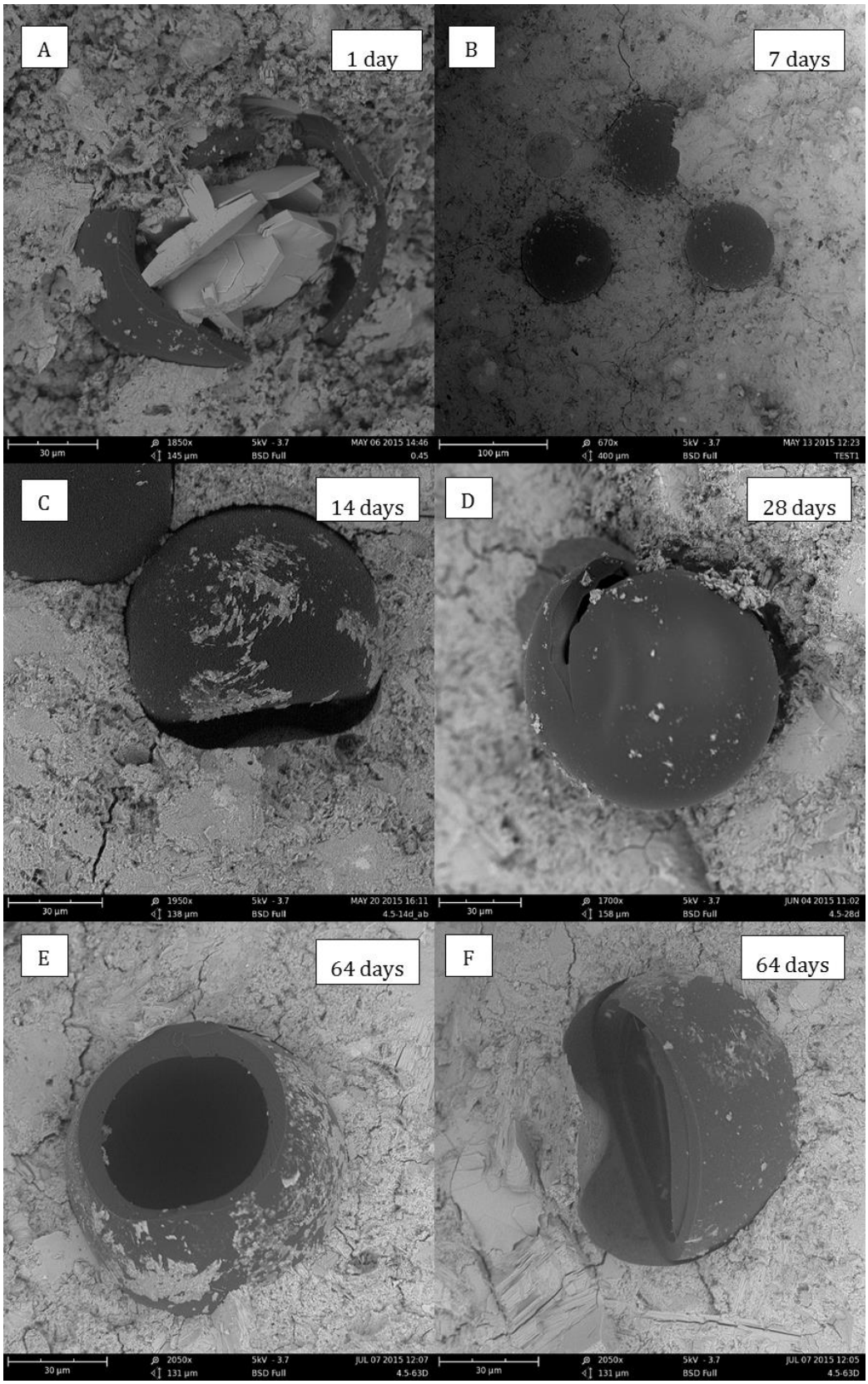

Figure 5.2 SEM images of the microcapsules BH-88/7 embedded on cement paste after (a) 1 day, (b) 7 days, (c) 14 days, (d) 28 days, (e) and (f) 64 days.

In order to numerically estimate the percentage of the BH-82/12 and BH-88/7 microcapsules that were broken under cracking, approximately 100 capsules were observed in the SEM. The capsules were separated into broken, debonded and deflated (e.g., Figure 5.2f) and the results are displayed in Figure 5.3.

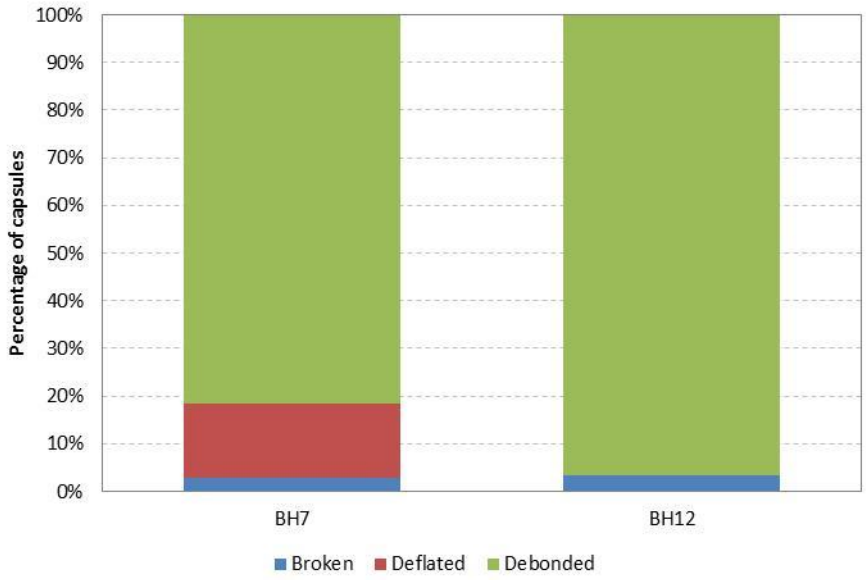

Figure 5.3 – The fate of microcapsules BH-88/7 and BH-82/12 after 64 days in the cement paste.

Although the likelihood of the thin-shelled microcapsules to rupture was expected to be higher, the result was not achieved and the percentage of broken capsules in both shell thicknesses was ~ 5%. For comparison, Lv et al. (2016) found that smaller sized microcapsules (50–200 μm) tended to be more easily ruptured by cracks in cement paste, reporting that around 30% of the microcapsules were mechanically triggered (Lv et al. 2016a). The low values of triggered microcapsules were attributed to four main reasons: (i) the poor interfacial bonding between the microcapsules and the matrix; (ii) the elevated shell thickness, particularly for sample BH-82/12; (iii) the loss of spherical shape of the microcapsules, particularly for sample BH-88/7; and (iv) the mechanical properties of the shell. The interfacial bonding between the shell and the cementitious materials was a concern, since other authors have reported debonding instead of rupture of the microcapsules (Wang et al. 2013; Lv et al. 2016a). The deformation of the capsules due to the loss of core material was also responsible for reducing the percentage of the mechanically triggered microcapsules, primarily for sample BH-88/7. To decrease the likelihood of buckling, the shell thickness could be increased, but it resulted in preventing the mechanical triggering, as shown for sample BH-82/12. Thus, to increase the likelihood of aqueous core microcapsules being mechanically activated, the properties of the acrylates were preliminary investigated, particularly the tensile strength.

5.1.3. TENSILE STRENGTH

5.1.3.1. EPOXY BASED SHELL

Preliminary investigation on the effect of mechanical properties on the likelihood of rupture considered the tensile strength of the acrylates. The copolymer of 25% HDDA and 75% BisGMA, more concentrated in BisGMA than the BH used for encapsulation, was reported to have a tensile strength of 56 MPa. On the other hand, the copolymer of 50% ETMPTA and 50% BisGMA presented a tensile strength of 40 MPa (Miller, 1989). Both copolymers presented high values of tensile stress prior to failure, especially when compared with the low tensile strength of concrete (2-6 MPa), and this may have been responsible for preventing the mechanical triggering. Nonetheless, the slightly reduced tensile strength of the copolymer with ETMPTA was appealing for the preliminary investigations on the mechanical properties. To examine the impact of a lower tensile strength, double emulsions with a middle fluid comprised of 80% wt of ETMPTA and 20% of BisGMA, named 20BE, were produced. This proportion of ETMPTA was determined after investigating the production of double emulsion with 50 and 40% wt BisGMA – both solutions were very viscous and difficult to pump. Then, the solution was diluted to 80% of ETMPTA and a double emulsion was produced using an inner aqueous solution 10 % wt of PVA and an outer fluid of PVA 2% wt. The elevated viscosity of PVA 10% wt facilitated the formation of the double emulsion in the dripping regime. The flow rates were 0.35, 1.2 and 36 μL/min (pressure of 308, 402 and 260 mbar) for the inner, middle and outer fluids, respectively. The pumps were calibrated for water, so the flow rates were inaccurate, but the pressure could act as a guideline for the reproduction of the experiment. The double emulsion was in-situ polymerised and the produced microcapsules were embedded in the cement paste (w/c=0.45). The double emulsion and microcapsules produced are shown in Figure 5.4, as well as the SEM of microcapsules embedded in the cement paste after 3 days.

The double emulsion produced in the dripping regime was highly monodisperse as observed in Figure 5.4A. However, with 20BE as the middle fluid, the middle layer was thick and very difficult to make thinner. After polymerisation, fully closed core-shell structures were formed, with an outer diameter of 86 μm and a shell thickness of 14 μm. The elevated shell to radius ratio (h = 0.32) indicated that the shell was unlikely to buckle due to water loss and the structural integrity of the capsule may have been preserved. This is demonstrated when the microcapsules were added to the cement paste, where no collapsed microcapsules was observed. Unfortunately, the thick shell also prevented the physical triggering and, despite the decrease in tensile strength, no ruptured microcapsules were observed. Interestingly, the adherence of cement on the surface of the microcapsules (Figure 5.4C and D) was better than the adherence in the BH microcapsules at 3 days. The increase in interfacial bonding was attributed to the ethoxylate groups present in the ETMPTA,

whereas HDDA had an alkyl hydrophobic backbone. The oxygen present in the ETMPTA chain facilitated hydrogen bonds with the polar groups in the cement paste, making the shell more hydrophilic. Nonetheless, the change in tensile strength and interfacial bonding was not sufficient to rupture the microcapsules upon crack formation. Thus, the reduction in shell thickness while retaining the structural integrity was necessary to promote mechanical triggering of the microcapsules.

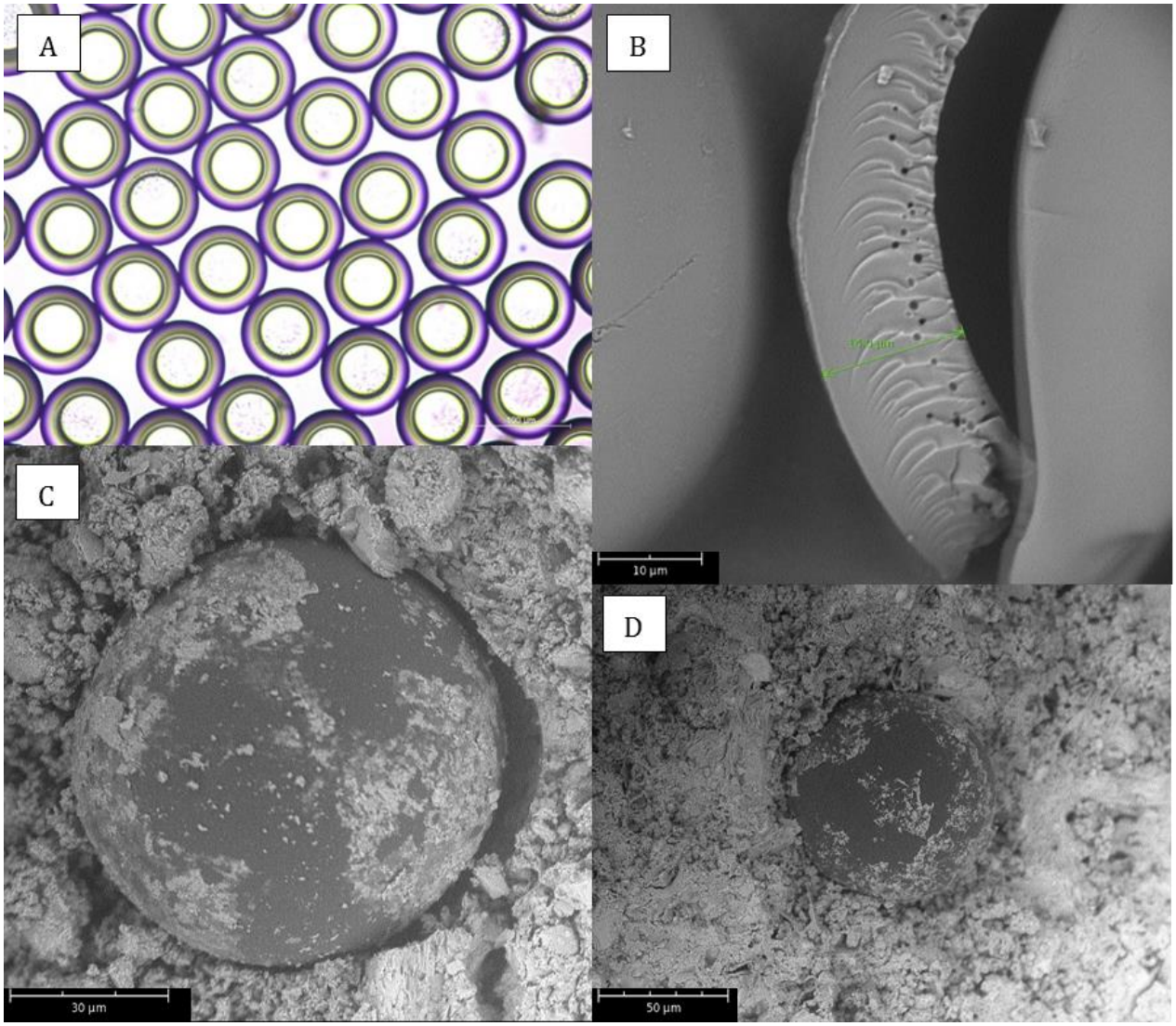

Figure 5.4 - Images of the capsules 20BE-86/14: (A) OM images of the double emulsion; (B) SEM image focusing on the shell; and (C and D): SEM images of the microcapsules embedded on cement paste for 3 days.

5.1.3.2. URETHANE BASED SHELL

In order to investigate the role of the oligomer in the performance of the microcapsules after integration in the cementitious matrix, a urethane-based acrylate was used as shell. The urethane acrylate MU3603 presents a low tensile strength (3.4 MPa) and Young's modulus (12 MPa) which

can contribute to the similar properties in the copolymer. The production of microcapsules using UH (urethane acrylate and HDDA) as shell was described in section 4.4.4. Furthermore, the microcapsules UHCS-125/7.5 with colloidal silica as core have a thinner shell to radius ratio (h = 0.12) which can facilitate the mechanical triggering. The produced microcapsules were washed to remove the PVA and kept in water prior to the mixing with cement to assure the retention of the water core. Then, the microcapsules were hand mixed with cement powder and water, cast, and observed in the SEM after 1 day of casting (Figure 5.5).

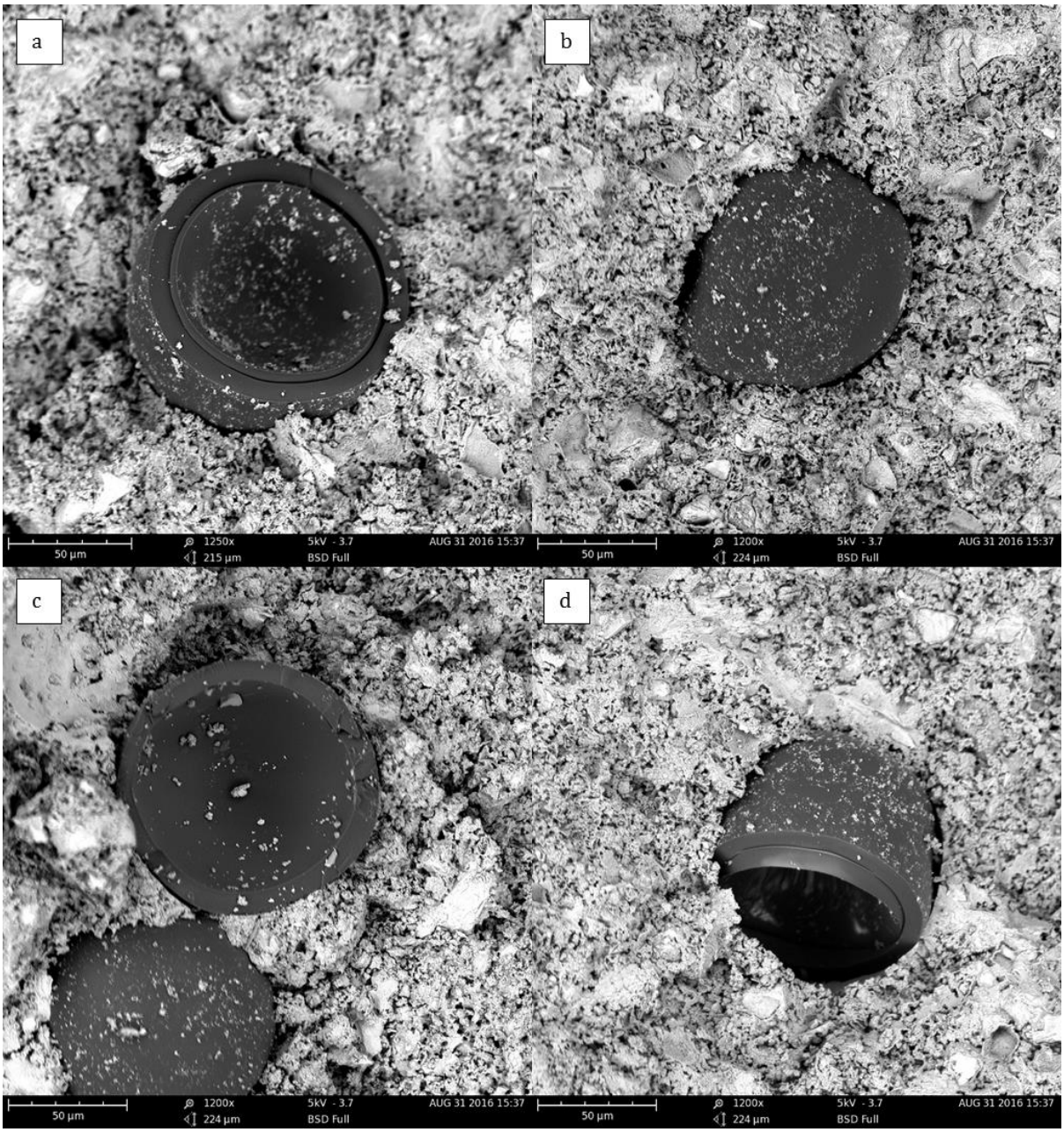

Figure 5.5 – SEM images of the microcapsules UHCS-125/7.5 embedded in the cement, showing microcapsules (a) deflated due to the water core, (b) debonded, (c) broken and (d) collapsed and forming a gap between the capsule and the matrix.

Although a broken microcapsule was observed (Figure 5.5c), most of the microcapsules were debonded (Figure 5.5b) or deflated (Figure 5.5a,d). Interestingly, when the microcapsules were dried in air, they kept their spherical shape during the process, as shown in Figure 4.24. However, the microcapsules dried in the cement paste were mostly buckled and collapsed due to the loss of water core. This hinted that the buckling pressure during the drying of the cement paste might have been higher than the buckling pressure in air. Furthermore, the combination of low shell-to-radius ratio and low Young's modulus reduced the minimum threshold buckling pressure and the microcapsules were more easily buckled. As discussed for the microcapsules BH-88/7, the buckling of the microcapsule during the drying of the cement diminished the interfacial bonding between the matrix and the shell. As a result, even if the tensile strength of the acrylate shell was reduced, the deformation of the microcapsules would still preclude the mechanical triggering. Since the buckling is caused by the loss of water core, microcapsules capable of retaining the core material were also investigated.

5.1.4. Organic core

The organic-cored microcapsules were also embedded in the cementitious matrix to investigate their performance during the integration. As discussed in section 4.4.1, the microcapsules containing organic core had thinner shells (around 2 μm) and they were capable of retaining the core material, thus they were more likely to be ruptured by crack formation. Although UH was likely to present a lower tensile strength, the production of organic core microcapsules with UH shell was not possible. Thus, BI was investigated as shell material, since the brittle nature of isobornyl acrylate has been reported in the literature (Chen et al. 2012). The production of microcapsules BIMO-110/2 containing mineral oil as core and BI as shell, was described in section 4.5.1. After being polymerised, the microcapsules were washed to remove the PVA and retained under water prior to being added to the cement paste. Since the loss of the surrounding water is one of the factors contributing to the buckling of the shell, the capsules were kept in water to minimise this effect. Prior to being inserted in the SEM, the crack surface was blasted with an air duster and vacuumed to remove the organic core of the ruptured microcapsules and Figure 5.6 shows the SEM images of the cast microcapsules after 1 day. Regarding the integration, despite the density difference – because of the oil core, the density of the microcapsules was less than 1g/L and thus floated on water – the microcapsules were well dispersed in the cement paste. Figure 5.6B shows the presence of holes in the shells, possibly formed during the polymerisation and also due to microcapsule debris, likely to have formed during the mixing process. The brittle nature of the BI shell makes the microcapsule more prone to physical triggering, but also more likely to be broken during the mixing. Due to the hydrophobic surface of the microcapsules, poor interfacial bonding was observed and most of the microcapsules debonded upon crack formation (Figure 5.6a).

Nonetheless, broken microcapsules were often observed (Figure 5.6c, d), due to the retention of organic core, thinner shell and more brittle material when compared with the BH microcapsules with aqueous cores. As expected, no deflated microcapsules were observed since the oil did not leak through the nanopores of the shell. The inhomogeneous shell thickness due to the density mismatch between the acrylate shell and the core material was observed in Figure 5.6d.

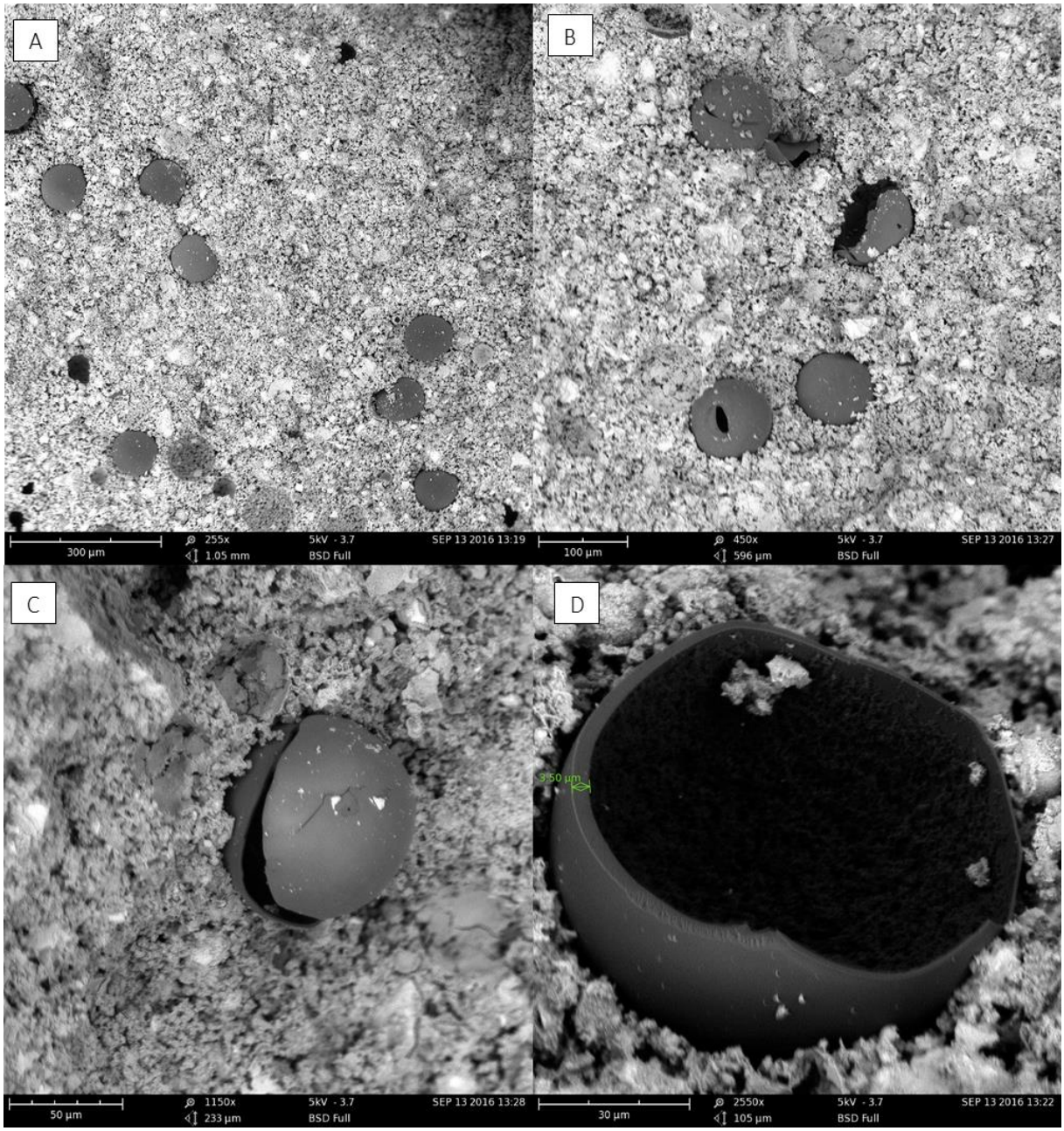

Figure 5.6 – SEM images of organic cored and hydrophobic shelled microcapsules BIMO-110/2 casted in cement paste after 1 day, showing (a) and (b) debonded microcapsules, (c) and (d) microcapsules ruptured upon crack.

These preliminary results indicated that the use of the double emulsion template of water-in-oil-in-water resulted in a smooth and hydrophobic shell surface, which hindered the interfacial bonding. Furthermore, the loss of water core played a key role in preventing physical triggering: if the shell was thin, the microcapsule would deform during the water evaporation; if the shell was thick, the capsule would not deform but also would not rupture upon crack formation. To overcome this issue, an organic core was used, since the material was retained inside the microcapsule, but the poor interfacial tension still prevented the mechanical triggering. Nonetheless, the use of a more brittle shell and the reduced shell thickness achieved with organic core resulted in an increased number of ruptured capsules. As result of this preliminary investigation, the mechanical properties of the shell material were investigated in more detail, to maximise the chances of mechanically triggering the microcapsules.

5.2. Mechanical Properties of the shell material

Suitable mechanical properties of the microcapsules' shell are considered essential to ensure the feasibility of self-healing. The properties of the microcapsules are directly associated with two important parameters in microcapsule-based self-healing: the mechanical properties of the matrix after embedding the capsules and the mechanical triggering of self-healing. Overall, the poor interfacial bonding and reduced elastic modulus of the microcapsules were associated with the decrease of mechanical properties of the matrix after incorporation of the microcapsules. As for mechanical triggering, the elastic modulus, fracture toughness and strength, and interfacial bonding are key factors for the likelihood of crack formation in the shell. Hence, this section explored some of the key parameters governing physical triggering, namely, the glass transition temperature, Young's modulus and tensile strength. The goal was to understand and acknowledge how these properties may vary for 5 different acrylates with potential to be used as shell material. From the data of the mechanical properties, the most suitable acrylate to be used as shell could be selected, aiming at the mechanical triggering. It was found that, despite the general importance of glass transition temperature and Young's modulus of the acrylates, the tensile strength, shell thickness and interfacial bonding were the main responsible for the physical triggering.

5.2.1. Glass Transition Temperature of the acrylates

The glass transition temperature (T_g) - the temperature at which the material ceases to be brittle and glassy and becomes ductile – needs to be considered for the application of self-healing. Ideally, the material should be brittle enough to rupture upon crack formation but ductile enough to survive mixing. The T_g is correlated to molecular structure of the polymer and the weaker secondary bonding between the neighbouring polymer chains. This can be explained by the

crankshaft model which treats the molecule as a collection of mobile segments with some degree of free movement (Mark 2007). These molecules are virtually frozen at very low temperatures, where the molecule is tightly compressed. As the material warms and expands, the free volume increases so that localised bond movements (bending and stretching) and side chain movements can occur. As the temperature and the free volume continue to increase, the whole side chains and localised groups begin to have enough space to move and the material starts to develop some toughness. This transition is called the beta transition (T_β) and a correlation with toughness has been seen empirically. As the heating continues, the T_g appears when the chain in the amorphous regions begin to coordinate large scale movements. This increased mobility in either side chains or small groups of adjacent backbone polymeric chain results in a greater compliance (lower modulus) of the material.

To investigate the influence of the molecular structure in the T_g, five different acrylates with potential to be used as shell were compared. The presence of side groups in the polymeric backbone increases the energy required to rotate the molecule, particularly in the case of bulky and/or rigid side groups. Thus, 4 different acrylate monomers, namely, PEA, IBOA, HDDA and s selected to investigate the role of the side groups. The T_g of the different polymers was found in the literature and was depicted in the black bars of Figure 5.7, together with the molecular structure of the monomers.

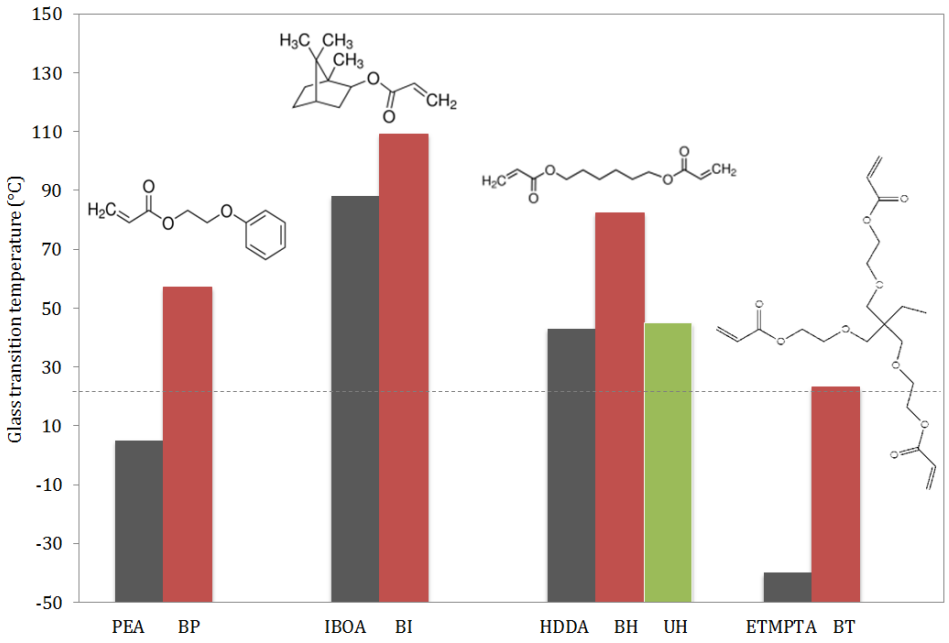

Figure 5.7 - Glass transition temperature of the four monomers individually (black) and the respective copolymer after the addition of BisGMA (red) and MU3603 (green). Dashed line indicates the room temperature at 20°C.

IBOA presented the highest T_g, 88°C, attributed to the bulky side group attached to the polymer backbone which restricts the molecular rotation. The linear structure of HDDA together with the difunctionalilty promoted a higher level of crosslinking and the second highest T_g, 43°C. The T_g of PEA and ETMPTA are the lowest ones, 5 and -40°C, respectively, mainly due to the ethoxylate group which present little steric hindrance to rotation. Especially for ETMPTA, as the ethoxy moiety becomes longer, the polymer chains are pushed further apart, creating additional free volume and decreasing the T_g.

Since the formation of droplets is facilitated by the increased viscosity (μ) of the middle fluid, the tuning of this parameter was performed for the formation of double emulsion. To increase the viscosity of the acrylate fluid and facilitate the formation of droplets, two viscous monomers were used: BisGMA and a urethane diacrylate. BisGMA has hydroxyl groups on the backbone and the π-π interactions given by the aromatic rings increase the initial viscosity. Copolymers composed of 1:1 in weight of BisGMA and the monomers PEA, IBOA, HDDA and ETMPTA was produced and named BP, BI, BH and BT, respectively. The aromatic urethane diacrylate (MU3603, Miramer, MW=3300g/mol, μ=4000 cP (at 60°C)) was also used, due to its high viscosity and low tensile strength. Also, increasing molecular weight of the urethane acrylate from 1000 to 4600 g/mol resulted in a decrease in the stress at break, Young's modulus, and glass transition temperature, while the elongation at break increases (Lin et al. 1984). Aiming at achieving a product with low tensile strength, the copolymer of urethane acrylate with HDDA in a proportion of 1:1 w/ww was produced and named UH. The exact structure of the polymer was not available, but a similar aromatic urethane diacrylate is shown below, where is possible to see the benzene rings, the presence of the urethane groups (-NHCOO-) and the acrylates by the end of the chain.

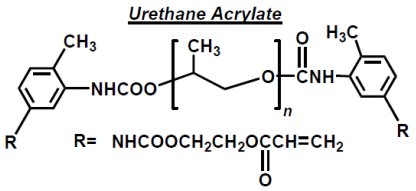

Figure 5.8 - Molecular structure of an aromatic urethane diacrylate (Ebecryl 270, Cytec).

The T_g of the copolymers was estimated using Fox equation (Fox and Flory 1954):

$$\frac{1}{T_g} = \frac{M_A}{T_{g,A}} + \frac{M_B}{T_{g,B}} \qquad \text{Equation 5.1}$$

Where M_A and M_B are the weight ratios of the monomers A and B, respectively and $T_{g,A}$ and $T_{g,B}$ are the glass transition temperatures of the homopolymers. Based on this equation, and considering

the T_g of BisGMA as 133°C (Sandner et al. 1997), the glass transition temperatures of the copolymers were estimated and they are shown in the red bars of Figure 5.7. The estimated values of T_g for the copolymers ranged between 23 and 109°C. The presence of BisGMA in the copolymer increased the T_g, once compared to the respective monomers. This was attributed to the phenyl hydrogen present in BisGMA, since it causes steric hindrance and the rotation at room temperature is impossible (Darvell 2009). Likewise the copolymers, BI, BH and BP presented the highest T_g values, above the room temperature, indicating a brittle behaviour is expected. BT presented an estimated T_g just above room temperature, and the material could be in the transition from brittle to ductile. The copolymer UH containing the polyurethane acrylate presented a measured glass transition temperature of 45°C, where the urethane acrylate T_g can be estimated to be around 44°C.

Dynamic mechanical analysis (DMA) was carried out to determine the elastic behaviour and T_g of the acrylates UH and BI. The values obtained in the DMA were used for comparison with the estimated values using the Fox equation. As observed in Figure 5.9, the values of storage modulus for both UH and BI were high at temperatures around -50°C.

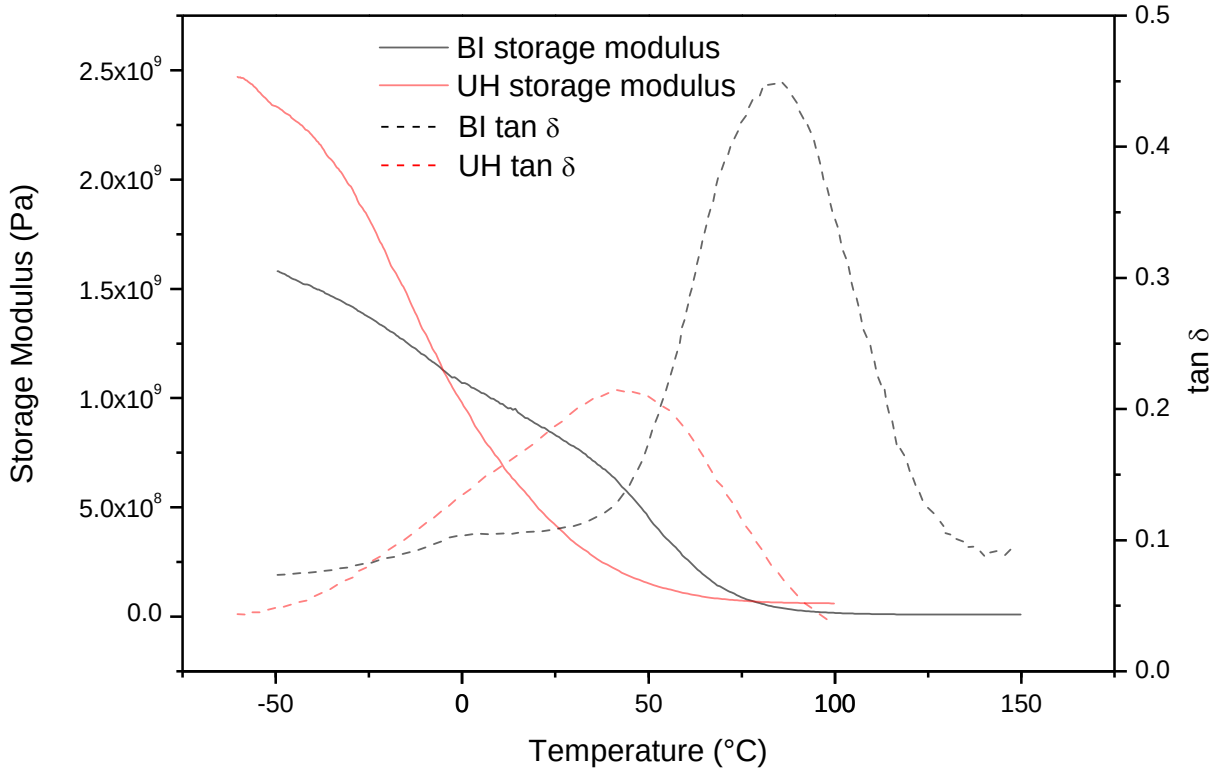

Figure 5.9 – Storage modulus (solid line) and tan δ (dashed line) in function of the temperature for the copolymers BI (black lines) and UH (red lines).

However, as the temperature increased, this value of storage modulus decreased and the slope was larger for UH when compared with the BI sample. The glass transition temperature was obtained

by the peak of tan δ and it was 42.8 °C for the UH and 84.3°C for the sample BI. This calculated value of T_g was used in Figure 5.7, since it was not possible to find data about the T_g of the urethane acrylate. For the BI, the value was 25°C below the T_g of 109°C estimated by the Fox equation. This difference could be due to the variety of ways used to determine the glass transition temperature. The broad tan δ peak observed especially for sample UH indicates the inhomogenous nature of the copolymer, e.g., wider range of polymeric chain length and chain branching within the copolymer. Future research looking at the DMA analysis of the 5 copolymers used in this work would be interesting in order to investigate more precisely the values of T_g.

The glass transition temperature of the copolymers used for the shell material impacts the plastic and elastic properties of the microcapsules. Ideally, the T_g of the shell material should be higher than the room temperature, to increase the elastic modulus and the brittle behaviour. This is also required in order to avoid elongation without rupture of the microcapsules for mechanically triggered self-healing. However, brittle materials are more likely to rupture during the mixing with the cementitious materials. Thus, the fine tuning of the glass transition temperature has been reported in the literature for the production of polymeric microcapsules. Considering the exothermic reaction that takes place during the production of cement, T_g can be adjusted so that the microcapsules are ductile during mixing and brittle after the hardening of the paste. To achieve that, vials were produced using co-extrusion and the shell comprised of poly(lactic acid) (PLA) (T_g = 59 °C), polystyrene (PS) (T_g = 102 °C) and poly(methyl methacrylate/n-butyl methacrylate) (P(MMA/n-BMA)) (T_g = 59 °C) (Hilloulin et al. 2015). The vials were heated prior to mixing with other components, shifting the mechanical properties from a brittle to a rubbery state, thus increasing the survival ratio. Thus, the T_g of UH and BT were very suitable for obtaining a more ductile material during mixing and more brittle after the hardening.

Besides the molecular structure, other factors could influence the T_g, such as the level of crosslinking, concentration of photo-initiator, relative molar mass of the monomers and the presence of plasticiser (Nicholson 2006). Although these parameters were not considered in this work, they are suggested as topics of further investigation for the production of microcapsules and their properties.

5.2.2. Ageing of the acrylates

Acrylates kept at temperatures below the T_g are subject to physical ageing which influences the physical properties (Hodge 1995; Hutchinson 1995). Below the T_g, the chains are not in their lowest-energy configuration and this nonequilibrium vitreous state have an excess of volume, enthalpy and entropy (Cowie and Arrighi 2010). Thus, the chains will attempt to achieve a state of thermodynamic equilibrium by losing these excess quantities by a variety of localised molecular

relaxations. To investigate the physical ageing, the polymer can be heated to temperatures above the T_g to accelerate the changes in properties. Above the T_g the relaxation times are short enough to enable the material properties to follow changes in temperature, but below T_g the retardation times become too long. Thus, the volume below T_g which is initially in a non-equilibrium state, evolves slowly towards equilibrium with time and the process is illustrated in Figure 5.10.

Physical changes in material properties are a consequence of the slow structural relaxation process. In terms of free volume theory, one can visualise that the loss in enthalpy involves increased stability via reduction in the free volume fraction towards its equilibrium, thus the mobility of chain segments is hindered. Hence, during physical ageing the material properties such as yield stress, tensile and flexural module, increase progressively while the fracture toughness, impact strength and compliance decrease (Hay 1995). However, there is a limiting temperature range in which ageing is observed. When the polymer is kept below the T_β, the polymer segments flexibility is strongly hindered and thus the physical ageing disappears. Furthermore, the rate of physical ageing is determined in part by how far below the T_g the polymer is used (Hodge 1995) – a shift in T_g a few tens of degree Celsius results in an increase (or decrease) of relaxation times by several orders of magnitude. Lai (1992) suggested that the equilibrium time will be 75 million years if the polymer is held at temperatures 40°C below the T_g, thus its ageing does not need to be considered. However, at temperatures 20°C below the T_g, the polymer will take 15 years to show differences in the mechanical properties. There are two important practical applications of this: first, in experimental studies of ageing, the equilibrium state will only be known by extrapolation from measured values at higher temperatures; second, physical ageing will occur throughout the lifetime of the polymer which is important to be considered for engineering applications (Hutchinson 1995).

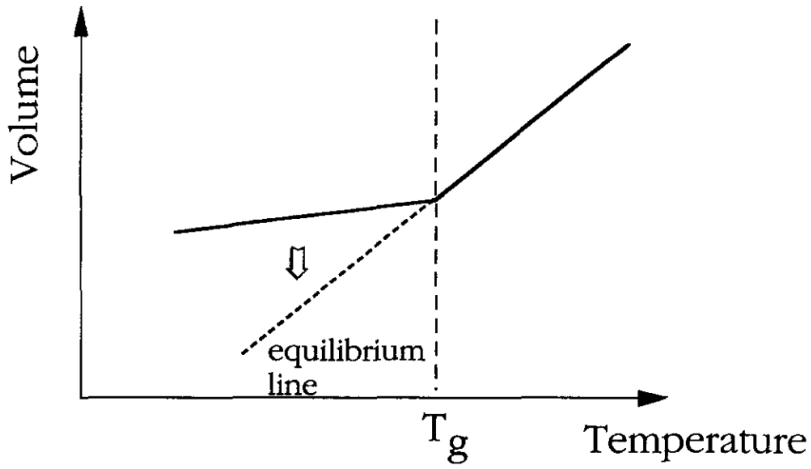

Figure 5.10 – Evolution of volume towards equilibrium in function of temperature. Adapted from (Brinson and Gates 1995)

Initial efforts to investigate the effect of physical ageing in the physical properties of the microcapsules were performed by measuring the microcapsule size variation over time. Microcapsules made with BH as shell material and colloidal silica as core were presented in section 4.3.2 and named BH-CS-88/9 due to their 88 µm of diameter and 9 µm of shell thickness measured using the optical microscope. Then the microcapsules were dried and observed in the SEM after 2 and 24 months (Figure 5.11). During the time between the production and the observation in the SEM, the microcapsules were kept in air atmosphere. The core-shell structure was preserved over time and the colloidal silica was retained inside of the microcapsules as indicated by the images of broken capsules after 2 and 24 months (Figure 5.11C and D).

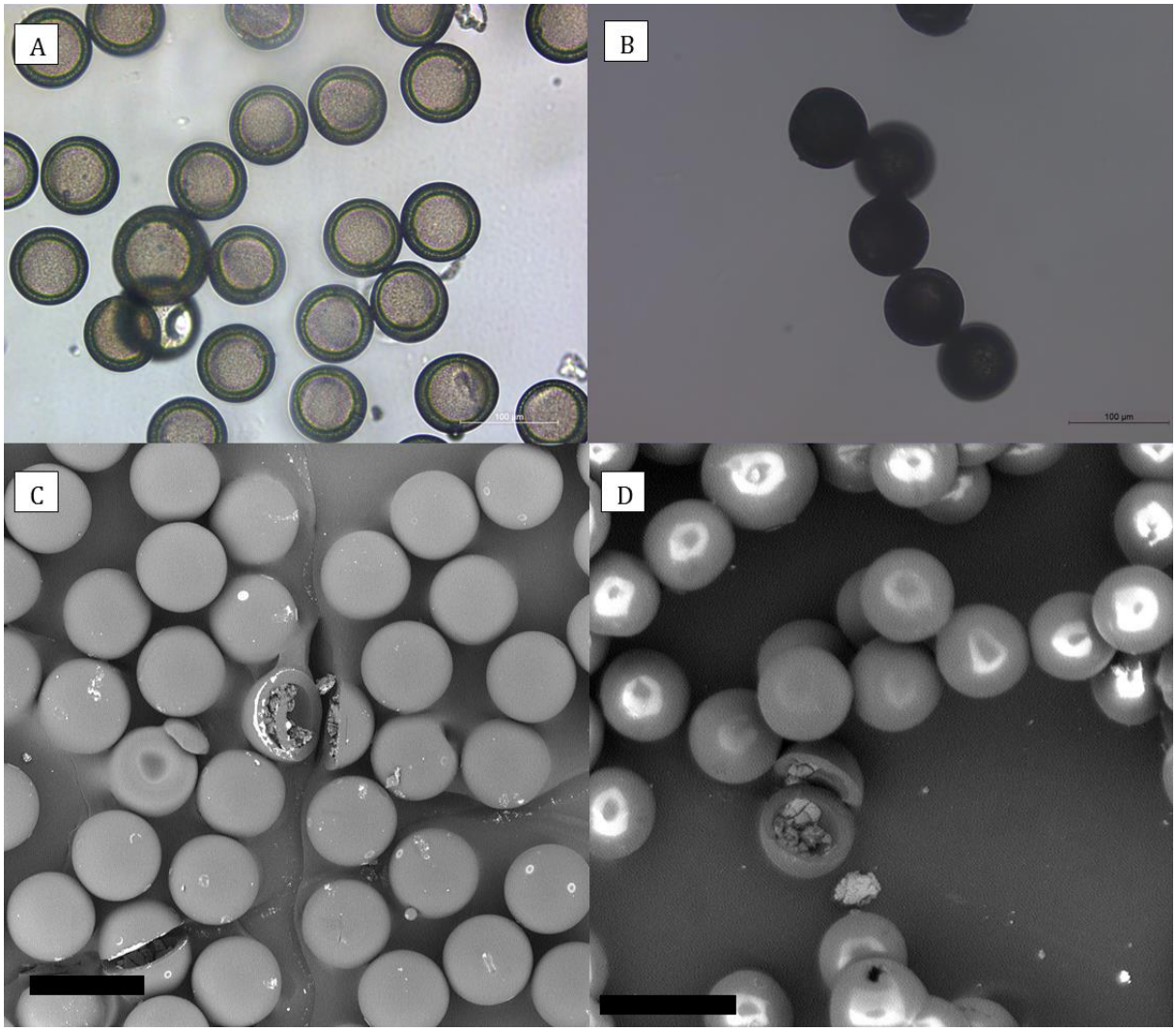

Figure 5.11 – Investigation of behaviour overtime of microcapsules BHCS-88/9. a) OM image of the microcapsules after polymerisation; b) OM image of the microcapsules after 24 months; c) SEM of microcapsules 2 months after the production; d) SEM of microcapsules 24 months after the production.

Furthermore, in both situations the microcapsules presented a smooth surface, with no signs of any cracks. No size difference was observed in the microcapsules despite the free volume present in the core, offering the possibility for the microcapsule to shrink freely. The T_g of BH was 82°C calculated with the Fox equation and considering that the sample was kept at room temperature (approx. 20°C), the volume shrinkage should take a longer period. However, there was a difference of approximately 25°C between the calculated and experimental values of T_g for BI, thus the T_g of BH could also be lower. Thus the polymer would still be kept 35°C below the Tg, in the best case scenario and changes in volume shrinkage should not be observed in 24 months. Interestingly, an initial size difference of the microcapsules after 2 and 24 months was observed in the SEM; however, after further investigation, it was noticed that the SEM was not calibrated. Furthermore, the microcapsules with BH shell did not show evidence of shrinkage after 64 days inside the cement paste, so the capsule could be considered to not have reached the equilibrium state before 64 days.

Further studies are necessary to investigate the role of shrinkage in shells with T_g just above room temperature, as it is important for mechanically triggered capsule-based self-healing. If the volume of the shell material is reduced during the lifetime, this volume reduction can decrease the interfacial bonding between the microcapsule and the matrix and preclude the mechanical triggering. Thus, it is important to measure and estimate the extension of volume shrinkage during the time-frame the microcapsules are supposed to be used. Furthermore, if the core is partially empty, the volume shrinkage can result in the reduction of volume of the core cavity; however, if the core is completely filled (e.g. encapsulating organic-based core or solid materials), the stress caused by volume shrinkage can lead to creep. The effect of physical ageing on the performance of microcapsules for drug-delivery with PLGA shell have shown variations in the enthalpy and T_g values (Rouse et al. 2007; Rawat and Burgess 2011). Additionally, the molecular mobility in the polymeric shell may lead to closure of microscopic pores and can affect the shell permeability over time (Allison 2008). Last, the time-frame of the changes of the physical properties are of paramount importance. If the equilibrium time is reached in a few minutes, the process will happen during the hardening of the cement and thus do not affect the self-healing. However, if the time-frame is during years, this data is important for designing the capsule shell. Even more when considering the use of shells that are ductile during mixing due to the exothermic reaction of cement hydration and thus the shell have a T_g slightly above room temperature.

5.2.3. Young's Modulus and hardness of the acrylates

Microindentation tests were performed in order to obtain the Young's modulus of the copolymers studied in this work. The elastic properties of the microcapsules affect the overall mechanical properties of the self-healing material and the likelihood of mechanical triggering to occur. Thus,

the calculation of the Young's modulus of the acrylate shell can offer a better understanding of how these parameters affect the self-healing process. Furthermore, the acrylates offer the option of easily producing bulk materials for the tests, whereas other methodologies to produce the microcapsules do not offer the same possibility. Hence, acrylates discs were photopolymerised and the load-displacement curves of the copolymers BP, BT, BI, BH and UH are shown in Figure 5.12. The curves were obtained using a Vickers indenter and 15 indentations were performed for each sample, and the load-displacement curve displayed in Figure 5.12 represents typical behaviour. The maximum load applied was 1000 mN, resulting in a deeper displacement of the samples BT, BP and UH when compared with the samples BH and BI. This resulted in a higher total (elastic plus plastic) work in the samples BT, BP and UH, as shown in detail in Figure 5.12. The area beneath the unload curve indicates the elastic energy used during recovery, indicating that the elastic work in samples BI and BH were the lowest ones. This translates into high resistance to elastic deformation and, thus, high stiffness in these samples. On the other hand, the plastic (total minus elastic) work expresses the material ability to undergo plastic deformation and informs about the ductility of the material. BP, BT and UH presented the highest values of plastic work indicating greater easiness in the polymers to slide their chains across each other. This also confirms the proximity of the T_g for these samples. All the materials were submitted to a 20s dwelling between loading and unloading, where the material is allowed to deform continuously at constant load in order to obtain an unloading response free from inelastic deformations.

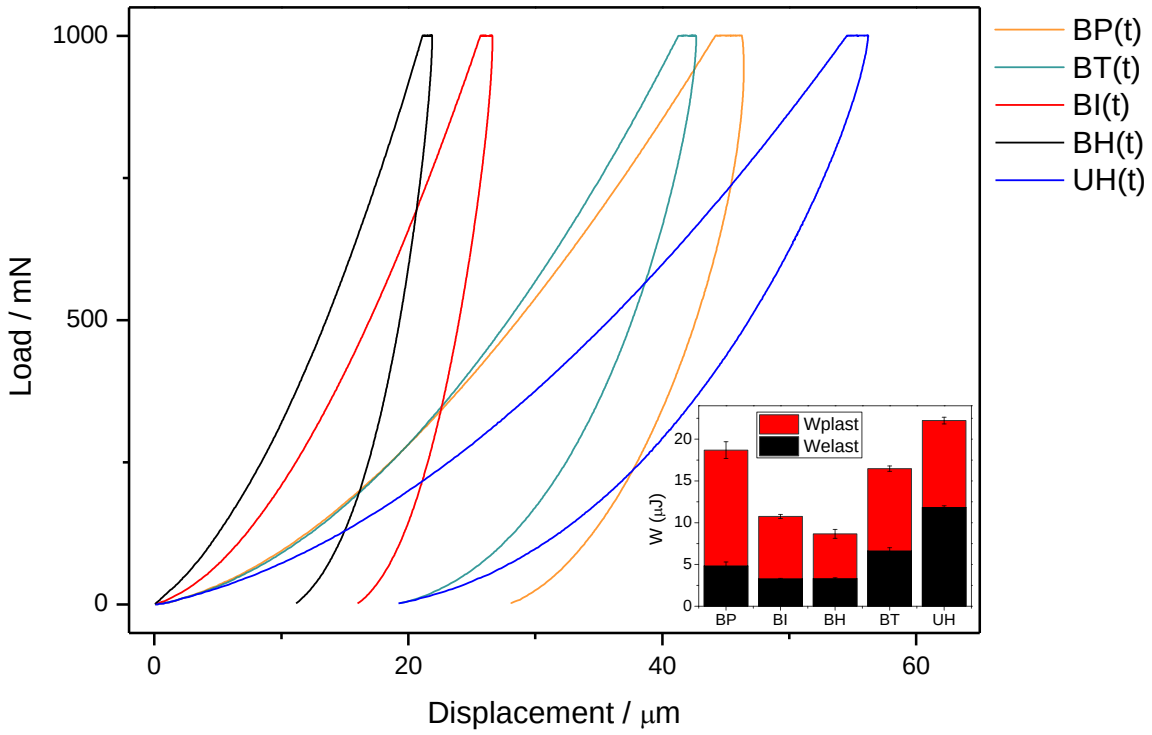

Figure 5.12 - Load-displacement curves of the copolymers containing BisGMA and polyurethane acrylate as oligomers. The graph in detail indicates the work for the samples.

The Young's Modulus was calculated according to Equation 3.9 and 3.10, where the unloading part of the curve, i.e., the elastic deformation, was used and it is shown in Figure 5.13. As described in the experimental methodology, the disc obtained for the microindentation was not uniformly polymerised: the bottom part was closer to the UV-lamp and the top part of the disc was polymerised in contact with water and then polished for the removal of the acrylate meniscus. This resulted in different values of Young's modulus for the indentation of the top (t) and bottom (b) surface of the disc. The indentation of the bottom of the disc presented the highest values of elastic modulus, between 0.459 and 3.558 GPa; on the other hand, the indentation of the top resulted in values of elastic modulus ranging between 0.261 and 2.644 GPa. The higher values of Young's modulus of the bottom part were attributed to the more intense polymerisation of the acrylate closer to the lamp, resulting in a more compact polymer. The top of the acrylate was more distant from the lamp and being shielded by the already polymerised bottom resulted in a different microstructure of the polymer. The elastic modulus of the acrylate shell in the microcapsule is possibly between the two values observed for the top and bottom sample. However, the values are expected to be closer to the top values, since the shell was polymerised in solution and it is expected that the water would shield part of the UV-light.

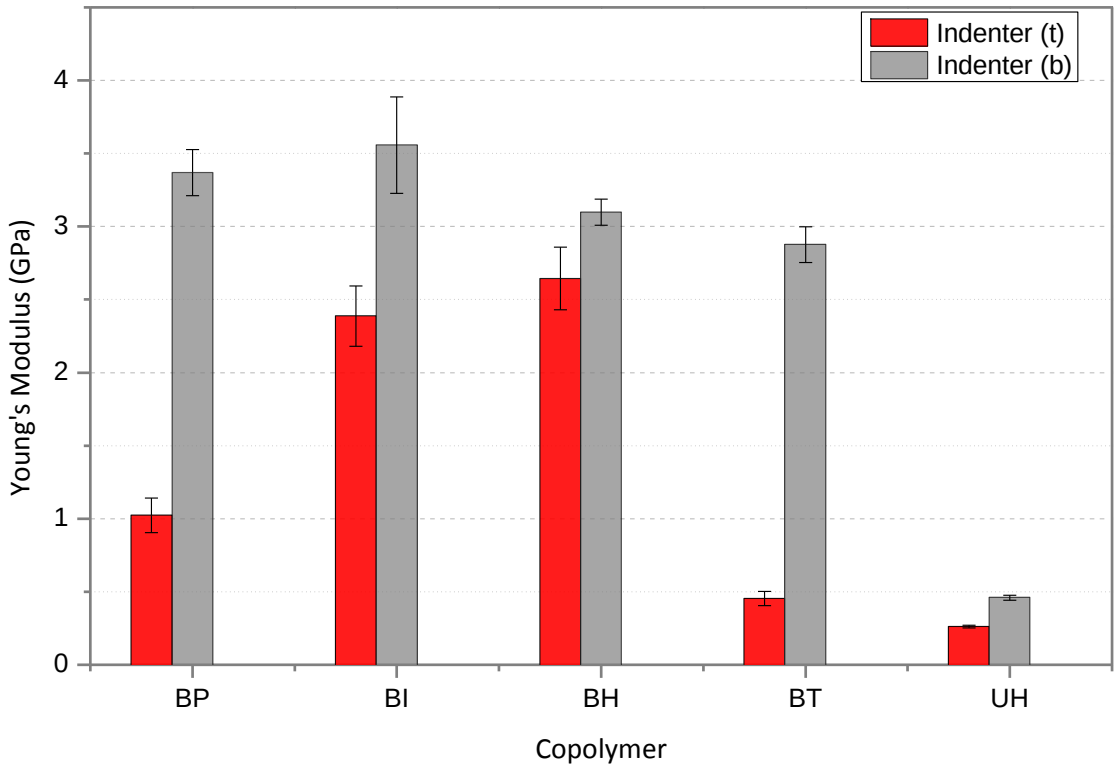

Figure 5.13 – Young's modulus of the copolymers with epoxy (BisGMA) and urethane (MU3603) acrylate. The indentation was performed in the top (red bars) and the bottom (grey bars) of the sample.

The epoxy-based copolymers presented the highest values of Young's modulus, associated with the presence of phenyl hydrogens in the bisphenol resulting in a steric hindrance and thus a rigid structure (Darvell 2009). The samples BH and BI used to produce the microcapsules discussed in the preliminary investigation (section 5.1), presented Young's modulus of 2.6 ± 0.2 and 2.4 ± 0.2 GPa, respectively. Although the structure of the urethane monomer is unknown, the high molecular mass indicates mobility of the branches in the triacrylate and the lowest value of Young's modulus was observed, 0.26 ± 0.01 GPa. This difference in the Young's modulus of the shell materials had a direct implication in the likelihood of the microcapsules buckling due to the loss of the water core. The pressure buckling is proportional to the Young's modulus of the shell (Equation 4.5), thus a capsule made of UH has a 10-fold decrease in the minimum pressure necessary to buckle when compared with the BH shell with the same dimensions. The easiness in which the microcapsules buckle and collapse inwardly plays an important role in the adhesion, and it may result in the debonding of the capsule. This will be determined by the interplay between the surface interactions and the mechanical of deformation energies of the shell and needs to be taking into account for the production of water core microcapsules.

Microindentation was also used to measure the elastic modulus of a single microcapsule. Figure 5.14a shows the load–displacement curve of single BH-CS-88/9 microcapsules comprised of BH as shell material, colloidal silica as core, the diameter of 88 μm and shell thickness of 9 μm. The microcapsule was linearly loaded up to 30 mN, held for 10s and linearly unloaded. During the loading, the microcapsules deformed elastically, up to 10 mN where the microcapsule was permanently deformed and ruptured, as shown in Figure 5.14b. Chen et al. (2012) reported a load at rupture of 58 mN for brittle microcapsules with diameter of 130 μm and shell thickness of 15 μm. The lower value of load at rupture for microcapsules, which is likely to be less brittle needs further investigation. After the yield point, the microcapsules deform plastically and elastically up to a maximum deformation of 2.8μm, representing 3% of the total size of the microcapsule. During the unloading, the force decreased to zero before the displacement recovered to zero, confirming the permanent deformation of the microcapsule. At the start of the unloading, the elastic recovery took place first and the calculated compliance was 2.6 ± 0.8 GPa. The value is close to the Young's modulus obtained for the bulk acrylate (2.6 ± 0.2 GPa), and the Young's modulus of 1.6 GPa reported for other acrylate microcapsules (Chen et al. 2014a).

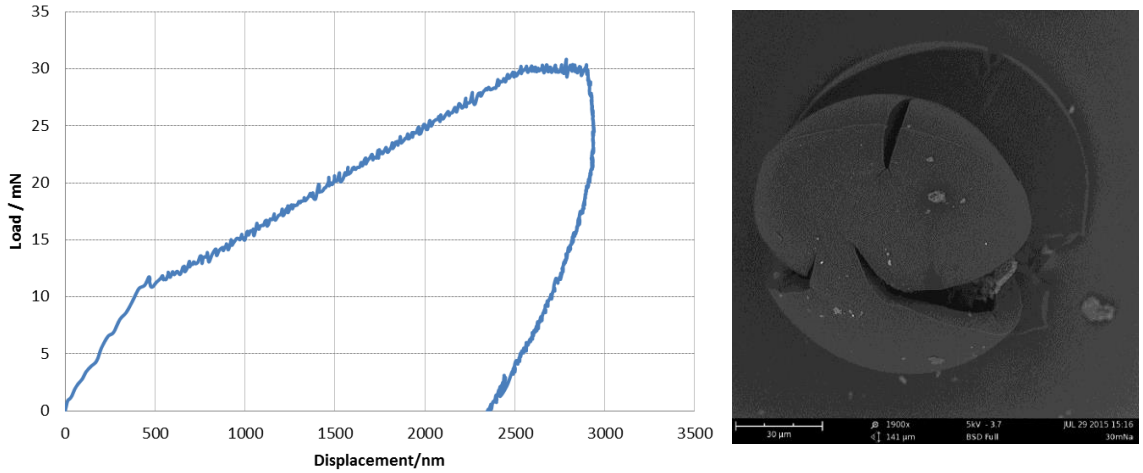

Figure 5.14 – Indentation of single capsule. (a) Load-displacement curve of single microcapsule BH-CS-88/9 (b) SEM of a microcapsule with a permanent deformation after the microindentation analysis.

The Young's modulus of the microcapsule is a structural property which can vary according to the size, shell thickness, shell and core material of the microcapsules (Su et al. 2015). The mechanical properties of microcapsules have been investigated using indentation. In general, the Young's modulus of the polymeric shells ranges between 1 and 5 GPa, with typical values around 2.7 GPa (Lee et al. 2012; Su et al. 2013; Ghorbanzadeh Ahangari et al. 2014; Su et al. 2015). These values are lower than the elastic modulus of concrete, typically ranging between 25-38 GPa. This mismatch between the Young modulus of the microcapsules and the one of the matrix favours the attraction of cracks, since softer particles attract the cracks (Ponnusami et al. 2015). Thus, when there is a good interfacial bonding between the matrix and the microcapsules, the mismatch favours the physical triggering of the microcapsules typically used for self-healing. On the other hand, the insertion of the microcapsules with reduced values of Young's modulus, compared with the matrix, may decrease the overall elastic modulus of the matrix (Young et al. 2016). Nonetheless, Kanellopoulous et al. (2016) reported that the addition of microcapsules comprised of pig gelatin shell did not significatively reduce the compressive strength of the mortar up to an addition of 8% of volume fraction (1.6% by weight of cement). Studies with a similar size range of microcapsule, between 98 to 632 μm, with average size of 290 μm, reported insignificant compressive strength changes at percentage microcapsules around 3%, relative to the cement weight (Wang et al. 2013). Alternatively, microcapsules with size around 5 μm decreased the compressive strength 10-15% with the addition of only 2 wt% (Wang et al. 2014). Theoretical results also show the trend of a diminishing Young's modulus as the volumetric fraction of the microcapsules increased. According to this result, the microcapsule content should be below 4 vol.% to ensure that at least 90% of the Young's modulus of the matrix is retained (Li et al. 2016a). Thus, there is no clear understanding of

the effects of microcapsules on the elastic properties of the matrix and further studies are needed to investigate the effect of the volume fraction, size, shell thickness, shell and core material of the microcapsules on the final mechanical properties of the self-healing matrix.

5.2.3.1. HARDNESS

Hardness (H) is a measure of a material's resistance to localised plastic deformation (e.g., a small dent or a scratch)(Callister 2011). Considering the indenter to be much stiffer than the probed acrylate, the hardness is defined as the maximum load (P_{max}) divided by the contact area of the indenter at the maximum load (A_c).

$$H = \frac{P_{max}}{A_c}$$

As the same load was used for all the materials, hardness is inversely proportional to the square of displacement, which can be seen in Figure 5.12. The results for hardness are shown in Figure 5.15.

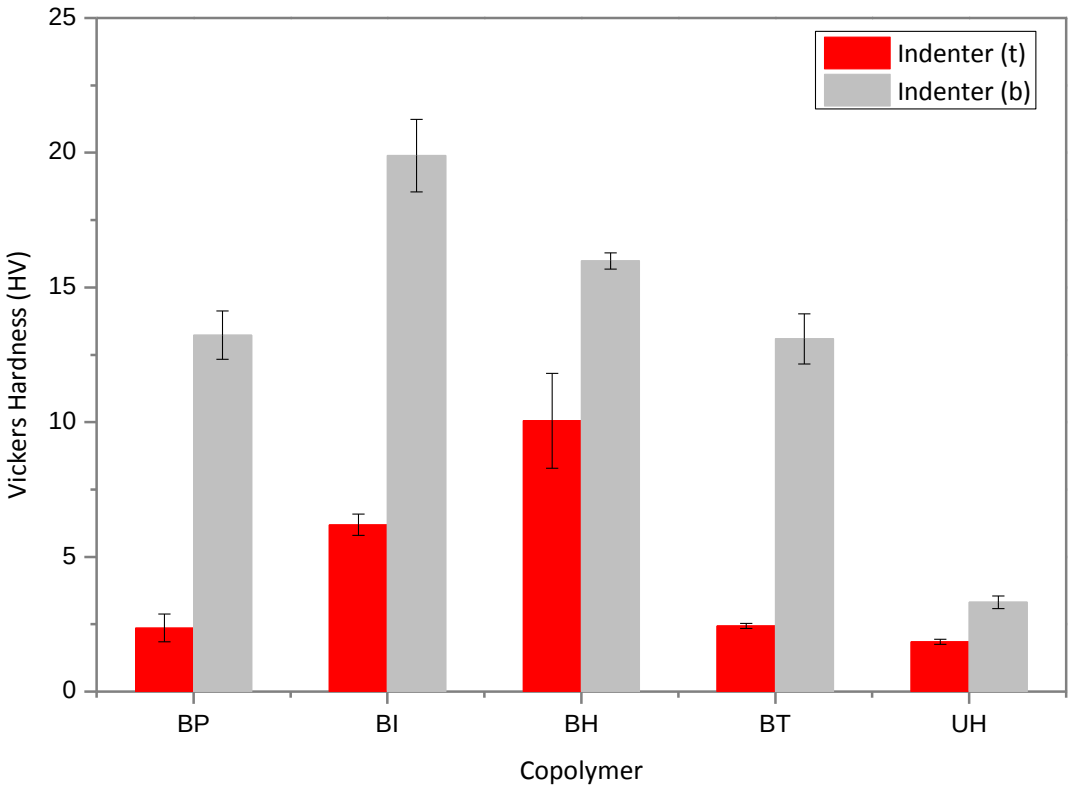

Figure 5.15 - Vickers hardness for different acrylates obtained using the microindenter.

The material presented very different behaviour at the top and the bottom during analysis. The results for hardness for the bottom of the sample show that they resisted more of the penetration of the indenter as shown in the load-displacement curves. This is likely to be caused by the different packing of the bottom sample since it was closer to the exposition lamp and it received more

intense exposition to the UV-light. On the other hand, the samples at the top of the cylinder received the UV-light after the light went through a layer of polymers. Thus the formation of radicals was less prolific and a different packing density was obtained and the displacement of the indenter was hence larger. In general samples BH and BI presented increased resistance to localised deformation and thus higher values of hardness – which is also associated with the brittle nature of both acrylates. Alternatively, the samples BP, BT and UH presented a more ductile behaviour and reduced hardness. All these values are below the reference value reported for PMMA, ranging between 16-21 HV (Ashby and Johnson 2014), which indicates increased mobility chain.

The values of hardness are not directly associated with the key properties governing the mechanical triggering of self-healing. Nonetheless, hardness can act as an indicator of other properties, such as yield and tensile strength. Furthermore, the values of hardness were important for the design of the experimental procedure for the use of the microindenter for the assessment of the acrylates properties. Low values of load resulted in higher values of hardness because of the meniscus and the resistance of the indentation. As shown in the Figure 5.16, for small values of displacement the hardness presented high values – for example, when the displacement was 4 μm, (load was around 70mN) the hardness was around 170 MPa. This is because at lower values of load, the meniscus played a role in the resistance to localised plastic deformation. However, with the increase of the load and consequently at higher values of displacement, the hardness decreased and approached a more realistic value. Because of that, the load of 1000 mN was selected to describe the hardness of the material.

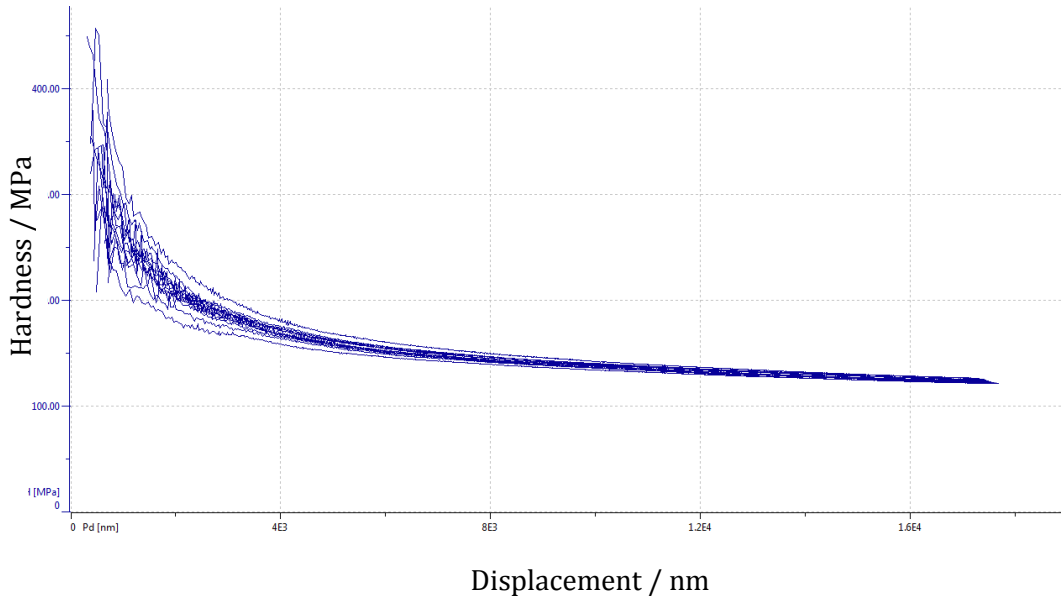

Figure 5.16 – Values of hardness in function of the displacement for the samples BH.

5.2.4. Tensile Strength of the acrylates

The tensile strength of bulk acrylates was obtained from uniaxial tensile tests and the stress-strain plots are displayed in Figure 5.17. The values of tensile stress the material can withstand before failure are associated with minimum stress necessary to rupture the capsule during the mechanical triggering. Thus, a thin layer of each of the acrylates BH, BI and BT was photopolymerised and cut into a rectangular shape to be used in the tensile tests. To determine the tensile strength, the load at fracture was divided by the initial undeformed cross-section area (typically around 8 x 0.4 mm). The tensile tests were conducted at room temperature, which is below the glass transition temperature of the copolymers and thus a complete brittle fracture took place. The copolymers presented stress at rupture of 14.7, 36.0 and 15.6 MPa, and strain values of 5.3, 9.7 and 8.1%, for BI, BH and BT, respectively. The plastic deformation occurred by the alignment and untangling of the chain structure and the more the tangled structure, the more resistant is to deformation. This resistance was observed in the sample BH, which presented the highest values of stress and strain at rupture. Furthermore, the presence of defects, low crosslinking density and weak forces between the chains can result in low tensile strength. In the sample BI, the bulky isobornyl groups preventing the sliding of the chain and the monoacrylate reducing the crosslinking density may be responsible for the lowest value of stress and strain. Sample BT presented an increased toughness, compared with BI which can be attributed to the mobility of the ethoxylate chains.

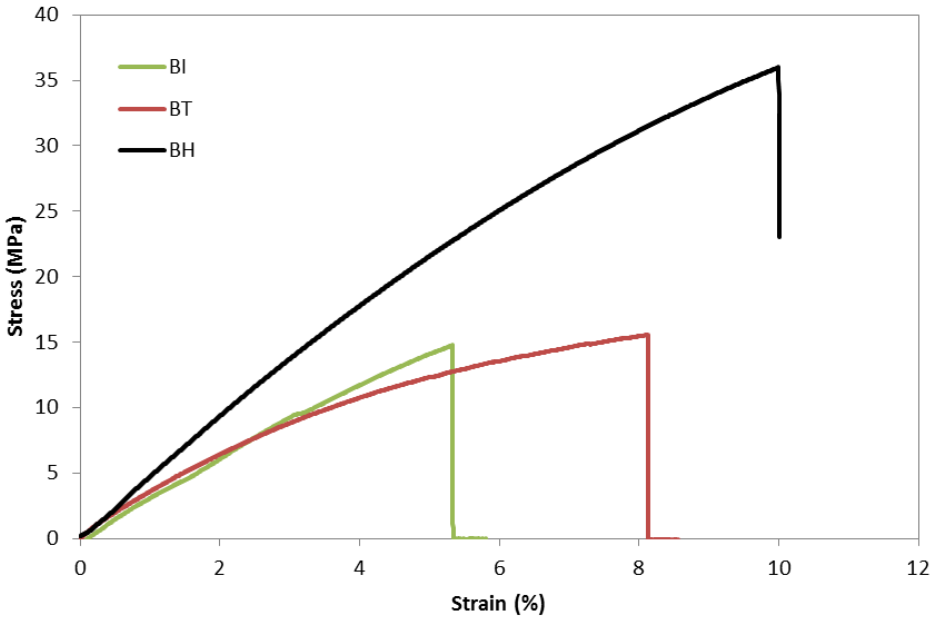

Figure 5.17 - Typical stress-strain curves of the copolymers BI, BH and BT.

According to Ponnusami et al. (2015) when a particle is embedded in a matrix, its fracture is dependent upon the mismatch in fracture strength and toughness, as shown in Figure 5.18. Overall,

the particle fracture is favoured when the particle is softer than the matrix, as in the case of microcapsules inserted in the cementitious matrix. Furthermore, the likelihood of a softer particle fracture is dependent upon the mismatch of fracture strength and toughness. Regarding fracture toughness, the typical values for concrete are 0.35-0.45 MPa $m^{1/2}$, whereas the values for acrylate such as PMMA are 0.7-1.6 MPa $m^{1/2}$. Considering the tensile strength of concrete around 2-5 MPa, the brittle BI microcapsules with shell thickness of 2 μm can be mechanically triggered even with the tensile strength of 15MPa. Alternatively, the BH microcapsules presented a higher toughness, tensile strength of 36 MPa and thicker shell which combined to preclude the shell fracture. There are no theoretical values of threshold of tensile strength and toughness for shell material of the microcapsules to ensure rupture under crack formation in the cementitious matrix. But it is important to notice that unlike particles in the matrix, the presence of the core of the microcapsules will facilitate the rupture of the shell. Thus, even though the tensile strength of BI is 15 MPa, the microcapsules might rupture given a good interfacial bonding and a thin shell.

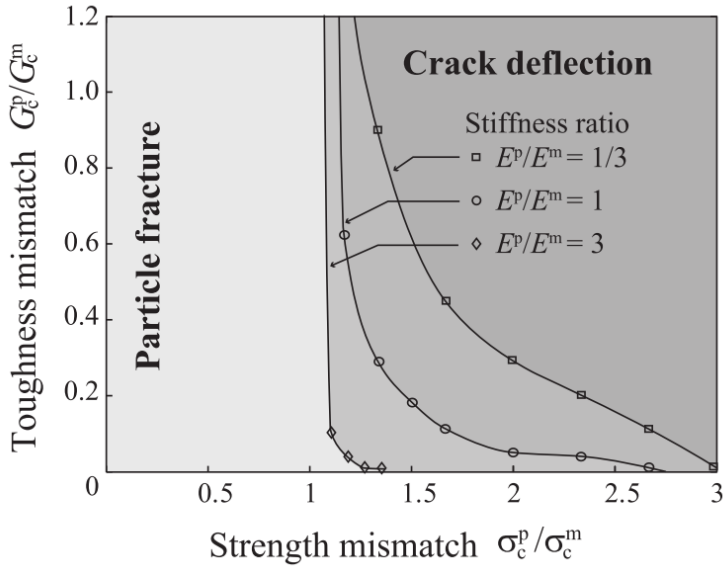

Figure 5.18 - Fracture map: The transition curves correspond to the boundary separating the regions in which particle fracture or crack deflection occurs. Three stiffness ratios are considered corresponding to stiffer particle, particle with same stiffness of the matrix and softer particle (Ponnusami et al. 2015)**.**

These results of tensile strength are preliminary and represent an indication to promote a better understanding of the key factors influencing the mechanical triggering of the microfluidics microcapsules. Precise values of stress-strain following the ISO protocol still need to be determined. For example, an inconsistency was observed between the value of tensile strength of 15.6 MPa observed for sample BT and the values of 40 MPa reported for the same polymer (H.Miller, 1989). Furthermore, a deeper investigation of the factors influencing the tensile strength is needed,

including the degree of conversion of the acrylates. Additionally, the use of methacylates (e.g., isobornyl methacrylate) can contribute to the increase of the steric hindrance and decrease the tensile strength.

5.3. Production of microcapsules for physical triggering

5.3.1. Shell functionalisation

The interfacial bonding between the shell and the cementitious matrix is a major concern when aiming at mechanically triggered self-healing. For polymeric material, the presence of the hydroxyl group is recognised as promoting a strong chemical bonding with cement (Li et al. 2002; Peled et al. 2008; Pakravan et al. 2012; Halvaei et al. 2014). This is because to produce cementitious materials, water is mixed with the cement powder (e.g., Portland cement) and with aggregates for the production of concrete. The main and most important constituent of Portland cement is tricalcium silicate ($3CaO.SiO_2$), which hydrates to form calcium silicate hydrate phase (CSH), the main responsible for the strength of cement based materials. During the mixing of the cement powder and water, the low chemical affinity between the cement paste and hydrophobic shells may result in the development of a gap between the shell and the matrix, as illustrated in Figure 5.19 (left). On the other hand, the use of shells such as gelatine (Kanellopoulos et al. 2016; Kanellopoulos et al. 2017) and silica (Perez et al. 2015b; Perez et al. 2015a) results in a good interfacial bonding with the cement paste due to the chemical reactions. This is caused by the hydroxyl groups (or other polar groups such as carboxylates) present in the surface of these shells which enables the nucleation and growth of hydration products of cement (Pakravan et al. 2012), as illustrated in Figure 5.19 (right). The hydroxyl groups can participate in the cement hydration taking part in the formation of hydration products (Kanellopoulos et al. 2016). However, some of the shells may be without hydroxyl or polar groups, particularly when using in situ polymerisation.

In the case of microfluidics, the formation of the double emulsion of water-in-oil-in-water relies on the hydrophobic nature of the oil middle layer. Thus, when the microcapsule is formed, the shell is also hydrophobic and precludes the chemical bonding with the cement paste. The smooth shell surface due to the surface tension during the polymerisation also hinders the physical interlock bonding with the cementitious matrix. Alternatively, a double emulsion of oil-in-water-in-oil (o/w/o) would result in the formation of a hydrophilic shell and it would be suitable for chemical bonding. However, the microfluidic device used in this work had a hydrophobic coating, allowing just the formation of hydrophobic middle layer, so the o/w/o template was not investigated. Furthermore, the presence of a hydrophilic middle layer may also facilitate the diffusion of hydrophilic healing agents through the shell (Lee et al. 2016b).

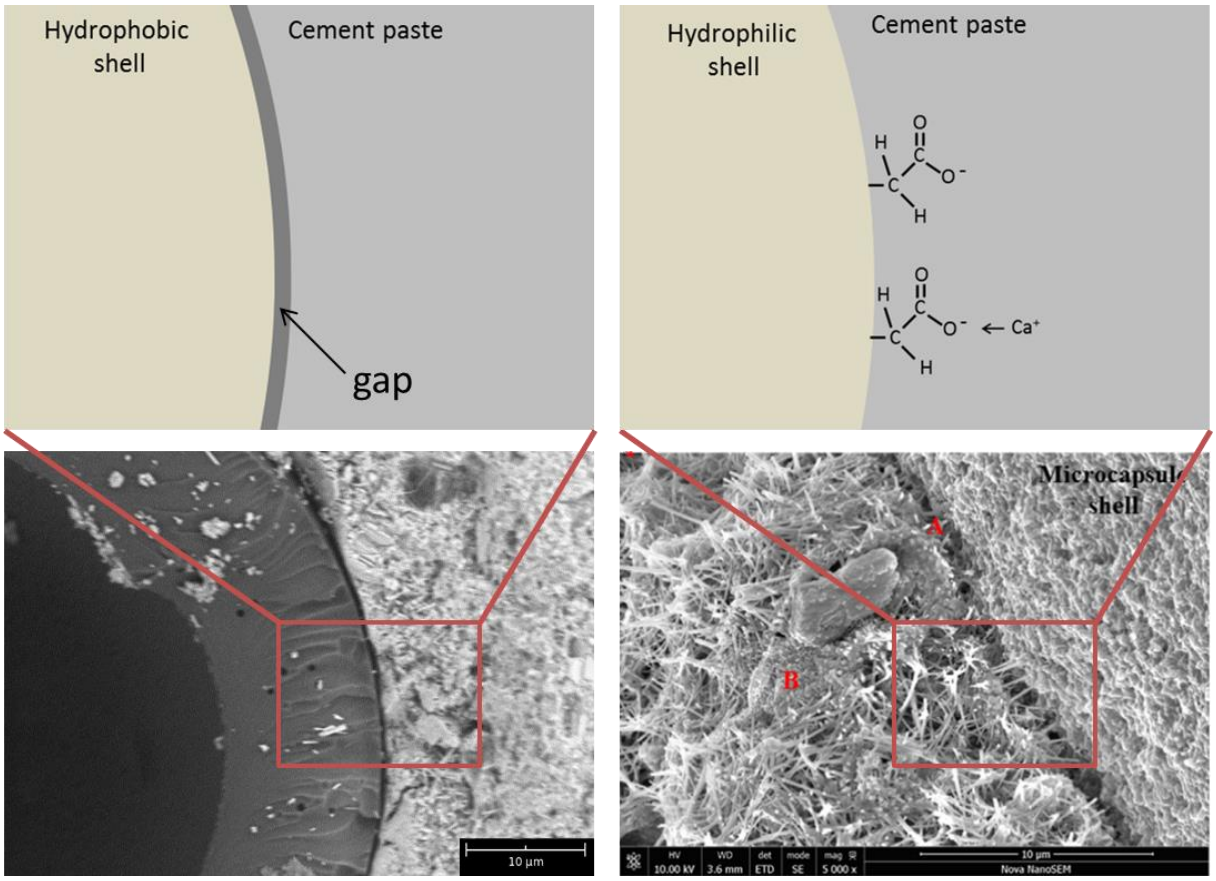

Figure 5.19 - Schematic representation of the interfacial bonding using hydrophobic (left) and hydrophilic shells (right). SEM of interface microcapsule-matrix in the bottom right was adapted from Kanellopoulos et al. (2016).

Hence, to enhance the interfacial bonding, while still using hydrophobic shells, the functionalisation of the shell surface with hydrophilic groups was proposed. To achieve that, the use of photopolymerisation was explored not only as a mechanism to solidify the shell but also functionalise the surface of the microcapsules. The process is schematically represented in Figure 5.20, showing the addition of acrylic acid to the outer fluid. During the photopolymerisation of the shell, the radicals also initiate the polymerisation of the acid, attaching a chain of carboxyl groups to the surface of the microcapsule. The process appears to be efficient in consuming most of the acrylic acid, since its distinct acrid odour was not noticed in the collecting solution.

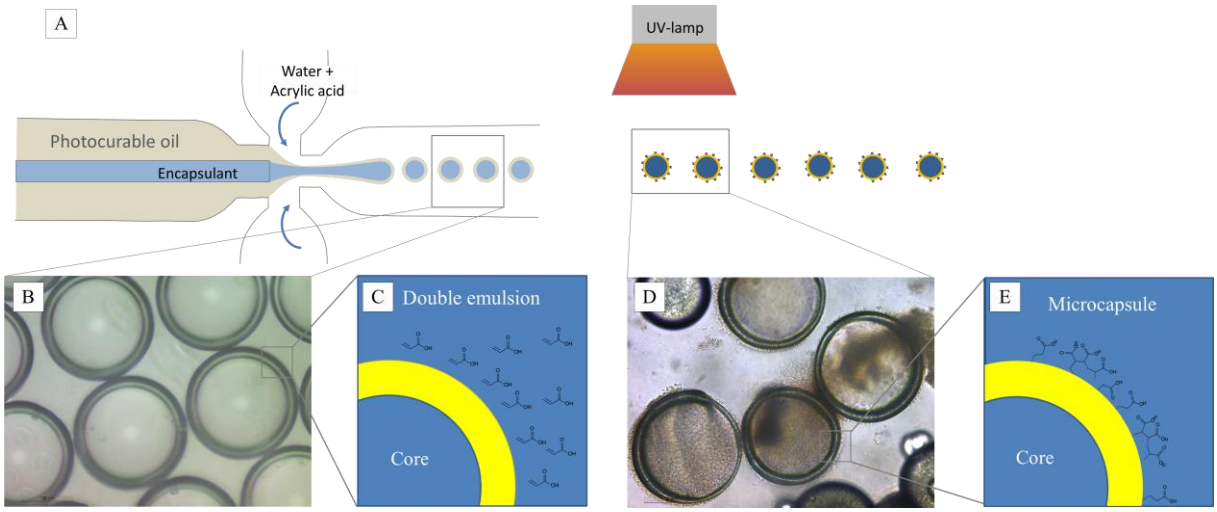

Figure 5.20 - Encapsulation of aqueous and non-aqueous cargo material and with the surface functionalised with poly(acrylic acid): (A) Schematic illustration of the microfluidic device used for the production of the double emulsion template and the photopolymerisation process, (B) Double emulsion template formed using microfluidic, (C) schematic illustration of the outermost part of the double emulsion surrounded by the acrylic acid pumped with the outer aqueous solution, (D) Microcapsules obtained after the photopolymerisation and (E) schematic illustration of the outermost part of the microcapsules functionalised with acrylic acid.

The addition of acrylic acid to the outer solution can be used to functionalise mono, di and triacrylates as middle layer and for w/o/w and o/o/w templates, resulting in hydrophilic surfaces. The main limitation of the approach is the interplay between the concentrations of acrylic acid and PVA in the aqueous solution. For instance, around 0.4% of acrylic acid in a 10% PVA solution results in poor functionalisation of the shell. On the other hand, when 2% of acrylic acid is added to the 10% PVA outer solution, it results in the polymerisation of a hydrogel containing the microcapsules, which is impossible to cast for self-healing. Furthermore, when 2% of acrylic acid in PVA solution of 2% was used, no polymerisation took place when using BI as shell – most likely the photoinitiator favoured the polymerisation of the acrylic acid instead of the shell. Thus, the work was realised with the concentration of 1% of acrylic acid.

5.3.2. Functionalised epoxy shell and water core

To investigate the role of surface functionalisation in promoting the mechanical triggering, microcapsules with BH shell were synthesised, as shown in Figure 5.21.

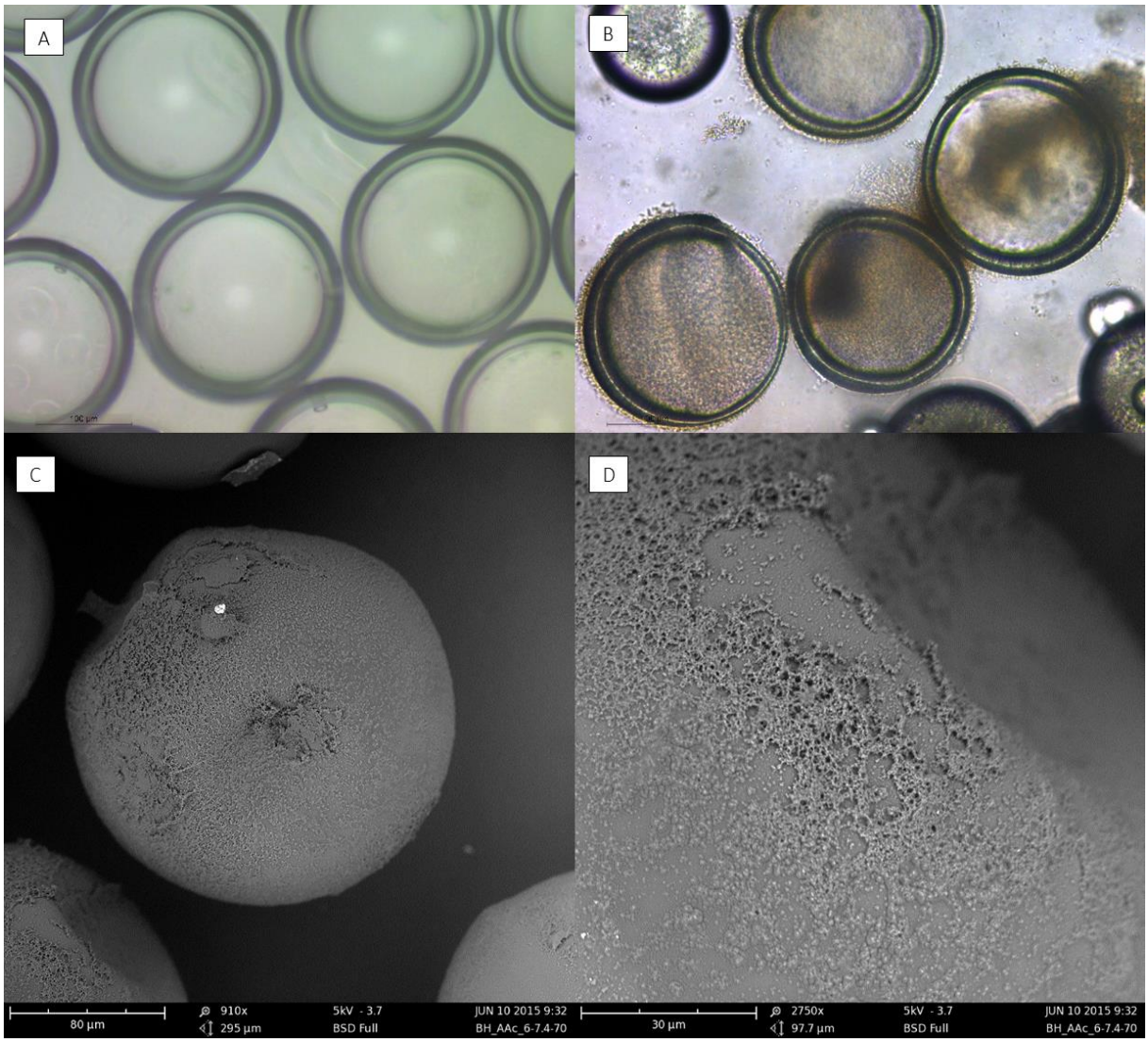

Figure 5.21 – Images of functionalised microcapsules with BH shell (a) OM images of the double emulsion surrounded with acrylic acid and (b) microcapsules functionalised with carboxyl groups, and (c) and (d) SEM images of the dried microcapsules functionalised with carboxyl groups.

The double emulsions were produced using an inner flow of PVA 2%, a middle flow of BH and an outer flow of PVA 2% containing 1% of acrylic acid. Despite the high tensile strength of BH, the copolymer was selected as shell to investigate the functionalisation of a mixture of diacrylates and to observe the performance of functionalised BH shell. The flow rates were calibrated for water and measured 6, 7.2 and 70 µL/min (pressure of 266, 1900 and 410 mbar) for inner, middle and outer fluids, respectively. The microcapsules were produced in the tubing regime, resulting in an outer diameter of 190 µm and a shell thickness of 15 µm. As shown in Figure 5.21A, the PVA in the outer solution was effective in stabilising the double emulsion, regardless the presence of acrylic acid. When the double emulsion was exposed to the UV-light, the photoinitiator formed the radicals that initiated the polymerisation of the shell. In addition, the radicals also initiated the polymerisation of

the acrylate present in the outer solution, resulting in the formation of a layer of poly(acrylic acid) surrounding the microcapsules. Figure 5.21B shows a brown cloudy material wrapping the microcapsules after the polymerisation, which was attributed to the swollen poly(acrylic acid) on the surface of the shell. Poly(acrylic acid) is a well-known hydrophilic material, capable of absorbing water and swelling while maintaining the polymeric structure and it is commonly used as a superabsorbent polymer. After drying the microcapsules, the shell had a rougher surface when compared with the non-functionalised ones, attributed to the presence of poly(acrylic acid) (Figure 5.21c and d).

After the production of the microcapsules, the material was filtered and incorporated in the cement paste to investigate the new surface properties. The acid dissociation constant (pKa) of polyacrylic acid was 4.2, meaning that when the pH is higher than 4.2, the polymer is deprotonated and the surface of the microcapsules acquires a negative charge. In the alkaline environment of the cement paste the carboxylate formed attracts cations, e.g., Ca^{2+} or Na^{+} promoting the chemical bond with the cementitious matrix (Hernández-Cruz et al. 2014). The optical microscope and SEM images of the microcapsules after the incorporation are shown in Figure 5.22.

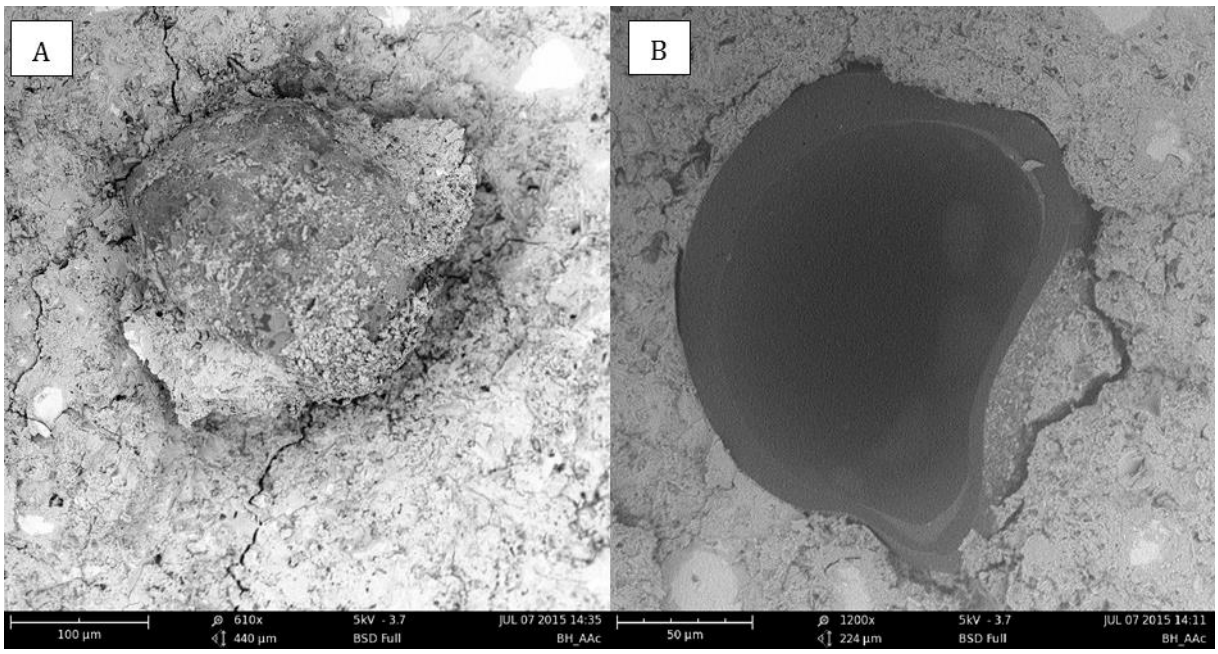

Figure 5.22 – SEM images of the microcapsules functionalised with carboxyl groups after being casted in the cement paste for 28 days.

The interfacial bonding was significantly increased, forming a layer of good intimate contact between the cement and the matrix. Nonetheless, the increase of interfacial bonding strength was not enough to assure mechanical triggering. Although it was possible to see broken capsules, most of them remained unbroken after 28 days of casting. Interestingly, instead of debonding the

capsule-matrix interface, the crack went through the cement paste and the unbroken microcapsules were camouflaged. This can be explained based on the low tensile strength of the cement paste at day 1 compared with the tensile strength of 36 MPa of the acrylate shell. Thus, the next step was to reduce the fracture strength of the microcapsules. Additionally, despite the low shell to radius ratio (h = 0.16), the shell thickness was around 15 μm, which was still thicker than most values reported in the literature. Thus, further investigation was needed to obtain thinner shell.

5.3.3. Functionalised urethane based shell and water core

To demonstrate the versatility of the methodology to functionalise different shells and to investigate the production of thinner shells with a water core, microcapsules with UH shell were produced. However, the production of thinner shells increased the likelihood of loss of the spherical shape of the microcapsules due to the loss of the water core. A possible way to overcome this issue was to maximise the adhesion of the shell to the matrix – in this way, the interplay between surface adhesion and the buckling pressure would favour the shell being attached to the matrix. Thus the microcapsule surface was functionalised with acrylic acid to investigate the role of interfacial bonding in preventing the collapse of the shell. For the production of the double emulsion, an aqueous solution containing 20% of colloidal silica and 5% of PVA was used as the inner phase, UH as the middle phase and 1% acrylic acid in 10% PVA aqueous solution was used as the outer phase. The flow rates were calibrated for water and measured to be 4, 2 and 60 μL/min (pressure of 1899, 2150 and 3626 mbar) for the inner, middle and outer fluids, respectively. Higher pressures were necessary to pump the fluids due to the high viscosity of the aqueous solution of PVA 10%. The microcapsules were produced in a tubing regime, and after the polymerisation microcapsules with a high coefficient of variation were obtained (Figure 5.23). Microcapsules with 100 μm diameter and around 5 μm shell thickness were observed, together with larger ones. The mechanism of formation of the microcapsules led to an increased variation in size, and hence to obtain more monodisperse microcapsules, the use of a new microfluidic chip was recommended. The clear formation of swollen material involving the microcapsules was not observed, but the texture of the microcapsule shell appeared to be different (compared with the non-functionalised UH shell in Figure 4.24).

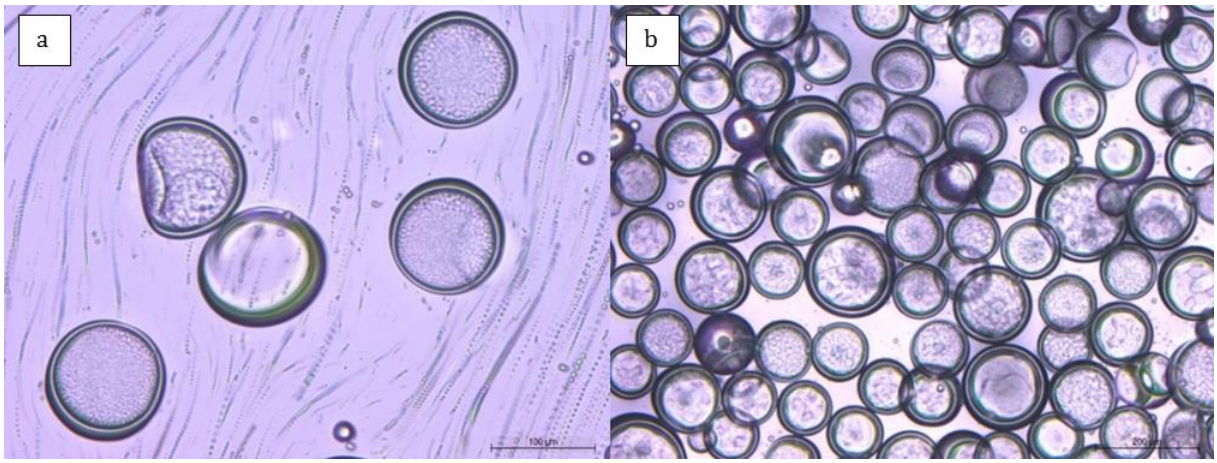

Figure 5.23 – Microcapsules with UH shell with the surface functionalised with acrylic acid: (a) detail of microcapsules texture after polymerisation and (b) large dispersion of the microcapsules produced in tubing regime.

The aqueous core microcapsules with hydrophilic functionalised surface were kept in water before being mixed within the cement paste to ensure the water is retained. Then, the microcapsules were hand-mixed with cement powder and water and cast for SEM observation after 1 day (Figure 5.24). The 5 μm shells shrunk due to the loss of core material (Figure 5.24a) or folded inwards and deformed (Figure 5.24c, d). Regarding the interfacial bonding, the microcapsules with the UH shell presented excellent adherence to the cement paste. The polar groups effectively enabled the formation of chemical bonds between shell and the matrix and the microcapsules were fully covered with it; particularly in Figure 5.24b, the polymers in the interface indicates that the material was bonding the shell to the cement paste, despite the shrinkage of the shell. The better adherence to the cement paste when compared to the functionalised BH shell was attributed to the presence of triacrylates which increased the potential of the shell to be functionalised.

The good interfacial bonding between the capsule and the matrix was not sufficient to prevent the buckling and collapse during the loss of water core. The process is schematically represented in Figure 5.24, where the microcapsules containing water core were embedded in the cement and occupied a certain volume.

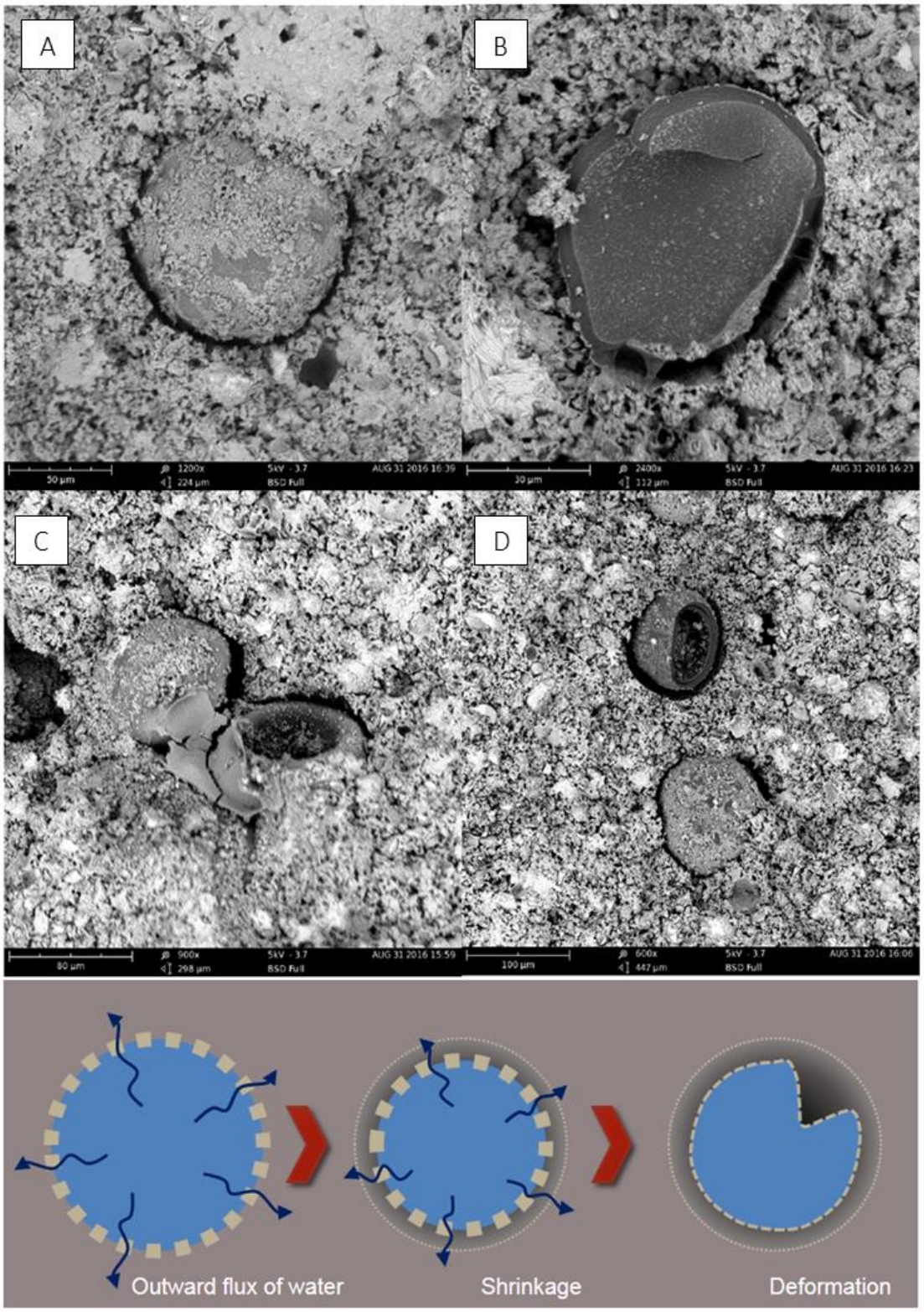

Figure 5.24 – SEM images of the sample UHA-4-2-60 casted in cement paste: (a) shrunk microcapsules, (b) broken capsules, (c, d) collapsed microcapsules due to water evaporation and schematic representation of the loss of water core inside of the cement paste.

When the encapsulated water escaped through the nanopores of the membrane, the shell shrunk and buckled due to a pressure decrease induced by the evaporation. Thin-shell microcapsules were easier to buckle and the dimple on the shell deepened as the core evaporated. Finally, most of the water in the core was drawn out, and the shells of the microcapsules folded inwards and were deformed, leaving a gap between the shell and the original shape of the microcapsule. Since the pressure buckling is proportional to Young's modulus of the shell (Equation 4.5), the UH shell were more likely to buckle given the low Young's modulus of the material (0.26 GPa).

To delay the loss of water and maintain the structural integrity of the microcapsules, the shell thickness could be increased. However, this would decrease the payload of healing material and likely to preclude the triggering, as demonstrated with the functionalised BH shell. The water permeability of the acrylate shells and the collapse of the capsule due to the water loss are well described in the literature of microfluidics (Abbaspourrad et al. 2013b; Kim et al. 2014a; Nabavi et al. 2016). Also, it is likely that other shell materials would have a similar issue when encapsulating water, since the shell is usually thinner. Although the encapsulation of water-based core for self-healing has been reported, such as aqueous sodium silicate encapsulated by polyurethane (Pelletier et al. 2011) or the encapsulation of calcium nitrate in urea formaldehyde (Hassan et al. 2016; Milla et al. 2016), more studies were needed to better understand their behaviour. First, no experiment was performed to confirm whether the water was retained within the microcapsules. This means that the retention time of the aqueous core is unknown, and, even more, the water may not have been encapsulated. Secondly, when the microcapsules were added to the cementitious material, no characterisation of the survivability or whether the microcapsules ruptured due to crack was performed; more importantly, if the water was encapsulated and the microcapsules survived, it is not entirely clear if the material remained inside of the microcapsules once no study was performed focusing on it. The lack of shells impermeable to water is unfortunate, since water is necessary for mineral- and biological-based self-healing. Furthermore, the presence of the dry core resulted in the low payload and relied on the ingress of water to diffuse the healing agent. Even if the shell was bonded to the cement matrix, the empty space inside of the capsule would result in a reduced Young's modulus of the capsules and also likely for the Young's modulus of the overall matrix. In the light of these findings, the encapsulation of organic materials seems to be the suitable route for the use of liquid cores for capsule-based self-healing.

5.3.4. Functionalised epoxy shell and organic core

The organic core microcapsules functionalised with hydrophilic groups were also embedded to investigate their performance during the integration and mechanical triggering. The organic core was investigated since it did not evaporate through the nanopores of the membrane and thus the

microcapsules maintained their spherical shape. Furthermore, the use of organic core resulted in a thinner shell, which is convenient for mechanical triggering and higher payload of the capsule. Although the potentially low tensile strength and ductile behaviour of the UH copolymer made it suitable to be used as shell, the formation of microcapsules with UH shell and organic core was not possible. Thus, BI was investigated as shell material due to its low tensile strength and high Young's modulus which may facilitate mechanical triggering and reduce the effect in the overall mechanical properties. The microcapsules were produced using an inner flow of mineral oil, a middle flow of BI and an outer flow of PVA 10% containing 1% of acrylic acid. The flow rates were calibrated for water and measured to be 1.65, 1 and 53 μL/min (pressure of 2270, 1860 and 4388 mbar) for the inner, middle and outer fluids, respectively. Figure 5.25 shows optical images of the microcapsules in solution and the SEM images of the formed microcapsules.

The microcapsules were formed in the tubing regime and they are not monodisperse. To improve the coefficient of variation, the double emulsion could be produced using a new microfluidic device, where the capillary tube is still perfectly hydrophobic. The oil was retained inside of the microcapsules, and a thin layer of acrylate shell was observed. In fact, the shell was so thin that it was hard to observe it in the optical microscope, as seen in Figure 5.25b. The small cloudy material around the microcapsules in Figure 5.25b was attributed to the functionalisation of the BI outer surface. To better observe the shell, the microcapsules were ruptured between two glass slides, washed with ethanol and vacuumed to remove the mineral oil. Then, the ruptured shell material was placed in the stub to be observed in the SEM (Figure 5.25c,d). The thin shells were observed in the SEM and measured around 2 μm. It was challenging to obtain the precise value because the density mismatch between the core and the shell resulted in an inhomogeneous shell thickness. The surface functionalisation with poly(acrylic acid) was not as prolific as in the BH or the UH shell, as observed in the sparse rugged islands in the surface of the shell (Figure 5.25c). The poor surface functionalisation was attributed to the use of isobornyl acrylate as monomer and the presence of fewer acrylate groups to functionalise the shell when compared with the di- and triacrylates in BH and UH. The formation of a porous material inside of the shell was observed in Figure 5.25c and d and it is likely to have been associated with the partial mixing of BI and mineral oil prior the photopolymerisation. As a result, during the polymerisation, the BI dispersed in the mineral phase was solidified in a porous inner surface. This also hints that the polymerisation of the shell needs to be as soon as possible to avoid the diffusion of the shell and loss of organic core.

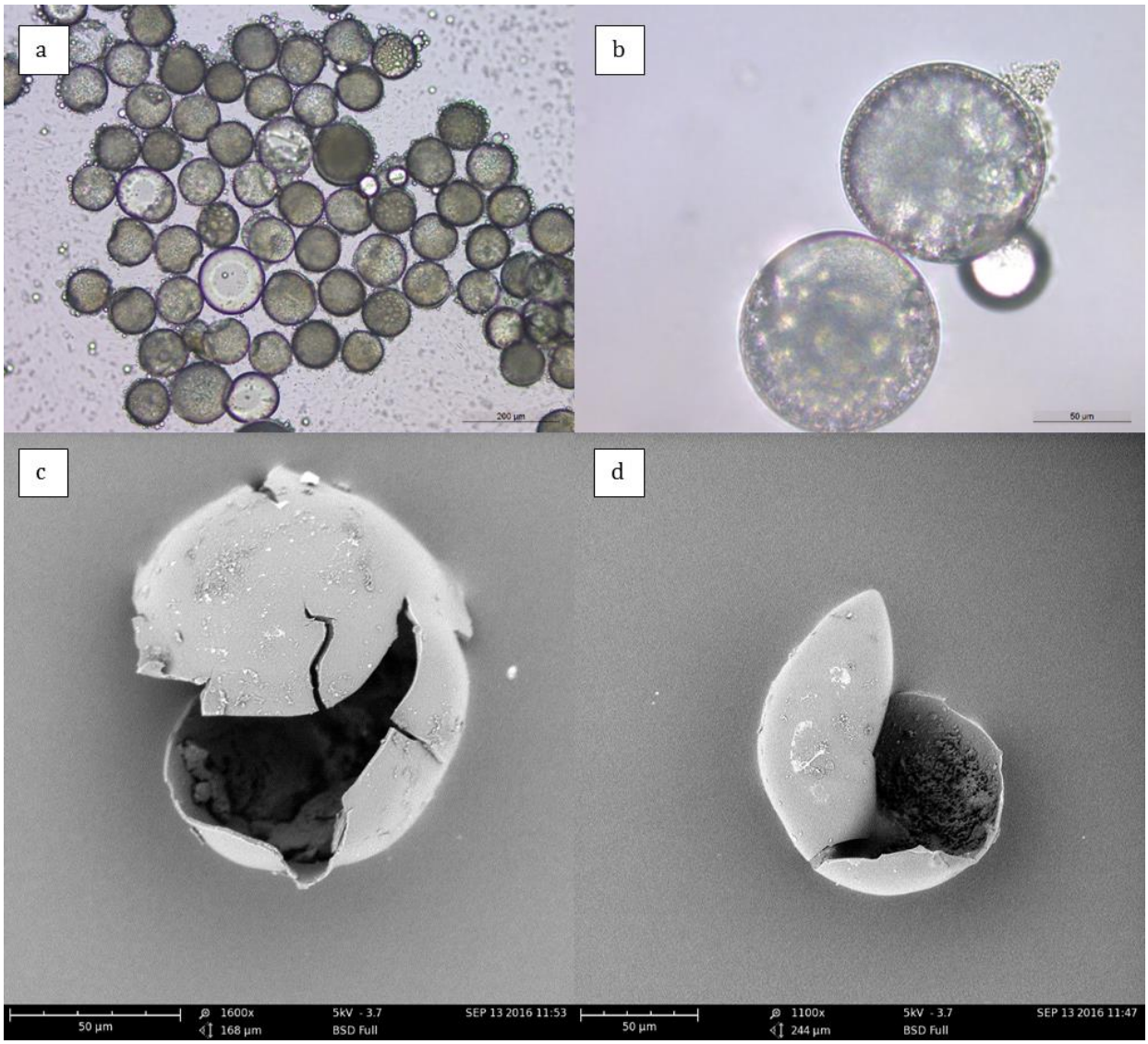

Figure 5.25 – Images of BIAMO-110/2 microcapsules: (a-b) optical microscope images of the microcapsules immersed in water and (c-d) SEM images of the ruptured microcapsules.

The microcapsules were washed to remove the outer PVA solution and were kept in water before being hand mixed with the cement paste. The cement paste was casted for 1 day before being broken to observe the microcapsules. Prior to being inserted in the SEM, the crack surface was blasted with an air duster and vacuumed to remove the organic core of the ruptured microcapsules. As observed in Figure 5.26, the microcapsules were well dispersed and virtually all the shells were ruptured at the cracked face. The chemical bond formed between the shell and the matrix was not as good as the one observed for the UH and the BH shell and attributed to the poor surface functionalisation. Although it is possible to see broken microcapsules ruptured upon crack (Figure 5.26a,b), some of them gave the impression that they were broken during the mixing process (Figure 5.26b), or during the drying process (Figure 5.26d). In particular, some shells appear to have blended with the cement during the drying process, as observed in Figure 5.26c. The

mechanism of this blend was unclear, but is probably associated with the thin part of the inhomogeneous shell formed due to the density mismatch.

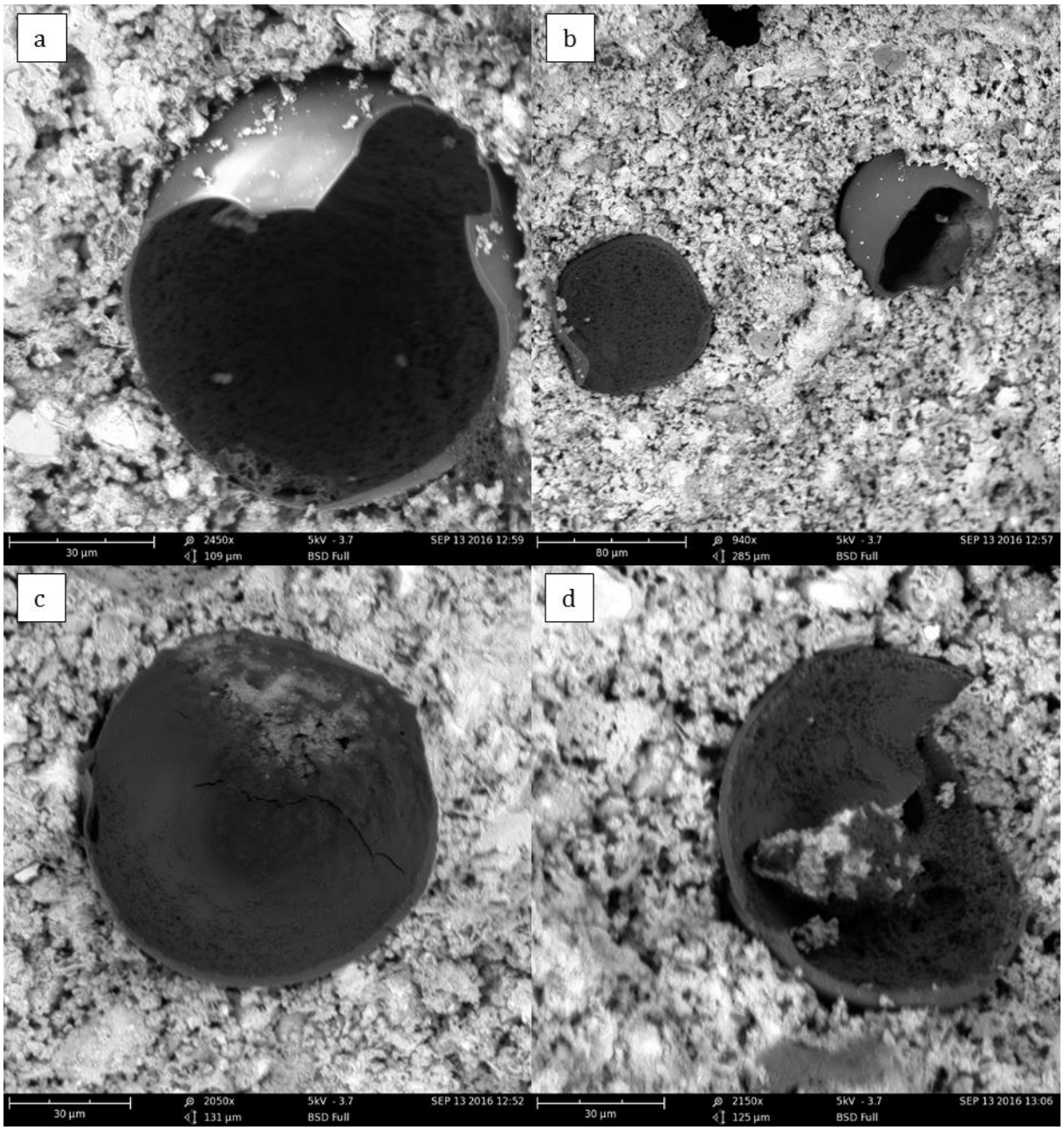

Figure 5.26 – SEM Images of the broken microcapsules BIAMO-110/2 casted in cement paste: (a) broken capsule with leaked core material, (b) presence of broken capsules and debris, (c,d) thin-shell interface with the matrix.

Microcapsules with an organic core and BI shell with a thinner shell were produced by increasing the inner flow. According to Arriaga et al. (2015), the formation of an inhomogeneous shell thickness due to density mismatch can be minimised by decreasing the shell thickness of the acrylate middle layer. This was attributed to the higher lubrication resistance of the thin layer of

acrylate (Kim et al. 2011; Arriaga et al. 2015). Thus, the double emulsion was produced using an inner flow of mineral oil, a middle flow of BI and an outer flow of PVA 10% containing 1% of acrylic acid. The flow rates were calibrated for water and measured 2.3, 1 and 40 μL/min for inner, middle and outer fluid, respectively. Figure 5.27a shows the formed double emulsion where is difficult to distinguish between the oil and the shell core. After the polymerisation, the formation of a non-uniform shell is still observed, but typically monodisperse microcapsules with a thin shell were produced, as shown in Figure 5.27b. The diameter of the microcapsules was ~140 μm and the shell thickness was ~2 μm, resulting in a shell to radius ratio (h) of 0.03.

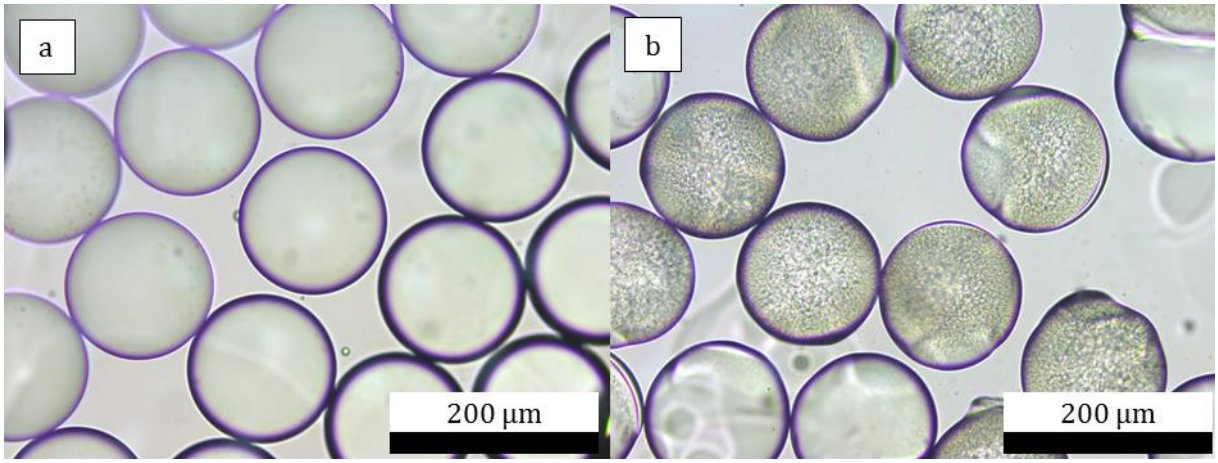

Figure 5.27 – Production of microcapsules BIAMO-140/2. (a) OM image of the double emulsion of o/o/w and (b) OM image of the polymerised shell.

The formed microcapsules were washed to remove the PVA and then hand mixed with cement powder and water, casted, and observed in the SEM after 1 day of casting, as shown in Figure 5.28. The microcapsules presented a thinner shell with more homogeneous thickness, when compared with microcapsules BIAMO-110/2 (Figure 5.26). Most of the microcapsules were broken, similarly to the ruptured microcapsules in Figure 5.26a,b. A few microcapsules detached from the cavity of the cement paste and partially deformed (Figure 5.28c,d). Since there was no cement paste inside the microcapsule, the debonding happened after the rupture of the capsule, perhaps during the blasting with the air duster or vacuum to remove the organic core. The debonding of the microcapsule after rupture hinted to the poor interfacial bonding between the shell and the matrix for the functionalised surface of BI at day 1. Furthermore, since all the microcapsules were ruptured in the crack surface, it also hints that the low tensile strength and the maintenance of the spherical shape of the microcapsules are more important than the interfacial bonding to assure the physical triggering.

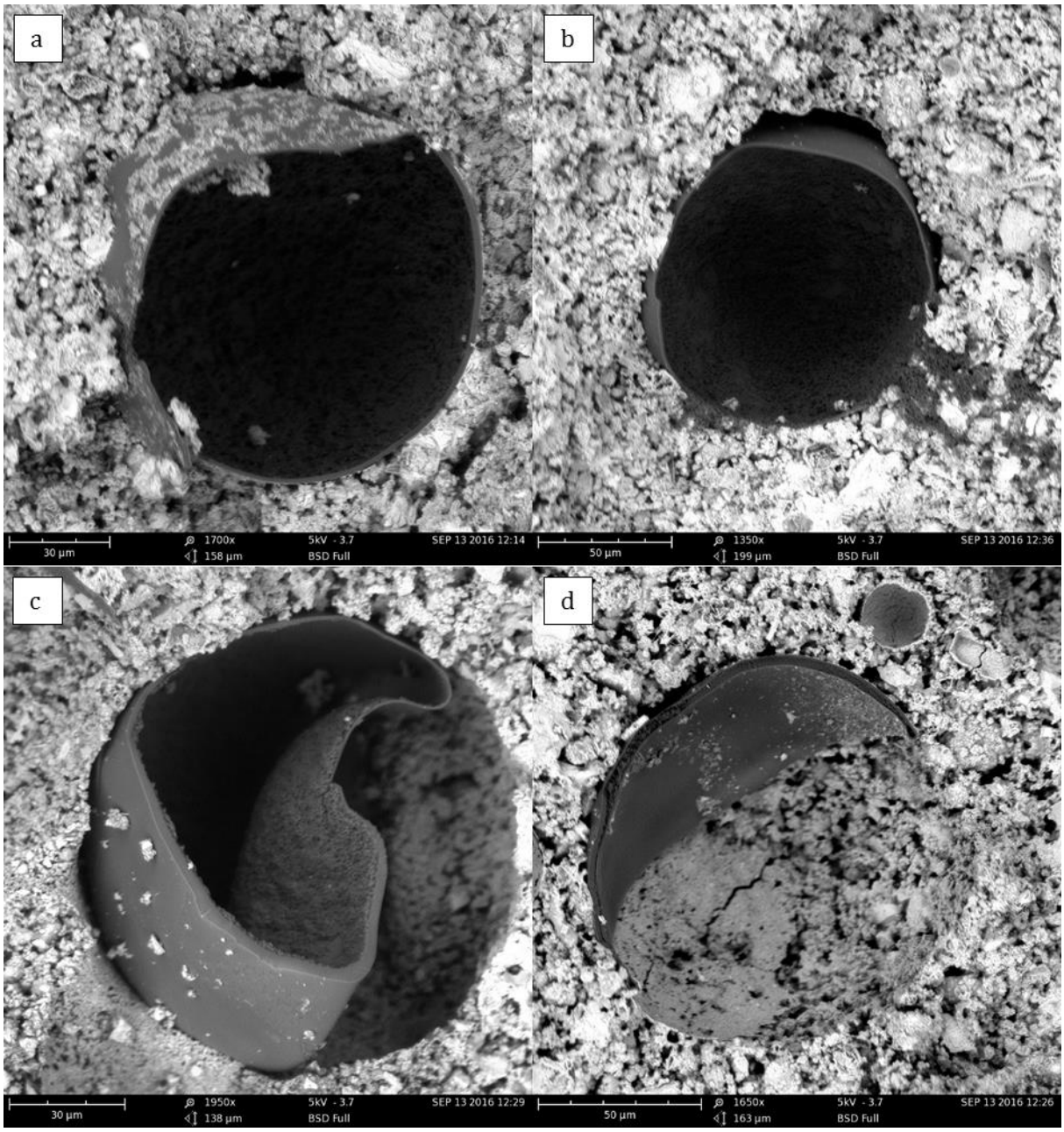

Figure 5.28 - SEM images of the microcapsules BIAMO – 140/2 casted in cement paste. (a,b) broken microcapsules and (c,d) microcapsules deformed after rupture.

To examine the long-term stability of the capsules, the microcapsules were also observed in the SEM after 9 months. Due to the alkaline environment, the shell could react and deteriorate, leading to leakage of core material. Nevertheless, the shell survived without any noticeable deterioration and it was ruptured upon crack formation, releasing the core material that was still retained. Figure 5.29 indicates the broken capsules upon crack with red arrows and the unbroken capsules with green arrow. A total of 60 microcapsules were observed in the cracked surface, from which 55% were ruptured upon crack, 6% remained unbroken, 13% were observed as debris and 25% uncertain – although they were ruptured, was unclear if it was due to the physical triggering.

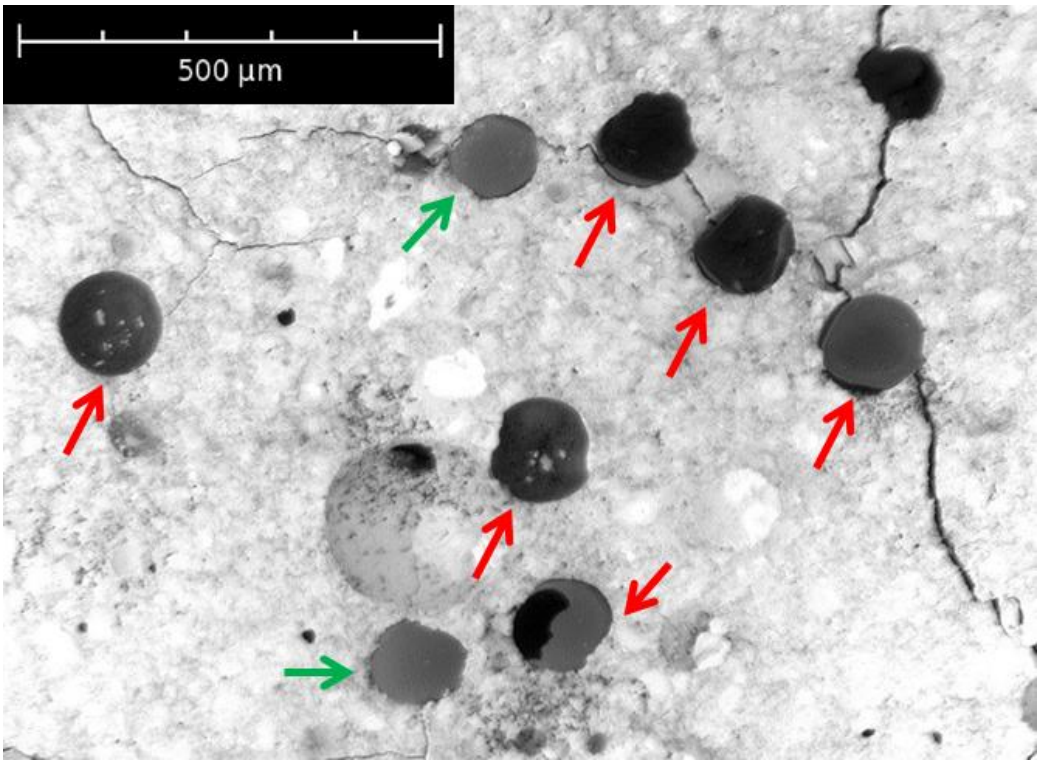

Figure 5.29 - SEM images of the microcapsules BIAMO – 140/2 casted for 9 months in the cement paste. Red arrows indicate broken microcapsules and green arrows indicate unbroken microcapsules.

In addition to survive and physically trigger, the microcapsules were also capable of retaining the core material after 9 months. As shown in Figure 5.30, the broken microcapsules presented an interior texture indicating the reaction of the shell with the core during the polymerisation. Alternatively, this texture could indicate the reminiscence of core material after being dried at room temperature, blasted with an air duster and vacuumed to remove the organic core. Nonetheless, in both cases it indicated the presence of core material. Furthermore, a similar texture was observed in the surrounding of the broken shell (Figure 5.30a,b), indicating that the mineral oil spilled over the matrix after rupture. The retention of core material was attributed to the integrity of the shell over time. This was achieved partially by the functionalisation of the shell – since there was a layer promoting the bonding between the shell and the matrix, the actual shell did not react with the cement paste. Therefore, it minimised the chances of deterioration of the shell and increases the longevity of the core retention.

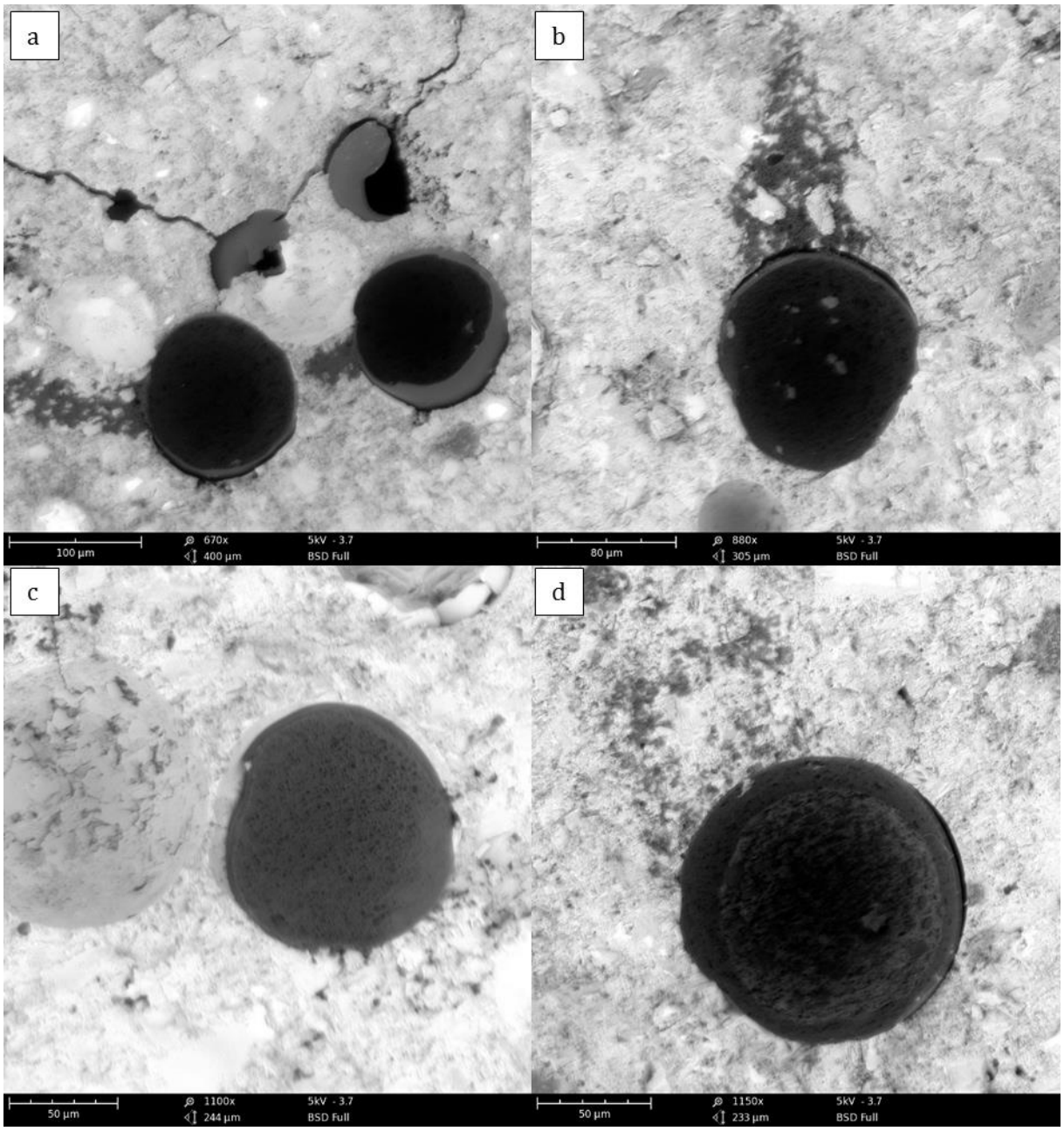

Figure 5.30 - SEM images of the microcapsules BIAMO – 140/2 casted for 9 months in the cement paste. (a,b) indication of leakage of the oil core during breakage and (c,d) broken microcapsule with porous inside.

The presence of broken capsules and the indication of core retained after 9 months indicate that the capsule may be suitable for long term self-healing. Thus, a better understanding of the time-frame of self-healing may help in the fine tuning of the properties. Before 28 days, it is expected that the bonding strength between the shell and the matrix is still increasing. Thus the microcapsules to be ruptured in this period need a good interfacial bonding with the matrix and low tensile strength. Then, if the self-healing will be considered for more than 64 days, intermediate values of tensile strength and interfacial bonding may be necessary, since they will increase with time. Furthermore,

although it was not discussed in this section, fine tuning the toughness may be necessary to ensure the survival in the cement mixers.

To conclude, the low tensile strength, low shell thickness, good interfacial bonding and maintenance of the spherical shape of the microcapsules resulted in their ruptured upon crack formation. To increase the survivability of the microcapsules during mixing, it would be interesting to investigate the formation of microcapsules with organic core and a more ductile shell, perhaps the BT. Furthermore, the use of triacrylate as monomers may increase the surface functionalisation and thus the interfacial bonding. Further studies to investigate the influence of the shell thickness and shell material in the mechanical properties are necessary, specially taking into consideration different core materials. Once the physical triggering and survivability of the capsules are assured, the self-healing performance of the microcapsules containing healing agent can be investigated.

5.4. Conclusion

The work undertaken on the development of mechanically triggered capsule-based self-healing was discussed in this chapter. Initial investigation included the integration of the microcapsules in the cementitious matrix to explore survival, dispersion and interfacial bonding. In addition, the preliminary investigation looked at the role of shell thickness, tensile strength, aqueous and organic core to assure the mechanical triggering. Due to lack of ruptured microcapsules under crack formation, the mechanical properties of the acrylate shell were investigated using DMA, microindentation and tensile tests. The focus was on the glass transition temperature (T_g), Young's modulus and tensile strength of 5 different acrylates with potential to be used as shell. The functionalisation of the shell was also proposed with the aim of increasing the interfacial bonding between the shell and the cementitious matrix. The functionalisation of three different shell materials was demonstrated, as well as the performance of the hydrophilic surface in the cement paste. The main outcomes of the research are summarised in Figure 5.31.

When the microcapsules are dispersed in the cement matrix, they disperse well and no reaction was noticed between the shell and the matrix. However, the encapsulation of hydrophilic core resulted in microcapsules with shell thickness ranging between 7-14 μm. For the thick shelled microcapsules, the shell would maintain its integrity during the loss of water core, but the physical triggering is precluded. For the thinner shelled microcapsules (~7 μm), the loss of water core resulted in shrinkage and/or buckling, also precluding the physical triggering. On the other hand, the encapsulation of organic core resulted in thinner shells (~2 μm) and retention of the core and structural integrity, increasing the likelihood of physical triggering. However, the poor interfacial bonding between the shell and the cementitious matrix also preclude the physical triggering.

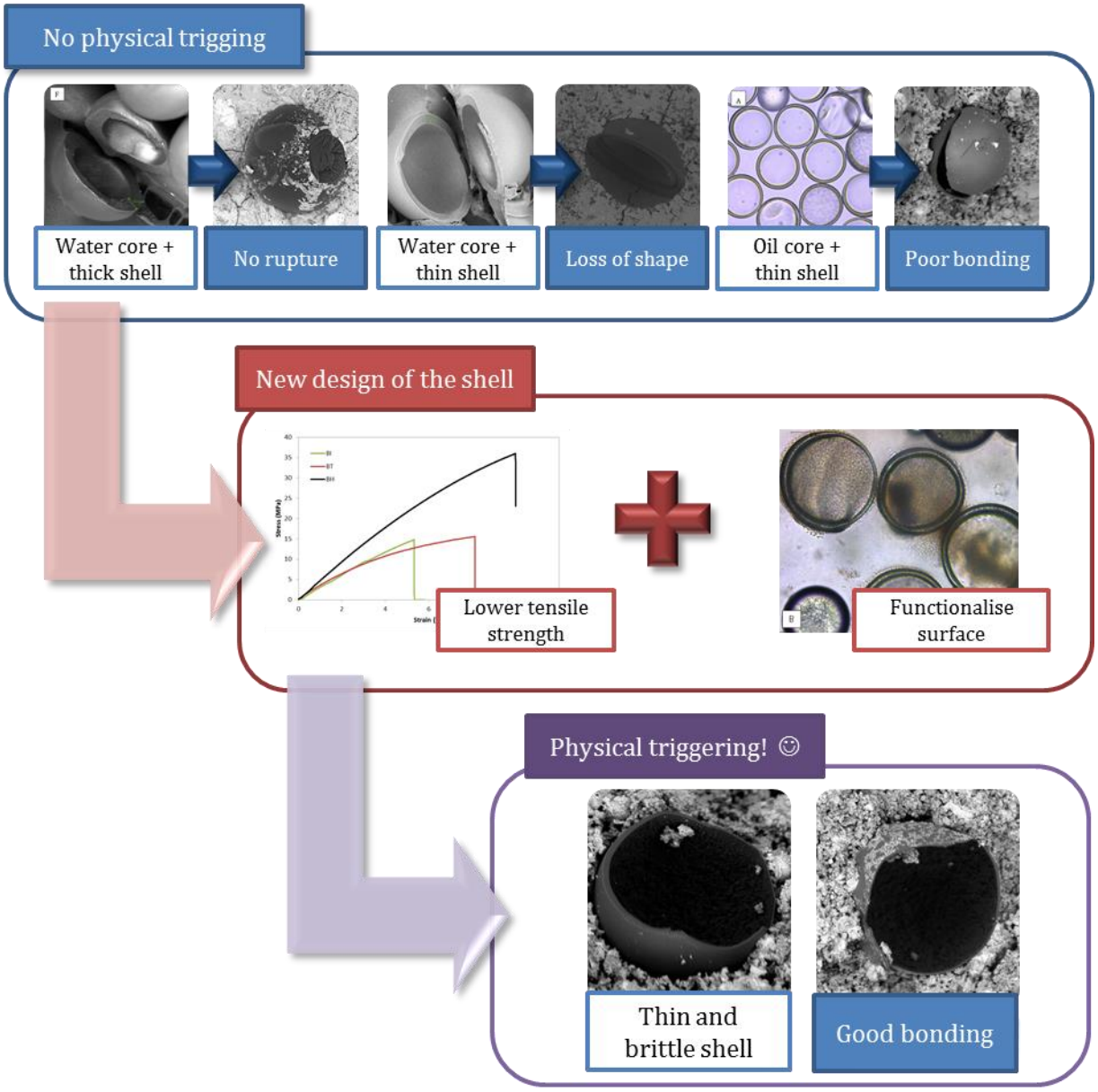

Figure 5.31 - Schematic representation summarising the outcomes of the Chapter 5.

Thus, to design microcapsules for the physical triggering, the properties of the shell were investigated. After characterising the glass transition temperature, the Young's modulus and the tensile strength of 5 different materials with potential to be used as shell, it was hypothesised that the main parameter controlling the physical triggering would be the tensile strength. Furthermore, the functionalisation of the hydrophobic acrylate was suggested to increase the interfacial bonding between the shell and the matrix. The functionalised shells used to encapsulate water core presented an improved bonding with the cementitious matrix, but the thick shells and loss of shape also prevented the physical triggering. Alternatively, when organic core were encapsulated with functionalised shells, virtually all the capsules were ruptured upon crack formation. This indicates

the physical triggering is favoured by thin shell, retention of spherical shape and good interfacial bonding. Furthermore, the results indicate that the organic core remained inside of the microcapsules up to 9 months, with no deterioration of the shell indicating good long term stability.

The research has also extended the knowledge about the behaviour of microcapsules in the cementitious matrix. It indicated good survival of acrylate microcapsules in the cement paste, the importance of tuning the shell thickness and the tensile strength to favour the mechanical triggering, particularly when the low tensile strength of cement is taken into account. Next steps include investigating the performance of physically triggered microcapsule-based self-healing, after the encapsulation of the healing agent.

6. Conclusions and Recommendations

This chapter summarises the main findings generated throughout this work and outline of the implications of this work to the field of research. Then, recommendations for future research within this area are given.

6.1. Conclusions

In **Chapter 1**, the background and rationale for the topic of research were presented. Concrete outperforms other common building materials and has been widely used for infrastructure development and expansion. However, due to the large volumes of material used, the cement industry contributes ~5% of annual anthropogenic CO_2 production, chiefly because of Portland cement (PC) clinker production. In order to produce a more sustainable concrete, several materials have been investigated as partial PC clinker replacements. Alternatively, improvements in durability have also been investigated, where the environmental impact of the concrete infrastructures is reduced by extending the service life and reducing life-cycle costs. However, concrete is inherently susceptible to crack formation, a phenomenon that impairs the material's integrity and durability. The cracks are preferential pathways for the ingress of potentially aggressive fluids that corrode the embedded steel reinforcement. For this reason, it is necessary to continuously inspect, maintain and repair reinforced concrete structures and these actions result in increased life-cycle costs significantly. In this context, the development of *self-healing* structures has been explored, where the formed crack is counteracted autonomously by a process of healing.

A critical state-of-the-art review on self-healing of cementitious materials was presented in **Chapter 2**. Intrinsically, cement-based materials possess a certain autogenous self-healing capability mainly due to the continued hydration and calcium carbonate formation. However, the autogenous healing is effective in the presence of water and crack width <0.15 mm and preferably < 0.05 mm (Reinhardt et al., 2013). Aiming at stimulating the intrinsic self-healing, several techniques have been proposed to restrict the crack width and enhance water supply. Crack restriction could be achieved by adding fibres, shape memory polymers and additional water could be provided by superabsorbent polymers (Li and Yang 2007; Jefferson et al. 2010; Snoeck et al. 2012; de Rooij et al. 2013; Snoeck et al. 2014; Fan and Li 2015; Mignon et al. 2017). The use of mineral admixtures has also been explored, resulting in the formation of new reaction products in the crack surface in the presence of water (Ahn and Kishi 2010). Alternatively, capsule-based self-healing can be used to isolate a healing material until the damage to the matrix causes its release and reactions, resulting in the healing of the fracture. These capsules can be easily added during mixing and allow the encapsulation of a wide variety of healing agents. As a result, capsules based self-healing has been

reported to heal cracks ranging from 0.2 to 1 mm and may potentially restore transport and mechanical properties of cementitious materials (Wang et al. 2014; Alghamri et al. 2016; Kanellopoulos et al. 2016; Giannaros et al. 2016).

Challenges associated with the design of the capsules for self-healing have yet to be overcome to promote the feasibility of the technique. In the design cycle, the first step is to consider the service conditions in which the self-healing will take place as it can help promote the mechanism of healing. For self-healing based in minerals or bacteria, the presence of water is essential and thus it is recommended as for submersed or underground structures (Huang et al. 2016). In places where the continuous supply of water is not available, the healing agent is preferred to be in a liquid form to be delivered to the cracks efficiently. Furthermore, the mechanism of healing should be water-free or moisture-based, using polymers such as epoxy and polyurethane. Once the service conditions are determined, the healing agent is selected and the encapsulation of the cargo can take place. To produce the bulk quantities of materials necessary to promote self-healing, typically two techniques are investigated: pan-coating for the encapsulation of solid cores and coacervation and emulsification polymerisation for the encapsulation of liquid cores (Dong et al. 2014a; Lee and Ryou 2014; Dong et al. 2014b; Perez et al. 2015a; Alghamri et al. 2016; Hassan et al. 2016; Milla et al. 2016; Lv et al. 2016b; Lee and Ryou 2016; Kanellopoulos et al. 2017). The techniques used to encapsulate the liquid healing agents resulted in capsules with a wide range of sizes and shell thicknesses, and thus restraining the understanding of the role of these parameters on the mechanical properties of the matrix and physical triggering. Although the produced microcapsules are mostly reported to survive mixing, the mechanical properties may result in the lack of physical triggering. For instance, the *in situ* polymerisation process may lead to the formation of hydrophobic shells which may cause debonding and prevent self-healing (Wang et al. 2013; Lv et al. 2016a). To overcome these limitations, the fine tuning of the tensile strength and the interfacial bonding is desired (Ponnusami et al. 2015). In addition, the pH and hydrophobic/hydrophilic nature of the core material affect the formation of the shell, consequently limiting the materials with potential to be encapsulated and investigated.

A promising route to produce a wide range of core-shell structures with fine control over the shell properties is the use of the microfluidic device. Microfluidics uses a double emulsion which is selectively photopolymerised to form a core-shell structure (Utada et al. 2005). The controlled conditions of reaction offer a route to explore the encapsulation of hydrophilic and hydrophobic cores, independent of pH (Chen et al. 2014b; Zieringer et al. 2015). In addition, a wide variety of shell materials with different properties can be adjusted to promote self-healing (Chen et al. 2012). This is achieved through the adjustment of the glass transition temperature, Young's modulus,

fracture strength and the interfacial bonding between the microcapsules and the matrix (Ponnusami et al. 2015). Thus, the following key factors governing the mechanical triggering can be tuned to enhance the rupture of the capsule and promote self-healing, namely: (i) thin shelled microcapsules; (ii) the retention of the core material; (iii) low fracture strength; and (iv) good interfacial bonding. Furthermore, the microfluidic encapsulation offers a platform to assess the properties of the shell associated with the permeability which is important to retain the core material and to prevent unwanted reactions.

Hence, the **main aim of this research** was to develop and optimise a microfluidic encapsulation protocol for physically triggered self-healing in cementitious materials. This aim was divided into specific objectives met in different sections of the thesis:

- Set-up a microfluidic station to produce double emulsions, followed by their photopolymerisation for the production of microcapsules (Chapter 4, Section 4.1);
- Investigate the role of flow regimes for the production of the double emulsion and the control over size and shell thickness (Chapter 4, Section 4.2);
- Synthesise microcapsules containing aqueous (Chapter 4, Section 4.3) and organic-based (Chapter 4, Section 4.4) core material and acrylate shell;
- Investigate the behaviour of the microcapsules in cementitious materials, focusing on survival during integration, dispersion, shell properties and physical triggering (Chapter 5, Section 5.1);
- Investigate the mechanical properties of specific materials suitable to be used as the shell for physical triggering (Chapter 5, Section 5.2);
- Synthesise microcapsules with shells suitable for physical triggering, focusing on shell functionalisation, core retention and tuning shell properties (Chapter 5, Section 5.3).

In **Chapter 3**, the materials and experimental methods used in the subsequent research work were presented. The flow-focusing and capillary devices investigated for the production of the double emulsion were described. Because of its reliable design and less laborious cleaning process, the flow-focusing device was selected to produce the double emulsion. The main parameters controlling the formation of the emulsions were presented, indicating the importance of the capillary number, i.e., the control over viscous stresses and interfacial forces to produce the double emulsion. Furthermore, the mechanism of consolidating the middle phase through free radical photopolymerisation is also explained. In total, 5 different materials were used as shells and 3 of them were functionalised to make their surfaces hydrophilic. As a result, colloidal silica and sodium silicate dispersed in water and emulsified in mineral oil were encapsulated. The microcapsules characterisation was performed using optical microscopy, SEM, SEM-EDX and TGA focusing on

demonstrating the formation of the core-shell structures and the retention of the core material. To investigate the behaviour of the microcapsules in the cementitious matrix, 3-5% of microcapsules (by weight of cement, bwoc) were added to the cement paste. The cement prisms containing the microcapsules were kept submerged and cracked at different days; the cracked surface was investigated for survival, dispersion, physical triggering and morphology of the microcapsules via SEM. Moreover, the mechanical properties of five different acrylates were characterised using DMA, microindentation and tensile tests due to their potentials as the shell materials. The aim was to characterise the glass transition temperature (Tg), Young's modulus, hardness and tensile strength of the acrylates.

In **Chapter 4**, the work undertaken to synthesise the microcapsules for self-healing of cementitious materials was discussed. Initial investigations included the setting-up an experimental platform to produce the double emulsion, using a flow-focusing device and syringe pumps. At this stage, the main challenge was to comprehend the importance of the order of added fluids, how to connect the tubing system and to discover the flow rates in which the double emulsions were produced. Using BH as middle fluid and PVA2% as inner and outer fluid, a double emulsion was produced only at flow rates of ~0.4, 0.4 and 4 mL/h for inner, middle and outer fluids, respectively. This protocol resulted in a double emulsion of water-in-oil-in-water (w/o/w) with 225 μm outer diameter and 26 μm of middle layer. To form the microcapsules, a double emulsion batch was exposed under the UV-light, which triggered the photopolymerisation of the middle acrylate phase containing the photoinitiator. This resulted in a core-shell structure encapsulating water containing PVA2%. However, during the drying process the produced microcapsules developed dimples and holes. This outcome was attributed to the gravitation settling caused by the density mismatch of the inner and middle fluids, resulting in the formation of inhomogeneous double emulsion template. The buckling of the inhomogeneous shell occurs within 20 min of exposure at room temperature due to the loss of water core. The leakage of water core was confirmed by TGA where no weight due to water evaporation was lost before 100°C. To obtain fully closed microcapsules, the fabrication process was switched to *in situ* photopolymerisation to minimise the gravitational settling. The UV-lamp was placed in the outlet tube containing the double emulsion. To overcome the limited control over the size and shell thickness provided by the syringe pumps, pressure pumps were acquired. The new pumps allowed a fine tune of the flow rates resulting in the production of microcapsules in the dripping and jetting regime – thus expanding the range of size from 80 up to 220 μm.

The diameter and shell thickness of the microcapsules were correlated with the flow rates and established flow regimes. The variation of the inner, middle and outer phase flow rates result in three different regimes for the formation of the double emulsion: tubing, jetting and dripping. At

high flow rates, around 7, 7 and 70 µl/min, the double emulsion was formed in a tubing regime, resulting in droplets ranging between 190-240 µm and higher yielding (~1 g/h). However, this system resulted in less uniform double emulsion and thick shells due to the enlarged size of the capsules. By decreasing the flow rate, the jetting regime was achieved but it was difficult to stabilise and produced inconsistent results. Hence, the dripping regime was typically used for the formation of the double emulsion, at flow rates of ~4, 4, 80 µl/min for inner, middle and outer phase, respectively. The dripping regime is very stable, producing microcapsules ranging between 70-130 µm with outstanding coefficient of variations as low as 0.7 and 1.8% for inner and outer diameter respectively. Nonetheless, the decrease in the flow rate also resulted in the decrease of the yield to approximately 0.5 g/h. Due to the mass conservation, the inner and middle flow rates are correlated to the internal and external diameter of the double emulsion. Thus, theoretical predictions and experimental data were used to show the correlation between the flow rate ratio of the middle and inner fluids and the shell thickness. This correlation was used to estimate the shell to radius ratio (h) of the double emulsion, with more than 90% accuracy. The minimum values of h of a w/o/w double emulsion were typically ~0.15. The parameter h is fundamental when considering the payload of core material, the retention of spherical shape and the likelihood of mechanical triggering.

To synthesise fully closed microcapsules containing an aqueous core, double emulsion templates of water-in-oil-in-water (w/o/w) were produced, followed by *in situ* photopolymerisation. By fine tuning the inner, middle and outer flow rates, microcapsules with BH shell and aqueous core with two sets of diameter and shell thickness were produced: 82 and 12 µm, termed BH-82/12 and 88 and 7 µm, termed BH-88/7. To prevent agglomeration of the capsules, the microcapsules were collected in a solution of PVA 10% in weight due to the higher viscosity and lower interfacial tension. However, the formation of dimples and buckled capsules was observed, particularly for BH-88/7 with the thinner shell (h = 0.16). The loss of spherical shape was attributed to the loss of aqueous core and evaporation of water surrounding the microcapsules. Depending on the Young's modulus of the shell material and h, the pressure created during the evaporation may result in buckled shells. Consequently, microcapsules BH-82/12 with 12 µm of shell thickness (h = 0.29) are stiff enough to remain spherical whereas for BH-88/7, buckling occurs. The uniformity of the shell is also important, since the density mismatch between the inner and middle solution resulted in the displacement of the core and then the polymerisation of asymmetrical microcapsules. This asymmetry favours the buckling in the thinner part of the shell during the water loss.

Colloidal silica suspension in water and sodium silicate aqueous solutions were investigated as core materials due to its superior self-healing properties as a mineral healing agent. In addition, these

materials could minimise the density mismatch in the double emulsion, resulting in homogenous shell thickness. Microcapsules were prepared containing ~20% in weight of pure colloidal silica suspended in water as core material and BH as shell, with 88 μm of outer diameter and 9 μm of shell thickness. EDX and SEM of the microcapsule core confirmed the retention of the colloidal silica but the loss of water. As for the sodium silicate, the double emulsions were formed containing the sodium silicate solution as core and the BH as shell. However, some of the core materials appeared to have escaped prior and during the batch photopolymerisation, minimising the core retention. Furthermore, the evaporation of water core during the drying process resulted in buckling and breakage of the microcapsules. Colloidal silica solution was also encapsulated by the urethane-based copolymer, UH, demonstrating the versatility of the double emulsion to produce shell with different materials. Additionally, the urethane monomer was chosen as it may favour physical triggering due to its low shrinkage, multiple functionality and low tensile strength. UH was successfully used to encapsulate a solution ~20% colloidal silica, resulting in well centralised capsules with the size of 125 μm and shell thickness of 7.5 μm (h = 0.12). The optical microscope observation of the UH shelled microcapsules drying at room temperature showed the buckling process occurred in less than 4 hours. The TGA results confirmed the encapsulation of water and the retention of only colloidal silica after 1 day of drying the microcapsules at room temperature.

The retention of core materials is enhanced by encapsulating non-aqueous solvent such as mineral oil because they are less likely to evaporate through the shell. Mineral oil served as a model compound to investigate the encapsulation of non-polar core and the retention of non-aqueous cargo. The use of oil-in-oil-in-water (o/o/w) double emulsion template hindered the polymerisation of the UH shell. However, the o/o/w template was effective in producing microcapsules with mineral oil as core and BI as shell, with size and shell thickness of 110 μm and 2 μm, respectively (h = 0.04). The formation of thin shelled capsules resulted in higher payload of core materials and the retention of mineral oil inside of the capsules was confirmed by TGA, showing a encapsulation efficiency of 66%. Although mineral oil does not participate directly in the self-healing process, its indirect use as a vehicle has been explored for the encapsulation of an emulsified healing agent. To demonstrate this concept, a solution of sodium silicate emulsified in mineral oil (25% v/v) was encapsulated by the BI shell using an o/o/w template. Likewise, a solution of colloidal silica was also emulsified in mineral oil (33% v/v) and encapsulated using a BI shell.

The microcapsules produced with microfluidics were cast in cement paste prims and the investigation of integration, survivability and triggering mechanism was described in **Chapter 5**. The capsules were well dispersed, with no preferential distribution and no debris formation

indicating the capsules were not broken during mixing. Microcapsules BH-82/12 mostly debonded under crack formation and microcapsules BH-88/7 buckled significantly which hindered the shell-matrix bond. As a result, both thin (7 μm) and thick (12 μm) shelled microcapsules resulted in less than 5% of broken capsules. The low incidence of ruptured capsules was attributed to the thick shells, the buckling of thinner shells due to the loss of water core, the high tensile strength of the acrylates and the poor interfacial bonding. Aiming at reducing the tensile strength of the shells, 20BE precursor was used, but the resultant microcapsules presented an elevated shell to radius ratio (h = 0.32), which prevented the physical triggering nonetheless. Interestingly, an increased interfacial bonding between the 20BE shell and the cement paste was observed and attribute to the presence of polar groups. UH microcapsules were also cast due to the reduced tensile strength, but the combination of low shell to radius ratio (h = 0.12) and low Young's modulus resulted in buckled capsules. This indicates that microcapsules with water core may not be suitable for physical triggering as the thin shelled microcapsules deform and the thick ones debond. Alternatively, microcapsules with the organic core and BI shell were capable of retaining the core material and thus preventing deformation of the shell. Furthermore, shells achieved through the o/o/w were thinner ~2 μm (h = 0.04), thus favouring the physical triggering. However, the poor interfacial bonding between the hydrophobic shell and the hydrophilic cementitious materials still resulted in debonded microcapsules.

The mechanical properties of five different copolymers (BP, BI, BH, BT and UH) with potential to be used as the shell material were characterised, focusing on achieving physical triggering. The T_g of the copolymers were estimated and ranged between 23 and 109°C. Furthermore, DMA was used to confirm the T_g of UH and BI, which was determined to be 43 and 84°C, respectively. This indicates that the copolymers are likely to present a brittle fracture at room temperature. The structures of the different monomer used affected the inherent mobility of the copolymer and therefore affect its T_g. The effect of ageing of the acrylates was also considered and microcapsules with BH were observed in the SEM after 2 and 24 months. With time they still presented a smooth surface, retention of core-shell shape, absence of cracks and no volume shrinkage. Young's modulus of the shell materials was measured using microindentation and ranged between 0.3-2.6 GPa. Furthermore, the Young's modulus of a single microcapsule with BH shell was measured to be 2.6 GPa. These values have a direct implication in the likelihood of microcapsules' buckling due to the loss of the water core, indicating UH is more likely to buckle than BI or BH. In addition, the Young's modulus is lower than the one of concrete and the mismatch favours the crack attraction, thus facilitating the rupture. However, it is expected that the insertion of the microcapsules with reduced values of Young's modulus, compared with the matrix, will decrease the overall elastic modulus of the matrix. The tensile tests showed stresses at rupture of 15, 36 and 17 MPa, and strain

values of 5, 10 and 8%, for BI, BH and BT, respectively. The high tensile strength for the sample BH was attributed as the main factor precluding the physical triggering.

The good interfacial bonding between the microcapsules and the cementitious matrix was considered as one of the factors contributing to prevent the physical triggering of the microcapsule. The microcapsules produced in the double emulsion template have a hydrophobic surface which hinders the bond with the cement matrix. To tackle this disadvantage, an innovative methodology was proposed to functionalise the surface of the microcapsules with hydrophilic groups. To achieve this, 1% v/v of acrylic acid was added to the outer solution surrounding the double emulsion. During the photopolymerisation of the acrylate shell, a chain of carboxyl groups was attached to the surface of the microcapsule, resulting in a hydrophilic surface. SEM observation of the surface-modified capsules showed a different morphology of the surface, indicating the acrylic acid was attached to the microcapsules. In addition, an increased interfacial bonding between the cement paste and the functionalised microcapsules was observed, demonstrating the effectiveness of the surface functionalisation. However, the interfacial bonding was not sufficient to prevent the buckling of thin shelled microcapsules due to the loss of water core. Thus the combination of low tensile strength, low shell thickness and good interfacial bonding was defined as key factor for enabling physical triggering. The importance of these parameters was demonstrated by the physical triggering of microcapsules with mineral oil as core and functionalised BI as shell, with size and shell thickness of 140 μm and 2 μm, respectively. Furthermore, SEM of the embedded microcapsules indicated that the mineral oil was retained after 9 months, indicating good stability and retention of the core.

The main limitation of using microfluidics arises from the difficulties in producing the large-scale quantities needed for civil construction. The microfluidic device used in this work produced at a typical rate of ~0.5g of microcapsules/h, which can be increased to produce no more than 26g of microcapsules/day. Although devices in parallel and tandem emulsification can be used to increase the production, the optimum values are still ~1.5 kg of microcapsules/day. For comparison, typical lab experiments to evaluate the effect of different proportions of microcapsules in the cementitious matrix and to assess self-healing performance need ~3 kg of microcapsules. Nonetheless, the microfluidic technique is the most suitable to investigate the properties and limitations of the microcapsules. As a result of this controlled methodology of the encapsulation, it was demonstrated that although water can be encapsulated, it is not retained inside of the microcapsule. Consequently, the healing agent remains dried inside of the capsule with low payload, and relies on the ingress of water in the crack to promote the healing mechanism. Alternatively, organic liquids are retained inside of the capsule and can be used as a delivery vehicle. The main implication of these findings is

the importance of considering the service conditions in which the self-healing takes place: if the water is present throughout the cracks, the use of solid-core microcapsules may be preferential, as the water is necessary to disperse the healing agent and as a reactant for healing. In this case, the use of other techniques to produce microcapsules with solid cores should be considered, since it would increase the payload of the core materials. On the other hand, when the autonomous diffusion of the healing agent outside the capsule is necessary, the organic core microcapsules could be considered. This may be suitable for service conditions with non-continuous water supply, possible using polymers such as epoxy or polyurethane as the healing agent.

The main goal of this thesis was to develop a microfluidic encapsulation protocol to investigate physically triggered self-healing in cementitious materials. It may be concluded therefore that this primary objective was met. The research has also extended the knowledge about the behaviour of microcapsules in the cementitious matrix and has several practical applications. Firstly, it indicated the survival of acrylate microcapsules in the cement paste. Furthermore, investigation of the microcapsules showed that they survive without changes in properties after 2 years. Thus, acrylate shells could potentially be used for the encapsulation of other materials, such as solid cores through pan-coating. Secondly, the tensile strength of the shell needs to be considered to favour the mechanical triggering, particularly when the low tensile strength of cement is taken into account. Thirdly, the poor chemical affinity between the polymeric microcapsules and the cementitious matrix may lead to debonding of the microcapsules and preclude physical triggering. Thus, the self-healing research should focus on the use of chemically compatible materials such as silica and hydrophilic shells or the functionalisation of hydrophobic shells. Last but not least, this is the first study in self-healing of cementitious materials addressing the leakage of core material through the shell and indicates the unfeasibility of using aqueous core microcapsules. Further research should take the permeability of the shell into consideration when selecting the core materials. The characterisation of the mechanical properties of the microcapsules may also help as data for modelling of the mechanical triggering.

6.2. Future directions

Microfluidic was used to produce the microcapsules, providing valuable insights about the encapsulation process and properties of the core and shell. However, the technique is still not suitable for the production of large quantities of microcapsules necessary to promote self-healing in constructions. Therefore, the investigation of parallelised systems to scale-up the production of microcapsules using microfluidics would be desirable. Furthermore, the findings of the work with microfluidics could be translated to bulk scale emulsification-polymerisation, steering the research towards production of organic cores and hydrophilic shells. Furthermore, the investigation of

likelihood of physically triggering water-core microcapsules with other shell materials is also necessary.

Although mineral oil was investigated as a model organic compound, the next step is the microfluidic encapsulation of organic healing agents such as epoxy and polyurethane prepolymer. And for the use of emulsified healing agents, the volume of the active materials needs to be optimised and the stability of the emulsion needs to be investigated. In addition, the effect of the organic phase in the cement properties also needs to be assessed and potentially used to promote self-healing as well. The determination of the permeability coefficient of the capsule shells would be also useful to compare the retention of different core materials.

In this thesis hand mixing was used to investigate the survival of the microcapsules. The use of realistic mixing equipment for investigation of microcapsules' behaviour in cementitious composites, e.g. cement and concrete mixers, is proposed in future studies to assess suitability of applications. In order to better understand the effect of microcapsules on the hardened cementitious materials, microcapsules need to be tested in mortar and concrete.

The mechanical properties of the acrylates and microcapsules could be further characterised to map the key properties governing self-healing. Standardised protocols to determine the stress-strain behaviour of the acrylate shells would result in precise values of tensile strength. Furthermore, experiments to quantify the fracture toughness of the acrylate copolymers also need to be performed. It would also be interesting to quantify the interfacial bonding between the hydrophilic/ hydrophobic shells and the cementitious materials.

Moreover, the scaling down typical set-up used to asses self-healing performance would facilitate the use of microcapsules produced in smaller quantities. Thus the tests of compressive strength, transport properties and crack closure with a wide range of sizes, shell thicknesses and shell materials could be performed. Ideally, the mapping of physical triggering could be achieved, correlating the mechanical properties of the microcapsules with size and shell thickness.

In this research, the work was focused on promoting the physical triggering of the microcapsules. However, it would be interesting to use microfluidics to investigate also the chemical triggering, particularly because the material would require less fine tuning on mechanical properties. Thus, thick shells and higher elastic modulus could be investigated, potentially reducing the effect of the addition of microcapsules in the overall mechanical properties of the cementitious matrix.

On a broader perspective, the future directions of research also include advancing the dialogue with construction industry. Thus, it is necessary to answer questions regarding compromising structural

integrity and fire safety. The challenge of demonstrating the reduction in life-cycle costs and long term durability of the autonomic self-healing also need to be addressed. Although self-healing concrete is much more possible now than 20 years ago, there is still a long way to go.

The place where autonomic self-healing works undoubtedly, is an imagined place or state of things in which everything is perfect, defined as utopia. In the words of the poet Eduardo Galeano:

> *"Utopia is on the horizon. I move two steps closer; it moves two steps further away. I walk another ten steps and the horizon runs ten steps further away. As much as I may walk, I'll never reach it. So what's the point of utopia? The point is this: to keep walking."*

REFERENCES

Abate AR, Weitz DA (2011) Faster multiple emulsification with drop splitting. Lab Chip 11:1911. doi: 10.1039/c0lc00706d

Abbaspourrad A, Carroll NJ, Kim S-H, Weitz DA (2013a) Polymer Microcapsules with Programmable Active Release. J Am Chem Soc 135:7744–7750. doi: 10.1021/ja401960f

Abbaspourrad A, Duncanson WJ, Lebedeva N, et al (2013b) Microfluidic fabrication of stable gas-filled microcapsules for acoustic contrast enhancement. Langmuir 29:12352–7. doi: 10.1021/la402598p

Ahn T-H, Kim H, Ryou J-S (2016) New Surface-Treatment Technique of Concrete Structures Using Crack Repair Stick with Healing Ingredients. Materials (Basel) 9:654. doi: 10.3390/ma9080654

Ahn T-H, Kishi T (2010) Crack Self-healing Behavior of Cementitious Composites Incorporating Various Mineral Admixtures. J. Adv. Concr. Technol. 8:171–186.

Al-Ansari M, Abu-Taqa AG, Hassan MM, et al (2017) Performance of modified self-healing concrete with calcium nitrate microencapsulation. Constr Build Mater 149:525–534. doi: 10.1016/j.conbuildmat.2017.05.152

Alghamri R, Kanellopoulos A, Al-Tabbaa A (2016) Impregnation and encapsulation of lightweight aggregates for self-healing concrete. Constr Build Mater 124:910–921. doi: 10.1016/j.conbuildmat.2016.07.143

Allison SD (2008) Effect Of Structural Relaxation On The Preparation And Drug Release Behavior Of Poly(lactic-co-glycolic)acid Microparticle Drug Delivery Systems. J Pharm Sci 97:2022–2035. doi: 10.1002/jps.21124

Amstad E, Chemama M, Eggersdorfer M, et al (2016) Robust scalable high throughput production of monodisperse drops. Lab Chip 16:4163–4172. doi: 10.1039/C6LC01075J

Andrade B, Song Z, Li J, et al (2015) New frontiers for encapsulation in the chemical industry. ACS Appl Mater Interfaces 7:6359–68. doi: 10.1021/acsami.5b00484

Anna SL, Bontoux N, Stone HA (2003) Formation of dispersions using “flow focusing” in microchannels. Appl Phys Lett 82:364. doi: 10.1063/1.1537519

Anton Paar (2014) Indentation software manual R0.2.1 (July 14).

References

Araújo M, Van Vlierberghe S, Feiteira J, et al (2016) Cross-linkable polyethers as healing/sealing agents for self-healing of cementitious materials. Mater Des. doi: 10.1016/j.matdes.2016.03.005

Arce GA, Hassan MM, Mohammad LN, Rupnow T (2017) Characterization of Self-Healing Processes Induced by Calcium Nitrate Microcapsules in Cement Mortar. J Mater Civ Eng 29:4016189. doi: 10.1061/(ASCE)MT.1943-5533.0001717

Arriaga LR, Amstad E, Weitz DA (2015) Scalable single-step microfluidic production of single-core double emulsions with ultra-thin shells. Lab Chip. doi: 10.1039/c5lc00631g

Ashby M, Johnson K (2014) Materials and Design, Third Edit. Elsevier

Benita S (2006) Microencapsulation : methods and industrial applications. Taylor & Francis

Bertolini L, Elsener B, Pedeferri P, et al (2013) Chloride-Induced Corrosion. Corrosion of Steel in Concrete. Wiley-VCH Verlag GmbH & Co. KGaA, pp 93–112

Bill Gates (2014) Have You Hugged a Concrete Pillar Today? In: GatesNotes blog Bill Gates. https://www.gatesnotes.com/Books/Making-the-Modern-World. Accessed 16 Jun 2017

Blaiszik BJ, Kramer SLB, Olugebefola SC, et al (2010) Self-Healing Polymers and Composites. Annu Rev Mater Res 40:179–211. doi: 10.1146/annurev-matsci-070909-104532

Boh B, Boštjan Šumiga, Šumiga B (2008) Microencapsulation technology and its applications in building construction materials. RMZ - Mater Geoenvironment 55:329–344.

Brinson LC, Gates TS (1995) Effects of physical aging on long term creep of polymers and polymer matrix composites. Int J Solids Struct 32:827–846. doi: 10.1016/0020-7683(94)00163-Q

Broomfield JP (2007) Corrosion of steel in concrete : understanding, investigation and repair, 2nd editio. Taylor & Francis, Oxon

Brown EN, Kessler MR, Sottos NR, White SR (2003) *In situ* poly(urea-formaldehyde) microencapsulation of dicyclopentadiene. J Microencapsul 20:719–730. doi: 10.3109/02652040309178083

Cailleux E, Pollet V (2009) Investigations on the development of self-healing properties in protective coatings for concrete and repair mortars. 2nd International Conference on Self Healing Materials. Chicago,

Callister WD (2011) Materials Science and Engineering, 8th Editio.

Chen C-Y, Huang C-K, Lin S-P, et al (2008) Low-shrinkage visible-light-curable urethane-modified epoxy acrylate/SiO2 composites as dental restorative materials. Compos Sci Technol 68:2811–2817. doi: 10.1016/j.compscitech.2008.06.015

Chen P, Brignoli J, Studart AR (2014a) Mechanics of thick-shell microcapsules made by microfluidics. Polym (United Kingdom) 55:6837–6843. doi: 10.1016/j.polymer.2014.10.060

Chen PW, Cadisch G, Studart AR (2014b) Encapsulation of aliphatic amines using microfluidics. Langmuir 30:2346–50. doi: 10.1021/la500037d

Chen PW, Erb RM, Studart AR (2012) Designer polymer-based microcapsules made using microfluidics. Langmuir 28:144–52. doi: 10.1021/la203088u

Choi C-H, Lee H, Abbaspourrad A, et al (2016) Triple Emulsion Drops with An Ultrathin Water Layer: High Encapsulation Efficiency and Enhanced Cargo Retention in Microcapsules. Adv Mater 28:3340–3344. doi: 10.1002/adma.201505801

Choi C-H, Yi H, Hwang S, et al (2011) Microfluidic fabrication of complex-shaped microfibers by liquid template-aided multiphase microflow. Lab Chip 11:1477. doi: 10.1039/c0lc00711k

Comunian TA, Abbaspourrad A, Favaro-Trindade CS, Weitz DA (2014) Fabrication of solid lipid microcapsules containing ascorbic acid using a microfluidic technique. Food Chem 152:271–275. doi: 10.1016/j.foodchem.2013.11.149

Conchouso D, Castro D, Khan SA, Foulds IG (2014) Three-dimensional parallelization of microfluidic droplet generators for a litre per hour volume production of single emulsions. Lab Chip 14:3011. doi: 10.1039/C4LC00379A

Cowie J (Iain) MG, Arrighi V (2010) Physical Aging. In: Leszek A. Utracki, Alexander M. Jamieson (eds) Polymer Physics: From Suspensions to Nanocomposites and Beyond. John Wiley & Sons, Inc., Hoboken, NJ, USA, pp 357–389

Crow JM (2008) The concrete conundrum. Chem World 5:62–66.

Cubaud T, Mason TG (2008) Capillary threads and viscous droplets in square microchannels. Phys Fluids 20:53302. doi: 10.1063/1.2911716

Darvell BW (2009) Chapter 6 – Resin Restorative Materials. Materials Science for Dentistry. pp 128–162

Datta SS, Abbaspourrad A, Amstad E, et al (2014) 25th anniversary article: double emulsion

templated solid microcapsules: mechanics and controlled release. Adv Mater 26:2205–18. doi: 10.1002/adma.201305119

Datta SS, Kim S-H, Paulose J, et al (2012) Delayed Buckling and Guided Folding of Inhomogeneous Capsules. Phys Rev Lett 109:134302. doi: 10.1103/PhysRevLett.109.134302

de Rooij MR, Tittelboom K Van, De Belie N, Schlangen E (2013) Self-Healing Phenomena in Cement-Based Materials: State-of-the-Art Report of RILEM Technical Committee 221-SHC: Self-Healing Phenomena in Cement-Based Materials. Springer

Decker C, Nguyen Thi Viet T, Decker D, Weber-Koehl E (2001) UV-radiation curing of acrylate/epoxide systems. Polymer (Guildf) 42:5531–5541. doi: 10.1016/S0032-3861(01)00065-9

Dias MI, Ferreira ICFR, Barreiro MF (2015) Microencapsulation of bioactives for food applications. Food Funct 6:1035–1052. doi: 10.1039/C4FO01175A

Dolomite Centre Double Emulsion Chip (100µm etch depth), water-oil-water. http://www.dolomite-microfluidics.com/images/stories/PDFs/datasheets/double_emulsion_chip_product_datasheet.pdf. Accessed 26 Apr 2017a

Dolomite Centre Mitos Sensor Units. http://www.dolomite-microfluidics.com/images/stories/PDFs/datasheets/mitos_sensor_units_product_datasheet.pdf. Accessed 26 Apr 2017b

Dong B, Fang G, Ding W, et al (2016) Self-healing features in cementitious material with urea–formaldehyde/epoxy microcapsules. Constr Build Mater 106:608–617. doi: 10.1016/j.conbuildmat.2015.12.140

Dong B, Fang G, Wang Y, et al (2017) Performance recovery concerning the permeability of concrete by means of a microcapsule based self-healing system. Cem Concr Compos 78:84–96. doi: 10.1016/j.cemconcomp.2016.12.005

Dong B, Wang Y, Ding W, et al (2014a) Electrochemical impedance study on steel corrosion in the simulated concrete system with a novel self-healing microcapsule. Constr Build Mater 56:1–6. doi: 10.1016/j.conbuildmat.2014.01.070

Dong B, Wang Y, Fang G, et al (2014b) Smart releasing behavior of a chemical self-healing microcapsule in the stimulated concrete pore solution. Cem Concr Compos. doi:

10.1016/j.cemconcomp.2014.10.006

Dry C, McMillan W (1996) Three-part methylmethacrylate adhesive system as an internal delivery system for smart responsive concrete. IOP Publishing

Dry CM (2001) Design of self-growing, self-sensing, and self-repairing materials for engineering application. In: Wilson AR, Asanuma H (eds) Smart Materials. International Society for Optics and Photonics, pp 23–29

Duarte ARC, Ünal B, Mano JF, et al (2014) Microfluidic production of perfluorocarbon-alginate core-shell microparticles for ultrasound therapeutic applications. Langmuir 30:12391–9. doi: 10.1021/la502822v

Edvardsen C (1999) Water permeability and autogenous healing of cracks in concrete. ACI Mater J 96:448–454.

Eggersdorfer ML, Zheng W, Nawar S, et al (2017) Tandem emulsification for high-throughput production of double emulsions. Lab Chip 17:936–942. doi: 10.1039/C6LC01553K

Emmons PH, Sordyl DJ (2006) The State of the Concrete Repair Industry, and a Vision for its Future. Concr Repair Bull 7–14.

Erb RM, Obrist D, Chen PW, et al (2011) Predicting sizes of droplets made by microfluidic flow-induced dripping. Soft Matter 7:8757. doi: 10.1039/c1sm06231j

Esser-Kahn AP, Odom SA, Sottos NR, et al (2011) Triggered Release from Polymer Capsules. Macromolecules 44:5539–5553. doi: 10.1021/ma201014n

Fan C, Tang J, Zhou X (2013) Role of ammonium chloride in preparing poly(urea-formaldehyde) microcapsules using one-step method. J Appl Polym Sci 129:2848–2856. doi: 10.1002/app.39008

Fan S, Li M (2015) X-ray computed microtomography of three-dimensional microcracks and self-healing in engineered cementitious composites. Smart Mater Struct 24:15021. doi: 10.1088/0964-1726/24/1/015021

Feiteira J, Gruyaert E, De Belie N (2016) Self-healing of moving cracks in concrete by means of encapsulated polymer precursors. Constr Build Mater 102:671–678. doi: 10.1016/j.conbuildmat.2015.10.192

Formia A, Irico S, Bertola F, et al (2016) Experimental analysis of self-healing cement-based

materials incorporating extruded cementitious hollow tubes. J Intell Mater Syst Struct 27:2633–2652. doi: 10.1177/1045389X16635847

Formia A, Terranova S, Antonaci P, et al (2015) Setup of Extruded Cementitious Hollow Tubes as Containing/Releasing Devices in Self-Healing Systems. Materials (Basel) 8:1897–1923. doi: 10.3390/ma8041897

Fox TG, Flory PJ (1954) The glass temperature and related properties of polystyrene. Influence of molecular weight. J Polym Sci 14:315–319. doi: 10.1002/pol.1954.120147514

Freyermuth CL (2001) Life-Cycle Cost Analysis for Large Bridges. Concr Int 23:89–95.

Fu Z, Su L, Li J, et al (2014) Elastic silicone encapsulation of n-hexadecyl bromide by microfluidic approach as novel microencapsulated phase change materials. Thermochim Acta 590:24–29. doi: 10.1016/j.tca.2014.06.008

García Calvo JL, Pérez G, Carballosa P, et al (2017) Development of ultra-high performance concretes with self-healing micro/nano-additions. Constr Build Mater 138:306–315. doi: 10.1016/j.conbuildmat.2017.02.015

Ghorbanzadeh Ahangari M, Fereidoon A, Jahanshahi M, Sharifi N (2014) Effect of nanoparticles on the micromechanical and surface properties of poly(urea–formaldehyde) composite microcapsules. Compos Part B Eng 56:450–455. doi: 10.1016/j.compositesb.2013.08.071

Ghosh SK (2006) Functional Coatings and Microencapsulation: A General Perspective. Functional Coatings. Wiley-VCH Verlag GmbH & Co. KGaA, Weinheim, FRG, pp 1–28

Giannaros P (2017) Laboratory and field investigation of performance of novel microcapsule-based self-healing concrete. University of Cambridge

Giannaros P, Kanellopoulos A, Al-Tabbaa A (2016) Sealing of cracks in cement using microencapsulated sodium silicate. Smart Mater Struct 25:84005. doi: 10.1088/0964-1726/25/8/084005

Gilabert FA, Garoz D, Paepegem W Van (2017a) Macro- and micro-modeling of crack propagation in encapsulation-based self-healing materials: application of XFEM and cohesive surface techniques. Mater Des. doi: 10.1016/j.matdes.2017.05.050

Gilabert FA, Garoz D, Van Paepegem W (2014) Stress concentrations and bonding strength in encapsulation-based self-healing materials. Mater Des. doi: 10.1016/j.matdes.2014.11.012

Gilabert FA, Van Tittelboom K, Tsangouri E, et al (2017b) Determination of strength and debonding energy of a glass-concrete interface for encapsulation-based self-healing concrete. Cem Concr Compos 79:76–93. doi: 10.1016/j.cemconcomp.2017.01.011

Gouin S (2004) Microencapsulation: industrial appraisal of existing technologies and trends. Trends Food Sci Technol 15:330–347. doi: 10.1016/j.tifs.2003.10.005

Grolman JM, Inci B, Moore JS (2015) PH-dependent switchable permeability from core-shell microcapsules. ACS Macro Lett 4:441–445. doi: 10.1021/acsmacrolett.5b00194

Gruyaert E, Van Tittelboom K, Sucaet J, et al (2016) Capsules with evolving brittleness to resist the preparation of self-healing concrete. Mater Construcción 66:e092. doi: 10.3989/mc.2016.07115

H. C. Miller (1989) Urethane Acrylates: Expansion of Radiation Curable Epoxy Acrylate Coatings. Radtech '89-Europe.

Halvaei M, Jamshidi M, Latifi M (2014) Investigation on pullout behavior of different polymeric fibers from fine aggregates concrete. J Ind Text 45:995–1008. doi: 10.1177/1528083714551437

Hassan MM, Milla J, Rupnow T, et al (2016) Microencapsulation of Calcium Nitrate for Concrete Applications. Transp Res Rec J Transp Res Board 2577:8–16. doi: 10.3141/2577-02

Hay JN (1995) The physical ageing of amorphous and crystalline polymers. Pure Appl Chem 67:1855–1858.

He F, Wang W, He X-H, et al (2016) Controllable Multi-Compartmental Capsules with Distinct Cores and Shells for Synergistic Release. ACS Appl Mater Interfaces. doi: 10.1021/acsami.6b01278

Heath HB (1981) Source book of flavors. Van Nostrand Reihnold

Hennequin Y, Pannacci N, de Torres CP, et al (2009) Synthesizing microcapsules with controlled geometrical and mechanical properties with microfluidic double emulsion technology. Langmuir 25:7857–61. doi: 10.1021/la9004449

Hernández-Cruz D, Hargis CW, Bae S, et al (2014) Multiscale characterization of chemical–mechanical interactions between polymer fibers and cementitious matrix. Cem Concr Compos 48:9–18.

Hilloulin B, Van Tittelboom K, Gruyaert E, et al (2015) Design of polymeric capsules for self-healing

concrete. Cem Concr Compos 55:298–307. doi: 10.1016/j.cemconcomp.2014.09.022

Hodge IM (1995) Physical Aging in Polymer Glasses.

Huang H, Ye G, Damidot D (2014a) Effect of blast furnace slag on self-healing of microcracks in cementitious materials. Cem Concr Res 60:68–82. doi: 10.1016/j.cemconres.2014.03.010

Huang H, Ye G, Qian C, Schlangen E (2016) Self-healing in cementitious materials: Materials, methods and service conditions. Mater Des 92:499–511. doi: 10.1016/j.matdes.2015.12.091

Huang H, Ye G, Shui Z (2014b) Feasibility of self-healing in cementitious materials – By using capsules or a vascular system? Constr Build Mater 63:108–118. doi: 10.1016/j.conbuildmat.2014.04.028

Huang M, Yang J (2011) Facile microencapsulation of HDI for self-healing anticorrosion coatings. J Mater Chem 21:11123. doi: 10.1039/c1jm10794a

Humphreys K, Mahasenan M (2002) Toward a Sustainable Cement Industry Substudy 8: Climate Change.

Hutchinson JM (1995) Physical aging of polymers. Prog Polym Sci 20:703–760. doi: 10.1016/0079-6700(94)00001-I

Iveson SM, Litster JD, Hapgood K, Ennis BJ (2001) Nucleation, growth and breakage phenomena in agitated wet granulation processes: a review. Powder Technol 117:3–39. doi: 10.1016/S0032-5910(01)00313-8

Janssen D (2011) Water encapsulation to initiate self-healing in cementitious materials. Delft University of Technology

Jefferson A, Joseph C, Lark R, et al (2010) A new system for crack closure of cementitious materials using shrinkable polymers. Cem Concr Res 40:795–801. doi: 10.1016/j.cemconres.2010.01.004

Jeong H-H, Yelleswarapu VR, Yadavali S, et al (2015) Kilo-scale droplet generation in three-dimensional monolithic elastomer device (3D MED). Lab Chip 15:4387–4392. doi: 10.1039/C5LC01025J

Jeong W, Kim J, Kim S, et al (2004) Hydrodynamic microfabrication via “on the fly” photopolymerization of microscale fibers and tubes. Lab Chip 4:576–580. doi: 10.1039/B411249K

Ji L, Chang W, Cui M, Nie J (2013) Photopolymerization kinetics and volume shrinkage of 1,6-hexanediol diacrylate at different temperature. J Photochem Photobiol A Chem 252:216–221. doi: 10.1016/j.jphotochem.2012.12.010

Jian-ping Wang, Xiao-peng Zhao *, Hui-lin Guo and, Zheng Q (2004) Preparation of Microcapsules Containing Two-Phase Core Materials. doi: 10.1021/LA0490902

Jiang Z, Li W, Yuan Z (2015) Influence of mineral additives and environmental conditions on the self-healing capabilities of cementitious materials. Cem Concr Compos 57:116–127. doi: 10.1016/j.cemconcomp.2014.11.014

Kanellopoulos A, Giannaros P, Al-Tabbaa A (2016) The effect of varying volume fraction of microcapsules on fresh, mechanical and self-healing properties of mortars. Constr Build Mater 122:577–593. doi: 10.1016/j.conbuildmat.2016.06.119

Kanellopoulos A, Giannaros P, Palmer D, et al (2017) Polymeric microcapsules with switchable mechanical properties for self-healing concrete: synthesis, characterisation and proof of concept. Smart Mater Struct 26:45025. doi: 10.1088/1361-665X/aa516c

Kanellopoulos A, Qureshi TS, Al-Tabbaa A (2015) Glass encapsulated minerals for self-healing in cement based composites. Constr Build Mater 98:780–791. doi: 10.1016/j.conbuildmat.2015.08.127

Karsa DR (ed) (1999) Design and Selection of Performance Surfactants. Sheffield Academic Press, Sheffield

Keller MW, Sottos NR (2006) Mechanical Properties of Microcapsules Used in a Self-Healing Polymer. Exp Mech 46:725–733. doi: 10.1007/s11340-006-9659-3

Kim S-H, Jeon S-J, Yang S-M (2008) Optofluidic encapsulation of crystalline colloidal arrays into spherical membrane. J Am Chem Soc 130:6040–6. doi: 10.1021/ja800844w

Kim S-H, Kim JW, Cho J-C, Weitz DA (2011) Double-emulsion drops with ultra-thin shells for capsule templates. Lab Chip 11:3162–6. doi: 10.1039/c1lc20434c

Kim S-H, Lee TY, Lee SS (2014a) Osmocapsules for direct measurement of osmotic strength. Small 10:1155–62. doi: 10.1002/smll.201302296

Kim S-H, Park J-G, Choi TM, et al (2014b) Osmotic-pressure-controlled concentration of colloidal particles in thin-shelled capsules. Nat Commun 5:3068. doi: 10.1038/ncomms4068

Klatter L, Vrouwenvelder T, van Noortwijk JM (2009) Societal and reliability aspects of bridge management in the Netherlands. Struct Infrastruct Eng 5:11–24. doi: 10.1080/15732470701322743

Koch GH, Brongers M, Thompson NG, et al (2002) Corrosion cost and preventive strategies in the United States.

Kumacheva E, Garstecki P (2011) Microfluidic Reactors for Polymer Particles. Microfluidic Reactors for Polymer Particles. John Wiley & Sons, Ltd, Chichester, UK, pp 41–94

Kumar VR, Bhuvaneshwari B, Maheswaran S, et al (2011) An overview of techniques based on biomimetics for sustainable development of concrete.

Lark R, Joseph C, Isaacs B, et al (2010) Experimental investigation of adhesive-based self-healing of cementitious materials. Mag Concr Res 62:831–843. doi: 10.1680/macr.2010.62.11.831

Leal-Calderon F, Bibette J, Schmitt V (2007) Emulsification. In: Leal-Calderon F, Bibette J, Schmitt V (eds) Emulsion Science: Basic Principles. Springer New York, New York, NY, pp 5–51

Lee H, Choi C-H, Abbaspourrad A, et al (2016a) Fluorocarbon Oil Reinforced Triple Emulsion Drops. Adv Mater. doi: 10.1002/adma.201602804

Lee H, Choi C-H, Abbaspourrad A, et al (2016b) Encapsulation and Enhanced Retention of Fragrance in Polymer Microcapsules. ACS Appl Mater Interfaces 8:4007–4013. doi: 10.1021/acsami.5b11351

Lee J, Zhang M, Bhattacharyya D, et al (2012) Micromechanical behavior of self-healing epoxy and hardener-loaded microcapsules by nanoindentation. Mater Lett 76:62–65. doi: 10.1016/j.matlet.2012.02.052

Lee SS, Abbaspourrad A, Kim S-H (2014) Nonspherical Double Emulsions with Multiple Distinct Cores Enveloped by Ultrathin Shells. ACS Appl Mater Interfaces 6:1294–1300. doi: 10.1021/am405283j

Lee TY, Choi TM, Shim TS, et al (2016c) Microfluidic production of multiple emulsions and functional microcapsules. Lab Chip 16:3415–3440. doi: 10.1039/C6LC00809G

Lee Y-S, Ryou J-S (2014) Self healing behavior for crack closing of expansive agent via granulation/film coating method. Constr Build Mater 71:188–193. doi: 10.1016/j.conbuildmat.2014.08.045

Lee Y-S, Ryou J-S (2016) Crack Healing Performance of PVA-Coated Granules Made of Cement, CSA, and Na2CO3 in the Cement Matrix. Materials (Basel) 9:555. doi: 10.3390/ma9070555

Li V, Wu C, Wang S, et al (2002) Interface tailoring for strain-hardening polyvinyl alcohol-engineered cementitious composite (PVA-ECC). ACI Mater J 463–472.

Li VC, Yang E-H (2007) Self Healing in Concrete Materials. In: Sybrand van der Zwaag (ed) Self Healing Materials. Springer Netherlands, pp 161–193

Li W, Jiang Z, Yang Z, et al (2013) Self-healing efficiency of cementitious materials containing microcapsules filled with healing adhesive: mechanical restoration and healing process monitored by water absorption. PLoS One 8:e81616. doi: 10.1371/journal.pone.0081616

Li W, Jiang Z, Yang Z, Yu H (2016a) Effective mechanical properties of self-healing cement matrices with microcapsules. Mater Des 95:422–430. doi: 10.1016/j.matdes.2016.01.124

Li W, Zhu X, Zhao N, Jiang Z (2016b) Preparation and Properties of Melamine Urea-Formaldehyde Microcapsules for Self-Healing of Cementitious Materials. Materials (Basel) 9:152. doi: 10.3390/ma9030152

Liang W-G, Yang C, Wen G-Q, et al (2014) A facile and controllable method to encapsulate phase change materials with non-toxic and biocompatible chemicals. Appl Therm Eng 70:817–826. doi: 10.1016/j.applthermaleng.2014.06.006

Ligon SC, Husár B, Wutzel H, et al (2014) Strategies to Reduce Oxygen Inhibition in Photoinduced Polymerization. Chem Rev 114:557–589. doi: 10.1021/cr3005197

Lin SB, Tsay SY, Speckhard TA, et al (1984) Properties of UV-cured polyurethane acrylates: effect of polyol type and molecular weight. Chem Eng Commun 30:251–273. doi: 10.1080/00986448408911131

Litina C, Kanellopoulos A, Al-Tabbaa A (2014) Alternative repair system for concrete using microencapsulated healing agents. Concr. Solut. 97–103.

Liu S, Deng R, Li W, Zhu J (2012) Polymer Microparticles with Controllable Surface Textures Generated through Interfacial Instabilities of Emulsion Droplets. Adv Funct Mater 22:1692–1697. doi: 10.1002/adfm.201103018

Liu X, Le JK, Kessler MR (2011) Microencapsulation of self-healing agents with melamine-urea-formaldehyde by the Shirasu porous glass (SPG) emulsification technique. Macromol Res 19:1056–1061. doi: 10.1007/s13233-011-1009-3

Lv L, Schlangen E, Yang Z, Xing F (2016a) Micromechanical Properties of a New Polymeric Microcapsule for Self-Healing Cementitious Materials. Materials (Basel) 9:1025. doi: 10.3390/ma9121025

Lv L, Yang Z, Chen G, et al (2016b) Synthesis and characterization of a new polymeric microcapsule and feasibility investigation in self-healing cementitious materials. Constr Build Mater 105:487–495. doi: 10.1016/j.conbuildmat.2015.12.185

Maes M, Van Tittelboom K, De Belie N (2014) The efficiency of self-healing cementitious materials by means of encapsulated polyurethane in chloride containing environments. Constr Build Mater 71:528–537. doi: 10.1016/j.conbuildmat.2014.08.053

Mark HF (2007) Encyclopedia of Polymer Science and Technology, Concise, 3rd editio. Wiley Subscription Services, Inc., A Wiley Company

Martins IM, Barreiro MF, Coelho M, Rodrigues AE (2014) Microencapsulation of essential oils with biodegradable polymeric carriers for cosmetic applications. Chem Eng J 245:191–200. doi: 10.1016/j.cej.2014.02.024

Mehta KP (2001) Reducing the Environmental Impact of Concrete. Concr. Int. 23:61–66.

Meyer C (2009) The greening of the concrete industry. Cem Concr Compos 31:601–605. doi: 10.1016/j.cemconcomp.2008.12.010

Mignon A, Snoeck D, Dubruel P, et al (2017) Crack Mitigation in Concrete: Superabsorbent Polymers as Key to Success? Materials (Basel) 10:237. doi: 10.3390/ma10030237

Milla J, Hassan MM, Rupnow T, et al (2016) Effect of Self-Healing Calcium Nitrate Microcapsules on Concrete Properties. Transp Res Rec J Transp Res Board 2577:69–77. doi: 10.3141/2577-09

Mindess S (1987) Bonding in cementitious composites: How important is it? Symp. on Cement Based Composites, Materials Research Society. pp 3–10

Miwon Specialty Chemical Co. The Solution in Energy Curing. http://www.miramer.com/bbs/E-Brochure.pdf. Accessed 17 May 2017

Mora-Huertas CE, Fessi H, Elaissari A (2010) Polymer-based nanocapsules for drug delivery. Int J Pharm 385:113–42. doi: 10.1016/j.ijpharm.2009.10.018

Muhammad NZ, Shafaghat A, Keyvanfar A, et al (2016) Tests and methods of evaluating the self-healing efficiency of concrete: A review. Constr Build Mater 112:1123–1132. doi:

10.1016/j.conbuildmat.2016.03.017

Müller N, Harnisch J (2007) How to Turn Around the Trend of Cement Related Emissions in the Developing World.

Nabavi SA, Vladisavljević GT, Gu S, Manović V (2016) Semipermeable Elastic Microcapsules for Gas Capture and Sensing. Langmuir 32:9826–9835. doi: 10.1021/acs.langmuir.6b02420

NACE International Corrosion Costs and Preventive Strategies In the United States. https://www.nace.org/uploadedFiles/Publications/ccsupp.pdf. Accessed 16 Jun 2017

Nam J-O, Kim J, Jin SH, et al (2016) Microfluidic preparation of a highly active and stable catalyst by high performance of encapsulation of polyvinylpyrrolidone (PVP)-Pt nanoparticles in microcapsules. J Colloid Interface Sci 464:246–253. doi: 10.1016/j.jcis.2015.11.037

Neubauer MP, Poehlmann M, Fery A (2014) Microcapsule mechanics: from stability to function. Adv Colloid Interface Sci 207:65–80. doi: 10.1016/j.cis.2013.11.016

Nicholson JW (2006) Chemistry of Polymers (3rd Edition).

Nie Z, Xu S, Seo M, et al (2005) Polymer particles with various shapes and morphologies produced in continuous microfluidic reactors. J Am Chem Soc 127:8058–63. doi: 10.1021/ja042494w

Nisisako T, Ando T, Hatsuzawa T (2014) Capillary-Assisted Fabrication of Biconcave Polymeric Microlenses from Microfluidic Ternary Emulsion Droplets. Small 10:n/a-n/a. doi: 10.1002/smll.201401269

Nisisako T, Torii T (2008) Microfluidic large-scale integration on a chip for mass production of monodisperse droplets and particles. Lab Chip 8:287–293. doi: 10.1039/B713141K

Nisisako T, Torii T, Higuchi T (2004) Novel microreactors for functional polymer beads. Chem Eng J 101:23–29. doi: 10.1016/j.cej.2003.11.019

Nisisako T, Torii T, Takahashi T, Takizawa Y (2006) Synthesis of Monodisperse Bicolored Janus Particles with Electrical Anisotropy Using a Microfluidic Co-Flow System. Adv Mater 18:1152–1156. doi: 10.1002/adma.200502431

Nunes JK, Tsai SSH, Wan J, Stone HA (2013) Dripping and jetting in microfluidic multiphase flows applied to particle and fiber synthesis. J Phys D Appl Phys 46:114002. doi: 10.1088/0022-3727/46/11/114002

Office for National Statistics (2016) Construction Statistics Annual Tables.

https://www.ons.gov.uk/businessindustryandtrade/constructionindustry/datasets/constructionstatisticsannualtables. Accessed 16 Jun 2017

Okushima S, Nisisako T, Torii T, Higuchi T (2004) Controlled production of monodisperse double emulsions by two-step droplet breakup in microfluidic devices. Langmuir 20:9905–8. doi: 10.1021/la0480336

Oliver WC, Pharr GM (1992) An improved technique for determining hardness and elastic modulus using load and displacement sensing indentation experiments. J Mater Res 7:1564–1583. doi: 10.1557/JMR.1992.1564

Oxley JD (2012) Coextrusion for food ingredients and nutraceutical encapsulation: Principles and technology. Encapsulation Technologies and Delivery Systems for Food Ingredients and Nutraceuticals. Elsevier Ltd, pp 131–150

Pakravan HR, Jamshidi M, Latifi M, Pacheco-Torgal F (2012) Evaluation of adhesion in polymeric fibre reinforced cementitious composites. Int J Adhes Adhes 32:53–60. doi: 10.1016/j.ijadhadh.2011.08.009

Palin D, Wiktor V, Jonkers HM (2016) A bacteria-based bead for possible self- healing marine concrete applications. Smart Mater Struct 25:84008–84013(6).

Pareek S, Shrestha KC, Suzuki Y, et al (2014) Feasibility of externally activated self-repairing concrete with epoxy injection network and Cu-Al-Mn superelastic alloy reinforcing bars. Smart Mater Struct 23:105027. doi: 10.1088/0964-1726/23/10/105027

Patil P, Chavanke D, Wagh M (2012) A Review On Ionotropic Gelation Method : Novel Approach for controlled Gastroretentive Gelispheres.

PCI (2000) The Use Of Specialty Acrylic Esters In Cure-In-Place Coating Technology. http://www.pcimag.com/articles/85843-the-use-of-specialty-acrylic-esters-in-cure-in-place-coating-technology. Accessed 18 May 2017

Peled A, Zaguri E, Marom G (2008) Bonding characteristics of multifilament polymer yarns and cement matrices. Compos Part A Appl Sci Manuf 39:930–939. doi: 10.1016/j.compositesa.2008.03.012

Pelletier MM, Brown R, Shukla A, Bose A (2011) Self-healing concrete with a microencapsulated healing agent. http://energetics.chm.uri.edu/system/files/Self healing concrete -7-11.pdf. Accessed 27 Jan 2017

Perez G, Erkizia E, Gaitero JJ, et al (2015a) Synthesis and characterization of epoxy encapsulating silica microcapsules and amine functionalized silica nanoparticles for development of an innovative self-healing concrete. Mater Chem Phys 165:39–48. doi: 10.1016/j.matchemphys.2015.08.047

Perez G, Gaitero JJJ, Erkizia E, et al (2015b) Characterisation of cement pastes with innovative self-healing system based in epoxy-amine adhesive. Cem Concr Compos 60:55–64. doi: 10.1016/j.cemconcomp.2015.03.010

Phillips AJ, Cunningham AB, Gerlach R, et al (2016) Fracture Sealing with Microbially-Induced Calcium Carbonate Precipitation: A Field Study. Environ Sci Technol. doi: 10.1021/acs.est.5b05559

Polenz I, Datta SS, Weitz DA (2014) Controlling the Morphology of Polyurea Microcapsules Using Microfluidics. Langmuir. doi: 10.1021/la503234z

Ponnusami SA, Turteltaub S, Zwaag S Van Der, van der Zwaag S (2015) Cohesive-zone modelling of crack nucleation and propagation in particulate composites. Eng Fract Mech 149:1–25. doi: 10.1016/j.engfracmech.2015.09.050

Qian S, Zhou J, de Rooij MR, et al (2009) Self-healing behavior of strain hardening cementitious composites incorporating local waste materials. Cem Concr Compos 31:613–621. doi: 10.1016/j.cemconcomp.2009.03.003

Qureshi TS, Al-Tabbaa A (2016) Self-healing of drying shrinkage cracks in cement-based materials incorporating reactive MgO. Smart Mater Struct 25:84004. doi: 10.1088/0964-1726/25/8/084004

Qureshi TS, Kanellopoulos A, Al-Tabbaa A (2016) Encapsulation of expansive powder minerals within a concentric glass capsule system for self-healing concrete. Constr Build Mater 121:629–643. doi: 10.1016/j.conbuildmat.2016.06.030

Rawat A, Burgess DJ (2011) Effect of physical ageing on the performance of dexamethasone loaded PLGA microspheres. Int J Pharm 415:164–168. doi: 10.1016/j.ijpharm.2011.05.067

Reinhardt HW, Jonkers H, Tittelboom K Van, et al (2013) Recovery against environmental action. Self-healing phenomena in cement-based materials. Springer, pp 65–117

Ren P-W, Ju X-J, Xie R, Chu L-Y (2010) Monodisperse alginate microcapsules with oil core generated from a microfluidic device. J Colloid Interface Sci 343:392–5. doi: 10.1016/j.jcis.2009.11.007

Roig-Flores M, Moscato S, Serna P, Ferrara L (2015) Self-healing capability of concrete with crystalline admixtures in different environments. Constr Build Mater 86:1–11. doi: 10.1016/j.conbuildmat.2015.03.091

Roig-Flores M, Pirritano F, Serna P, Ferrara L (2016) Effect of crystalline admixtures on the self-healing capability of early-age concrete studied by means of permeability and crack closing tests. Constr Build Mater 114:447–457. doi: 10.1016/j.conbuildmat.2016.03.196

Romanowsky MB, Abate AR, Rotem A, et al (2012) High throughput production of single core double emulsions in a parallelized microfluidic device. Lab Chip 12:802–7. doi: 10.1039/c2lc21033a

Rouse JJ, Mohamed F, van der Walle CF (2007) Physical ageing and thermal analysis of PLGA microspheres encapsulating protein or DNA. Int J Pharm 339:112–120. doi: 10.1016/j.ijpharm.2007.02.026

Saeki D, Sugiura S, Kanamori T, et al (2010) Microfluidic preparation of water-in-oil-in-water emulsions with an ultra-thin oil phase layer. Lab Chip 10:357–362. doi: 10.1039/B916318B

Sahmaran M, Yildirim G, Erdem TK (2013) Self-healing capability of cementitious composites incorporating different supplementary cementitious materials. Cem Concr Compos 35:89–101. doi: 10.1016/j.cemconcomp.2012.08.013

Saihi D, Vroman I, Giraud S, Bourbigot S (2006) Microencapsulation of ammonium phosphate with a polyurethane shell. Part II. Interfacial polymerization technique. React Funct Polym 66:1118–1125. doi: 10.1016/j.reactfunctpolym.2006.02.001

Sandner B, Baudach S, Davy KWM, et al (1997) Synthesis of BISGMA derivatives, properties of their polymers and composites. J Mater Sci Mater Med 8:39–44. doi: 10.1023/A:1018590229166

Segurola J, Allen N, Edge M, Roberts I (1999) Photochemistry and photoinduced chemical crosslinking activity of acrylated prepolymers by several commercial type I far UV photoinitiators. Polym Degrad Stab 65:153–160. doi: 10.1016/S0141-3910(99)00003-8

Seiffert S (2013) Small but Smart: Sensitive Microgel Capsules. Angew Chemie Int Ed 52:11462–11468. doi: 10.1002/anie.201303055

Shang L, Cheng Y, Wang J, et al (2016) Osmotic pressure-triggered cavitation in microcapsules. Lab Chip 16:251–255. doi: 10.1039/C5LC01286D

Shannaq R Al, Farid MM (2015) Microencapsulation of phase change materials (PCM) for thermal

energy storage systems. Advances in Thermal Energy Storage Systems: Methods and Applications. p 247

Silva BFB, Rodríguez-Abreu C, Vilanova N (2016) Recent advances in multiple emulsions and their application as templates. Curr Opin Colloid Interface Sci 25:98–108. doi: 10.1016/j.cocis.2016.07.006

Sisomphon K, Copuroglu O, Fraaij A (2011) Application of encapsulated lightweight aggregate impregnated with sodium monofluorophosphate as a self-healing agent in blast furnace slag mortar. Heron 56:13–32.

Sisomphon K, Copuroglu O, Koenders EAB (2012) Self-healing of surface cracks in mortars with expansive additive and crystalline additive. Cem Concr Compos 34:566–574. doi: 10.1016/j.cemconcomp.2012.01.005

Snoeck D, Dewanckele J, Cnudde V, De Belie N (2015) X-ray computed microtomography to study autogenous healing of cementitious materials promoted by superabsorbent polymers. Cem Concr Compos. doi: 10.1016/j.cemconcomp.2015.10.016

Snoeck D, Steuperaert S, Van Tittelboom K, et al (2012) Visualization of water penetration in cementitious materials with superabsorbent polymers by means of neutron radiography. Cem Concr Res 42:1113–1121. doi: 10.1016/j.cemconres.2012.05.005

Snoeck D, Van Tittelboom K, Steuperaert S, et al (2014) Self-healing cementitious materials by the combination of microfibres and superabsorbent polymers. J Intell Mater Syst Struct 25:13–24. doi: 10.1177/1045389X12438623

Soens H, De Belie N, Wang J, Durka M (2014) Microcapsules and concrete containing the same.

Squires TM, Quake SR (2005) Microfluidics: Fluid physics at the nanoliter scale. Rev Mod Phys 77:977–1026. doi: 10.1103/RevModPhys.77.977

Su J-F, Qiu J, Schlangen E, Wang Y-Y (2015) Investigation the possibility of a new approach of using microcapsules containing waste cooking oil: In situ rejuvenation for aged bitumen. Constr Build Mater 74:83–92. doi: 10.1016/j.conbuildmat.2014.10.018

Su J-F, Schlangen E, Qiu J (2013) Design and construction of microcapsules containing rejuvenator for asphalt. Powder Technol 235:563–571. doi: 10.1016/j.powtec.2012.11.013

Tan NPB, Keung LH, Choi WH, et al (2016) Silica-based self-healing microcapsules for self-repair in concrete. J Appl Polym Sci 133:43090. doi: 10.1002/app.43090

Tong X-M, Zhang T, Yang M-Z, Zhang Q (2010) Preparation and characterization of novel melamine modified poly(urea–formaldehyde) self-repairing microcapsules. Colloids Surfaces A Physicochem Eng Asp 371:91–97. doi: 10.1016/j.colsurfa.2010.09.009

Trenkel ME (1997) Controlled-Release and Stabilized Fertilizers in Agriculture. Paris

Tziviloglou E, Tittelboom K Van, Palin D, et al (2016) Bio-Based Self-Healing Concrete: From Research to Field Application. 1–41. doi: 10.1007/12_2015_332

U.S. Geological Survey (2017) Mineral commodity summaries 2017: U.S. Geological Survey.

UNCTAD Infrastructure Report UN (2001) Infrastructure as an agent for economic development.

Utada A, Fernandez-Nieves A, Stone H, Weitz D (2007) Dripping to Jetting Transitions in Coflowing Liquid Streams. Phys Rev Lett 99:94502. doi: 10.1103/PhysRevLett.99.094502

Utada AS, Lorenceau E, Link DR, et al (2005) Monodisperse double emulsions generated from a microcapillary device. Science 308:537–41. doi: 10.1126/science.1109164

van Breugel K (2007) Is there a market for self-healing cement based materials? Proceedings of the First International Conference on Self Healing Materials. Noordwijk aan Zee, The Netherlands,

van der Zwaag S (2007) An Introduction to Material Design Principles: Damage Prevention versus Damage Management. In: Zwaag S van der (ed) Self-Healing Materials. pp 1–18

Van Tittelboom K, De Belie N (2013) Self-Healing in Cementitious Materials—A Review. Materials (Basel) 6:2182–2217. doi: 10.3390/ma6062182

Van Tittelboom K, De Belie N, Lehmann F, Grosse CU (2012) Acoustic emission analysis for the quantification of autonomous crack healing in concrete. Constr Build Mater 28:333–341. doi: 10.1016/j.conbuildmat.2011.08.079

Van Tittelboom K, De Belie N, Van Loo D, Jacobs P (2011) Self-healing efficiency of cementitious materials containing tubular capsules filled with healing agent. Cem Concr Compos 33:497–505. doi: 10.1016/j.cemconcomp.2011.01.004

Van Tittelboom K, Tsangouri E, Hemelrijck D Van, Belie N De (2014) The efficiency of self-healing concrete using alternative manufacturing procedures and more realistic crack patterns. Cem Concr Compos. doi: 10.1016/j.cemconcomp.2014.12.002

Van Tittelboom K, Wang J, Araújo M, et al (2016) Comparison of different approaches for self-healing concrete in a large-scale lab test. Constr Build Mater 107:125–137. doi:

10.1016/j.conbuildmat.2015.12.186

Vericella JJ, Baker SE, Stolaroff JK, et al (2015) Encapsulated liquid sorbents for carbon dioxide capture. Nat Commun 6:6124. doi: 10.1038/ncomms7124

Vilanova N, Rodríguez-Abreu C, Fernández-Nieves A, Solans C (2013) Fabrication of novel silicone capsules with tunable mechanical properties by microfluidic techniques. ACS Appl Mater Interfaces 5:5247–52. doi: 10.1021/am4010896

Wang J-Y, Jin Y, Xie R, et al (2011) Novel calcium-alginate capsules with aqueous core and thermo-responsive membrane. J Colloid Interface Sci 353:61–68. doi: 10.1016/j.jcis.2010.09.034

Wang J, Van Tittelboom K, De Belie N, Verstraete W (2012) Use of silica gel or polyurethane immobilized bacteria for self-healing concrete. Constr Build Mater 26:532–540.

Wang JY, Soens H, Verstraete W, De Belie N (2014) Self-healing concrete by use of microencapsulated bacterial spores. Cem Concr Res 56:139–152. doi: 10.1016/j.cemconres.2013.11.009

Wang R, Tian Q, Zhang S, et al (2016) Improving efficiency of calcium oxide expansive additives by polylactic acid film. Mag Concr Res 68:1070–1078. doi: 10.1680/jmacr.15.00529

Wang X, Sun P, Han N, Xing F (2017) Experimental Study on Mechanical Properties and Porosity of Organic Microcapsules Based Self-Healing Cementitious Composite. Materials (Basel) 10:20. doi: 10.3390/ma10010020

Wang X, Xing F, Zhang M, et al (2013) Experimental Study on Cementitious Composites Embedded with Organic Microcapsules. Materials (Basel) 6:4064–4081. doi: 10.3390/ma6094064

Wang Y, Fang G, Ding W, et al (2015) Self-immunity microcapsules for corrosion protection of steel bar in reinforced concrete. Sci Rep 5:18484. doi: 10.1038/srep18484

White SR, Moore JS, Sottos NR, et al (2014) Restoration of large damage volumes in polymers. Science 344:620–3. doi: 10.1126/science.1251135

White SR, Sottos NR, Geubelle PH, et al (2001) Autonomic healing of polymer composites. Nature 409:794–7. doi: 10.1038/35057232

Wiktor V, Jonkers HM (2015) Field performance of bacteria-based repair system: Pilot study in a parking garage. Case Stud Constr Mater 2:11–17. doi: 10.1016/j.cscm.2014.12.004

Wiktor V, Jonkers HM (2016) Bacteria-based concrete: from concept to market. Smart Mater Struct

25:84006. doi: 10.1088/0964-1726/25/8/084006

Worrell E, Price L, Martin N, et al (2001) Carbon dioxide emissions from the global cement industry. Annu Rev Energy Environ 26:303–329. doi: 10.1146/annurev.energy.26.1.303

Xiong W, Tang J, Zhu G, et al (2015) A novel capsule-based self-recovery system with a chloride ion trigger. Sci Rep 5:10866. doi: 10.1038/srep10866

Xu S, Nie Z, Seo M, et al (2005) Generation of Monodisperse Particles by Using Microfluidics: Control over Size, Shape, and Composition. Angew Chemie 44:3799–3799. doi: 10.1002/ange.200462226

Yang B, Huang WM, Li C, Li L (2006) Effects of moisture on the thermomechanical properties of a polyurethane shape memory polymer. Polymer (Guildf) 47:1348–1356. doi: 10.1016/j.polymer.2005.12.051

Yang J, Keller MW, Moore JS, et al (2008) Microencapsulation of Isocyanates for Self-Healing Polymers. Macromolecules 41:9650–9655. doi: 10.1021/ma801718v

Yang Z, Hollar J, He X, Shi X (2011) A self-healing cementitious composite using oil core/silica gel shell microcapsules. Cem Concr Compos 33:506–512. doi: 10.1016/j.cemconcomp.2011.01.010

Yang Z, Hollar J, He X, Shi X (2010) Laboratory Assessment of a Self-Healing Cementitious Composite. Transp Res Rec J Transp Res Board 2142:9–17. doi: 10.3141/2142-02

Yoon D, Hasegawa K, Kaneko Y, et al (2015) Formation of Polymeric Hollow Microcapsules and Microlenses Using Gas-in-Organic-in-Water Droplets. Micromachines 6:622–633. doi: 10.3390/mi6050622

Young BA, Fujii AMK, Thiele AM, et al (2016) Effective elastic moduli of core-shell-matrix composites. Mech Mater 92:94–106. doi: 10.1016/j.mechmat.2015.09.006

Zhao Y, Cheng Y, Shang L, et al (2015) Microfluidic Synthesis of Barcode Particles for Multiplex Assays. Small 11:151–174. doi: 10.1002/smll.201401600

Zieringer MA, Carroll NJ, Abbaspourrad A, et al (2015) Microcapsules for Enhanced Cargo Retention and Diversity. Small 11:2903–2909. doi: 10.1002/smll.201403175

Zuidam NJ, Shimoni E (2010) Overview of Microencapsulates for Use in Food Products or Processes and Methods to Make Them. Encapsulation Technologies for Active Food Ingredients and Food

Processing. Springer New York, New York, NY, pp 3–29